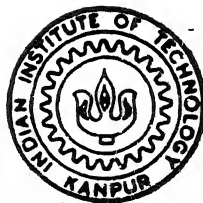


**Three-Dimensional Computation of Laminar and
Turbulent Flows with Heat Transfer in a
Channel with Built-in Longitudinal
Vortex Generators**

by

PRASANTA DEB

TH
ME/1994/D
D35t



**DEPARTMENT OF MECHANICAL ENGINEERING
INDIAN INSTITUTE OF TECHNOLOGY KANPUR**

April 1994

Three-Dimensional Computation of Laminar and
Turbulent Flows with Heat Transfer in a
Channel with Built-in Longitudinal
Vortex Generators

*A Thesis Submitted
in Partial Fulfillment of the Requirements
for the Degree of*

DOCTOR OF PHILOSOPHY

by
PRASANTA DEB

to the
DEPARTMENT OF MECHANICAL ENGINEERING
INDIAN INSTITUTE OF TECHNOLOGY

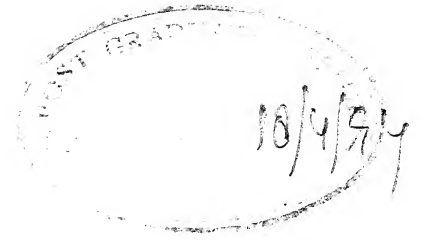
APRIL, 1994

3 1 JUL 1996
CENTRAL LIBRARY
I. I. T., KANPUR
No. A. 121961



A121961

ME-1994-D-DEB-THR



Certificate

It is certified that the work contained in the thesis entitled "*Three-Dimensional Computation of Laminar and Turbulent Flows with Heat Transfer in a Channel with Built-in Longitudinal Vortex Generators*", by **Prasanta Deb**, has been carried out under my supervision and that this work has not been submitted elsewhere for a degree.

Gautam Biswas

Dr. Gautam Biswas
Department of Mechanical Engineering
Indian Institute of Technology,
Kanpur

April, 1994

To My Parents

Synopsis

Flow and heat transfer characteristics in a rectangular channel, containing built-in vortex generators of both the slender delta-wing and winglet-pair type have been analyzed by means of solution of the full Navier-Stokes and energy equations. Each wing or winglet pair induces the creation of streamwise longitudinal vortices behind it. The spiraling flow of these vortices serves to entrain fluid from their outside into their core. These vortices also disrupt the growth of the thermal boundary layer and serve ultimately to bring about the enhancement of heat transfer between the fluid and the channel walls. The geometrical configuration considered in the study are representative of single elements of either a compact gas-liquid fin-tube crossflow heat exchanger or a plate-fin crossflow heat exchanger. Physically, these vortex generators can be mounted on the flat surfaces of the above mentioned heat exchangers by punching or embossing the flat surfaces. They can also act as spacers for the plate-fins. Because of the favorable pressure gradient in the channel, the longitudinal vortices are stable and their influence persists over an area which is many times the area of the slender vortex generators.

The present study gives a quantitative performance data for a delta wing and winglet-pair in a channel with different angles of attack and a wide range of operating conditions. The study is also extended for turbulent flows where the closure problem is solved with the well known $k - \epsilon$ model.

The time averaged Navier Stokes equations for incompressible flows where the Reynolds stresses are expressed via the eddy-viscosity concept have been used as governing equations. These equations are written in a Cartesian tensor form as

$$\frac{\partial \bar{U}_j}{\partial X_j} = 0 \quad (1)$$

$$\frac{D\bar{U}_j}{Dt} = -\frac{\partial(P + 2k_n/3)}{\partial X_j} + \frac{1}{Re} \frac{\partial}{\partial X_i} \left[(1 + \nu_{t,n}) \left(\frac{\partial \bar{U}_i}{\partial X_j} + \frac{\partial \bar{U}_j}{\partial X_i} \right) \right] \quad (2)$$

$$\frac{D\bar{\theta}}{Dt} = \frac{1}{Re.Pr} \frac{\partial}{\partial X_i} \left[(1 + \alpha_{t,n}) \frac{\partial \bar{\theta}}{\partial X_i} \right] \quad (3)$$

where \bar{U}_j and $\bar{\theta}$ are nondimensional time-mean velocity components and temperature, $\nu_{t,n}$ is the nondimensional kinematic viscosity, $\alpha_{t,n}$ is the nondimensional eddy diffusivity

and k_n is the nondimensional kinetic energy of turbulence. The subscripts i and j can take the values 1, 2 or 3 in the three coordinate directions X_1 , X_2 and X_3 respectively. The X_1 , X_2 and X_3 are equivalent to X , Y and Z in Cartesian coordinates. The Reynolds number Re is defined on the basis of average axial velocity at the inlet and the laminar viscosity as $Re = \bar{U}_o H / \nu$. The Prandtl number of the fluid is Pr .

The turbulent kinematic viscosity $\nu_{t,n}$ is given by

$$\nu_{t,n} = C_\mu Re k_n^2 / \epsilon_n \quad (4)$$

In the above equation C_μ is a constant (equal to 0.09) and ϵ_n is the dissipation rate of turbulent kinetic energy (normalized with respect to U_o^3/H). The nondimensional eddy diffusivity $\alpha_{t,n}$ is given by

$$\alpha_{t,n} = C_\mu Re Pr k_n^2 / (\sigma_t \epsilon_n) \quad (5)$$

where σ_t is the turbulent Prandtl number. Generally, $\sigma_t = 0.9$. The modeled transport equations for k_n and ϵ_n are

$$\frac{Dk_n}{Dt} = \frac{1}{Re} \frac{\partial}{\partial X_i} \left[\frac{\nu_{t,n}}{\sigma_k} \frac{\partial k_n}{\partial X_i} \right] + G_n - \epsilon_n \quad (6)$$

$$\frac{D\epsilon_n}{Dt} = \frac{1}{Re} \frac{\partial}{\partial X_i} \left[\frac{\nu_{t,n}}{\sigma_\epsilon} \frac{\partial \epsilon_n}{\partial X_i} \right] + C_1 \epsilon_n G_n / k_n - C_2 \epsilon_n^2 / k_n \quad (7)$$

Here G_n is the generation of turbulent kinetic energy(nondimensional) given by

$$G_n = \frac{(1 + \nu_{t,n})}{Re} \left(\frac{\partial U_i}{\partial X_j} + \frac{\partial \bar{U}_j}{\partial X_i} \right) \frac{\partial \bar{U}_i}{\partial X_j} \quad (8)$$

and $\sigma_k, \sigma_\epsilon, C_1, C_2$ are empirical constants : $\sigma_k = 1.0, \sigma_\epsilon = 1.3, C_1 = 1.44, C_2 = 1.92$. These are based on wide range of experimental data.

The equations are solved by a numerical procedure based on MAC (Marker and Cell) method. It may be mentioned that for the laminar flow computations, $\nu_{t,n}$ and k_n in equation (2) and $\alpha_{t,n}$ in equation (3) are taken as zero. Possibly it is needless to say that for the laminar flows, the barred quantities should be read as unbarred variables.

Figure S-1 compares the numerical flow visualization with its experimental counterpart due to a research group in the Ruhr University Bochum of Germany. The aspect ratio, Λ , and the angle of attack, β , of the winglet for this study are 1 and 35° respectively. In the experimental study, at the rear edge of the winglet, a primary longitudinal vortex of elliptical shape, is seen. The Reynolds number of this flow visualization study is 1350 and the flow is laminar. In the numerical flow visualization given, the secondary velocity vectors enable a view of the vortex transport at different regions of the cross-sections of the channel. A qualitative comparison between these numerical and the experimental flow visualizations implicates favorable agreement between the two. How-

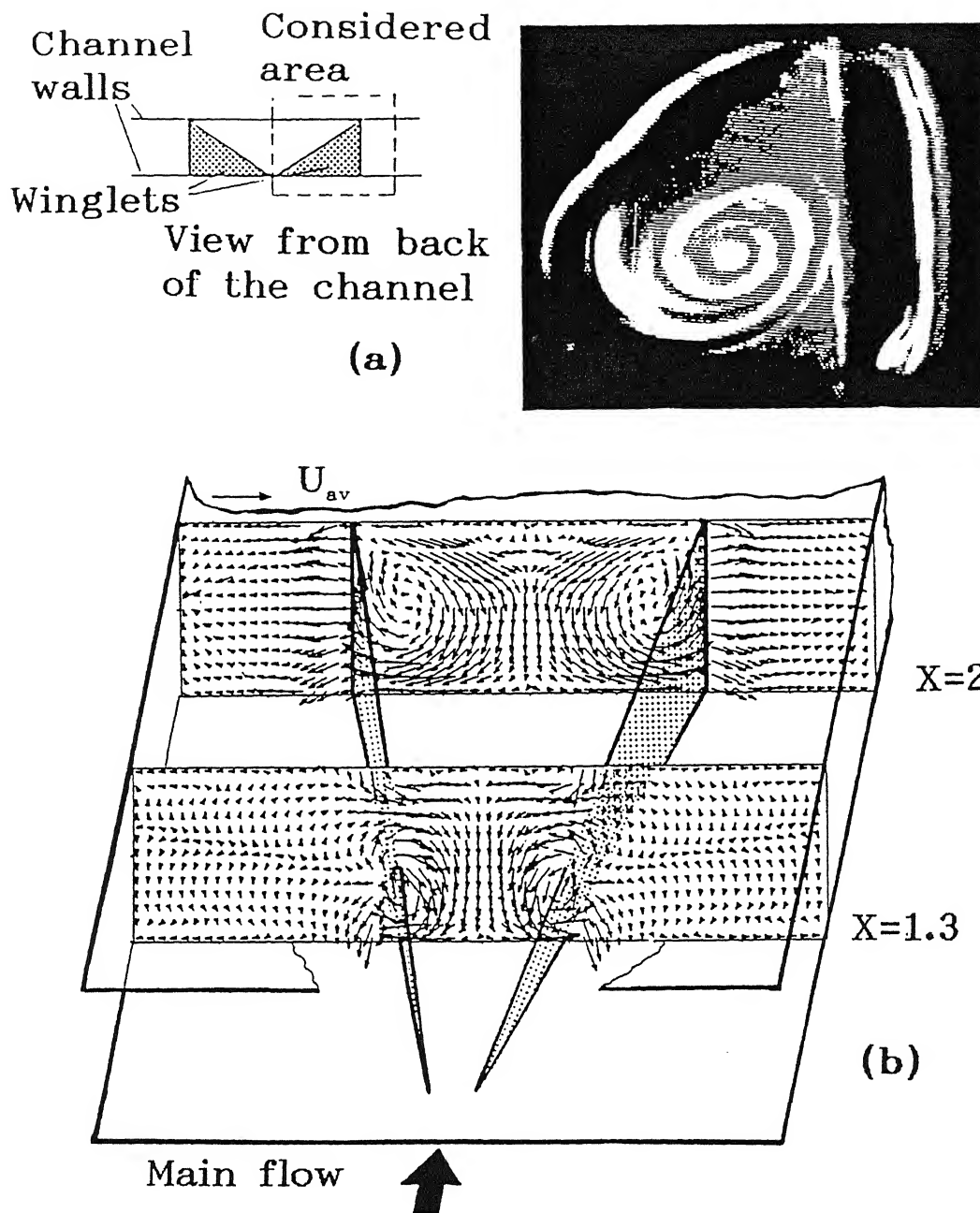


Fig. S-1 Formation of longitudinal vortices just behind the delta winglet-pair (a) experimental result (b) present computation

ever, a detailed evaluation of the performance parameters with regard to the enhancement of heat transfer using various wing-type vortex generators has been accomplished in this study.

From heat transfer point of view, delta wing is found to be more effective than winglet-pair. However, in the case of convective heat transfer two type of losses of useful work is encountered; one due to fluid friction resulting in viscous heat generation and other due to heat transfer across finite temperature gradient. Both these phenomena are manifestations of irreversibility and therefore for a complete evaluation of a heat transfer augmentation technique a detailed thermodynamic analysis is required. Thus, the present study incorporates an in-depth discussion about the influence of vortex generators (wings/winglets) on entropy generation and irreversibility.

It may be mentioned that the study of laminar flow in the present work is not for computational simplification. Usually, the fin spacing is so small and the mean velocity range is such that the flows are often laminar. However, for some special applications the velocity becomes very high and one may encounter turbulent flows in plate-fin heat exchangers. In the present study, results for turbulent flow have been obtained for a range of Reynolds number between 5000 and 100000. An effort has been undertaken to evaluate the accuracy of $k - \epsilon$ model in predicting such flows. In order to accomplish this, our computational results have been compared with a well documented experiment of another research group in Stanford University of the USA. The computational results agree reasonably well with their experimental counterpart.

Acknowledgements

As I recapitulate the sweet memories of past four years, I realize how much I am indebted to this Institute and numerous individuals who have given a soul to this passage with their love and support.

At the very outset I would like to take the opportunity to express my deep and sincere gratitude to my respected teacher and thesis supervisor Prof. Gautam Biswas for initiating me into this interesting problem and giving invaluable guidance, cordial advice and constant encouragement throughout this research. He has been not only the thesis supervisor but also my real friend, philosopher and guide. I have learned to develop the ideas for combining knowledge and practical applications and a true sense of scientific research through numerous discussions with him. His effective guidance, dynamism, coupled with his clarity of thoughts have directed the work towards completion. I feel very fortunate to have opportunity to work with him and I shall always remain obliged to his greatness in devoting a large share of his valuable time and knowledge to this work. It is not possible for me to express my full gratitude to him in above few words.

I wish to express my deep sense of gratitude to Prof. Martin Fiebig, Prof. N. K. Mitra and Dipl. Ing. Armin Eichholz of the Ruhr University Bochum, Germany for their generous help and encouragement.

I am indebted to Prof. John K. Eaton of Stanford University, the USA for his benevolent help in providing us with the experimental results related to the measurement of turbulent flows.

I am especially thankful to Dr. T. Sundararajan for his valuable suggestions and encouragement. I would gratefully recall the constructive criticism and enlightening suggestions received from Dr. Sangeeta Kohli during the concluding year of this program.

I also express my gratefulness to Prof. A. Ghosh, Prof. S. G. Dhande, Dr. V. Eswaran, Dr. K. Muralidhar, Dr. Amitabha Mukerjee for their help whenever required.

I gratefully acknowledge the facilities received from the Computational Fluid Dynamics

Laboratory of the Mechanical Engineering Department.

I am especially thankful to Dr. K. M. Singh and Dr. Manab Das for providing valuable suggestions time to time. I shall never forget their deep involvement in this work.

I shall be failing in my duty if I do not express thanks to my friends and colleagues Aniruddha Mukhopadhyay, Probodh Maji, Sudipta Biswas, Mausam Sarkar, Arun Saha, Pramod Choudhary and Anshul Gupta for their ungrudging help and suggestions.

I am grateful to Mr. Shambhu Sharma, Mr. S.R.K. Bharadwaj and Mr. Bhartiya for their help and cooperation.

I shall always carry the fond memories of the time I have spent with Niloy, Dada, Verma, Shamshi, Mota, Patel, Tiwari, Subhash, Sneha and Ravindra.

I am thankful to Mr. Khuswa and Mr. Shukla for preparation of drawings.

The silent support, inspiration, good wishes and blessings from my family have really been indispensable.

I shall be always grateful to those invisible persons whose support cannot be expressed in words.

Prasanta Deb

Contents

Certificate	iii
Synopsis	vii
Acknowledgements	xi
Contents	xiii
List of Figures	xvii
Nomenclature	xxi
1 Introduction	1
1.1 Description of the Problem	1
1.2 The Scope of the Present Work	2
1.3 Layout of the Thesis	3
2 Review of Literature	5
2.1 Introduction	5
2.2 Enhancement of Heat Transfer by Mounting Protrusions on the Surfaces	6
2.2.1 Internal Flows in Tubes and Ducts	6
2.2.2 Flows in Parallel Plate Channels Formed by Two Neighboring Fins of Plate -fin or Fin-tube Heat Exchangers	9
2.3 Development of Numerical Methods for Solving Full Navier-Stokes Equa- tions	14
2.3.1 Methods Developed on Regular Geometries	14
2.3.2 Methods on Complex Geometries	15
2.3.3 Modelling of Convection-Diffusion Equations	16
2.4 A Review on Turbulence Modelling	18
2.4.1 General	18
2.4.2 Various Approaches for Modelling Turbulent Flows	18
2.5 Remarks	23

3	Mathematical Formulation	25
3.1	Introduction	25
3.2	Statement of the Problem	25
3.2.1	Governing Equations for Laminar Flow	27
3.2.2	Boundary Conditions for Laminar Flow	27
3.2.3	Governing Equations for Turbulent Flow	28
3.2.4	Boundary Conditions for Turbulent Flow	29
3.3	Grid System Used	31
3.4	Numerical Boundary Conditions	33
3.4.1	Boundary Conditions for Confining Walls	33
3.4.2	Boundary Conditions for the Obstacle	34
3.5	Method of Solution	40
3.5.1	MAC Algorithm	40
3.5.2	Discretization Technique for k and ϵ Equations	44
3.5.3	Solution of the Energy Equation	45
3.5.4	Numerical Stability Considerations	47
3.6	More on Discretization of Governing Equations	47
3.6.1	Some Improvements on Discretization of Convective Terms	48
3.6.2	Comparison of Results based on Model Problem	51
3.7	Spatial Grid Independence	57
3.8	Computational Time	58
4	Evaluation of Performance Parameters for Laminar Flow	59
4.1	Introduction	59
4.2	Performance of Delta Wing-Type Vortex Generators	59
4.3	Performance of Delta Winglet-Pair Type Vortex Generators	75
4.4	Comparison with Experiments	81
5	A Second Law Based Optimization for the Choice of Vortex Generators in the Laminar Flow Regime in the Laminar Flow Regime	89
5.1	Introduction	89
5.2	Irreversibility Approach to Heat Transfer Process A Brief Review	90
5.3	The Calculation Procedure for the Thermodynamic Optimization	91
5.3.1	Nusselt number and Skin friction	91
5.3.2	Entropy Generation	91
5.3.3	Merit Function	93
5.4	Results and Discussions	94
5.5	Appraising Remarks	98

6	Turbulent Flow and Heat Transfer	101
6.1	Introduction	101
6.2	Basis of the Wall-Function Treatment in Turbulence Modeling	102
6.3	Present Investigation	104
6.4	Comparison of Numerical and Experimental Results	104
6.4.1	The Test Section and the Computational Domain	104
6.4.2	Comparison and Discussion	105
6.5	Prediction of Pertinent Performance Parameters	108
7	Concluding Remarks	125
	Bibliography	127
A	The Program Substructure	143

List of Figures

S-1	Formation of longitudinal vortices just behind the delta winglet-pair (a) experimental result (b) present computation	ix
1.1	Typical arrangement of heat exchanger cores (a) Gas-liquid fin-tube cross-flow (b) Plate-fin (single or multi pass)	2
1.2	Protrusions in the form of (a) delta wing and (b) winglet pair on the flat surface to enhance heat transfer	3
2.1	(a) Plate-fin heat exchanger and its surface geometries : (b) plain rectangular fins (c) plain triangular fins (d) wavy fins (e) offset strip fins (f) perforated fins (g) louvered fins; after Webb (1987)	7
2.2	Various methods of making enhanced tubes: (a) helical rib on inner surface and integral fin on outer surface (b) internal fins on inner surface and porous coating on outer surface (c) twisted tape insert on inner surface and integral fins on outer surface	8
2.3	Vortices formed by a slender delta wing; after van Dyke (1982)	10
2.4	Flow around a tube on a plate	12
3.1	Flow model for computation	26
3.2	Cross-section of the computational domain	29
3.3	(a) Grid spacing in the computational domain and the location of the wing-type vortex grid showing the discretized variables (b) Three-dimensional staggered grid showing the locations of the locations of the discretized variables	32
3.4	Boundary conditions and fictitious boundary cells	33
3.5	Relative location of velocity components and wing on X-Y plane at Z=0	35
3.6	Side edge of the wing-type vortex generator on Y-Z plane	36
3.7	Relative location of the spanwise velocity components and the wing-type vortex generator on X-Y plane	37
3.8	Thermal boundary conditions on the wing-type vortex	38
3.9	Periodic boundary conditions for pressure and velocities on the top and the bottom wall	39
3.10	Dependent variables on a rectangular mesh for describing QUICK scheme	48

3.11	Velocity vectors in a lid-driven square cavity for $Re=400$ (42×42 grid); discretization due to Weighted average scheme	52
3.12	Velocity vectors in a lid-driven square cavity for $Re=400$ (42×42 grid); discretization due to QUICK scheme	53
3.13	Velocity vectors in a lid-driven square cavity for $Re=400$ (42×42 grid); discretization due to third-order upwinding scheme	54
3.14	Variation of U velocity along the vertical midplane for the lid-driven flow in a square cavity	55
3.15	Variation of V velocity along the horizontal midplane for the lid-driven flow in a square cavity	56
3.16	Comparison of weighted average scheme with QUICK	57
4.1	Cross-stream velocity vectors at different axial locations behind the wing showing generation and deformation of vortices in the channel	61
4.2	Static pressure distribution at different axial locations behind the delta wing	62
4.3	Contours of normalized streamwise vorticity at different cross-sections of the channel in presence of a delta wing	63
4.4	Isolines for axial velocity at two different cross-stream planes (a) 0.58 wing-chord downstream and (b) 1.74 wing-chord downstream of a delta wing	64
4.5	Isotherms at different cross-planes in the channel in presence of built-in delta wing	65
4.6	Effect of angle of attack of the delta wing on the distribution of combined spanwise-average-Nusselt-number in the channel	67
4.7	Effect of stamping on cross-stream velocity vectors at different axial locations in the channel with delta wing as the obstacle	68
4.8	Effect of stamping on the distribution of combined spanwise average Nusselt number in the channel; simultaneously developing flow	69
4.9	Lateral distribution of local Nusselt number at different axial locations in the channel	70
4.10	Effect of Reynolds number on the distribution of combined spanwise average Nusselt number in the channel with and without the delta wing	72
4.11	Effect of angle of attack of delta wing on the distribution of combined spanwise-average-friction-coefficient in the channel	73
4.12	Effect of stamping on the distribution of combined spanwise average friction coefficient in the channel; simultaneously developing flow	74
4.13	Effect of Reynolds number on the distribution of combined spanwise average friction coefficient in the channel with and without the delta wing	76
4.14	Cross-stream velocity vectors at different axial locations behind the winglet-pair in a channel	77

4.15	Contours of normalized streamwise vorticity at different cross-sections of the channel in presence of the winglet-pair	78
4.16	Isotherms at different cross-planes in a channel in presence of a built-in winglet-pair	79
4.17	Effect of angle of attack of winglet-pair on the distribution of combined spanwise-average-Nusselt-number in the channel developed profile at the inlet	80
4.18	Effect of winglet-pair on combined spanwise average Nusselt number distribution of the channel for different Reynolds numbers	82
4.19	Effect of angle of attack of the winglet-pair on the distribution of combined spanwise average skin friction in the channel; developed profile at the inlet	83
4.20	Effect of Reynolds number on the distribution of combined spanwise-average-skin-friction in the channel with built-in winglet-pair	84
4.21	Comparison of computed results with experimental observation	86
4.22	Comparison between computational and experimental results for Colburn factor as a function of Reynolds number at different angles of attack	87
5.1	Effect of type of obstacle on the distribution of combined spanwise average Nusselt number in the channel; developed profile at the inlet	95
5.2	Effect of type of obstacle on the distribution of combined spanwise average friction coefficient in the channel; developed profile at the inlet	96
5.3	Effect of type of obstacle on the variation of volumetric entropy generation with Reynolds number	97
5.4	Effect of type of obstacle on the variation of merit function with Reynolds number	98
6.1	Schematic of the test section of Pauley and Eaton (1988 a,b)	105
6.2	Vector Plots of secondary flow: $Re_{H/2}=67000$	106
6.3	Contours of streamwise velocity at different cross-sections for $Re_{H/2} = 67000$	107
6.4	Isolines for turbulent kinetic energy at different cross-sections for $Re_{H/2} = 67000$	109
6.5	Streamwise velocity profiles at axial station $x=142$ cm for $Re_{H/2} = 67000$	110
6.6	Streamwise velocity profiles at axial station $x=188$ cm for $Re_{H/2} = 67000$	111
6.7	Turbulent kinetic energy profiles at axial station $x=188$ cm for $Re_{H/2} = 67000$	112
6.8	Isolines of static pressure at different cross-sections for $Re=5000$; trailing edge of the winglet is located at $X=2.5$ from the inlet	114
6.9	Isolines of static pressure at different cross-sections for $Re=15000$; trailing edge of the winglet is located at $X=2.5$ from the inlet	115

6.10	Isolines of turbulent kinetic energy at different cross-sections for $Re=5000$; trailing edge of the winglet is located at $X=2.416$ from the inlet	116
6.11	Distribution of spanwise average Nusselt number on the bottom plate for different Reynolds numbers	117
6.12	Cross-stream velocity vectors at $X=2.5$ from the inlet of the channel for two different Reynolds numbers	118
6.13	Spanwise variation of local Nusselt number for different Reynolds numbers at $X=4.325$	119
6.14	Distribution of spanwise average Nusselt number on the bottom plate for different angles of attack	120
6.15	Distribution of spanwise average skin friction on the bottom plate for different Reynolds numbers	122
6.16	Distribution of spanwise average skin friction on the bottom plate for different angles of attack	123

Nomenclature

B	channel width, m
H	channel height, m
b	wing span, m
L	characteristic length, m
t	time, s
Br	ratio of wing span to width of the channel (b/B)
S	wing area, m^2
T	temperature, K
r	ratio of wall temperature to ambient temperature, T_w/T_∞
θ	temperature (nondimensional), $(T - T_\infty)/(T_w - T_\infty)$
\bar{T}_b	average bulk temperature for the entire channel, K
$\bar{\theta}_b$	average nondimensional bulk temperature for the entire channel, $(\bar{T}_b - T_\infty)/(T_w - T_\infty)$
D	divergence of velocity vectors equation (1)
c_p	specific heat of the fluid, kJ/kg.K
E_c	Eckert number, $U_{av}^2/c_p T_\infty$
I	turbulent intensity
k	thermal conductivity of the fluid, W/mK
h	heat transfer coefficient, $-k(\partial T/\partial y)_w/(T_w - T_b)$, W/m ² K
q	wall heat flux, W
q_w	wall heat flux for turbulent flow, W
$q_{w,n}$	wall heat flux for turbulent flow (nondimensional)
j	mean Colburn factor, $\overline{Nu}_c/(RePr^{1/3})$
C_f	skin friction, $[2(\partial u/\partial y)_w]/(\rho U_{av}^2)$
\bar{C}_f	combined spanwise average friction coefficient equation (4.2)
Ns_3	rate of nondimensional entropy generation per unit volume equation (5.6)
Nu	local Nusselt number based on bulk temperature of the fluid
Nu_{xe}	local Nusselt number based on entry temperature of the fluid ,equation (4.3)
\overline{Nu}	spanwise average Nusselt number
\overline{Nu}_{sa}	combined spanwise average Nusselt number, equation (4.1)
\overline{Nu}_c	average Nusselt number for the entire channel
p	static pressure, N/m ²
P	nondimensional static pressure, $p/\rho U_{av}^2$
Pr	Prandtl number, $\mu c_p/k$

Re	$U_{av}H/\nu$
$Re_{H/2}$	$U_oH/2\nu$
x, y, z	axial, vertical or normal, and spanwise dimension of coordinates, m
X, Y, Z	axial, vertical or normal, and spanwise coordinates(normalized by H)
u, v, w	axial, vertical, spanwise components of velocity, m/s
u', v', w'	axial, vertical, spanwise components of fluctuating velocity, m/s
$\bar{u}', \bar{v}', \bar{w}'$	axial, vertical, spanwise components of time-mean fluctuating velocity, m/s
U, V, W	axial, vertical, spanwise components of laminar velocity (nondimensional)
$\bar{U}, \bar{V}, \bar{W}$	axial, vertical, spanwise components of time-mean velocity (nondimensional)
$\bar{\theta}$	time-mean temperature component (nondimensional)
k	turbulent kinetic energy, m^2/s^2
k_n	k/\bar{U}_o^2 , turbulent kinetic energy (nondimensional)
ϵ	dissipation rate of turbulent kinetic energy, m^2/s^3
ϵ_n	$\epsilon/\bar{U}_o^3/L$, dissipation rate of turbulent kinetic energy (nondimensional)
$\bar{\epsilon}_n$	average dissipation rate of turbulent kinetic energy (nondimensional)
τ_w	wall shear stress, N/m^2
$\tau_{w,n}$	wall shear stress (nondimensional)
$\tau_{w,n}^x$	x-component of wall shear stress (nondimensional)
$\tau_{w,n}^z$	z-component of wall shear stress (nondimensional)
u_τ	$\sqrt{\tau_w/\rho}$, friction velocity, m/s
$u_{\tau,n}$	$\sqrt{\tau_{w,n}}$, friction velocity (nondimensional)
ν_t	$C_\mu k^2/\epsilon$, turbulent kinematic viscosity, m^2/s
$\nu_{t,n}$	$C_\mu Re k_n^2/\epsilon_n$, turbulent kinematic viscosity (nondimensional)
Y^+	yu_τ/ν or $YReu_{\tau,n}$, nondimensional distance from the wall in the law of the wall
C_μ	empirical constant
P_{fn}	Pee function
χ	von Karman constant and equal to 0.42
E	function of wall roughness in the law of the wall
G	generation of turbulent kinetic energy, N/m^2s
G_n	generation of turbulent kinetic energy (nondimensional)
$\alpha_{t,n}$	eddy diffusivity (nondimensional)

Greek symbols

δ_{ij}	Kronnecker delta
α	aspect ratio of the channel, B/H
μ	dynamic viscosity of the fluid, $N.s/m^2$
σ	stress tensor
ν	kinematic viscosity of the fluid, m^2/s
τ	nondimensional time

- λ a constant and equal to 0.09
- Λ aspect ratio of the wing
- ρ density of the fluid
- Δ Divergence of velocity vectors, $\partial u_k / \partial x_k$

Subscripts

- w wall
- b bulk condition
- av average
- 1 bottom fin-plate
- 2 top fin-plate
- sa spanwise combination of top and bottom plate
- o condition in the free-stream
- p corresponding to grid point adjacent to the the wall

Chapter 1

Introduction

1.1 Description of the Problem

Fin-tubes are generally used in gas-liquid heat exchangers where the gas is in the crossflow to the tubes and the liquid flows inside the tubes. Figure 1(a) shows the arrangement of the core region of a fin-tube crossflow heat exchanger. The purpose of the fin is to enhance the heat transfer coefficient on the gas side to a value comparable to the liquid side. The area ratio of the fins to the tubes varies depending on the application and may reach a value of 30. Plate-fin heat exchangers also find application in many industrial processes. Such heat exchangers may be used to exchange energy between two different gases or liquids. Figure 1(b) illustrates the basic arrangement of the core region of a plate-fin heat exchanger. In forced convection heat transfer between a gas and a liquid, the heat transfer coefficient of the gas may be 10 to 50 times smaller than that of the liquid. In order to increase the heat transfer on the gas side, the fin geometry can be manipulated (Webb, 1987) in various ways. In addition, compactness of the heat exchangers is demanded for effective utilization of energy and to bring about a save on material and space. The performance of heat exchanger surfaces can be enhanced by mounting protrusions on the surfaces. The offset strip-fin and the louvered fins have been widely used for this purpose (Webb, 1987). The basic mechanism involved in the above mentioned cases is the periodic interruption of the boundary layer by separation, wake recovery and generation of thin developing boundary layer with high Nusselt numbers.

A somewhat different concept for the reduction of the thermal resistance is to induce longitudinal streamwise vortices in the flow field. The longitudinal vortices can be generated by mounting delta wing or winglet-type vortex generators on the flat surfaces (Fig. 1.2). The longitudinal vortices develop along the side edge of the wing-shaped vortex generator due to the pressure difference between the front surface facing flow and the back surface. These streamwise vortices interact with an otherwise two-dimensional boundary layer and produce a three dimensional swirling flow that mixes near wall

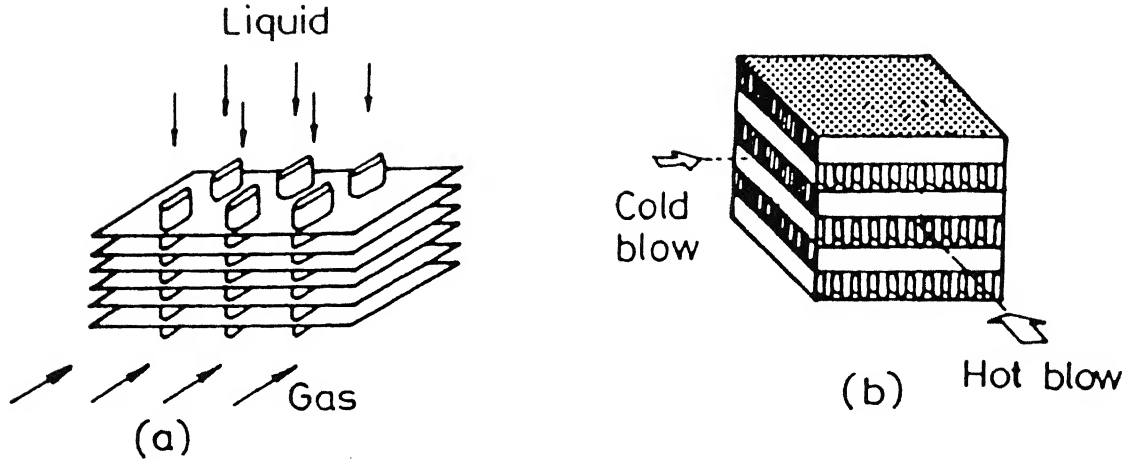


Figure 1.1: Typical arrangement of heat exchanger cores (a) Gas-liquid fin-tube cross-flow (b) Plate-fin (single or multi pass)

fluid with the free stream. This mechanism strongly enhances the exchange of fluid between the wall and the core region of the flow field which causes high heat transfer augmentation. The additional pressure losses are modest because the form drag for such wing-type slender bodies is low. A complete numerical evaluation of heat transfer in a fin-tube or plate-fin crossflow heat exchanger would be extremely difficult. In order to understand the basic mechanisms involved in enhancement of heat transfer and to evaluate the performance parameters quantitatively, a need is felt to analyze three-dimensional flow and heat transfer in a horizontal channel with built-in vortex generators.

A number of experimental investigations (Edwards and Alker, 1974; Russel *et al.*, 1982; Fiebig *et al.*, 1986) in fields relevant to the present problem have been reported in the literature. Computational studies on related topics have been performed by Fiebig *et al.* (1989) and Biswas and Chattopadhyay (1992) for laminar flows. Arising out of the practical and academic importance of the configuration of interest, it is conjectured that a detailed analysis of the longitudinal vortices embedded in a shear flow will provide a better understanding of the complex phenomena and facilitate a more accurate estimation of the pertinent performance parameters.

1.2 The Scope of the Present Work

Since, the details of the interactions between the longitudinal streamwise vortices, the enhancement of heat transfer and the associated flow losses for laminar and turbulent flows are not still clearly understood, there is a general agreement that more research

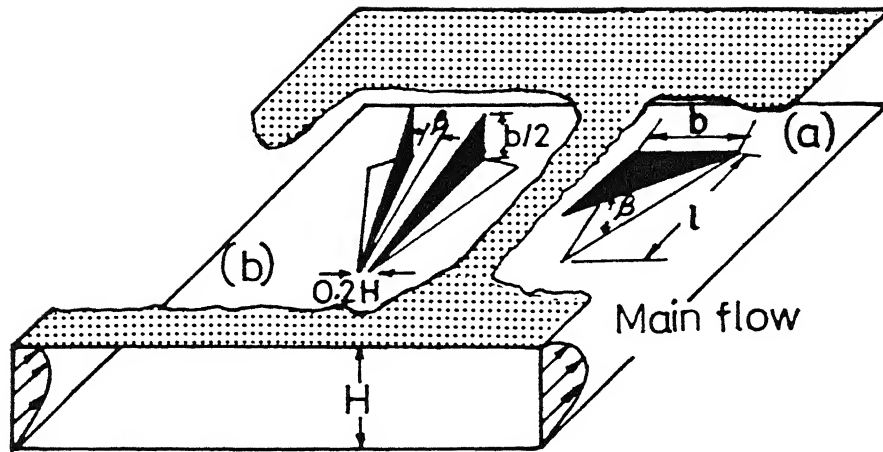


Figure 1.2: Protrusions in the form of (a) delta wing and (b) winglet pair on the flat surface to enhance heat transfer

on the subject is required.

In this thesis, a detailed three-dimensional numerical model has been formulated which is able to provide a clear understanding of the physics of the flow. Grid independent numerical solutions have been envisaged which carefully track the development of swirling flows, in order to estimate more accurately the performance parameters. In the numerical model, the full Navier-Stokes equations together with the governing equation for energy have been solved in a rectangular channel with built-in wing-type vortex generators. The present investigation also highlights the thermodynamic optimization of the heat transfer with respect to variation in geometrical parameters involved in transport-enhancement. An attempt has also been made to compute turbulent flows with suitably adapted $k-\epsilon$ model. An assessment regarding the validation of the model has been tried as well through the comparison with experimental results due to Pauley and Eaton (1988a, b).

1.3 Layout of the Thesis

Chapter-2 of the thesis provides a review of literature relevant to the basic mechanisms involved in augmentation of heat transfer with special emphasis on generation of longitudinal streamwise vortices. A concise review of the modeling aspects of turbulent flow has also been focussed in this chapter. The mathematical formulation of the problem for simulation is presented in chapter-3. In this chapter, the geometry, governing equations, boundary conditions, method of solution of the governing equations to obtain the numerical results are described in detail. Chapter-4 discusses the

results for laminar flows. Basically a detailed appraisal of the performance parameters is accomplished in this chapter. Two different wing-type vortex generators have been investigated numerically, *viz.*, delta wings and delta winglet pairs. In chapter-3, relative performance of the wing and winglet-pair has been compared. The basis of comparison has been a second law analysis. Most convective heat transfer processes encounter two types of losses, namely, losses due to fluid friction and those due to heat transfer across a finite temperature gradient. These two phenomena are the manifestations of thermodynamic irreversibility and the investigation of a process from this standpoint is known as second law analysis. Chapter-6 presents the results for turbulent flows. This chapter serves bivalent purposes. On one hand, a critical appraisal of the numerical model is accomplished through comparison with a well documented experimental data base of a research group in Stanford University and on the other hand, a parametric study is presented predicting the effects of various geometric and operating variables in the turbulent regime. Chapter-7 includes the concluding remarks and the scope for further research.

Chapter 2

Review of Literature

2.1 Introduction

The objectives of the present study have been briefly outlined in the previous chapter. A variety of experimental and a considerable amount of analytical and computational research have been carried out on the enhancement of heat transfer. Especially, the enhancement of heat transfer through manipulation of surface geometry has concerned many researchers and practitioners since the earliest documented studies of heat transfer. In this chapter a survey of the relevant literature is presented to indicate the extent of work already reported in open literature pertaining to the enhancement of heat transfer by introducing protrusions mounted on the heat transfer surfaces. In order to analyze the flow structure and heat transfer in such applications a detailed computational study is needed. The flow regime for such applications can be both laminar and turbulent. In the present literature review the attention is also focussed, by and large, on important numerical techniques developed in the recent past for solving the governing conservation equations for complex flows and heat transfer. Although the numerical solution of the governing conservation equations for laminar flows has become a realizable goal, the solution for turbulent flows even for simpler geometry is indeed a formidable task. The relevant literature on turbulence modeling has also been looked into with intent to understand various modeling and computational strategies. However, this survey also helps in suggesting further work that should be carried out to accomplish the objectives enumerated in the earlier chapter. The literature is reviewed from three different view points. In the first section, an overview of past work done by various researchers in the area of augmentation of heat transfer is presented and discussed. The second section presents a review of investigations pertaining to the numerical methods with regard to the task of computing flow fields in complex geometries. Basically, this section deals with the available schemes for solving the full Navier-Stokes equations. In the third, a comprehensive review on modeling aspects of turbulent flow has been undertaken with a view to suggest a suitable turbulent-closure-model for our problem.

2.2 Enhancement of Heat Transfer by Mounting Protrusions on the Surfaces

The subject of enhanced heat transfer is of serious interest in heat exchanger applications. Concepts like space and energy optimization in power and process industries call for more and more compact designs of heat exchangers. Specially designed surfaces use protrusions mounted on them to enhance heat transfer. Some typical examples of the enhanced heat transfer surfaces which are very popular in different industrial applications (Webb, 1987) are shown in Fig. 2.1. There have been a number of recent survey articles and handbook sections prepared that deal with the augmentation of heat transfer for different applications (Bergles, 1978, 1983, 1985). Special surface geometries bring about the transport-enhancement by establishing a higher " hA " per unit base surface area. It may be mentioned that $(1/hA)$ is the thermal resistance associated with heat transfer by convection at a surface. Some well known methods of manipulation of surface-geometry are:

- (a) Inserting twisted tapes or turbulence promoters for internal flows in circular tubes.
- (b) Roughening the surfaces for channel flows in closely spaced parallel plate channels, typical of plate -fin and plate type heat exchangers.
- (c) Improving flow structure in external flows normal to tubes and tube banks.

2.2.1 Internal Flows in Tubes and Ducts

Some useful methods of enhancing heat transfer on the inner surfaces of the tubes have been documented by Webb (1987). For tubular heat exchangers, enhancement is desirable for the inner side, outer side or both sides of the tube. Fig. 2.2 shows some doubly enhanced tubes where the enhancement is applied to both inner and outer surfaces. Generally the enhancement applied to the innerside is caused by imparting a swirl to the flowing fluid. Date (1974) has performed numerical predictions for the twisted tape in fully developed laminar flow for constant heat flux with constant properties. His analysis shows that the Nusselt number increases with increasing Prandtl and Reynolds numbers, contrary to laminar flow in smooth tubes which is independent of Re and Pr . Date (1973) has also proposed a correlation for the friction factor for the range $5000 < Re < 70,000$.

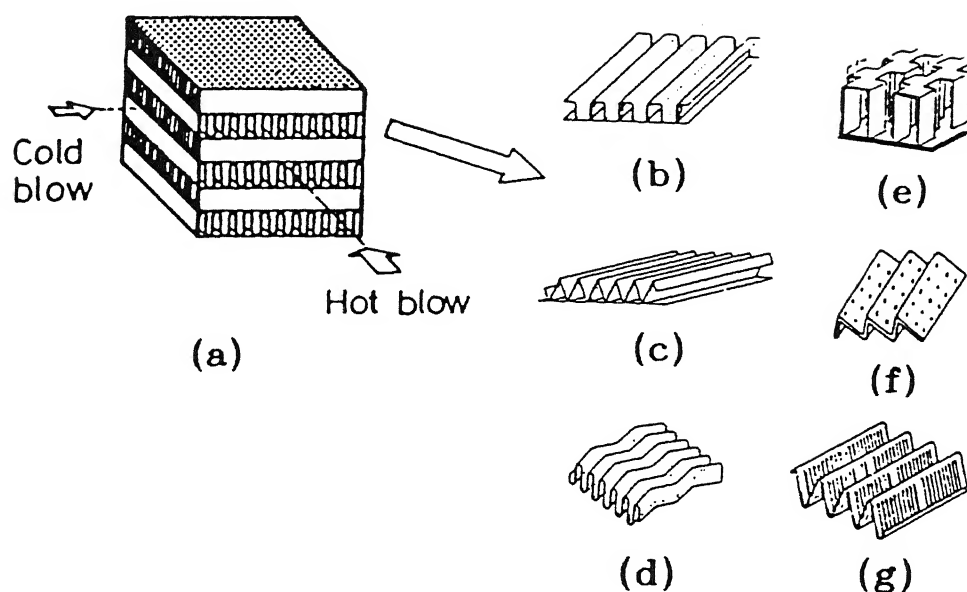
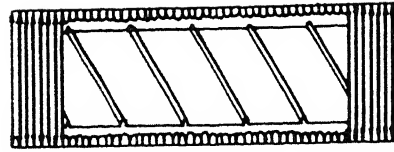
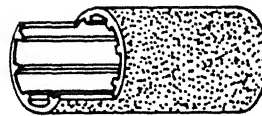


Figure 2.1: (a) Plate-fin heat exchanger and its surface geometries : (b) plain rectangular fins (c) plain triangular fins (d) wavy fins (e) offset strip fins (f) perforated fins (g) louvered fins; after Webb (1987)

Bergles et al. (1980) have reported a bibliography of different augmentation techniques. Nondecaying swirl flow has been the subject of many investigations (see Kreith and Margdis, 1959; Gambill and Bundy, 1963; Smithberg and Landis, 1964; Hong and Bergles, 1976). Blum and Oliver (1966) and Migay and Golubev (1970) have shown that there is significant increase in heat transfer due to free swirling flow. An analytical study of the heat transfer characteristics in decaying turbulent swirl flow generated by short twisted tapes placed at the entrance of the test section is carried out by Algifri and Bharadwaj (1985). They have shown that the augmentation in the local heat transfer can be as high as 80 percent and the augmentation is worthwhile up to an initial length of about 60 tube diameters. Bergles and Joshi (1983) provide an excellent summary of performance data on the twisted tape-inserts for the constant wall temperature and constant wall heat flux boundary conditions. Sparrow and Chaboki (1984) have performed an experimental study on swirl affected turbulent air flow and heat transfer in a tube. The swirling motion has been found to enhance heat transfer substantially in the initial portion of the tube. Compared with the heat transfer coefficient encountered in the conventional thermal entrance region in a nonswirling pipe flow, those associated with swirl are found to be remarkably greater. Junkhan et al. (1985) have conducted experimental studies of three different type of tape inserts for fire tube boilers. These tapes are termed as turbulators. Two commercial turbulators consisting of narrow, thin

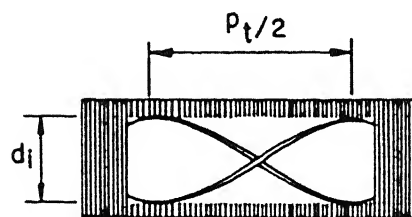


(a)



(b)

$$\text{Twist ratio} \\ = r_t = p_t / 2d_i$$



(c)

p_t = Axial distance through
which the tape is twisted
by 180°

Figure 2.2: Various methods of making enhanced tubes: (a) helical rib on inner surface and integral fin on outer surface (b) internal fins on inner surface and porous coating on outer surface (c) twisted tape insert on inner surface and integral fins on outer surface

metal strips bent and twisted in zig-zag fashion to allow a periodic contact with tube wall, have displayed 135 and 175 percent increase in heat transfer coefficient at a high Reynolds number. A third turbulator consisting of a twisted strip, with width slightly less than the tube diameter, has provided a 65 percent increase in the heat transfer coefficient while the increase in the friction factor is small as compared to the other two turbulator inserts.

2.2.2 Flows in Parallel Plate Channels Formed by Two Neighboring Fins of Plate -fin or Fin-tube Heat Exchangers

It may be mentioned here that we are particularly interested in enhancement of heat transfer in the gas side of fin-tube heat exchangers (with flat fins) and enhancement of heat transfer in plate-fin heat exchangers. With this intent, we would like to study different investigations related to augmentation of heat transfer suitable for preceding applications.

Augmentation of heat transfer is of special interest in channel flows where the rate of the heat transfer between the fluid and the channel walls deteriorates as the boundary layer grows on the channel walls and the flow tends to become fully developed. Protrusions can be mounted on these channel walls in order to disrupt the growth of the boundary layer and thereby enhance the heat transfer between the flowing fluid and the channel walls. Two relevant applications using this kind of flow configuration are the heat transfer between the gas and the fin in the case of gas-liquid fin-tube cross-flow heat exchangers and the heat transfer between flowing fluid and plates in the case of plate-fin heat exchangers (Fig. 1.1). The evolution towards a fully developed flow can be disturbed by using a multi-louvered surface geometry for the plates. Investigation by Achaichia and Cowell (1988) provides a detailed performance data for louvered fin surfaces. However in using louvered fins, enhancement is obtained at the price of high pressure drop. To circumvent this difficulty, protrusions in the form of slender delta wings or winglets can be deployed (Fig. 1.2). As shown, the base of the wing remains attached to the fin and the apex faces the incoming stream with an angle of attack with this configuration. The longitudinal vortices are generated along the side edge of the wing-shaped vortex generator due to the pressure difference between the front surface facing the flow and the back surface (Fig. 2.3). These longitudinal vortices, generated by the vortex generators, can be made to disrupt the growth of boundary layer in a channel by exchanging the fluid from the near-wall-region with the channel-core-region and thus they can serve to enhance the heat transfer rate while producing less of a pressure drop. Use of longitudinal vortices for boundary layer control is well known (Pearcey, 1961) and the vortex generators are used in commercial air-planes for this purpose.

Formation of streamwise longitudinal vortices behind a slender aerodynamic object is a research topic of considerable interest for several years. Both the theoretical and

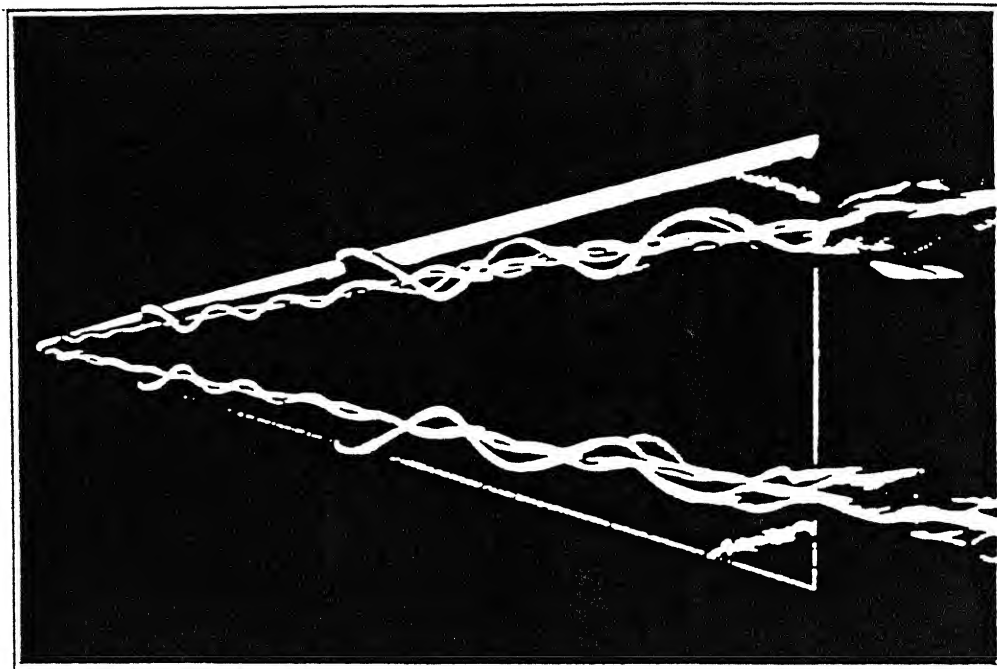


Figure 2.3: Vortices formed by a slender delta wing; after van Dyke (1982)

experimental investigations on flow past a delta wing have been conducted and reported in literature by a number of researchers. Among them Winter (1956), Fink (1956), Marsden et al. (1958) and Lawford (1964) are noteworthy. The physics of vortex formation has been furnished by Brown et al. (1954), Mangler et al. (1959) and Smith et al. (1968). Use of thin aerofoil theory provides good approximation of the strength of the leading edge vortices and the lift, though in trailing edge part their results show some discrepancy with experiments. Rehbach (1976) and Kandil et al. (1976) have obtained better results with non-conical theory. Computational solution of non-conical flow field and pressure distribution on wing surface has also been attempted by Johnson et al. (1976) and Weber et al. (1976). Their study suffers from some numerical complications in the vicinity of the trailing edge. Hummel and Srinivasan (1967) have made important contribution in revealing the complex flow structure behind a delta wing. They have conducted experiments and presented pressure distribution and vortex structure of the flow around a delta wing of unit aspect ratio with an angle of attack of 20° .

Thomas et al. (1990) have computed low-speed laminar flow over a low aspect ratio delta wing up to 40° angle of attack using an upwind biased finite volume algorithm. The differencing scheme used are second-order accurate and a multigrid algorithm is employed to promote convergence to steady state. The predicted results and lift coefficient of the wing have remarkable agreement with experiments due to Hummel (1973).

At 40° angle of attack, a bubble-type vortex breakdown is evident in the computations.

Experimental investigations due to Edwards and Alker (1974), Russels et al. (1982), Fiebig et al (1986), Fiebig et al (1991) and Tiggelbeck et al. (1992) can be referred to in connection with augmentation of heat transfer by means of longitudinal vortices. Experimental investigation due to Fiebig et al. (1991) is the first systematic study to compare the performance of different kinds of vortex generators, viz., delta wing, rectangular wing, delta winglet pair and rectangular winglet pair in the Reynolds number range of 1360 and 2270. Their observations depict that the delta wing is the best vortex generator from heat transfer point of view. Another important feature of their observations is that the heat transfer coefficient increases with increase in angle of attack till the vortex break down takes place. Tiggelbeck et al. (1992) use multiple rows of vortex generators in an aligned arrangement within a channel and observe their influence on flow structure. The flow structure in the wake of the second row is qualitatively similar to that of the first row. Their flow visualization by a laser light sheet technique has revealed that the concentrated vortex pair generated by a small aspect ratio delta wing at large angle of attack has elliptic shape due to the influence of channel walls. They also observe that the peak value of spanwise-averaged Nusselt number at the wake of the second row is strongly dependent on the spacing of the two rows.

Computational studies on related topics have been performed by Fiebig et al. (1989) and Biswas and Chattopadhyay (1992) for laminar flows in a geometrical configuration of delta wing placed inside a channel. Both studies have discussed the influence of angle of attack and Reynolds number on velocity and temperature fields.

When the flow velocity is not very high and the temperature difference between the body surface and ambient fluid is large, flow and heat transfer characteristics are strongly influenced by thermal buoyancy forces. Even without a vortex generator, buoyancy can induce longitudinal vortices and multiple plumes which can enhance heat transfer and alter the length of entrance region in mixed convection flows in ducts (Patankar et al., 1978; Incropera and Schutt, 1985; Incropera et al., 1987). Biswas et al. (1989) characterize the mixed-convection condition by buoyancy driven secondary flows that form counter rotating longitudinal vortices and enhance heat transfer. In another study, Biswas et al. (1990) observe that the critical Reynolds number in a channel flow with built-in obstacle may be lower in the case of mixed convection than in the case of forced convection alone. It is observed that for a given Reynolds number, the heat transfer is improved up to a certain Grashof number and deteriorates if the Grashof number is further increased. Nandakumar et al. (1985) have obtained dual solutions for the case of a duct flow. In one solution a two vortex pattern emerges while in the other solution a four vortex pattern evolves.

It has already been discussed that the gas side heat transfer coefficient in gas-liquid fin-tube crossflow heat exchangers is small as compared to that of the liquid side. The mechanism of heat transfer between the gas and the solid surfaces in such cases is to be understood in detail. Let us consider only one tube on a plate-fin (Fig. 2.4). The flow

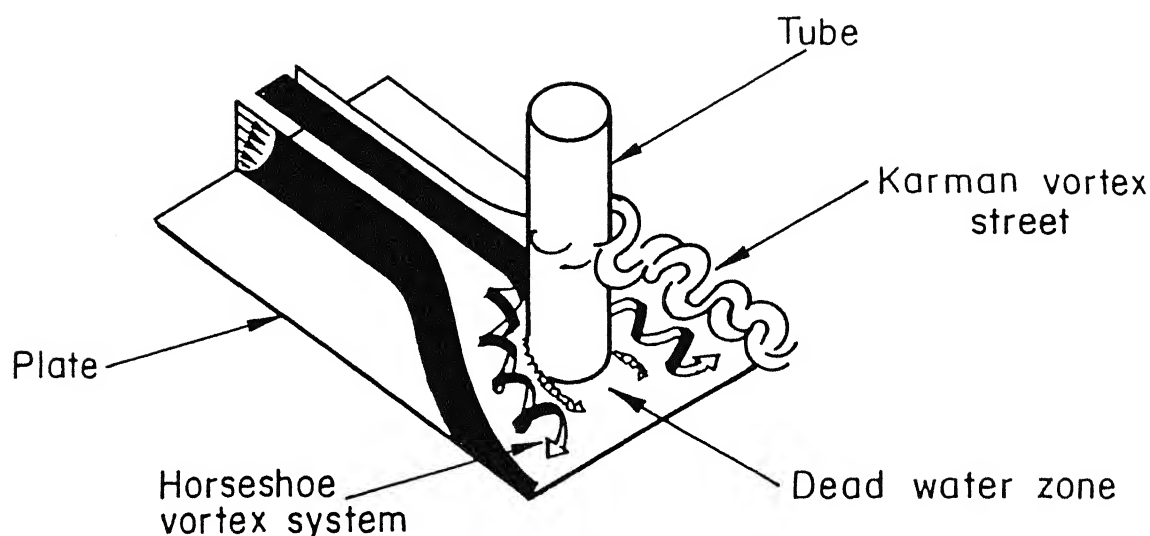


Figure 2.4: Flow around a tube on a plate

field consists of a horseshoe vortex system, a dead water zone at the juncture of the tube and the plate and a von-Karman vortex street in the middle. In order to enhance heat transfer in such a flow configuration, vortex generators can be mounted on the plates which makes the flow field extremely complicated. Recently, Dong (1989) and Valencia (1992) have conducted experimental investigations to observe the influence of winglet-type vortex generators in a channel with a built-in circular tube. Sanchez et al. (1989) have computed laminar flows around a circular cylinder in a rectangular channel with a pair of delta winglets on the bottom plate of the channel. Their results show that the longitudinal vortices generated by the winglets placed in the wake, control the spread of the wake zone behind the cylinder and damp the periodic vortex street. Biswas et al. (1994) have observed that in the absence of the winglet-type vortex generators, relatively little heat transfer takes place in the downstream of the circular tube which is a recirculation region with low velocity fluid. However, they observe an enhancement of heat transfer as high as 240 percent in the wake region behind the cylinder in presence of winglet-type longitudinal vortex generators.

Recently, computational studies have been extended to periodic configurations which are realistic in terms of plate-fin heat exchangers with perforated fins or slotted channels. Heat transfer surfaces periodically interrupted along the streamwise direction have been widely used in order to obtain improved performance of the heat-exchange devices. Such an arrangement may be viewed as a succession of collinear plate-segments aligned parallel to the flow with slots between successive plates. Each slot enables the interruption of the thermal boundary layer where the highest resistance to the heat flux occurs and a new boundary layer with lower thermal resistance begins. It also allows

a very good mixing of the flow with self-sustained oscillation when the system is operating above the critical conditions (Reynolds number). The channels which have such operating conditions have been classified as communicating channels. As it has been told, above a critical value of the Reynolds number (much within the laminar regime), the initially steady flow becomes unstable to small disturbances. At this instant, the flow is set to have undergone a bifurcation from steady state to a time periodic, self-sustaining oscillatory regime. These flows are characterized by supercritical bifurcation and narrow band excitation (Ghaddar et al., 1986a; Ghaddar et al., 1986b; Amon and Patera, 1989). Appreciable transport augmentation takes place in this range of Reynolds number (Majumdar and Amon, 1992).

Webb and Ramadhyani (1985) have analyzed fluid flow and heat transfer characteristics through a parallel plate channel with transverse ribs which act as vortex generators. Significant heat transfer augmentation is obtained in their study for fluids such as water or fluorocarbons. Acharya et al. (1991) explain vortex interaction between two such ribs in a channel for the subharmonic excitation of shear layer. In a similar study, significant augmentation is obtained by positioning vortex generators at key locations in the flow (Myrum et al., 1992).

Many researchers have observed longitudinal vortices in various complex flow configurations. Naturally, the interaction of such vortices with boundary layer and its effect on heat transfer is a subject of interest to them. Some examples are Taylor-Görtler vortices in boundary layers on concave curved surfaces, horseshoe vortices formed by an obstruction protruding from a surface and wingtip vortices impinging on a downstream surface. The embedded vortex is capable of strongly perturbing the boundary layer thickness and influencing the heat transfer characteristics. In addition, longitudinal vortices usually maintain their coherence over a long streamwise distance. As a consequence, the heat transfer effects behind a vortex generator are very persistent. Eibeck and Eaton (1987), Westphal and Mehta (1987) have worked extensively in this field with more focus to the turbulent boundary layer. Eibeck and Eaton (1987) have conducted experiments on longitudinal vortices embedded in a turbulent boundary layer and resultant heat transfer effects. Longitudinal vortices are found to influence the heat transfer behaviour significantly. Local Stanton number is increased by as much as 24 percent resulting in a net increase in spanwise average heat transfer coefficient. Despite the presence of turbulent diffusion, the influence of longitudinal vortices on momentum and energy transport can be traced at a location as far downstream as 60 wing chords behind the delta wing.

Westphal and Mehta (1987) have studied the effect of oscillating vortex on a turbulent boundary layer. The meander is simulated by forcing a periodic lateral translation of a half-delta wing vortex generator at a low frequency of 1 Hz and one-half amplitude of 0.5 cm. The effect of the meander is found to flatten the vorticity contours at the stations where they are originally round. The Reynolds stresses are also found to be significantly affected. Ligrani et al. (1991) have presented results that illustrate the

effects of embedded longitudinal vortices on heat transfer and also the effect of injecting a fluid downstream of a row of film-cooling holes in a turbulent boundary layer. In some circumstances, the protection provided by film cooling is augmented because of secondary flows, which cause extra injectant to accumulate near upwash regions.

2.3 Development of Numerical Methods for Solving Full Navier-Stokes Equations

2.3.1 Methods Developed on Regular Geometries

Different solution techniques for full Navier-Stokes equations have been developed during the past three decades. As it has been seen, the major difficulty encountered during the solution of incompressible flows is the non-availability of any obvious equation for pressure. This difficulty can be resolved in the stream function-vorticity approach. But the stream function-vorticity approach loses its attractiveness when three-dimensional flow is computed because of the absence of a single scalar stream function in the three-dimensional space. A three dimensional problem demands a primitive-variable approach. Efforts have been made so that two-dimensional as well as three-dimensional problems could be computed following a primitive variable approach without encountering non-physical wiggles in pressure distribution. As a remedy, it has been suggested to employ a different grid for each-dependent variable. Harlow and Welch (1965) have used such a staggered grid for the dependent variables in their well known MAC (Marker and Cell) method. The MAC method of Harlow and Welch is one of the earliest and widely used explicit methods for solving full Navier-Stokes equations. In this method, solutions of velocities are obtained in two folds. In the first fold, provisional value of velocity components are computed explicitly using advection, diffusion and pressure gradients of the earlier time step. This explicitly advanced provisional velocity field may not ensure a divergence free velocity field. In the subsequent second fold, pressure and velocity components are corrected through the solution of a Poisson equation for pressure. A related technique developed by Chorin (1967) involves a simultaneous iteration on pressures and velocity components. Vicelli (1971) has shown that the two methods as applied to the MAC method are equivalent. The original version of the MAC method has been modified by Harlow and Amsden (1970), Nichols and Hirt (1971) and Hirt and Cook (1972) for application to free surface flows. The MAC method uses a layer of imaginary cells around the boundary of the physical domain necessitate updating of boundary conditions after every change in internal velocity and pressure values. The MAC method has been extensively used by many researchers to solve flow in complex geometry. For example, Braza, Chassaing and Ha-Minh (1986) have obtained the unsteady wake behind circular cylinder. Mukhopadhyay, Biswas and Sundararajan (1993) have obtained the periodic wake behind a rectangular obstacle. In fact, the MAC method has been

successfully used even to simulate highly unsteady turbulent flows (Robichaux, Tafti and Vanka, 1992). It has been experienced that the MAC method is indeed very efficient in the studies of temporal flow development but it has stability restrictions on the time step values which slow down the calculations for steady flow considerably. Since implicit methods have no such restrictions, they are obviously very attractive. Patankar and Spalding (1972) have introduced an efficient implicit method known as SIMPLE (Semi-Implicit Method for Pressure Linked Equations). This method is based on a finite volume discretization of the governing equations on a staggered grid. In order to improve the convergence involved in the pressure-velocity coupling, several variants of SIMPLE algorithm have been developed. The SIMPLER algorithm of Patankar (1981) and the SIMPLEC algorithm of van Doormaal and Raithby (1984) may be referred to with regard to such improvement on SIMPLE algorithm. Although, the necessary changes to incorporate SIMPLEC into a SIMPLE algorithm is minor, the consequences can be great as it eliminates the approximations made in SIMPLE while deriving the pressure-velocity corrections. A comparative illustration between the operator splitting algorithm, viz., the PISO of Issa (1986) and the SIMPLE family of algorithm has been reported by Jang, Jetli and Acharya (1986).

2.3.2 Methods on Complex Geometries

In regular geometry, the orthogonality of the coordinate frame makes it possible to decouple the integrands so as to carry out individual line integration products for evaluating the surface integrals. Thus, many researchers have tried to generate orthogonal grids for complex solution domains while considerable effort has also been directed towards solving the equations on general non-orthogonal curvilinear grids.

In order to extend the aforesaid established flow solvers to the complex geometries, generalized orthogonal body-conforming coordinate systems have been used in different combinations. Pope (1978) has applied the conservative forms of the equations with finite volume method to compute turbulent recirculating flows in diffusers. Gosman and Rapley (1980) have used a similar procedure for fully developed flows in ducts of arbitrary cross-section. Lawal and Mujumdar (1985) have performed calculations in the entrance region of an arbitrary shaped cross section. In this case, collocated cartesian velocity components on orthogonal grids in each cross-sectional plane have been solved along with a Poisson equation for pressure. Garg and Maji (1987) have applied SIMPLEC method for the solution of viscous flows through periodically converging-diverging tubes. In another numerical investigation, Velusamy and Garg (1993) have solved the complete set of Navier-Stokes equations for the three-dimensional developing flow in elliptical cross-section ducts.

In non-orthogonal systems, general curvilinear coordinates are employed which exactly coincide with the boundaries of the physical domain. The governing partial differential equations are transformed in terms of these curvilinear coordinates and finite dif-

ference representations are derived in the transformed domain. Gal-chen and Somerville (1975) and Faghri et al. (1984) have used algebraic coordinate transformation. While the former use a MAC-like grid arrangement coinciding with the grid lines, latter used covariant components of velocities. Thompson et al. (1982) have made remarkable contributions to the development of numerical grid generation techniques for solving elliptic partial differential equations related to both external and internal flow problems. Vanka et al. (1980), Maliska and Raithby (1984) and Shyy et al. (1985) have extended the available solvers of different flow problems to irregular geometries. The basic flow solvers have been based on the SIMPLE algorithm. The adaptive grid procedure of Acharya and Patankar (1985) for parabolic flows may be mentioned here for its detailed discussion on the choice of different discretization schemes and their performance in the adaptive grid layout. However, application of finite volume methods using non-orthogonal coordinates and collocated grids are reported by Rhie and Chow (1983) and Peric (1985). Peric et al. (1988) have shown that the collocated arrangement converges faster than the staggered variable arrangement and has advantages when extensions such as multigrid techniques and non-orthogonal grids are considered. It may be worthwhile to note from Benard and Thompson (1984) that while staggered grid is a direct solution to avoid pressure split with conventional finite difference interpolations of flow variables, proper interpolation of velocities still remains crucial to avoid oscillatory velocity field even on a staggered grid. An appropriate pressure interpolation avoids pressure splits in these methods of collocated grids. A finite volume based procedure has been very successfully developed by Majumdar et al. (1992) using such collocated velocities and pressure. The concept of "momentum interpolation" of cell face pressures from nodal values has been established showing equivalence in the methods of staggered and collocated arrangements. Mukhopadhyay et al. (1993) have developed a numerical method for predicting viscous flows in complex geometries. Integral mass and momentum conservation equations are deployed and these are discretized into algebraic form through numerical quadrature. The physical domain is divided into a number of non-orthogonal control volumes which are isoparametrically mapped on to standard rectangular cells. Numerical integration for unsteady momentum equations is performed over such non-orthogonal cells. The algorithm is tested on some complex problems. The results exhibit good accuracy and justify the applicability of the algorithm.

2.3.3 Modelling of Convection-Diffusion Equations

During the development of flow solvers, emphasis is given to efficient handling of non-linear convection terms in the flow equations. As such entire treatment of convection-diffusion equations is somewhat tricky due to the presence of the first-order nonlinear spatial derivatives that describe the convective flux. Especially, in the case of transient equations, the interaction between space and time dependence in the convection-diffusion equation requires that the temporal and spatial derivatives be accurately ap-

proximated in order to obtain a satisfactory solution. Solutions based on conventional finite difference or finite element spatial discretizations suffer from spurious oscillations due to space-centered discretization of the convective terms. The possible improvement is to use a first-order upwinding technique. However, the first-order upwind schemes introduce significant amount of artificial (numerical) diffusion into the physical problem. Roache (1972), Roberts and Wiess (1966) and Bozeman and Dalton (1973) have criticized the idea of introducing this "artificial viscosity" into the physical problem through upwind schemes which are first-order accurate. Roache (1972) has estimated the amount of false diffusion due to such schemes and proved that its contribution may be too high to be ignored. Spalding (1972) and Cristie (1976) have presented a local analytical solution of convection-diffusion equations which is superior to central differencing schemes, when the local Peclet number of the grid is large. Leonard (1979) has developed a second-order upwinding scheme, known as Quadratic Upstream Interpolation for Convective Kinematics (QUICK) in order to avoid the stability problems of central differencing. However, this second-order upwinding involves a dispersive third-derivative in the truncation error. Raithby (1976) has introduced two schemes, namely, Skew Upstream Differencing Scheme (SUDS) and Skew Upstream Weighted Difference Scheme (SUWDS) to reduce the error, brought about in the flow region when the grid line and velocity directions are not aligned. These schemes are capable of reducing the disadvantages of upstream differencing. A simple stable mass-flow-weighted skew upwind scheme has been proposed by Hassan et al. (1983). Leonard (1984) has shown that the third-order upwinding provides a robust discretization procedure in the modeling of convection-diffusion terms of Navier Stokes equations. Runchal (1987) has modified central difference scheme by introducing a controlled amount of numerical diffusion based on local gradients. This proposed technique for Controlled Numerical Diffusion with Internal Feedback (CONDIF) eliminates the undesirable feature of the space-centered schemes. Shirayama (1992) has constructed the modified third-order upwinding schemes for stretched meshes using Lagrangian interpolation formula. This method prevents numerical instability, preserves third-order accuracy and produces realistic results. Although upwind differencing scheme has its dissipative nature, it is probably the best choice for high Reynolds number ($Re > 1000$) flows. Patankar (1980) has mentioned about various approximative schemes, namely, upwind, hybrid, exponential and power-law schemes and discussed on their relative merits and demerits. Galpin and Raithby (1986) have linearized the nonlinear convective terms by Newton-Raphson linearization method and found that such a linearization enhances convergence, especially when grid curvature effects are important. Pollard and Siu (1982) and Thakur and Shyy (1993) have successfully used upwind, hybrid and QUICK schemes in computation of complex flows. Tamamidis et al. (1993) have made use of hybrid, third-order, QUICK and fifth-order upwind schemes for modeling turbulent flows using SIMPLEC algorithm. The results show that accurate solutions can be efficiently obtained on grids of moderate size by using high-order-accuracy schemes.

It is clear that substantial progress has been made on development of higher order schemes which are suitable over a large range of velocities. However, none of the prescriptions is universal. Depending on the nature of flow and geometry etc., one can always go for the best suited discretization procedure (see Vanka, 1987; Fletcher, 1988). It is also very difficult to be conclusive about any algorithm with its universal sense of applicability. In a recent investigation, Kim and Benson (1992) have compared three well known algorithms for modeling unsteady flows. They have concluded that a modified version of MAC algorithm (Harlow and Amsden, 1970; Braza et al., 1986) is highly accurate and has some specific advantages on other schemes. However, the variants of MAC algorithm are not without problems of their own. Although, these variants have all usual disadvantages of the explicit methods, we prefer to use the MAC method because of the following advantages : it does not need boundary conditions for pressure, it can describe unsteady flows well, it is robust and uses primitive variable which are preferable in 3-D flow calculations.

2.4 A Review on Turbulence Modelling

2.4.1 General

Any flow whether laminar or turbulent, is fully represented by the Navier Stokes equations. The Navier Stokes equations can be solved on a fine enough grid with an exceptionally accurate discretization method so that both the fine scale and large scale aspects of turbulence can be calculated. This is termed as the Direct Numerical Simulation (DNS) of turbulence (Rai and Moin, 1991). The modeling effort and simplifications that are employed in the study of turbulence are the consequences of the difficulty encountered in solving the full Navier Stokes equations on a fine grid. In numerical solutions, where DNS of turbulence is performed, the mesh spacings and the time steps need to be significantly less than those over which appreciable variation of velocity occurs, otherwise details of the evolution will not be correctly reproduced by the numerical prediction. The length-scale-range of the eddies of varying sizes (smallest eddies of the order of mm's in the domain where the mean velocity is not much greater than 100 m/s) and the time-scale-range of the velocity fluctuations due to the eddy-ing motion cannot be economically resolved by ordinary discretization methods. This difficulty is circumvented through turbulence modeling.

2.4.2 Various Approaches for Modelling Turbulent Flows

Launder and Spalding (1972) describe the modeling approaches for turbulent flows comprehensively. The basis of turbulence modeling is to decompose the high frequency fluctuating instantaneous velocity of the fluid into a mean and a fluctuating component, and solving for the mean velocities, while the effect of the fluctuating components on

the mean motion is modeled after empirical relations obtained for specific cases from experiments. The Navier Stokes equations together with the equation of mass conservation form a closed system of equations. When the velocity components are decomposed we have more unknowns than number of available equations. The modified system of equations cannot be closed within itself unless empirical relations are supplied from experiments to correlate the fluctuating components with the mean motion. This is termed as the closure problem.

The averaging of the equations to get the mean components can be done in various ways (see Hinze, 1987). The time averaging is suitable for the flows in which mean flow would be stationary or slowly varying in time. The ensemble averaging is basically a statistical concept which signifies the same meaning as time averaging for stationary flows, but is somewhat more meaningful for transient mean flows. A third alternative is the space averaging. The first two methods have been well tested and established while the third is used in a technique known as Large Eddy Simulation. The Large Eddy Simulation (LES) is another emerging area of turbulent research (see Schumann, 1975; Schmidt and Schumann, 1989; Robichaux, Tafti and Vanka, 1992). In LES, large scale motions are calculated from DNS and subgrid scales are modeled. The most important aspect of this method is spatial filtering of the flow quantities i.e., decomposing the variables into resolvable and subgrid components before analysis. The interpretation of the results in physical terms is also quite tricky and complicated.

The time averaged equations of motion completely resemble the original transport equations, except that they have a few additional terms containing the contribution of the fluctuating components of velocities to the transport mechanism. These terms are same for time average and ensemble average for stationary and homogeneous turbulence and the assumption is known as ergodic hypothesis. Since turbulence is considered as eddying motion and the aforesaid additional terms are added to the viscous stresses due to mean motion in order to explain the complete stress field, these terms are called turbulence stresses or Reynolds stresses named after Osborne Reynolds. Space averaging culminates into a few more additional terms besides the Reynolds stress terms.

Ferziger (1987) discusses in detail various alternative approaches to turbulence modeling and explains the relative merits and demerits of these approaches. It is observed that many of the widely used models are based upon the eddy viscosity concept of Boussinesq. The most important effect of turbulence on mean flow is that it absorbs kinetic energy from the mean flow and increases the rate of transport of mass, momentum and energy in the direction normal to the streamlines of the flow. As both of these effects are mediated by the viscosity in laminar flows, it is natural to assume that the effects of turbulence on the mean flow can be represented as an increased viscosity. This helps in expressing the turbulent stress as

$$-\rho \overline{u'_i u'_j} = \mu_t \left(\frac{\partial \overline{u_i}}{\partial x_j} + \frac{\partial \overline{u_j}}{\partial x_i} \right) - \frac{2}{3} \rho k \delta_{i,j}$$

where μ_t is called eddy viscosity and is attributed to random fluctuations of turbulent motion, k is the turbulent kinetic energy of turbulence and $\delta_{i,j}$ is the Kronecker delta.

The eddy viscosity models are indeed popular, although they are criticized for assuming the turbulent eddy action to be isotropic by associating it to a viscosity. However, in order to determine the eddy viscosity, Prandtl proposed a mixing length hypothesis by analogy of eddy activity to molecular interaction (Schlichting, 1987). Thus, a need was felt for determination of a characteristic length and a velocity scale to define the eddy viscosity completely. The various models described in turbulent flow literature based on the eddy viscosity concept, necessarily attempt at determining a suitable velocity scale and a length scale to calculate μ_t .

The kinetic energy of fluctuating velocity components which defines the amount of energy available for eddy action is proposed to be a good representative of turbulent velocity scale. The first step beyond the mixing length is such a model in which the transport equation for the above mentioned kinetic energy is derived. The length scale of eddies is continued to be derived algebraically. Such models are called as one equation models.

The rate of dissipation of the turbulent kinetic energy (ϵ) is subsequently proposed to represent the length scale of turbulence and the well known Prandtl-Kolmogorov relation is obtained as $\mu_t = \rho C_\mu k^2 / \epsilon$. This gave rise to a family of two equation models (Rodi and Spalding, 1970; Jones and Launder, 1972; Launder and Spalding, 1974) where the equation for turbulent kinetic energy determines the velocity scale. This equation can be derived from Navier Stokes equations by subtracting the mean equation from the unaveraged equations to obtain an equation for the fluctuating velocity. Taking the scalar product of this equation with the fluctuating velocity and averaging yields the equation for the turbulent kinetic energy. An equation for the dissipation can be derived from a Navier Stokes equation by an extension of the method used to derive the energy equation. The two equation models are quite successful and have become very popular. With only little modification, they are able to simulate a large variety of flows with reasonably good degree of accuracy. A comprehensive review of different kind of two equation models is available in open literature (Nallasamy, 1987). The equations derived in the above mentioned way apply to fully developed turbulence.

The laminar region near a wall is handled by wall function treatment. In standard wall function approach (Launder and Spalding, 1974), the wall shear stress is related to the values of average velocity, kinetic energy and the distance outside the viscous layer using the generalized logarithmic law. This wall function approach, by not requiring the integration up to the wall, has a very beneficial effect on the economy of a calculation procedure. The viscous sublayer need not be integrated and therefore, a coarse grid can be used for calculation purpose, making it computationally economical.

Although the thickness of the viscous zone is usually two or more orders of magnitude smaller than the overall width of the flow, its effects extend over the whole flow field

since nearly 50 percent of the velocity change from the wall to the freestream occurs in this region. Amano (1984) suggests a model where the near-wall region is divided into two distinct parts, a viscous sublayer region ($0 < Y^+ < 11$) and an overlap layer ($11 < Y^+ < 400$). In the viscous sublayer region, kinetic energy shows parabolic variation with Y^+ and in the overlap region it increases linearly. Amano (1984) proposes a three-layer model for the near-wall region that consists of a viscous sublayer ($0 < Y^+ < 5$), a buffer layer ($5 < Y^+ < 30$) and an overlap layer ($30 < Y^+ < 400$). The behaviour of the turbulent kinetic energy, k and turbulent shear stress are proposed in the viscous sublayer and the buffer layer. Bakewell and Lumley (1967) suggest that within the viscous sublayer the streamwise fluctuating velocity increases linearly with the distance from the wall, y and increases approximately as $y^{0.5}$ in the buffer layer. The suggestions of Bakewell and Lumley are implemented in the near-wall three-layer model of Amano (1984).

Though the wall function approach is an economical method from the point of view of computer resources, the areas of steep gradients in the viscous sublayer are not resolved properly if the first point on the grid is placed away from the wall outside the viscous sublayer ($Y^+ > 11.63$). The wall functions relating to the velocity and turbulent quantities at the first grid point depend heavily on the assumption of a logarithmic velocity distribution and of local equilibrium of turbulence. These assumptions are not valid for separated flows and if there is a secondary flow extending into the sublayer. Therefore, considerable effort has gone into developing models that simulate the effect of viscosity and other turbulent quantities near the wall. Jones and Launder (1973) have extended the $k - \epsilon$ model to the low Reynolds number form which allows a calculation right to the wall. Since viscous diffusion of k and ϵ are of the same order of magnitude as the turbulence diffusion in the near wall region, the molecular viscosity is also included in the respective diffusion terms in different directions. A function f_μ is introduced in the eddy viscosity equation to mimic the direct effect of molecular viscosity on the shear stress and the eddy viscosity is given by, $\mu_t = f_\mu C_\mu \rho k^2 / \epsilon$. The function f_μ is so chosen that it damps down from unity in the fully turbulent layer to zero at the wall. In all the models, f_μ is assumed to be a van Driest type of experimental damping function of local Reynolds number of turbulence ($R_t = k^2 / \epsilon \nu_t$) and a similar independent variable ($R_k = k^{1/2} y / \nu_t$). Another function f_1 is introduced in the production term of the $k - \epsilon$ equations in order to increase the magnitude of ϵ near the wall to account for the additional dissipation. In addition to these, a function f_2 is used in the destruction term of ϵ equation to indicate the low Reynolds number effects on the decay of isotropic turbulence. All these concepts are simplified and implemented in a somewhat more convenient way by Lam and Bremhorst (1981). From the evaluation of DNS data for channel flow a new model has been proposed by Rodi and Mansour (1993) which simulates the net effect of production terms and consequential increase in destruction term of the $k - \epsilon$ model near the wall more accurately.

An isotropic eddy viscosity model gives equal turbulent intensities in all directions.

The drawback of assuming isotropy is overcome by using Reynolds stress model. The Reynolds stresses are evaluated from exact transport equation for $\overline{u_i' u_j'}$ which may be obtained by taking a velocity-weighted moment of the Navier Stokes equation and averaging. This will result in six partial differential equations. Many of the terms of this equation are not directly determinable and must be modeled. It is beyond the scope of the present study to give a comprehensive review on methods for closing the additional equations. But the contributions from Launder et al. (1975), Gibson and Launder (1978), Hogg and Leschziner (1989a, 1989b) indicate the successful implementation of this concept. However, it seems that the Reynolds stress model is not without problems of its own. On the deficit side, Reynolds stress model continues to be a computationally intensive option even on extremely powerful computers.

An Algebraic Stress Model is proposed by Rodi (1976, 1984) which predicts anisotropy without requiring the solution of differential equations for these stress components. This approach begins with the exact transport equations for Reynolds stresses. Subsequently, it assumes isotropic dissipation, a modeled pressure strain term, and that transport of $\overline{u_i' u_j'}$ is proportional to the transport of k . Using these assumptions, the partial differential equations for the Reynolds stresses are reduced to a system of algebraic equations at each point in the flow. Equations for the turbulent kinetic energy and dissipation rate are written. So, finally six algebraic equations are solved together with the $k - \epsilon$ equations. This model has considerable appeal and will keep on improving. It may be mentioned that the time scale for the Algebraic Stress Model is the same as other $k - \epsilon$ models (k/ϵ).

The commonly used $k - \epsilon$ models of turbulence are thought to be incapable of accurately predicting turbulent flows where the normal Reynolds stresses play an important role (mean velocity has a gradient). Speziale (1987) has developed non-linear $k - \epsilon$ model by adding a non-linear term to the linear Boussinesq approximation for the stress used in the standard $k - \epsilon$ model. However, his non-linear model shows improvement both in the prediction of turbulent stresses and in the mean flow field. Speziale has also developed non-linear model equations to account for the anisotropic behaviour of the turbulent stresses without disturbing the tensorially invariant eddy viscosity structure of the two equation model. The model adds second order derivatives to the Boussinesq approximation of the turbulent stresses in the momentum equations. Dutta and Acharya (1993) extend Speziale's non-linear model to heat transfer studies. The modified $k - \epsilon$ model (Leschziner and Rodi, 1981) is another significant improvement on the standard $k - \epsilon$ model by incorporating the effects of streamwise curvature. The improvement of the velocity related terms is expected to improve heat transfer. Therefore, it can be argued that the curvature effect should also be incorporated in the expression for the turbulent Prandtl number which in turn may bring about a change in the rate of the heat transfer. Dutta and Acharya show that the heat transfer prediction of the non-linear $k - \epsilon$ model is found to be similar to that of the standard $k - \epsilon$ model. However, heat transfer predictions of Dutta and Acharya with the modified $k - \epsilon$ model agree

excellently with the experimental data of Aung and Goldstein (1972).

As can be seen from the cited literature on turbulence modeling, no generalized turbulence model has yet been devised which can be applied through a modest computation effort. For turbulence models, comparison with experimental data is the only way to assess the accuracy and applicability of a model for a specific physical problem. Recently, Zhu, Fiebig and Mitra (1993) have computed a three dimensional turbulent flow with longitudinal vortices embedded in the boundary layer on a channel wall. They use standard $k - \epsilon$ model for their simulation. Although the behaviour of $k - \epsilon$ model is not known for such highly vortical flows, the comparison between the measurements of Pauley and Eaton (1988 a,b) and the computed results of Zhu, Fiebig and Mitra shows that the interaction of the longitudinal vortices with the boundary layer within a turbulent channel flow is captured quite correctly by the numerical simulation.

It is envisaged that the $k - \epsilon$ model with some modifications in the wall function treatment will be able to predict our flow field which is also dictated by the longitudinal vortex induced swirling motion. For the validation of the model we also propose to compare our results with the experimental data of Pauley and Eaton (1988 a,b).

2.5 Remarks

The present state of art of enhanced surfaces with respect to the augmentation of heat transfer has been outlined in the section 2.2 of this survey. The prediction of the details of the flow field over such enhanced surfaces and to determine the influence of different geometrical parameters on the flow and temperature fields by numerical solution of governing conservation equations are the essential goals of this study. Such prediction methods have been under development over more than two decades now. In section 2.3 of the present chapter we have discussed the salient features of predictive procedures. The section 2.4 gives an account of various modeling techniques for resolving the issues related to turbulent flows. Apart from the references cited in the earlier sections, there is a host of other articles which will be discussed in the subsequent chapters together with the analyses presented therein.

Chapter 3

Mathematical Formulation

3.1 Introduction

Arising out of the practical and academic importance of the flow configuration and thermal conditions as described in the previous chapters, a need is felt to compute three-dimensional laminar and turbulent flows in a horizontal channel with built-in wing-type obstacles. For detailed investigations, only one delta wing or a winglet-pair inside a horizontal channel has been considered (Fig. 3.1). The numerical simulation enables us to obtain a quantitative information on flow structure and heat transfer in the entire domain, with their dependence on the various governing parameters.

3.2 Statement of the Problem

As it has been stated above, computation is performed in a channel which is formed by two neighboring fins (Fig. 3.1). An obstacle in the form of a delta wing or winglet-pair (of zero thickness) is placed inside the channel. The base of the wing is fixed on the bottom wall and the apex faces the incoming flow stream at an angle of attack. In the case of winglet-pair, one side of each is fixed on the bottom wall and the trailing edge of each is free. Since symmetry prevails in the central vertical plane of the channel, the flow field in only half of the channel is computed. In the present study, the numerical simulations deal with two different regimes of flow, *viz.*, laminar and turbulent. In the subsequent sections, the governing conservation equations for laminar and turbulent flows and the appropriate boundary conditions will be discussed.

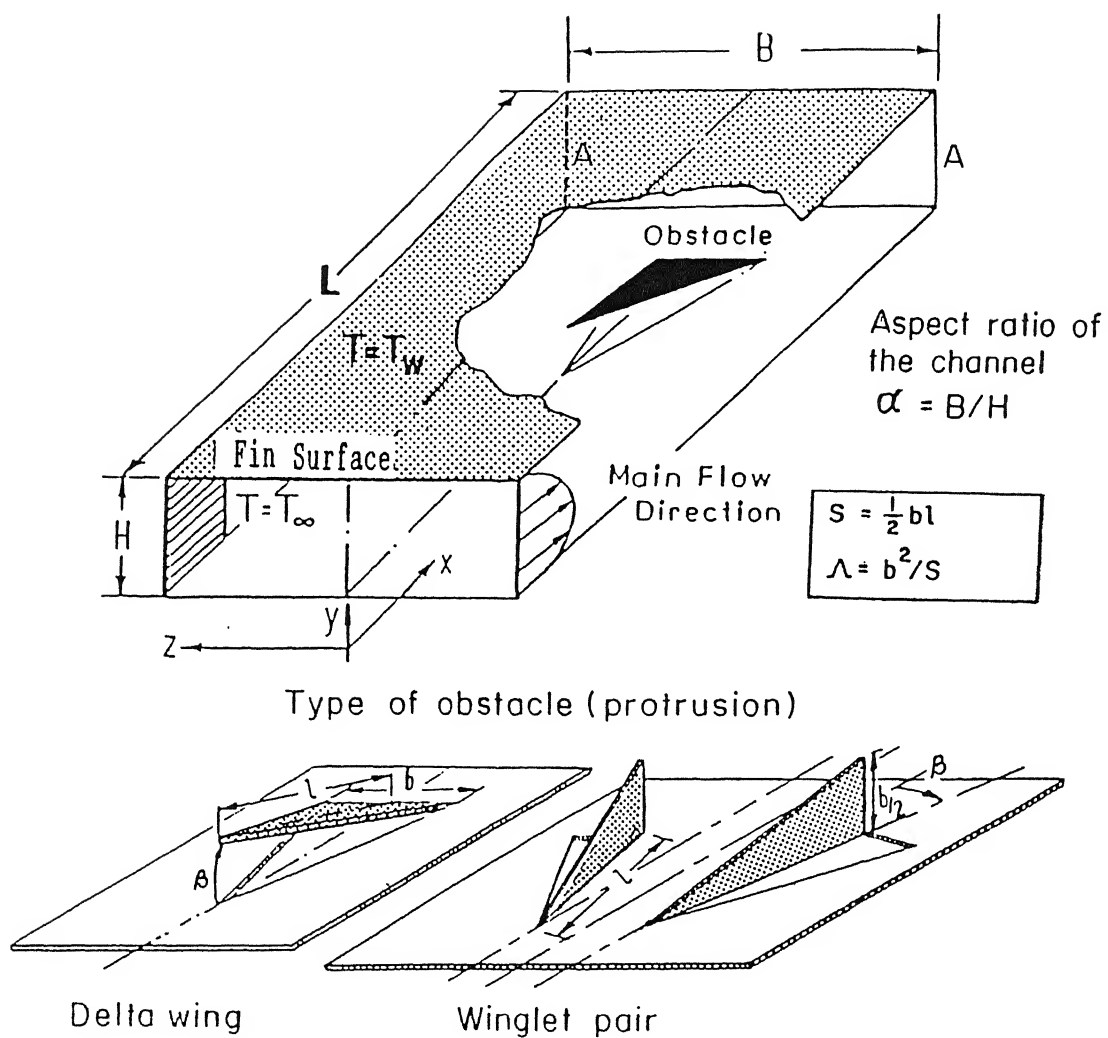


Figure 3.1: Flow model for computation

3.2.1 Governing Equations for Laminar Flow

The dimensionless equations for continuity, momentum and energy for laminar incompressible flow may be expressed in their conservative forms as following :

$$D \equiv \frac{\partial U}{\partial X} + \frac{\partial V}{\partial Y} + \frac{\partial W}{\partial Z} = 0 \quad (3.1)$$

$$\frac{\partial U}{\partial \tau} + \frac{\partial U^2}{\partial X} + \frac{\partial UV}{\partial Y} + \frac{\partial UW}{\partial Z} = -\frac{\partial P}{\partial X} + \frac{\nabla^2 U}{Re} \quad (3.2)$$

$$\frac{\partial V}{\partial \tau} + \frac{\partial UV}{\partial X} + \frac{\partial V^2}{\partial Y} + \frac{\partial VW}{\partial Z} = -\frac{\partial P}{\partial Y} + \frac{\nabla^2 V}{Re} \quad (3.3)$$

$$\frac{\partial W}{\partial \tau} + \frac{\partial UW}{\partial X} + \frac{\partial VW}{\partial Y} + \frac{\partial W^2}{\partial Z} = -\frac{\partial P}{\partial Z} + \frac{\nabla^2 W}{Re} \quad (3.4)$$

$$\frac{\partial \theta}{\partial \tau} + \frac{\partial U\theta}{\partial X} + \frac{\partial V\theta}{\partial Y} + \frac{\partial W\theta}{\partial Z} = \frac{\nabla^2 \theta}{Re.Pr} \quad (3.5)$$

In the above equations, velocities have been nondimensionalized with the average incoming velocity U_{av} at the channel inlet, all lengths with the channel height H , the pressure with ρU_{av}^2 and the nondimensional temperature is defined as $\theta = (T - T_\infty)/(T_w - T_\infty)$. The Reynolds number and Prandtl number are defined by Re and Pr respectively.

3.2.2 Boundary Conditions for Laminar Flow

The boundary conditions of interest in this investigation are (refer to Fig. 3.1):

- Top and bottom plates:

$$U = V = W = 0; \quad \theta = 1 \quad (3.6)$$

- Side wall ($z = B/2$) and midplane ($z = 0$):

$$W = \left(\frac{\partial V}{\partial Z} \right) = \left(\frac{\partial U}{\partial Z} \right) = 0; \quad \left(\frac{\partial \theta}{\partial Z} \right) = 0 \quad (3.7)$$

- At the channel inlet:

$$U = U(Y), \quad V = W = 0; \quad \theta = 0 \quad (3.8)$$

- At the exit, a smooth transition through the outflow boundary is ensured by setting:

$$\frac{\partial^2 U}{\partial X^2} = \frac{\partial^2 V}{\partial X^2} = \frac{\partial^2 W}{\partial X^2} = 0; \quad \frac{\partial^2 \theta}{\partial X^2} = 0 \quad (3.9)$$

No-slip boundary conditions for the velocities on the obstacles are used. The details of kinematic boundary condition on the surface of the vortex-generators will be discussed in a subsequent chapter. The temperature of the obstacle is considered constant and equal to T_w .

3.2.3 Governing Equations for Turbulent Flow

The time averaged Navier Stokes equations for turbulent incompressibl flow where the Reynolds stresses are expressed via the eddy-viscosity concept have been used as governing equations. These equations are written in a Cartesian tensor form as

$$\frac{\partial \bar{U}_j}{\partial X_j} = 0 \quad (3.10)$$

$$\frac{D\bar{U}_j}{Dt} = -\frac{\partial(P + 2k_n/3)}{\partial X_j} + \frac{1}{Re} \frac{\partial}{\partial X_i} \left[(1 + \nu_{t,n}) \left(\frac{\partial \bar{U}_i}{\partial X_j} + \frac{\partial \bar{U}_j}{\partial X_i} \right) \right] \quad (3.11)$$

$$\frac{D\bar{\theta}}{Dt} = \frac{1}{RePr} \frac{\partial}{\partial X_i} \left[(1 + \alpha_{t,n}) \frac{\partial \bar{\theta}}{\partial X_i} \right] \quad (3.12)$$

where \bar{U}_j and $\bar{\theta}$ are nondimensional time-mean velocity components and temperature, $\nu_{t,n}$ is the nondimensional kinematic viscosity, $\alpha_{t,n}$ is the nondimensional eddy diffusivity and k_n is the nondimensional kinetic energy of turbulence. The subscripts i and j can take the values 1, 2 or 3 in the three coordinate directions X_1 , X_2 and X_3 respectively. The X_1 , X_2 and X_3 are equivalent to X , Y and Z in Cartesian coordinates. The Reynolds number Re is defined on the basis of average axial velocity at the inlet and the laminar viscosity as $Re = \bar{U}_o H / \nu$. The Prandtl number of the fluid is denoted by Pr .

The turbulent kinematic viscosity $\nu_{t,n}$ is given by

$$\nu_{t,n} = C_\mu Re k_n^2 / \epsilon_n \quad (3.13)$$

In the above equation C_μ is a constant (equal to 0.09) and ϵ_n is the dissipation rate of turbulent kinetic energy (normalized with respect to U_o^3/H). The nondimensional eddy diffusivity $\alpha_{t,n}$ is given by

$$\alpha_{t,n} = C_\mu Re Pr k_n^2 / (\sigma_t \epsilon_n) \quad (3.14)$$

where σ_t is the turbulent Prandtl number. Generally, $\sigma_t = 0.9$. The modeled transport equations for k_n and ϵ_n are

$$\frac{Dk_n}{Dt} = \frac{1}{Re} \frac{\partial}{\partial X_i} \left[\frac{\nu_{t,n}}{\sigma_k} \frac{\partial k_n}{\partial X_i} \right] + G_n - \epsilon_n \quad (3.15)$$

$$\frac{D\epsilon_n}{Dt} = \frac{1}{Re} \frac{\partial}{\partial X_i} \left[\frac{\nu_{t,n}}{\sigma_\epsilon} \frac{\partial \epsilon_n}{\partial X_i} \right] + C_1 \epsilon_n G_n / k_n - C_2 \epsilon_n^2 / k_n \quad (3.16)$$

Here, G_n is the generation of turbulent kinetic energy (nondimensional) given by

$$G_n = \frac{(1 + \nu_{t,n})}{Re} \left(\frac{\partial \bar{U}_i}{\partial X_j} + \frac{\partial \bar{U}_j}{\partial X_i} \right) \frac{\partial \bar{U}_i}{\partial X_j} \quad (3.17)$$

and $\sigma_k, \sigma_\epsilon, C_1, C_2$ are empirical constants : $\sigma_k = 1.0, \sigma_\epsilon = 1.3, C_1 = 1.44, C_2 = 1.92$. These are based on wide range of experimental data. The argument for choosing these values are given in Launder and Spalding (1972).

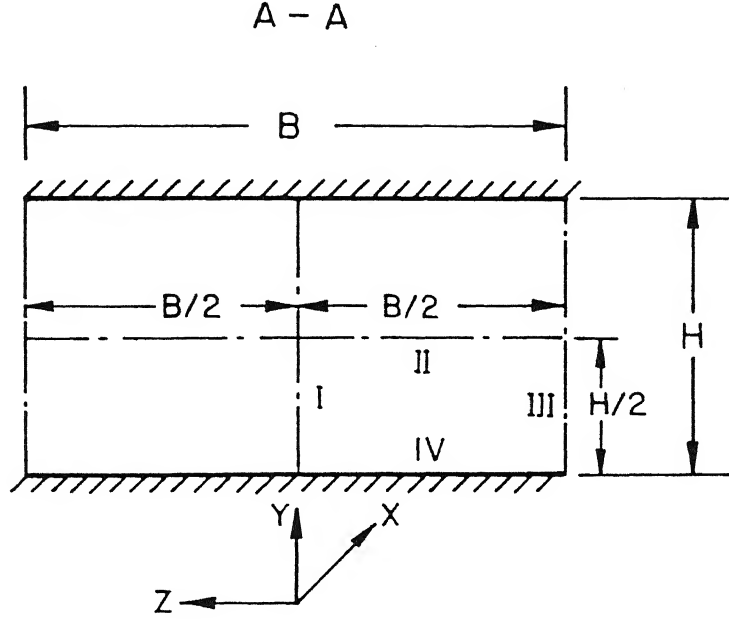


Figure 3.2: Cross-section of the computational domain

3.2.4 Boundary Conditions for Turbulent Flow

The inlet conditions for velocity and temperature can be specified using the profiles we want to use. The turbulent kinetic energy k_n and its dissipation rate are calculated from the value of turbulent intensity specified at the inlet.

The inlet boundary conditions can be specified as following:

$$\left. \begin{aligned} U(Y) &= (u_{\tau,n} \ln(EY^+))/\chi \\ V &= 0 \\ W &= 0 \\ k_n &= 1.5 I^2 \\ \epsilon_n(Y) &= (k_n^{3/2} C_\mu^{3/4})/\chi Y \quad \text{for } Y < (\lambda/\chi) \\ &= (k_n^{3/2} C_\mu^{3/4})/\lambda \quad \text{for } Y > (\lambda/\chi) \end{aligned} \right\} \quad (3.18)$$

where, $u_{\tau,n}$ is nondimensional friction velocity, Y^+ is given by yu_τ/ν , I is turbulent intensity, $\chi = 0.42$ which is known as von Karman constant, λ is a constant prescribing ramp distribution of mixing length in boundary layers and equal to 0.09 and $E=9.0$.

The boundary conditions for the outlet and the confining walls (both no-slip and free-slip) as shown in Fig. 3.2 are treated as follows:

- outlet:

$$\frac{\partial f}{\partial X} = 0; \quad f = (\bar{U}, \bar{V}, \bar{W}, \bar{\theta}, k_n, \epsilon_n) \quad (3.19)$$

- free-slip (symmetric) wall (plane I, III):

$$\bar{W} = 0, \quad \frac{\partial f}{\partial Z} = 0; \quad f = (\bar{U}, \bar{V}, \bar{\theta}, k_n, \epsilon_n) \quad (3.20)$$

- free-slip wall (plane II):

$$\bar{V} = 0, \quad \frac{\partial f}{\partial Y} = 0; \quad f = (\bar{U}, \bar{W}, \bar{\theta}, k_n, \epsilon_n) \quad (3.21)$$

- no-slip wall (plane IV):

$$\bar{U} = \bar{V} = \bar{W} = 0, \quad \bar{\theta} = 1 \quad (3.22)$$

The wall functions due to Launder and Spalding (1974) and Amano (1984) are used to mimic the near wall region.

- For $Y_p^+ < 11.63$

$$\tau_{w,n}^x = \frac{\bar{U}_p}{ReY_p} \quad (3.23)$$

$$\tau_{w,n}^z = \frac{\bar{W}_p}{ReY_p} \quad (3.24)$$

- and for $Y_p^+ \geq 11.63$.

$$\tau_{w,n}^x = \frac{\bar{U}_p C_\mu^{\frac{1}{4}} k_{n,p}^{\frac{1}{2}} \chi}{\ln(EY_p^+)} \quad (3.25)$$

$$\tau_{w,n}^z = \frac{\bar{W}_p C_\mu^{\frac{1}{4}} k_{n,p}^{\frac{1}{2}} \chi}{\ln(EY_p^+)} \quad (3.26)$$

where, $Y_p^+ = Y_p Re C_\mu^{\frac{1}{4}} k_{n,p}^{\frac{1}{2}}$. The subscript p refers to the grid point adjacent to the wall. The production rate of k_n and the average dissipation rate of $\bar{\epsilon}_n$ over a near wall cell for the equation (3.15) at point p are computed from the following

$$G_{n,p} = \left(\sqrt{(\tau_{w,n}^x)^2 + (\tau_{w,n}^z)^2} \right) \left(\sqrt{\bar{U}_p^2 + \bar{W}_p^2} \right) / Y_p \quad (3.27)$$

$$\bar{\epsilon}_{n,p} = \frac{1}{Y_p} \int_0^{Y_p} \epsilon dY = \frac{C_\mu^{\frac{3}{4}} k_{n,p}^{\frac{3}{2}} \ln(EY_p^+)}{\chi Y_p} \quad (3.28)$$

Instead of using equation (3.16) near the wall, the ϵ_n at point p is computed from

$$\epsilon_{n,p} = \frac{C_\mu^{\frac{3}{4}} k_{n,p}^{\frac{3}{2}}}{\chi Y_p} \quad (3.29)$$

In order to calculate the wall functions for temperature, the heat flux at the wall can be expressed in the following way:

- For $Y_p^+ < 11.63$

$$q_{w,n} = \frac{(\bar{\theta} - \bar{\theta}_w) C_\mu^{\frac{1}{4}} k_{n,p}^{\frac{1}{2}}}{Pr Y_p^+} \quad (3.30)$$

- and for $Y_p^+ \geq 11.63$

$$q_{w,n} = \frac{(\bar{\theta} - \bar{\theta}_w) C_\mu^{\frac{1}{4}} k_{n,p}^{\frac{1}{2}}}{(\sigma_t \ln(EY_p^+)/\chi) + P_f n} \quad (3.31)$$

where, $q_{w,n}$ is the nondimensional heat flux at the wall given by

$$q_{w,n} = \frac{q_w}{\rho c_p U_o (T_w - T_\infty)} \quad (3.32)$$

It may be mentioned that P_{fn} in equation (3.31) is the Pee function which may be written as (see Dutta and Acharya, 1993)

$$P_{fn} = 9 \left[\frac{Pr}{\sigma_t} - 1 \right] \left[\frac{Pr}{\sigma_t} \right]^{-\frac{1}{4}} \quad (3.33)$$

3.3 Grid System Used

Computational domain is divided into a set of rectangular cells (Fig. 3.3a) and a staggered grid arrangement is used such that the velocity components are defined at the center of the cell faces to which they are normal (Fig. 3.3b). The pressure and temperature are defined at the center of the cell. In such an arrangement, pressure difference between two adjacent cells is the driving force for the velocity component located between the interface of these cells. The pressure field will accept a reasonable pressure distribution for a correct velocity field. Another important advantage of such a grid system is that transport rates across the faces of the control volumes can be computed without interpolation of velocity components.

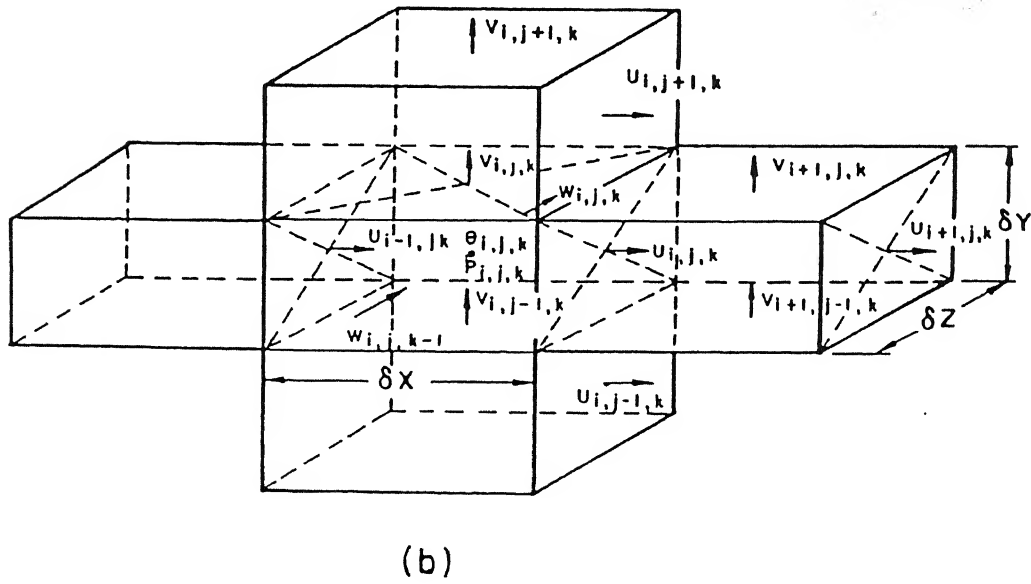
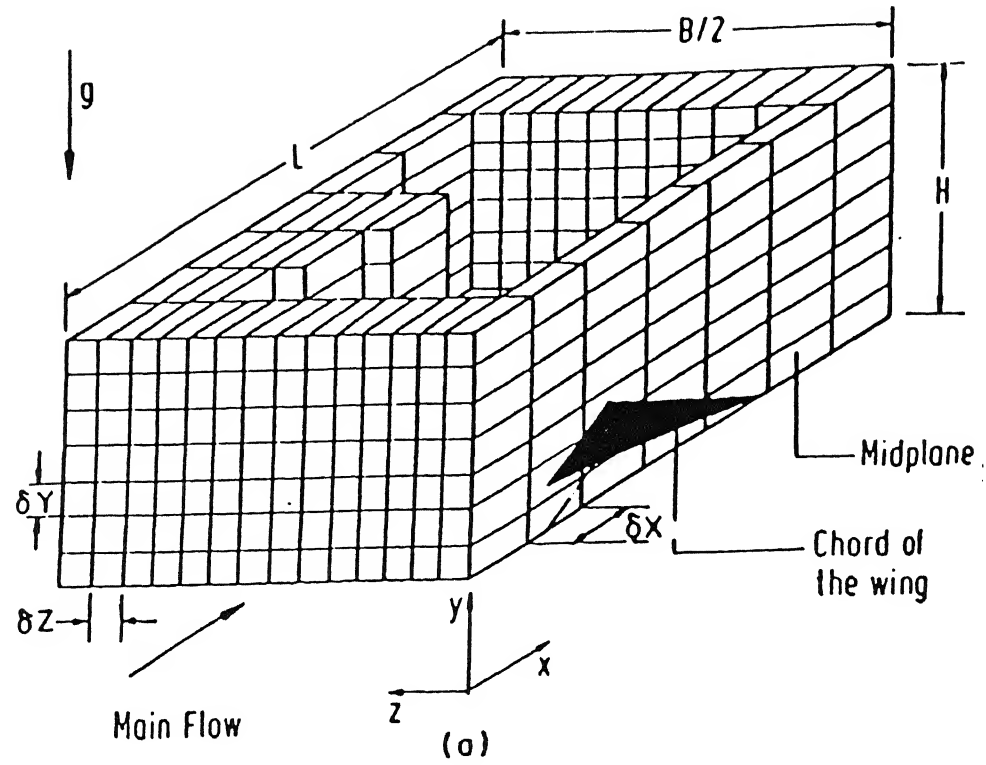


Figure 3.3: (a) Grid spacing in the computational domain and the location of the wing-type vortex grid showing the discretized variables (b) Three-dimensional staggered grid showing the locations of the locations of the discretized variables

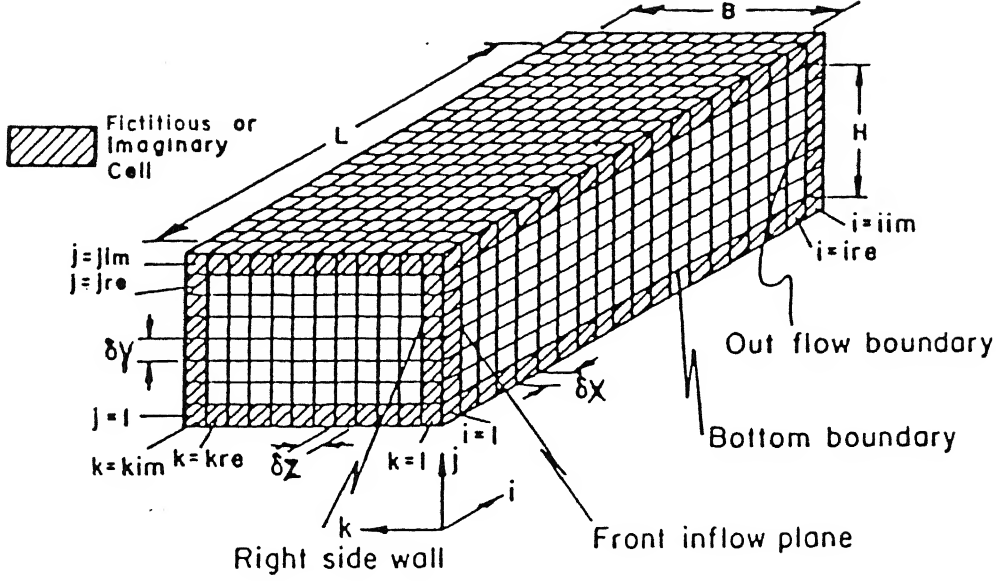


Figure 3.4: Boundary conditions and fictitious boundary cells

3.4 Numerical Boundary Conditions

So far, we have discussed boundary conditions for laminar and turbulent flows in symbolic form. In this section, we will briefly discuss the implementation technique of the boundary conditions in the solution code. The boundary conditions are imposed by setting appropriate velocities in the fictitious cells surrounding the physical domain (Fig. 3.4).

3.4.1 Boundary Conditions for Confining Walls

Since, the equations are elliptic in space, we need boundary conditions on all confining walls, - even at the outlet. Consider, for example, the bottom boundary of the computing (physical) mesh. If this boundary is to be a rigid no-slip wall, the normal velocity on the wall must be zero and the tangential velocity components should also be zero. Here, we are considering a stationary wall. With reference to Fig. 3.4, we have

$$\left. \begin{aligned} V_{i,1,k} &= 0 \\ U_{i,1,k} &= -U_{i,2,k} \\ W_{i,1,k} &= -W_{i,2,k} \end{aligned} \right\} \begin{aligned} &\text{for } i = 2 \text{ to } ire \\ &\text{and } k = 2 \text{ to } kre \end{aligned} \quad (3.34)$$

If the right side wall is a free-slip (vanishing shear) boundary, the normal velocity

must be zero and the tangential velocities should have no normal gradient.

$$\left. \begin{aligned} W_{i,j,1} &= 0 \\ U_{i,j,1} &= U_{i,j,2} \\ V_{i,j,1} &= V_{i,j,2} \end{aligned} \right\} \begin{aligned} &\text{for } i = 2 \text{ to } ire \\ &\text{and } j = 2 \text{ to } jre \end{aligned} \quad (3.35)$$

The front plane is to be provided with inflow boundary condition. Any desired functional relationship may be recommended. Generally, normal velocity components are set to zero and a uniform or parabolic axial velocity may be deployed. Hence, with reference to Fig. 3.4, we can write

$$\left. \begin{aligned} V_{1,j,k} &= -V_{2,j,k} \\ W_{1,j,k} &= -W_{2,j,k} \\ U_{1,j,k} &= 1.0 \\ \text{or, } U_{1,j,k} &= 1.5 \left[1 - \left(\frac{j_m - j}{j_m} \right)^2 \right] \end{aligned} \right\} \begin{aligned} &\text{for } j = 2 \text{ to } jre \\ &\text{and } k = 2 \text{ to } kre \end{aligned} \quad (3.36)$$

where, j_m is the horizontal midplane.

Continuative or outflow boundaries always pose a problem for low-speed calculations, because whatever prescription is chosen it can affect the entire flow field upstream. What is needed is a prescription that permits fluid to flow out of the mesh with a minimum of upstream influence. In MAC family of algorithms, the second derivatives of the dependent variables in flow direction are set to zero in order to ensure smooth transition through the outflow boundary. These are implemented in the following way:

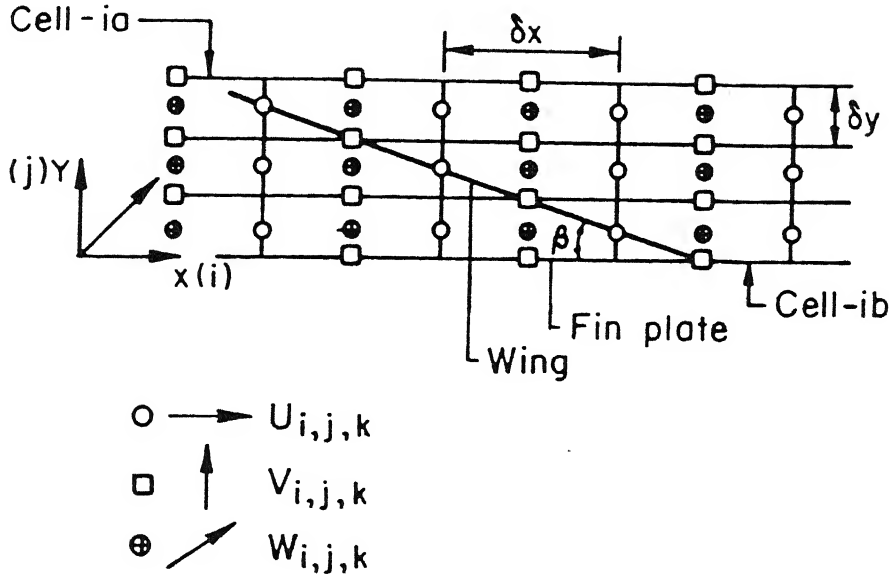
$$\left. \begin{aligned} U_{i+1,j,k} &= 2U_{i,j,k} - U_{i-1,j,k} \\ V_{i+1,j,k} &= 2V_{i,j,k} - V_{i-1,j,k} \\ W_{i+1,j,k} &= 2W_{i,j,k} - W_{i-1,j,k} \end{aligned} \right\} \begin{aligned} &\text{for } j = 2 \text{ to } jre \\ &\text{and } k = 2 \text{ to } kre \\ &i = iim - 2 \end{aligned} \quad (3.37)$$

3.4.2 Boundary Conditions for the Obstacle

A special effort is required to satisfy the kinematic boundary conditions on the vortex generator. From Fig. 3.5, the angle of attack of the wing-type vortex generator can be expressed as $\beta = \tan^{-1}(\delta Y / \delta X)$. Figure 3.5 further reveals that the U and V components of velocity fall directly on the surface of the obstacle in the region of the wing and are therefore set equal to zero. Implementation of no-slip condition for U component velocity at the side edge of the obstacle needs some manipulations. From Fig. 3.6, it is found that $U_{i,j,k+1/2} = 0$. In other words, we can write

$$\left. \begin{aligned} U_{i,j,k} &= -U_{i,j,k+1} \\ &(\text{for } i = ia \text{ to } ib, j = 2 \text{ to } ja \text{ and } k = 2 \text{ to } kc) \end{aligned} \right\} \quad (3.38)$$

It may be mentioned that the difference of count between kc and 2 is equal to that between ib and ia. The W component of velocity also needs manipulation for its zero value on the surface of the obstacle. From Fig. 3.7

Figure 3.5: Relative location of velocity components and wing on X-Y plane at $Z=0$

$$\left. \begin{aligned}
 W_{i,j,k} &= -W_{i,j-1,k} \\
 W_{i,j,k} &= -W_{i-1,j,k} \\
 W_{i,j-1,k} &= -W_{i,j,k} \\
 W_{i-1,j,k} &= -W_{i,j,k} \\
 &(\text{for } i = ia \text{ to } ib, j = 2 \text{ to } ja \text{ and } k = 2 \text{ to } kc)
 \end{aligned} \right\} \quad (3.39)$$

The temperature boundary conditions on the wing-type obstacle are diagrammatically shown in Fig. 3.8. The obstacle boundary conditions for temperature are :

$$\left. \begin{aligned}
 \theta_{i,j,k} &= 2\theta_w - \theta_{i-1,j,k} \\
 \theta_{i,j,k} &= 2\theta_w - \theta_{i,j-1,k} \\
 \theta_{i-1,j+1,k} &= 2\theta_w - \theta_{i-1,j,k} \\
 \theta_{i-1,j+1,k} &= 2\theta_w - \theta_{i-2,j+1,k} \text{ etc.} \\
 &(\text{for } i = ia \text{ to } ib, j = 2 \text{ to } ja \text{ and } k = 2 \text{ to } kc)
 \end{aligned} \right\} \quad (3.40)$$

In practice, the vortex generators can easily be manufactured by punching or embossing the wall. In some computational results, the effects due to the hole beneath the vortex generator have been taken into account. It is considered that the heat exchanger cores have a number of plates and on each plate the vortex generators are punched out in such a way that the holes are perfectly aligned. In our computational domain, a small part of top and bottom boundaries must be set to identify the punched holes. For this purpose spacewise-periodic boundary conditions on the location of the punched holes have to be applied in the y - direction (Fig. 3.9). Here, the period length

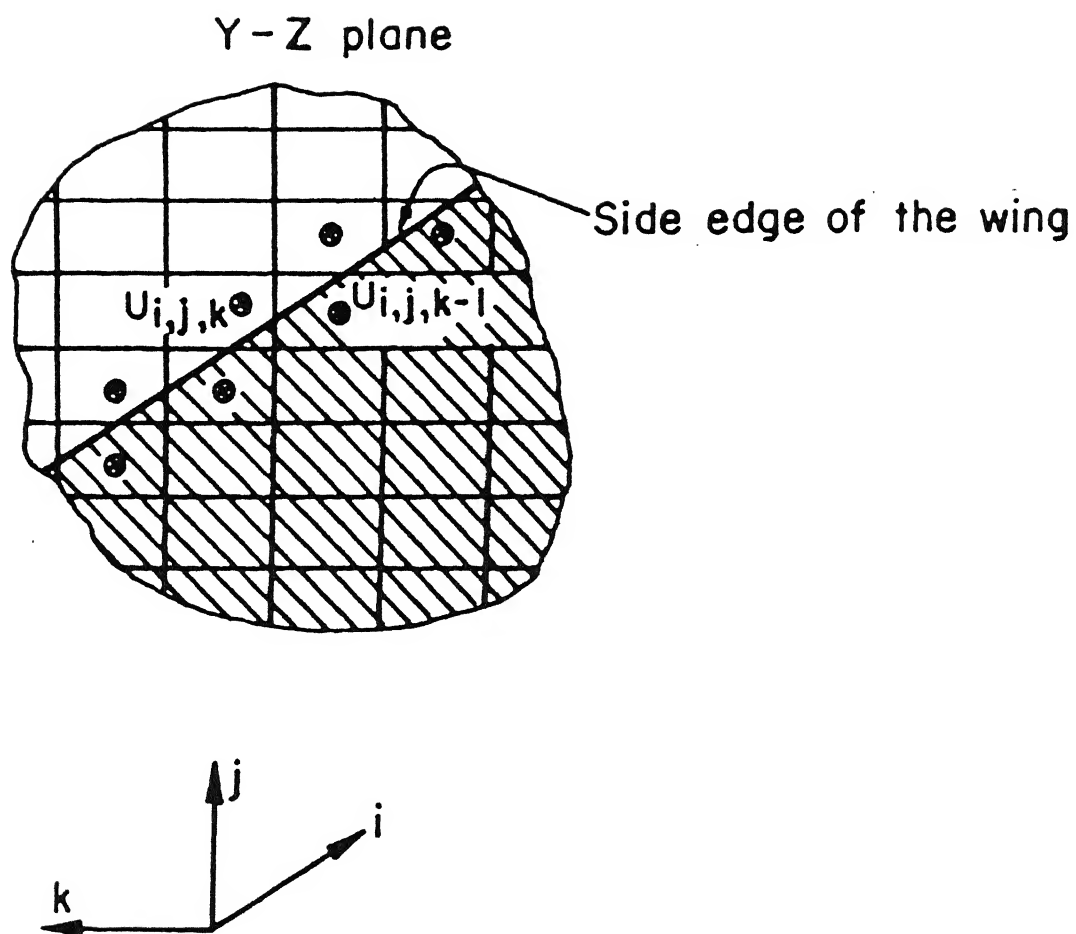


Figure 3.6: Side edge of the wing-type vortex generator on Y-Z plane

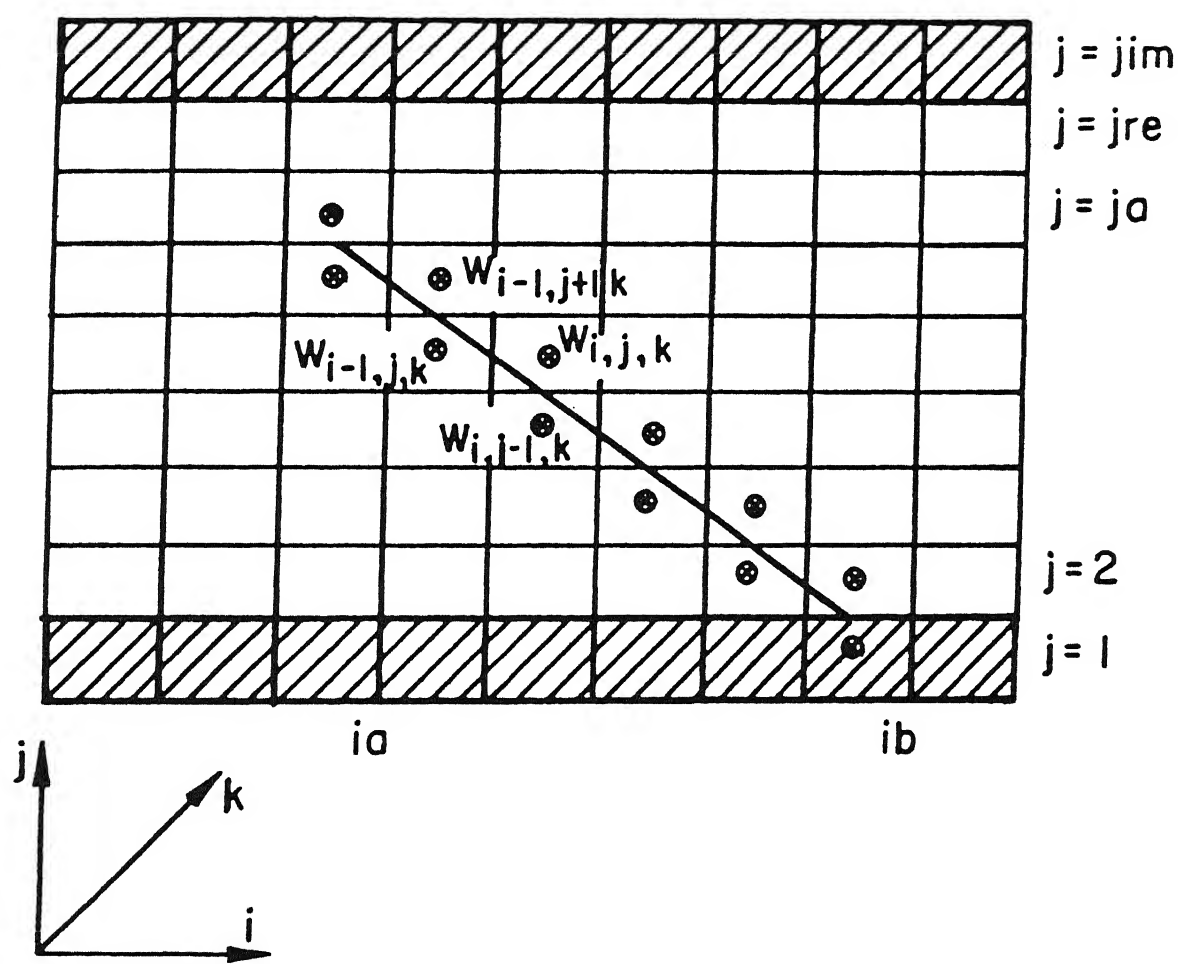


Figure 3.7: Relative location of the spanwise velocity components and the wing-type vortex generator on X-Y plane

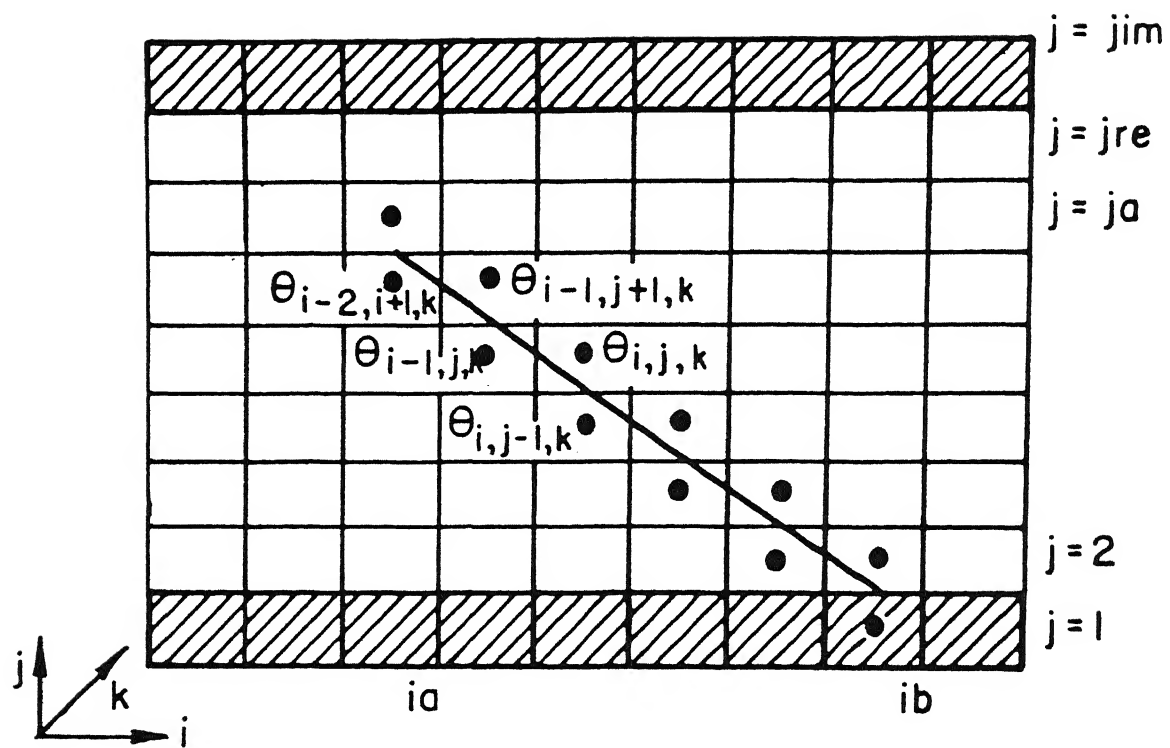


Figure 3.8: Thermal boundary conditions on the wing-type vortex

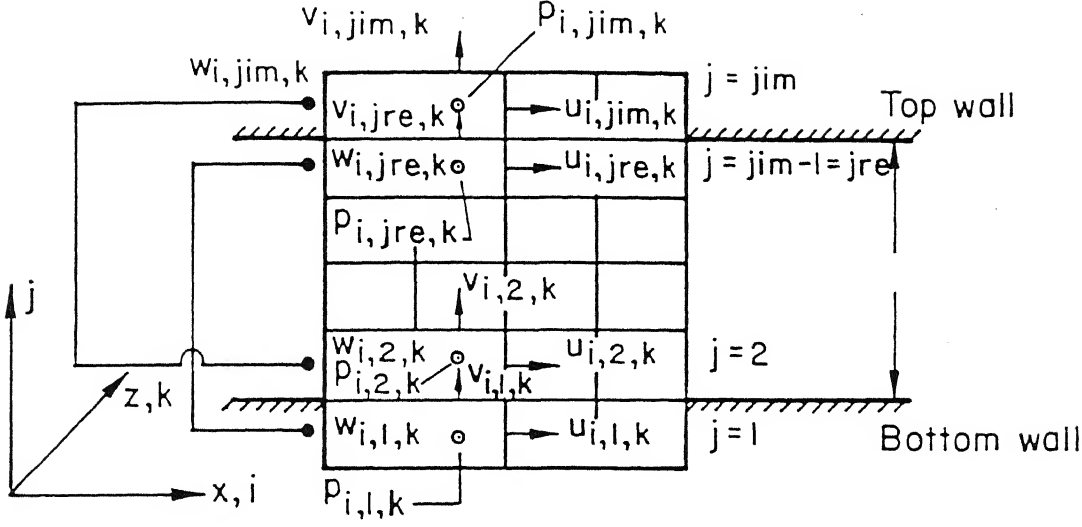


Figure 3.9: Periodic boundary conditions for pressure and velocities on the top and the bottom wall

is channel height H . However, the boundary conditions for the fictitious cells on the bottom are :

$$\left. \begin{aligned} U_{i,1,k} &= U_{i,jre,k} \\ V_{i,1,k} &= 0.5(V_{i,jre,k} + V_{i,1,k}) \\ W_{i,1,k} &= W_{i,jre,k} \\ P_{i,1,k} &= P_{i,jre,k} \\ &(\text{for all } i, k \text{ in the punched holes}) \end{aligned} \right\} \quad (3.41)$$

and on the top

$$\left. \begin{aligned} U_{i,jim,k} &= U_{i,2,k} \\ V_{i,jim,k} &= V_{i,2,k} \\ V_{i,jre,k} &= 0.5(V_{i,jre,k} + V_{i,1,k}) \\ W_{i,jim,k} &= W_{i,2,k} \\ P_{i,jim,k} &= P_{i,2,k} \\ &(\text{for all } i, k \text{ in the punched holes}) \end{aligned} \right\} \quad (3.42)$$

Such boundary conditions have also been discussed by *Hirt et al.* (1975) and *Biswas and Chattopadhyay* (1992). However, for plate-fin heat exchangers, a different manufacturing technique for mounting the vortex generators is adapted. For this case, no hole exists underneath the vortex-generators in order to avoid mixing of the hot and cold streams.

3.5 Method of Solution

A modified version of Marker and Cell (MAC) method due to Harlow and Welch (1965) and Hirt and Cook (1972) is used to obtain the numerical solution of the governing equations.

3.5.1 MAC Algorithm

Because of staggered grid arrangement (Fig 3.3(b)), the velocities are not defined at the nodal points. Whenever required, the velocities at the nodal points are to be found by interpolation. For example, with uniform grids, we can write $U_{i+1/2,j,k} = 0.5(U_{i,j,k} + U_{i+1,j,k})$. Where a product or square of such quantity appears, it is to be averaged first and then the product is to be formed.

Convective terms of the momentum equations are discretized using a weighted average of second upwind and space centered scheme (Hirt *et al.*, 1975). Diffusive terms are discretized by a central difference scheme. Let us consider the discretized terms of x -momentum equation (refer to Figure 3.3(b)).

$$\begin{aligned}
 \left[\frac{\partial U^2}{\partial X} \right]_{i,j,k} &= \frac{1}{4\delta X} [(U_{i,j,k} + U_{i+1,j,k})(U_{i,j,k} + U_{i+1,j,k}) \\
 &+ \alpha_p |(U_{i,j,k} + U_{i+1,j,k})| (U_{i,j,k} - U_{i+1,j,k}) \\
 &- (U_{i-1,j,k} + U_{i,j,k})(U_{i-1,j,k} + U_{i,j,k}) \\
 &- \alpha_p |(U_{i-1,j,k} + U_{i,j,k})| (U_{i-1,j,k} - U_{i,j,k})] \\
 &\equiv \text{DUUDX}
 \end{aligned} \tag{3.43}$$

$$\begin{aligned}
 \left[\frac{\partial UV}{\partial Y} \right]_{i,j,k} &= \frac{1}{4\delta Y} [(V_{i,j,k} + V_{i+1,j,k})(U_{i,j,k} + U_{i+1,j,k}) \\
 &+ \alpha_p |(V_{i,j,k} + V_{i+1,j,k})| (U_{i,j,k} - U_{i+1,j,k}) \\
 &- (V_{i,j-1,k} + V_{i+1,j-1,k})(U_{i,j-1,k} + U_{i,j,k}) \\
 &- \alpha_p |(V_{i,j-1,k} + V_{i+1,j-1,k})| (U_{i,j-1,k} - U_{i,j,k})] \\
 &\equiv \text{DUVDY}
 \end{aligned} \tag{3.44}$$

$$\begin{aligned}
 \left[\frac{\partial UW}{\partial Z} \right]_{i,j,k} &= \frac{1}{4\delta Z} [(W_{i,j,k} + W_{i+1,j,k})(U_{i,j,k} + U_{i,j,k+1}) \\
 &+ \alpha_p |(W_{i,j,k} + W_{i+1,j,k})| (U_{i,j,k} - U_{i,j,k+1}) \\
 &- (W_{i,j,k-1} + W_{i+1,j,k-1})(U_{i,j,k-1} + U_{i,j,k}) \\
 &- \alpha_p |(W_{i,j,k-1} + W_{i+1,j,k-1})| (U_{i,j,k-1} - U_{i,j,k})] \\
 &\equiv \text{DUWDZ}
 \end{aligned} \tag{3.45}$$

$$\frac{\partial P}{\partial X} = \frac{P_{i+1,j,k} - P_{i,j,k}}{\delta X} \equiv DPDX \quad (3.46)$$

$$\frac{\partial^2 U}{\partial X^2} = \frac{U_{i+1,j,k} - 2U_{i,j,k} + U_{i-1,j,k}}{(\delta X)^2} \equiv D2UDX2 \quad (3.47)$$

$$\frac{\partial^2 U}{\partial Y^2} = \frac{U_{i,j+1,k} - 2U_{i,j,k} + U_{i,j-1,k}}{(\delta Y)^2} \equiv D2UDY2 \quad (3.48)$$

$$\frac{\partial^2 U}{\partial Z^2} = \frac{U_{i,j,k+1} - 2U_{i,j,k} + U_{i,j,k-1}}{(\delta Z)^2} \equiv D2UDZ2 \quad (3.49)$$

with, $\alpha_p \rightarrow 1$, the scheme tends to Second upwind and $\alpha_p \rightarrow 0$, the scheme tends to Space centered.

The factor α_p is chosen in such a way that the differencing scheme retains 'something' of second order accuracy and the required upwinding is done for the sake of stability. A typical value of α_p is between 0.2 and 0.3.

Solutions for the velocities are obtained in two folds. First the velocity components are advanced explicitly using the previous state of the flow, having calculated accelerations caused by convection, diffusion and pressure gradients through a time step $\delta\tau$. The explicit time increment may not necessarily lead to a velocity field with zero mass divergence in each cell. In the subsequent fold, adjustment of pressure and velocity is done by an iterative process in order to ensure mass conservation in each cell. If the explicitly advanced provisional velocity is termed as $\tilde{U}_{i,j,k}^{n+1}$, then from equation (3.2) we can write

$$\tilde{U}_{i,j,k}^{n+1} = U_{i,j,k}^n + \delta\tau[RESIDU]_{i,j,k}^n \quad (3.50)$$

where

$$\begin{aligned} [RESIDU]_{i,j,k}^n &= [(-DUUDX - DUVDY - DUWDZ) - DPDX \\ &+ (1/Re)(D2UDX2 + D2UDY2 + D2UDZ2)] \end{aligned} \quad (3.51)$$

In a similar manner we evaluate

$$\tilde{V}_{i,j,k}^{n+1} = V_{i,j,k}^n + \delta\tau[RESIDV]_{i,j,k}^n \quad (3.52)$$

$$\tilde{W}_{i,j,k}^{n+1} = W_{i,j,k}^n + \delta\tau[RESIDW]_{i,j,k}^n \quad (3.53)$$

As discussed earlier, the explicitly advanced tilde velocities may not necessarily lead to a flow field with zero mass divergence in each cell. This implies that at this stage the pressure distribution is not correct. Pressure in each cell will be corrected in such a way that there is no net mass flow in or out of the cell. In the original MAC method, the

corrected pressures are obtained from the solution of a Poisson equation for pressure. A related technique developed by Chorin(1967) involved a simultaneous iteration on pressures and velocity components. Vicelli(1971) has shown that the two methods as applied to the MAC method are equivalent. We shall make use of the iterative correction procedure of Chorin (1967) in order to obtain a divergence-free velocity field. The mathematical methodology of this iterative pressure-velocity correction procedure will be discussed herein.

The relationship between the explicitly advanced velocity component and the velocity at the previous time step may be written as

$$\tilde{U}_{i,j,k}^{n+1} = U_{i,j,k}^n + \frac{\delta\tau[P_{i,j,k}^n - P_{i+1,j,k}^n]}{\delta X} + \delta\tau[CONDIFU]_{i,j,k}^n \quad (3.54)$$

$$[CONDIFU]_{i,j,k}^n = [RESIDU]_{i,j,k}^n + [DPDX]_{i,j,k}^n \quad (3.55)$$

where, on the other hand, the corrected velocity-component (unknown) will be related to the correct pressure (also unknown) in the following way:

$$U_{i,j,k}^{n+1} = U_{i,j,k}^n + \delta\tau \frac{[P_{i,j,k}^{n+1} - P_{i+1,j,k}^{n+1}]}{\delta X} + \delta\tau[CONDIFU]_{i,j,k}^n \quad (3.56)$$

From equations (3.55) and (3.56) we can write

$$U_{i,j,k}^{n+1} - \tilde{U}_{i,j,k}^{n+1} = \frac{\delta\tau[P'_{i,j,k} - P'_{i+1,j,k}]}{\delta X} \quad (3.57)$$

where the pressure correction may be defined as

$$P'_{i,j,k} = P_{i,j,k}^{n+1} - P_{i,j,k}^n \quad (3.58)$$

Neither the pressure corrections nor $U_{i,j,k}^{n+1}$ are known explicitly at this stage so one can not be calculated with the help of the other. Calculations are done in an iterative cycle and we write

$$U_{i,j,k}^{n+1} = \tilde{U}_{i,j,k}^{n+1} + \frac{\delta\tau[P'_{i,j,k} - P'_{i+1,j,k}]}{\delta X} \quad (3.59)$$

In a similar way, we can formulate the following array:

Corrected	→	Estimated	Correction	
$U_{i,j,k}^{n+1}$	→	$\tilde{U}_{i,j,k}^{n+1}$	$+\frac{\delta\tau[P'_{i,j,k} - P'_{i+1,j,k}]}{\delta X}$	(3.60)

$U_{i-1,j,k}^{n+1}$	→	$\tilde{U}_{i-1,j,k}^{n+1}$	$-\frac{\delta\tau[P'_{i,j,k} - P'_{i-1,j,k}]}{\delta X}$	(3.61)
---------------------	---	-----------------------------	---	--------

$V_{i,j,k}^{n+1}$	→	$\tilde{V}_{i,j,k}^{n+1}$	$+\frac{\delta\tau[P'_{i,j,k} - P'_{i,j+1,k}]}{\delta Y}$	(3.62)
-------------------	---	---------------------------	---	--------

$$V_{i,j-1,k}^{n+1} \rightarrow \tilde{V}_{i,j-1,k}^{n+1} - \frac{\delta\tau[P'_{i,j,k} - P'_{i,j-1,k}]}{\delta Y} \quad (3.63)$$

$$W_{i,j,k}^{n+1} \rightarrow \tilde{W}_{i,j,k}^{n+1} + \frac{\delta\tau[P'_{i,j,k} - P'_{i,j,k+1}]}{\delta Z} \quad (3.64)$$

$$W_{i,j,k-1}^{n+1} \rightarrow \tilde{W}_{i,j,k-1}^{n+1} - \frac{\delta\tau[P'_{i,j,k} - P'_{i,j,k-1}]}{\delta Z} \quad (3.65)$$

The correction is done through continuity equation. Plugging-in the above relationship into the continuity equation (3.1) we shall obtain

$$\begin{aligned} & \left[\frac{U_{i,j,k}^{n+1} - U_{i-1,j,k}^{n+1}}{\delta X} + \frac{V_{i,j,k}^{n+1} - V_{i,j-1,k}^{n+1}}{\delta Y} + \frac{W_{i,j,k}^{n+1} - W_{i,j,k-1}^{n+1}}{\delta Z} \right] \\ = & \left[\frac{\tilde{U}_{i,j,k}^{n+1} - \tilde{U}_{i-1,j,k}^{n+1}}{\delta X} + \frac{\tilde{V}_{i,j,k}^{n+1} - \tilde{V}_{i,j-1,k}^{n+1}}{\delta Y} + \frac{\tilde{W}_{i,j,k}^{n+1} - \tilde{W}_{i,j,k-1}^{n+1}}{\delta Z} \right] \\ - & \delta\tau \left[\frac{P'_{i+1,j,k} - 2P'_{i,j,k} + P'_{i-1,j,k}}{(\delta X)^2} + \frac{P'_{i,j+1,k} - 2P'_{i,j,k} + P'_{i,j-1,k}}{(\delta Y)^2} \right. \\ & \left. + \frac{P'_{i,j,k+1} - 2P'_{i,j,k} + P'_{i,j,k-1}}{(\delta Z)^2} \right] \end{aligned} \quad (3.66)$$

or,

$$\begin{aligned} & \left[\frac{U_{i,j,k}^{n+1} - U_{i-1,j,k}^{n+1}}{\delta X} + \frac{V_{i,j,k}^{n+1} - V_{i,j-1,k}^{n+1}}{\delta Y} + \frac{W_{i,j,k}^{n+1} - W_{i,j,k-1}^{n+1}}{\delta Z} \right] \\ = & \left[\frac{\tilde{U}_{i,j,k}^{n+1} - \tilde{U}_{i-1,j,k}^{n+1}}{\delta X} + \frac{\tilde{V}_{i,j,k}^{n+1} - \tilde{V}_{i,j-1,k}^{n+1}}{\delta Y} + \frac{\tilde{W}_{i,j,k}^{n+1} - \tilde{W}_{i,j,k-1}^{n+1}}{\delta Z} \right] \\ + & \left[\frac{2\delta\tau(P'_{i,j,k})}{\delta X^2} + \frac{2\delta\tau(P'_{i,j,k})}{\delta Y^2} + \frac{2\delta\tau(P'_{i,j,k})}{\delta Z^2} \right] \end{aligned} \quad (3.67)$$

$$(3.68)$$

In deriving the above expression, it is assumed that the pressure corrections in the neighboring cells are zero. Back to the calculations, we can write

$$\begin{aligned} 0 &= (D)_{i,j,k} + P'_{i,j,k} \left[2\delta\tau \left(\frac{1}{\delta X^2} + \frac{1}{\delta Y^2} + \frac{1}{\delta Z^2} \right) \right] \\ \text{or, } P'_{i,j,k} &= \frac{-(D)_{i,j,k}}{\left[2\delta\tau \left(\frac{1}{\delta X^2} + \frac{1}{\delta Y^2} + \frac{1}{\delta Z^2} \right) \right]} \end{aligned} \quad (3.69)$$

In order to accelerate the calculation, the pressure correction equation is modified as

$$P'_{i,j,k} = \frac{-\omega_o(D)_{i,j,k}}{\left[2\delta\tau \left(\frac{1}{\delta X^2} + \frac{1}{\delta Y^2} + \frac{1}{\delta Z^2} \right) \right]} \quad (3.70)$$

where ω_o is the overrelaxation factor. A value of $\omega_o = 1.7$ is commonly used. After calculating $P'_{i,j,k}$, the pressure in the cell (i,j,k) is adjusted as

$$P_{i,j,k}^{n+1} \rightarrow P_{i,j,k}^n + P'_{i,j,k} \quad (3.71)$$

Now the pressure and velocity components for each cell are corrected through an iterative procedure in such a way that for the final pressure field, the velocity divergence in each cell vanishes. The process is continued till divergence-free velocity field is reached with a prescribed upper bound; here a value of 0.0001 is recommended. This solution scheme is continued until a steady flow is obtained.

Finally we discuss another important observation. If the velocity boundary conditions are correct and a divergence-free converged velocity field has been obtained, eventually correct pressure will be determined in all the cells including the cells at the boundary. Thus, this method avoids the application of pressure boundary conditions. This typical feature of modified MAC method has been discussed in more details by Peyret and Taylor(1983).

3.5.2 Discretization Technique for k and ϵ Equations

Convective terms of the k and ϵ equations are also discretized using a weighted average of second upwind and space centered scheme (Hirt *et al.*, 1975). Diffusive terms are discretized by a central difference scheme.

Let us consider the discretized terms of the k equation (refer to Figure 3.3(b); here the location of P or θ is similar to the location of k)

$$\begin{aligned} \left[\frac{\partial k U}{\partial X} \right]_{i,j,k} &= \frac{1}{2\delta X} [(k_{i,j,k} + k_{i+1,j,k}) U_{i,j,k} \\ &+ \alpha_p (k_{i,j,k} - k_{i+1,j,k}) | U_{i,j,k} | \\ &- (k_{i-1,j,k} + k_{i,j,k}) U_{i-1,j,k} \\ &- \alpha_p | U_{i-1,j,k} | (k_{i-1,j,k} - k_{i,j,k})] \\ &\equiv DkUDX \end{aligned} \quad (3.72)$$

$$\begin{aligned} \left[\frac{\partial}{\partial X} \left(\nu_t \frac{\partial k}{\partial X} \right) \right]_{i,j,k} &= \frac{1}{2(\delta X)^2} [((\nu_t)_{i,j,k} + (\nu_t)_{i+1,j,k}) (k_{i+1,j,k} - k_{i,j,k}) \\ &- ((\nu_t)_{i-1,j,k} + (\nu_t)_{i,j,k}) (k_{i,j,k} - k_{i-1,j,k})] \\ &\equiv DIFFkX \end{aligned} \quad (3.73)$$

The difference quotients involved in the Generation term are discretized as following.

$$\frac{\partial U}{\partial X} = \frac{U_{i,j,k} - U_{i-1,j,k}}{\delta X} \equiv DUDX \quad (3.74)$$

$$\frac{\partial V}{\partial Y} = \frac{V_{i,j,k} - V_{i,j-1,k}}{\delta Y} \equiv DV DY \quad (3.75)$$

$$\frac{\partial W}{\partial Z} = \frac{W_{i,j,k} - W_{i,j,k-1}}{\delta Z} \equiv DW DZ \quad (3.76)$$

$$\begin{aligned} \frac{\partial U}{\partial Y} &= \frac{1}{4\delta Y} [(U_{i,j,k} + U_{i-1,j,k} + U_{i,j+1,k} + U_{i-1,j+1,k}) \\ &\quad - (U_{i,j,k} + U_{i-1,j,k} + U_{i,j-1,k} + U_{i-1,j-1,k})] \\ &\equiv DUDY \end{aligned} \quad (3.77)$$

$$\begin{aligned} \frac{\partial V}{\partial X} &= \frac{1}{4\delta X} [(V_{i,j,k} + V_{i,j-1,k} + V_{i+1,j,k} + V_{i+1,j-1,k}) \\ &\quad - (V_{i,j,k} + V_{i,j-1,k} + V_{i-1,j,k} + V_{i-1,j-1,k})] \\ &\equiv DV DX \end{aligned} \quad (3.78)$$

$$\begin{aligned} \frac{\partial W}{\partial X} &= \frac{1}{4\delta X} [(W_{i,j,k} + W_{i,j,k-1} + W_{i+1,j,k} + W_{i+1,j,k-1}) \\ &\quad - (W_{i,j,k} + W_{i,j,k-1} + W_{i-1,j,k} + W_{i-1,j,k-1})] \\ &\equiv DW DX \end{aligned} \quad (3.79)$$

$$\begin{aligned} \frac{\partial U}{\partial Z} &= \frac{1}{4\delta Z} [(U_{i,j,k} + U_{i-1,j,k} + U_{i,j,k+1} + U_{i-1,j,k+1}) \\ &\quad - (U_{i,j,k} + U_{i-1,j,k} + U_{i,j,k-1} + U_{i-1,j,k-1})] \\ &\equiv DUDZ \end{aligned} \quad (3.80)$$

$$\begin{aligned} \frac{\partial V}{\partial Z} &= \frac{1}{4\delta Z} [(V_{i,j,k} + V_{i,j-1,k} + V_{i,j,k+1} + V_{i,j-1,k+1}) \\ &\quad - (V_{i,j,k} + V_{i,j-1,k} + V_{i,j,k-1} + V_{i,j-1,k-1})] \\ &\equiv DVDZ \end{aligned} \quad (3.81)$$

$$\begin{aligned} \frac{\partial W}{\partial Y} &= \frac{1}{4\delta Y} [(W_{i,j,k} + W_{i,j,k-1} + W_{i,j+1,k} + W_{i,j+1,k-1}) \\ &\quad - (W_{i,j,k} + W_{i,j,k-1} + W_{i,j-1,k} + W_{i,j-1,k-1})] \\ &\equiv DW DY \end{aligned} \quad (3.82)$$

In terms of the difference quotients, the ϵ equation consists of the similar quotients as the k equation.

3.5.3 Solution of the Energy Equation

After evaluating the correct velocities, the energy equation is solved with an Successive Over-Relaxation technique to determine the temperature field. We shall discuss the solution procedure of the energy equation in this section.

The steady state energy equation, neglecting the dissipation term, may be written

in the following conservative form as

$$\frac{\partial U\theta}{\partial X} + \frac{\partial V\theta}{\partial Y} + \frac{\partial W\theta}{\partial Z} = \frac{\nabla^2\theta}{Pe} \quad (3.83)$$

Equation (3.83) may be rewritten as

$$\nabla^2\theta = Pe[CONVT]_{i,j,k}^m \quad (3.84)$$

where, $[CONVT]_{i,j,k}$ is the discretized convective terms on the left hand side of equation (3.83) and m stands for iterative counter. To start with, we can assume any guess value of θ throughout the flow field. U, V, W are known from the solution of momentum equation hence equation (3.83) is now a linear equation. However, from the guess values of θ and known correct values of U, V , and W the left hand side of equation (3.84) is evaluated. A weighted average scheme may be adapted for discretization of the convective terms. After discretizing and evaluating right hand side of equation (3.84) we obtain a Poisson equation for temperature with a source term on the right hand side. Now, we can follow a SOR technique for solving equation (3.84). Consider a discretized equation as

$$\frac{\theta_{i+1,j,k} - 2\theta_{i,j,k} + \theta_{i-1,j,k}}{(\delta X)^2} + \frac{\theta_{i,j+1,k} - 2\theta_{i,j,k} + \theta_{i,j-1,k}}{(\delta Y)^2} + \frac{\theta_{i,j,k+1} - 2\theta_{i,j,k} + \theta_{i,j,k-1}}{(\delta Z)^2} = S^{*m}$$

where $S^{*m} \equiv Pe[CONVT]_{i,j,k}^m$

or,

$$A^{*m} - \theta_{i,j,k} \left[\frac{2}{(\delta X)^2} + \frac{2}{(\delta Y)^2} + \frac{2}{(\delta Z)^2} \right] = S^{*m}$$

$$\text{or, } \theta_{i,j,k} = \frac{A^{*m} - S^{*m}}{\left[\frac{2}{(\delta X)^2} + \frac{2}{(\delta Y)^2} + \frac{2}{(\delta Z)^2} \right]} \quad (3.85)$$

where,

$$A^{*m} = \frac{\theta_{i+1,j,k} + \theta_{i-1,j,k}}{(\delta X)^2} + \frac{\theta_{i,j+1,k} + \theta_{i,j-1,k}}{(\delta Y)^2} + \frac{\theta_{i,j,k+1} + \theta_{i,j,k-1}}{(\delta Z)^2}$$

$\theta_{i,j,k}$ in equation (3.85) may be assumed to be the most recent value and it may be written as $\theta_{i,j,k}^{m'}$. In order to accelerate the speed of computation we introduce a overrelaxation factor ω and

$$\theta_{i,j,k}^{m+1} = \theta_{i,j,k}^m + \omega[\theta_{i,j,k}^{m'} - \theta_{i,j,k}^m] \quad (3.86)$$

where $\theta_{i,j,k}^m$ is the previous value, $\theta_{i,j,k}^{m'}$ is the most recent value and $\theta_{i,j,k}^{m+1}$ is the calculated better guess. The procedure will continue till the required convergence is achieved.

3.5.4 Numerical Stability Considerations

For accuracy, the mesh size must be chosen small enough to resolve the expected spatial variations in all dependent variables.

Once a mesh has been chosen, the choice of the time increment is governed by two restrictions, namely, the Courant-Friedrichs-Lewy (CFL) condition and the restriction on the basis of grid-Fourier numbers.

According to the CFL condition, material cannot move through more than one cell in one time step. Therefore, the time increment must satisfy the inequality

$$\delta\tau < \min \left\{ \frac{\delta X}{|U|}, \frac{\delta Y}{|V|}, \frac{\delta Z}{|W|} \right\} \quad (3.87)$$

where the minimum is with respect to every cell in the mesh. Typically, $\delta\tau$ is chosen equal to one-fourth to one-third of the minimum cell transit time. When the viscous diffusion terms are more important, the condition necessary to ensure stability is dictated by the restriction on the grid Fourier numbers, which results in

$$\delta\tau < \frac{1}{2} \frac{(\delta X)^2(\delta Y)^2(\delta Z)^2}{(\delta X^2 + \delta Y^2 + \delta Z^2)} Re \quad (3.88)$$

The final $\delta\tau$ for each time increment is the minimum of the $\delta\tau$'s obtained from equations (3.87) and (3.88).

3.6 More on Discretization of Governing Equations

We have already seen that the continuity equation is discretized by a simple first-order differencing in such a way that the mass conservation is maintained in each cell. The temporal terms and the terms corresponding to the pressure gradients are also discretized by first order differencing. The discretized viscous terms are second order accurate. All these terms have been presented in the previous section. The convective terms have been discretized by using a weighted average scheme which combines upwind and central differencing to achieve the stability of the upwind method and better formal accuracy of the central differencing. We have already discussed that the factor, α_p serves to balance the upwind contribution. If $\alpha_p \rightarrow 0$, the difference equations are centered in space. In the present investigation, the factor α_p is restricted between 0.2 and 0.3 so that the formulation can retain "something" of the second order accuracy (Roache, 1972). Runchal and Wolfstein (1969) and Timin and Esmail (1983) used this discretization scheme to compute driven cavity flows. Their results compare favorably with those of the second order schemes.

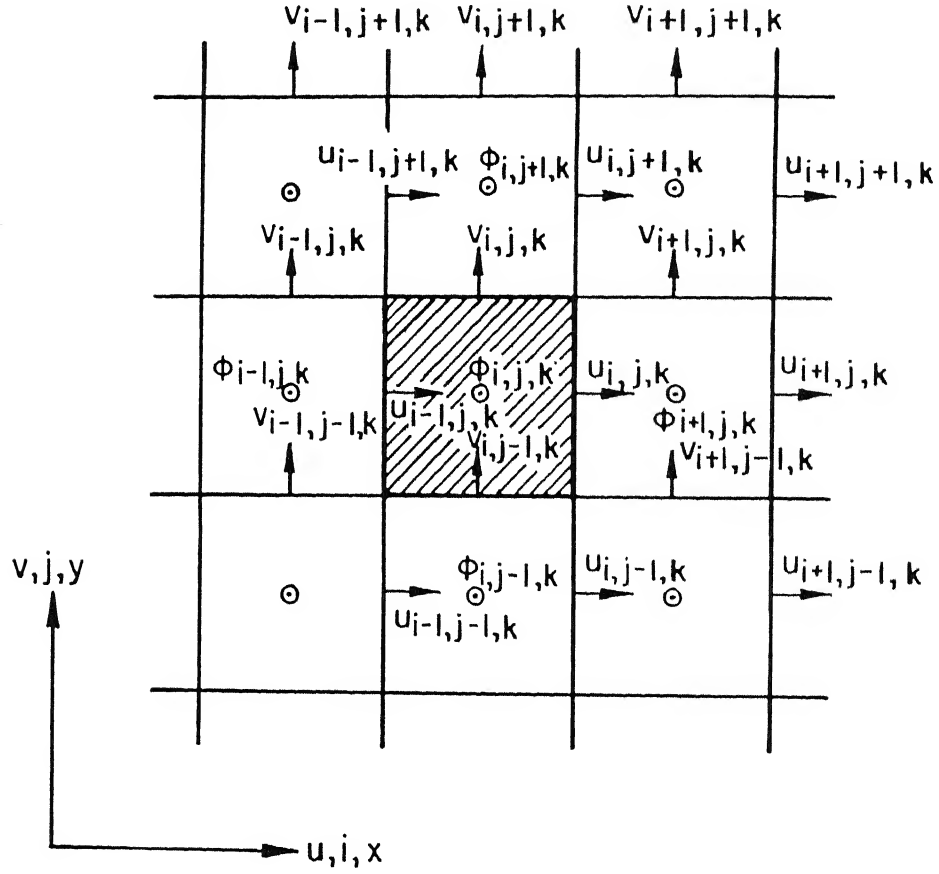


Figure 3.10: Dependent variables on a rectangular mesh for describing QUICK scheme

3.6.1 Some Improvements on Discretization of Convective Terms

Perhaps more accurate solutions are obtained if the convective terms are discretized by higher order schemes. Davis and Moore (1982) use the MAC method with a multidimensional third-order upwinding scheme. Needless to mention that their marching algorithm for the momentum equation is explicit and the stability restriction concerning the CFL condition $[(U\delta\tau/\delta X) \leq 1, (V\delta\tau/\delta Y) \leq 1 \text{ and } (W\delta\tau/\delta Z) \leq 1]$ is satisfied.

The multidimensional third-order upwinding is, in principle similar to one-dimensional quadratic upstream interpolation scheme introduced by Leonard (1979). Consider Fig. 3.10. Let ϕ be any property which can be convected and diffused. The convective term $\partial(U\phi)/\partial X$ may be represented as

$$\frac{\partial(U\phi)}{\partial X} = \frac{(U\phi)_{i+\frac{1}{2},j,k} - (U\phi)_{i-\frac{1}{2},j,k}}{\delta X} \quad (3.89)$$

where, the variables $(U\phi)_{i+\frac{1}{2},j,k}$, $(U\phi)_{i-\frac{1}{2},j,k}$ are defined as

$$\begin{aligned} (U\phi)_{i+\frac{1}{2},j,k} &= \frac{1}{2}[(U\phi)_{i,j,k} + (U\phi)_{i+1,j,k}] \\ &- \frac{\xi}{3}[(U\phi)_{i-1,j,k} - 2(U\phi)_{i,j,k} + (U\phi)_{i+1,j,k}] \quad \text{for } U_{i,j,k} > 0 \end{aligned} \quad (3.90)$$

and

$$\begin{aligned} (U\phi)_{i-\frac{1}{2},j,k} &= \frac{1}{2}[(U\phi)_{i,j,k} + (U\phi)_{i-1,j,k}] \\ &- \frac{\xi}{3}[(U\phi)_{i-2,j,k} - 2(U\phi)_{i-1,j,k} + (U\phi)_{i,j,k}] \quad \text{for } U_{i,j,k} > 0 \end{aligned} \quad (3.91)$$

The parameter ξ can be chosen to increase accuracy or to alter the diffusion-like characteristics. It may be pointed out that $\xi = 3/8$ corresponds to the QUICK scheme of Leonard (1979). However, the discretized second term of the x -momentum equation after the QUICK scheme may be written as

$$\begin{aligned} \left[\frac{\partial(UV)}{\partial Y} \right] &= \frac{0.25}{8\delta Y} [3U_{i,j+1,k}(V_{i,j+1,k} + V_{i,j,k} + V_{i+1,j+1,k} + V_{i+1,j,k}) \\ &+ 3U_{i,j,k}(V_{i,j,k} + V_{i,j-1,k} + V_{i+1,j,k} + V_{i+1,j-1,k}) \\ &- 7U_{i,j-1,k}(V_{i,j-1,k} + V_{i,j-2,k} + V_{i+1,j-1,k} + V_{i+1,j-2,k}) \\ &+ U_{i,j-2,k}(V_{i,j-2,k} + V_{i,j-3,k} + V_{i+1,j-2,k} + V_{i+1,j-3,k})] \\ &\quad \text{for } U_{i,j,k} > 0 \end{aligned} \quad (3.92)$$

and

$$\begin{aligned} \left[\frac{\partial UV}{\partial Y} \right] &= \frac{0.25}{8\delta Y} [-U_{i,j+2,k}(V_{i,j+2,k} + V_{i,j+1,k} + V_{i+1,j+2,k} + V_{i+1,j+1,k}) \\ &+ 7U_{i,j+1,k}(V_{i,j+1,k} + V_{i,j,k} + V_{i+1,j+1,k} + V_{i+1,j,k}) \\ &- 3U_{i,j,k}(V_{i,j,k} + V_{i,j-1,k} + V_{i+1,j,k} + V_{i+1,j-1,k}) \\ &- 3U_{i,j-1,k}(V_{i,j-1,k} + V_{i,j-2,k} + V_{i+1,j-1,k} + V_{i+1,j-2,k})] \\ &\quad \text{for } U_{i,j,k} < 0 \end{aligned} \quad (3.93)$$

We have combined the QUICK scheme of Leonard and a upwind scheme in order to improve the accuracy of discretized convective terms of the governing equations. The upwind discretization of the second term of the x -momentum equation has been accomplished in the following way:

$$\begin{aligned} \left[\frac{\partial UV}{\partial Y} \right]_{up} &= \frac{1}{4\delta Y} [(V_{i,j,k} + V_{i+1,j,k})(U_{i,j,k} + U_{i,j+1,k}) \\ &+ |(V_{i,j,k} + V_{i+1,j,k})|(U_{i,j,k} - U_{i,j+1,k}) \\ &- (V_{i,j-1,k} + V_{i+1,j-1,k})(U_{i,j-1,k} + U_{i,j,k}) \\ &- |(V_{i,j-1,k} + V_{i+1,j-1,k})|(U_{i,j-1,k} - U_{i,j,k})] \end{aligned} \quad (3.94)$$

Finally, the discretization of the term $\partial(uv)/\partial y$ for the x -momentum equation has been accomplished in the following way:

$$\left[\frac{\partial(UV)}{\partial Y} \right] = (1 - \alpha_y) \left[\frac{\partial(UV)}{\partial Y} \right]_{\text{quick}} + \alpha_y \left[\frac{\partial(UV)}{\partial Y} \right]_{\text{up}} \quad (3.95)$$

where, α_y is contribution of the upwind factor. The factor α_y can be found in the following way:

$$\alpha_y = \frac{Re_{\Delta}^c - Re_{\Delta}^{\min}}{Re_{\Delta}^{\max} - Re_{\Delta}^{\min}} \quad (3.96)$$

where,

$$\begin{aligned} Re_{\Delta}^{\min} & \text{ (minimum cell Reynolds number) } = \min \left[\left| \frac{U\delta X}{\nu} \right|, \left| \frac{V\delta Y}{\nu} \right|, \left| \frac{W\delta Z}{\nu} \right| \right] \\ Re_{\Delta}^{\max} & \text{ (maximum cell Reynolds number) } = \max \left[\left| \frac{U\delta X}{\nu} \right|, \left| \frac{V\delta Y}{\nu} \right|, \left| \frac{W\delta Z}{\nu} \right| \right] \\ Re_{\Delta}^c & = \text{calculated cell Reynolds number of any cell.} \end{aligned}$$

The modified third-order upwind scheme is represented by blending the fourth-order central difference of the first derivative and the fourth-order dissipation term. As an example, the discretized second term of the x -momentum equation becomes

$$\begin{aligned} \left[\frac{\partial(UV)}{\partial Y} \right]_{\text{third}} &= \frac{1}{12\delta Y} [U_{i,j,k}V_a - 8U_{i,j-1,k}V_b + 8U_{i,j+1,k}V_c - U_{i,j+2,k}V_d] \\ &+ \frac{\alpha_y |V_e|}{V_e} \times \frac{1}{12\delta Y} \times [U_{i,j-2,k}V_a - 4U_{i,j-1,k}V_b \\ &+ 6U_{i,j,k}V_c - 4U_{i,j+1,k}V_d + U_{i,j+2,k}V_d] \end{aligned} \quad (3.97)$$

where,

$$\begin{aligned} V_a &= 0.25(V_{i,j-2,k} + V_{i,j-1,k} + V_{i+1,j-2,k} + V_{i+1,j-1,k}) \\ V_b &= 0.25(V_{i,j-1,k} + V_{i,j,k} + V_{i+1,j-1,k} + V_{i+1,j,k}) \\ V_c &= 0.25(V_{i,j+1,k} + V_{i,j,k} + V_{i+1,j+1,k} + V_{i+1,j,k}) \\ V_d &= 0.25(V_{i,j+2,k} + V_{i,j+1,k} + V_{i+1,j+2,k} + V_{i+1,j+1,k}) \\ V_e &= 0.25(V_{i,j,k} + V_{i,j+1,k} + V_{i+1,j,k} + V_{i+1,j+1,k}) \end{aligned}$$

The term, α_y is the blending parameter. For $\alpha_y=1$, present third-order scheme becomes similar to another scheme proposed by Leonard (1984). Following a recommendation of Kawamura *et al.* (1986) and Shirayama (1992) $\alpha_y = 3$ has been used in the present investigation.

3.6.2 Comparison of Results based on Model Problem

Three different discretization schemes which have been already discussed in the earlier sections are tested on a model problem of flow in a lid-driven square cavity. In this section, the results obtained by the above mentioned discretization schemes are reported and comparisons are made with the available results.

The computational domain consists of a two dimensional lid-driven square cavity with no-slip and impervious boundary conditions at the bottom and side walls except at the top, where u is a non-zero constant and equal to ULID. In the governing equations, the velocities have been nondimensionalized with respect to ULID. All lengths have been scaled with respect to cavity height H , and the Reynolds number is defined as $Re = (ULID.H)/\nu$. In order to display quantitative information on the velocity field, the velocity vectors for the above mentioned flow field for three different discretization schemes have been shown in Figs. 3.11, 3.12 and 3.13

In Fig. 3.14 u velocity components at the vertical mid plane of the square cavity for a Reynolds number of 400 are plotted. A (42×42) grid is used and the results due to three different discretization schemes are compared with the results obtained by Ghia *et al.* (1982). It may be mentioned that Ghia *et al.* (1982) have employed a 129×129 grid via a multigrid technique. However, Fig. 3.14 shows reasonably good agreement between Ghia *et al.*'s result and all the three cases of present computation. Even otherwise, the positions and the values of the minimum u velocity in position and value of all the computations agree with each other on an overall assessment. The v velocity components at the horizontal mid plane for the same Reynolds number ($Re=400$) are shown in Fig. 3.15. It is evident that the results obtained due to all the three schemes demonstrate reasonably good agreement with the results due to Ghia *et al.* (1982).

This has also been observed that the weighted average scheme takes considerably less CPU time to compute (discussion on computational time has been presented in a subsequent section). The computational accuracy of the weighted average scheme is also calibrated by comparing the peripheral average local Nusselt numbers predicted by our numerical scheme with those of available literature (Shah and London, 1978) for thermally developing and hydrodynamically developed flow through parallel plates. The results are found to be within about 3 percent for a Reynolds number of 500 and uniform wall temperature boundary condition. As such, in the present investigation, we have used weighted average schemes of discretization for computing laminar flows. The turbulent flows have been computed by making use of QUICK-upwinding scheme. For laminar flows, weighted average scheme has been found to be time optimized and reasonably accurate.

We may mention that for laminar flows we have also compared the results due to our weighted average scheme of discretization with those due to QUICK discretization scheme for the problem of our investigation. The combined-spanwise-average Nusselt number ($\overline{Nu_{sa}}$) distribution and the combined-spanwise-average skin friction coefficient

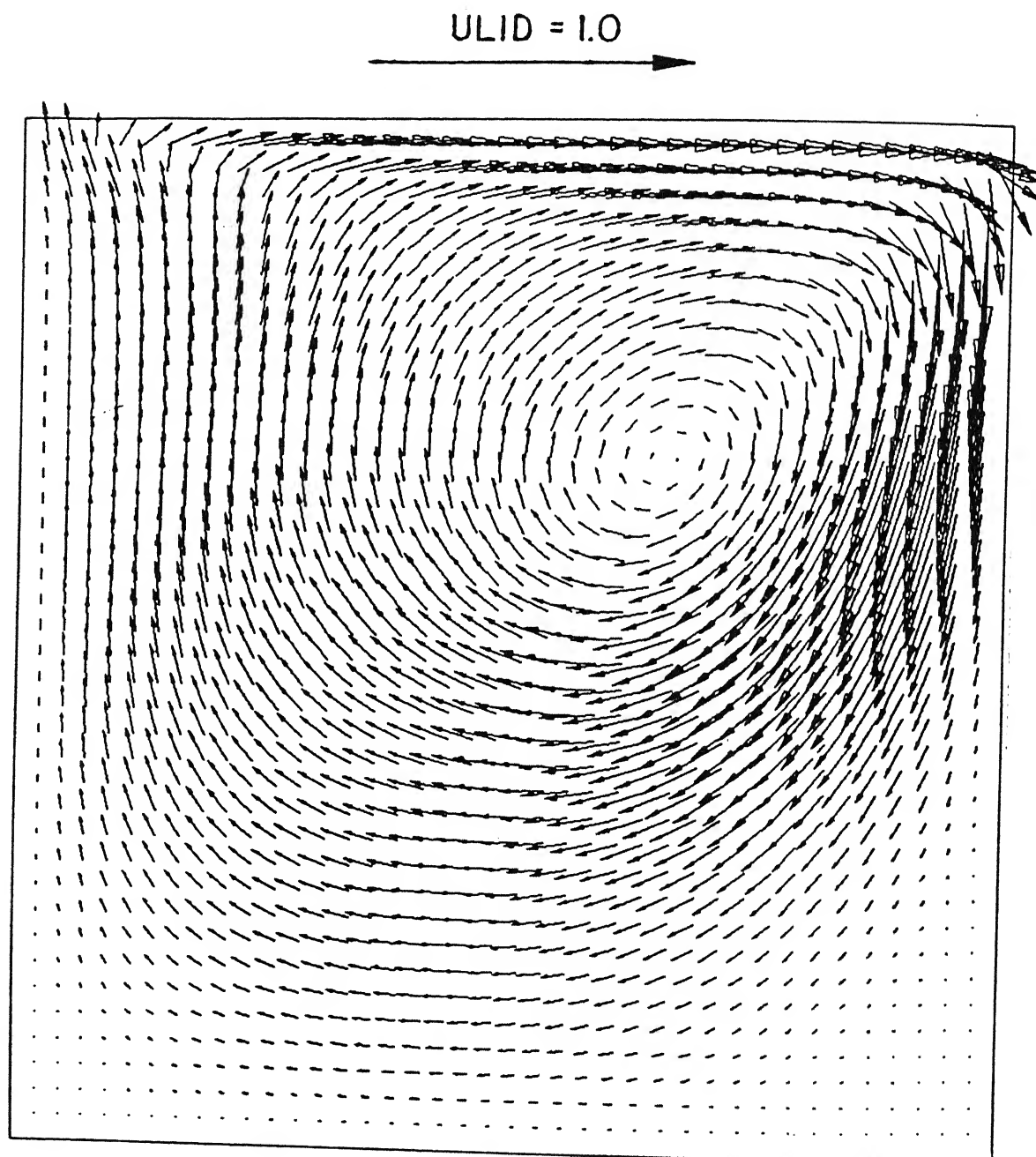


Figure 3.11: Velocity vectors in a lid-driven square cavity for $Re=400$ (42×42 grid); discretization due to Weighted average scheme

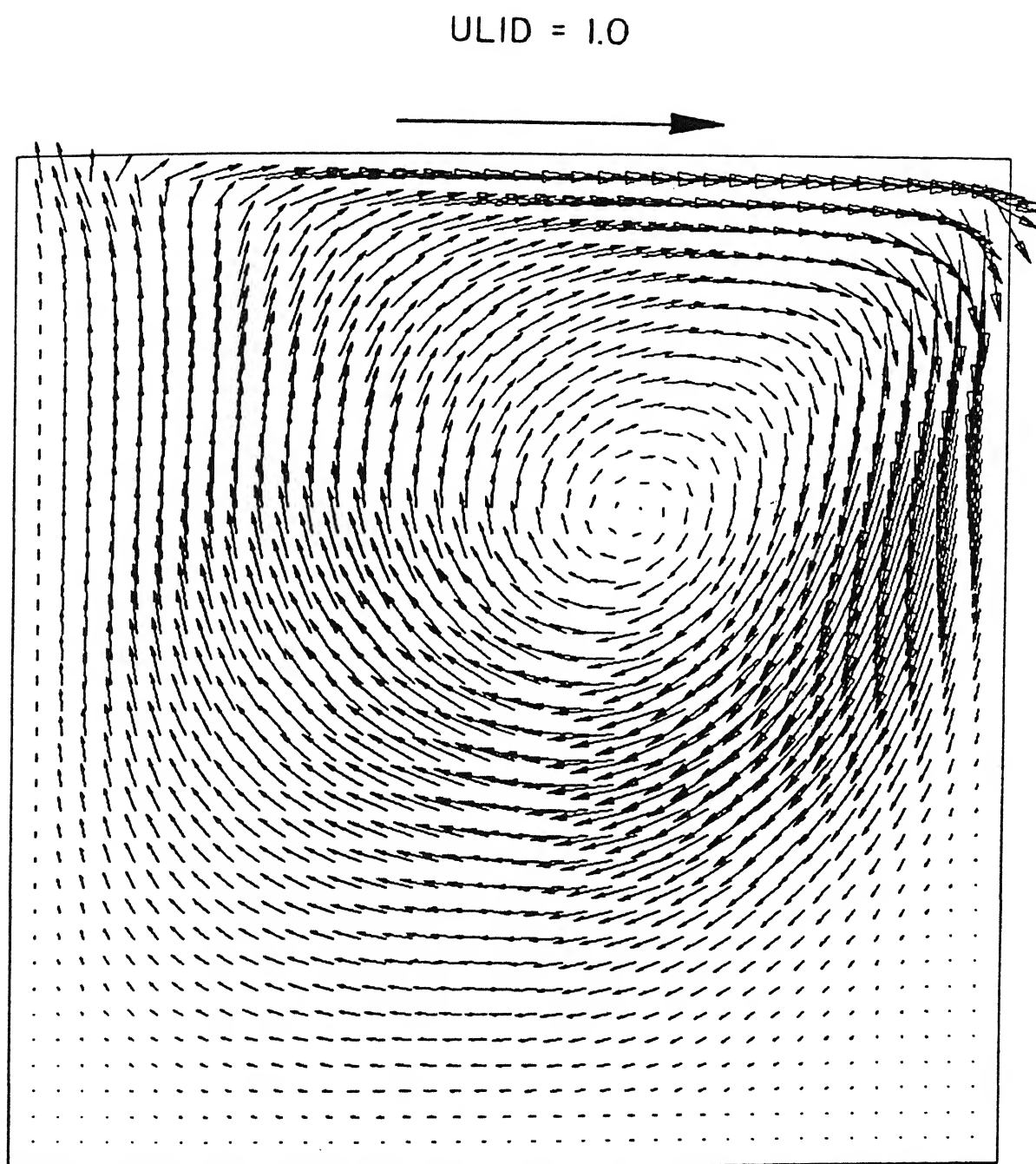


Figure 3.12: Velocity vectors in a lid-driven square cavity for $Re=400$ (42×42 grid); discretization due to QUICK scheme

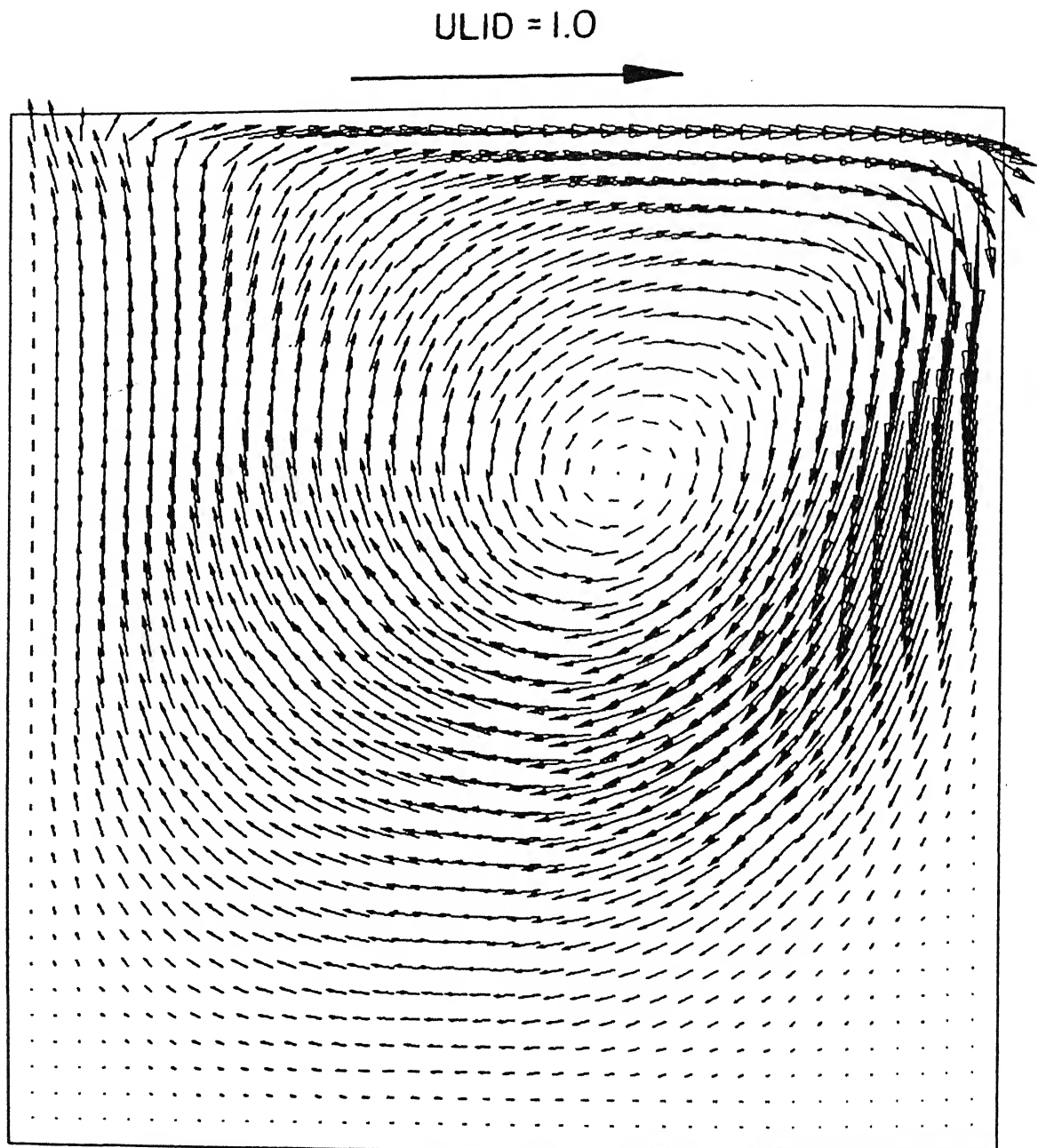


Figure 3.13: Velocity vectors in a lid-driven square cavity for $Re=400$ (42×42 grid); discretization due to third-order upwinding scheme

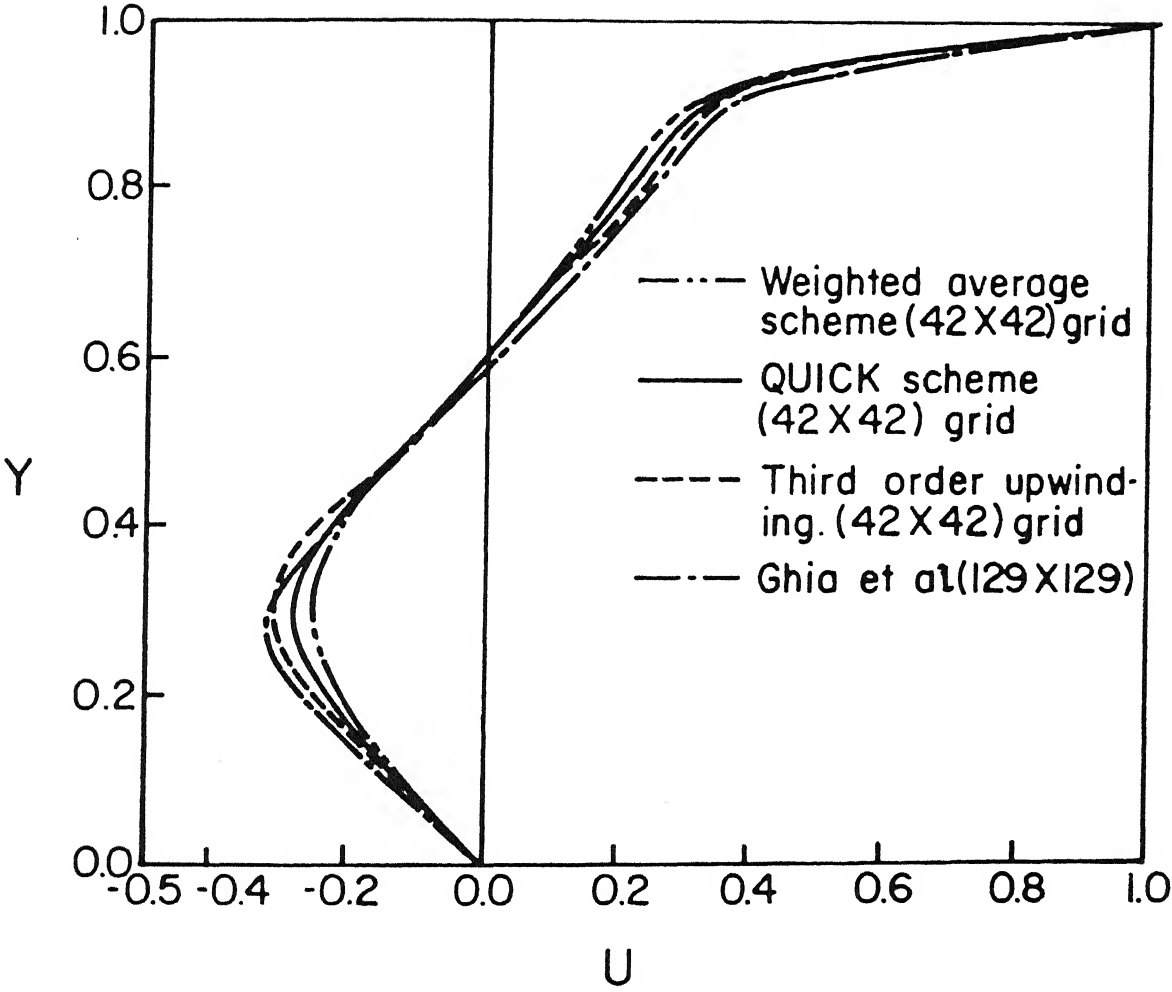


Figure 3.14: Variation of U velocity along the vertical midplane for the lid-driven flow in a square cavity

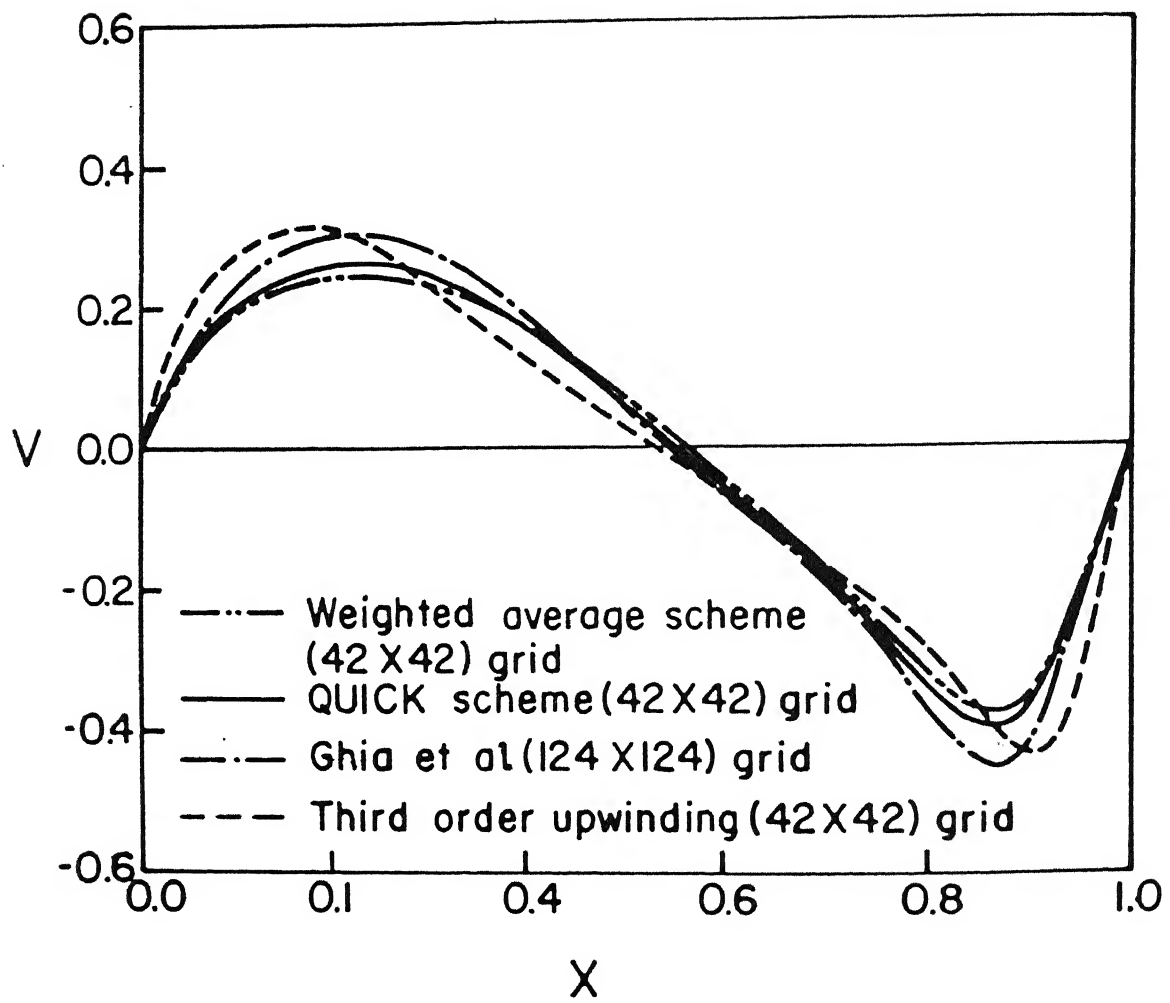


Figure 3.15: Variation of V velocity along the horizontal midplane for the lid-driven flow in a square cavity

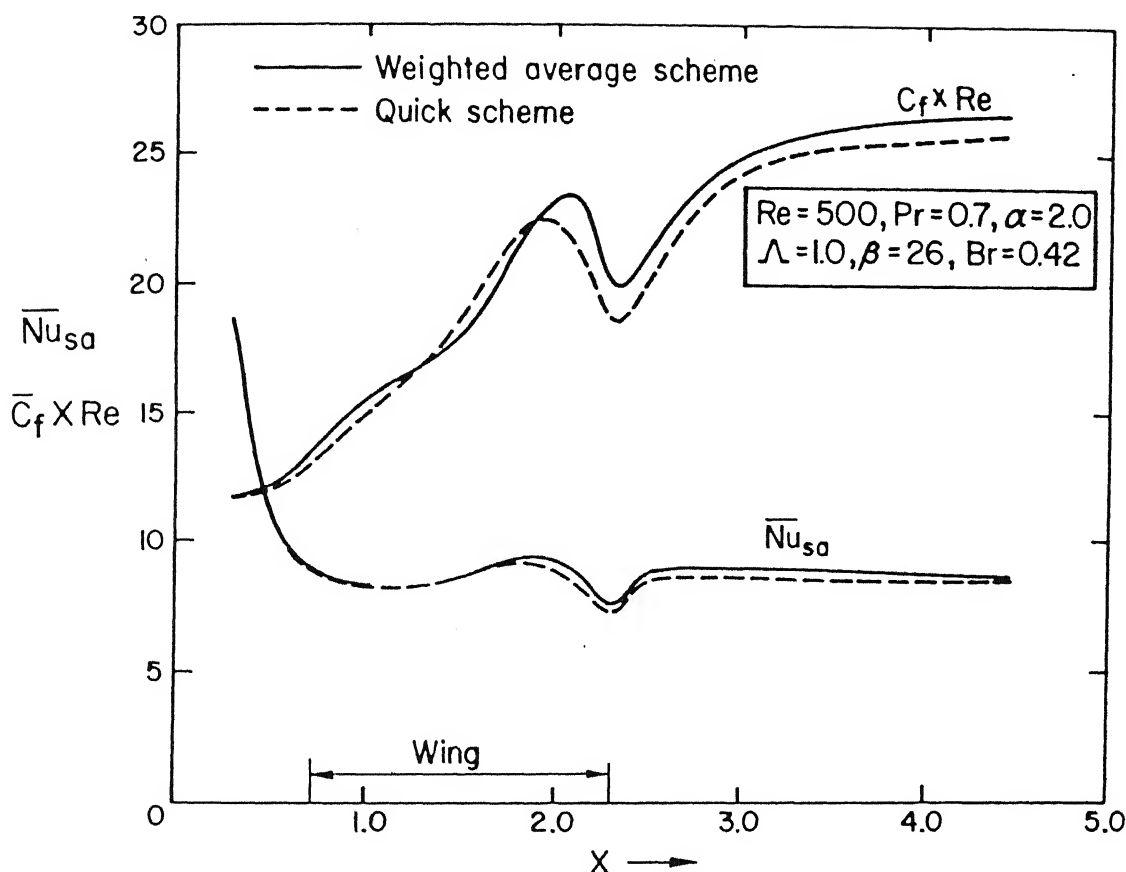


Figure 3.16: Comparison of weighted average scheme with QUICK

$(\overline{C_f} \times Re)$ distribution in a rectangular channel with a built-in delta wing are the parameters which form basis of this comparison. The comparison is shown in Fig. 3.16. Maximum discrepancy in the prediction of \overline{Nu}_{sa} is found to be less than 3 percent.

3.7 Spatial Grid Independence

An effort is undertaken to obtain grid independent results. For $Re=500$ and $Pr=0.7$, in a channel ($\alpha=2$) with a built-in delta wing ($\Lambda=1$) at an angle of attack (β) of 26° , reasonable agreement between the results obtained for 15×26 and 20×30 cross-stream grids is found. In the foregoing specification of cross-stream grids, 15 and 20 refer to the number of grids in the y direction. Similarly, 26 and 30 refer to the number of grids in the z direction. It may be mentioned that for a 15×26 cross-stream grids, 60 grid nodes are taken in x direction for a nondimensional length of 8.4.

Computations are also performed for a shorter channel of nondimensional length 4.3 for three different grids. Other geometrical and flow parameters concerning these computations remain same as the earlier one. Computations for grids $30 \times 10 \times 13$, $30 \times 15 \times 26$ and $30 \times 30 \times 52$ have been carried out. The grids are specified in x , y and z directions respectively. However, the extrapolated grid-independent average Nusselt number differs from the corresponding Nusselt number obtained with the coarsest grid by less than 10 percent. A grid size of $30 \times 15 \times 26$ produces average Nusselt number which differs from this extrapolated grid-independent average Nusselt number by less than 3 percent. Hence most of the computations are done by using a 15×26 cross-stream grids. In some cases, cross-stream grids finer than (15×26) are used for special requirements, *viz.*, accommodating some typical obstacle position and obtaining a closer point near the wall in the case of turbulent flow computations. The grids in the streamwise directions are suitably chosen to cover the required length of the channel with a reasonably good accuracy.

3.8 Computational Time

In the problem of a channel with a built-in delta wing, for a grid size of $60 \times 15 \times 26$ (in x , y and z directions respectively) and Reynolds number of 1000 (laminar flow) the CPU time with respect to steady solution is 157 min.

For a Reynolds number of 15000 (turbulent flow), the corresponding CPU time with respect to steady solution is 620 min and the grid size is $30 \times 15 \times 27$.

The laminar flow computations are performed on a HP-9000/850 series computer whereas the computations for the turbulent flows are performed on a CONVEX C-220 computer. The CONVEX C-220 consists of 2 processors with 128 MB RAM and 2 GB disk space.

Chapter 4

Evaluation of Performance Parameters for Laminar Flow

4.1 Introduction

Transport-enhancement in fin-tube and plate-fin heat exchangers is the essential goal of this investigation. Improvement in heat transfer is attributed to the decrease in thermal resistance owing to the spiraling motion of the flowing fluid. Thus the main quantities of interest are the enhancement of heat transfer and the corresponding flow losses. In this study a detailed numerical simulation has been done on an element of an heat exchanger which is representative of a part in the core region of the above mentioned heat exchangers. This chapter presents the results of the simulation for flow and heat transfer in a channel with both the vortex generators, viz., delta wing and delta winglet-pair. The first part of this chapter presents the performance of a delta wing as a vortex generator. In order to evaluate performance of the winglet-pair as the promoters of enhanced heat transfer, the latter part of this chapter presents simulation of flow and heat transfer in the configuration of a channel with built-in winglet-pair. The results presented in this chapter are in the laminar-flow regime.

4.2 Performance of Delta Wing-Type Vortex Generators

A number of computations have been performed at different angles of attack (β) with a delta wing as a vortex generator. For slender delta wing in an infinite medium, leading edge vortices have a spiraling structure and they diverge slightly. Now, when we envision a wing moving in an infinite medium, the wake grows longer and basically becomes a swirling flow supported by trailing vortices. However the flow in a channel with an attached delta wing shows no trailing edge vortices. Figure 4.1 shows the generation of

vortices and their deformation as they move along the channel in presence of a delta wing. Deformation takes place due to the reduction in strength of the vortices which is brought about by the viscous resistance of the wall. The cross stream velocity vectors at different axial locations are shown in this figure.

Figure 4.2 illustrates the static pressure distribution on the cross planes at the same axial locations for the same geometrical and flow parameters as those of Fig. 4.1. The nondimensional static pressure ($p/\rho U_{av}^2$) contours follow the same qualitative trends as those observed in experiments conducted by Hummel (1978).

Development of streamwise vorticity, normalized with the mean axial velocity and the channel height, is presented in Fig. 4.3. Dotted lines indicate negative vorticity. Peak vorticity occurs in the vortex centers. However, the peak vorticity in the vortex core decreases in the downstream direction. Reynolds number for this case is 1000 and the angle of attack of the wing is 20° .

The isolines for the axial velocity at two different axial locations behind the wing are shown in Fig. 4.4. On the base plate behind the wing, the vortices lead to a thinning of velocity boundary layer in the downwash region at the wing symmetry plane and thickening at the array symmetry plane.

Figure 4.5 shows the isotherms over eight cross-planes located at eight different axial locations in a channel for $Re = 1500$ and $Pr = 0.7$. It is seen that as the fluid stream moves from an axial distance $X = 1.268$ to $X = 5.706$, the value of the isotherms in the core region increases and consequently the bulk temperature keeps on rising. The relative location of the wing has been shown clearly in this figure. Due to the spiraling structure of the flow behind the wing, there is a mixing of cooler stream of the core with the hot fluid from the wall and thus, as can be observed, the core temperature rises in the downstream.

However, the heat transfer and the skin friction coefficients, the major performance parameters are dependent on the type of the obstacle (wing or winglet pair), the Reynolds number and the geometrical parameters of the obstacle. In the following sections we shall discuss the influence of these governing parameters on the performance of vortex generators. Air has been assumed as the working fluid; hence the Prandtl number of this study is fixed at a constant value of 0.7.

In order to have a quantitative distinction of the heat transfer performance, the combined spanwise Nusselt number

$$\overline{Nu}_{sa} = \frac{B(q_1 + q_2) (H/k)}{2 \int_0^{B/2} (T_{w1}(x, z) - T_b(x)) dz + 2 \int_0^{B/2} (T_{w2}(x, z) - T_b(x)) dz} \quad (4.1)$$

has been calculated at each longitudinal location to depict heat transfer at any axial position in the channel.

Fig. 4.6 shows the influence of angle of attack on heat transfer. It is observed that the combined spanwise average Nusselt number increases with increasing angle of attack. Wings with higher angles of attack (until vortex breakdown takes place) produce vortices

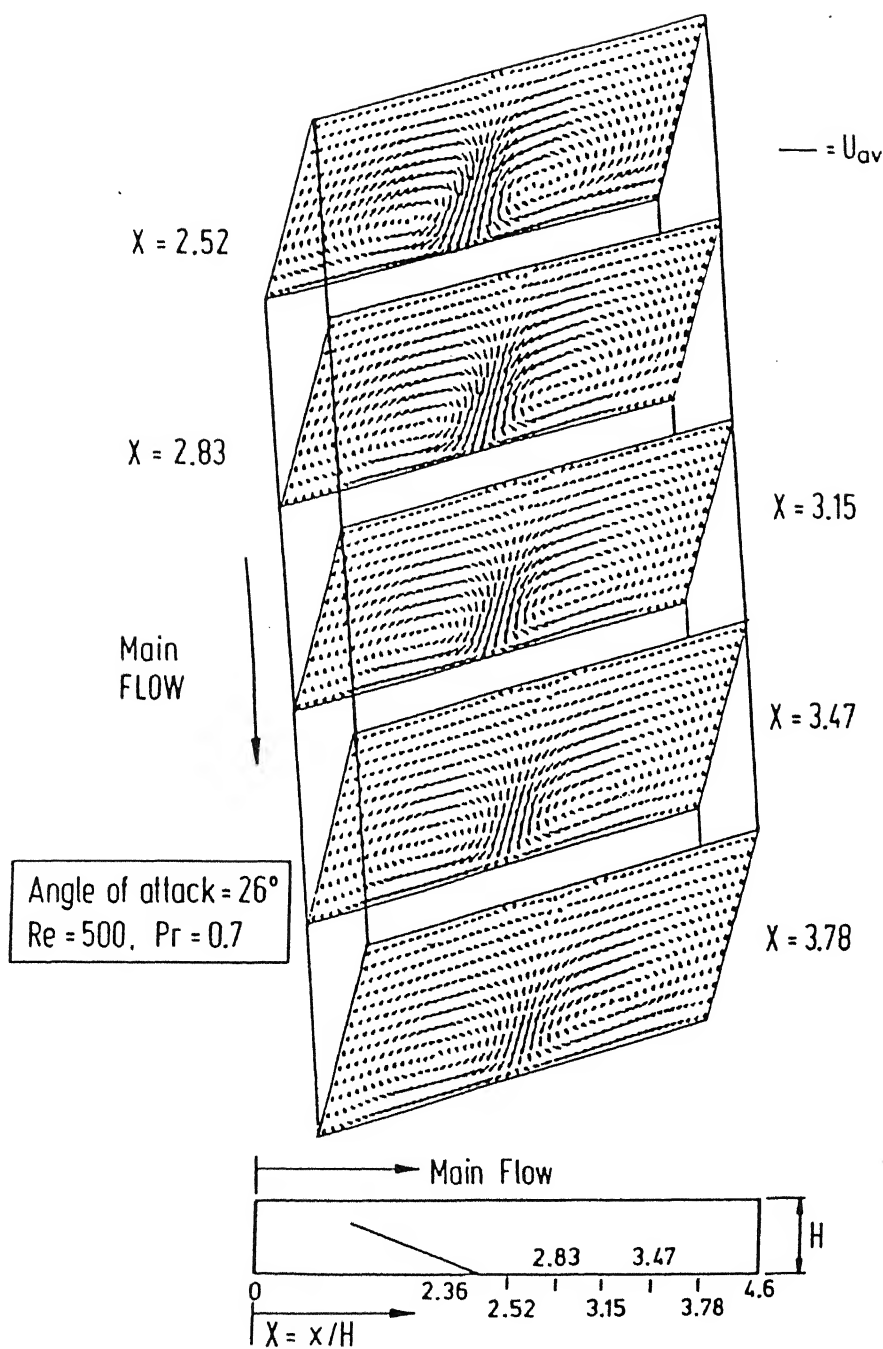


Figure 4.1: Cross-stream velocity vectors at different axial locations behind the wing showing generation and deformation of vortices in the channel

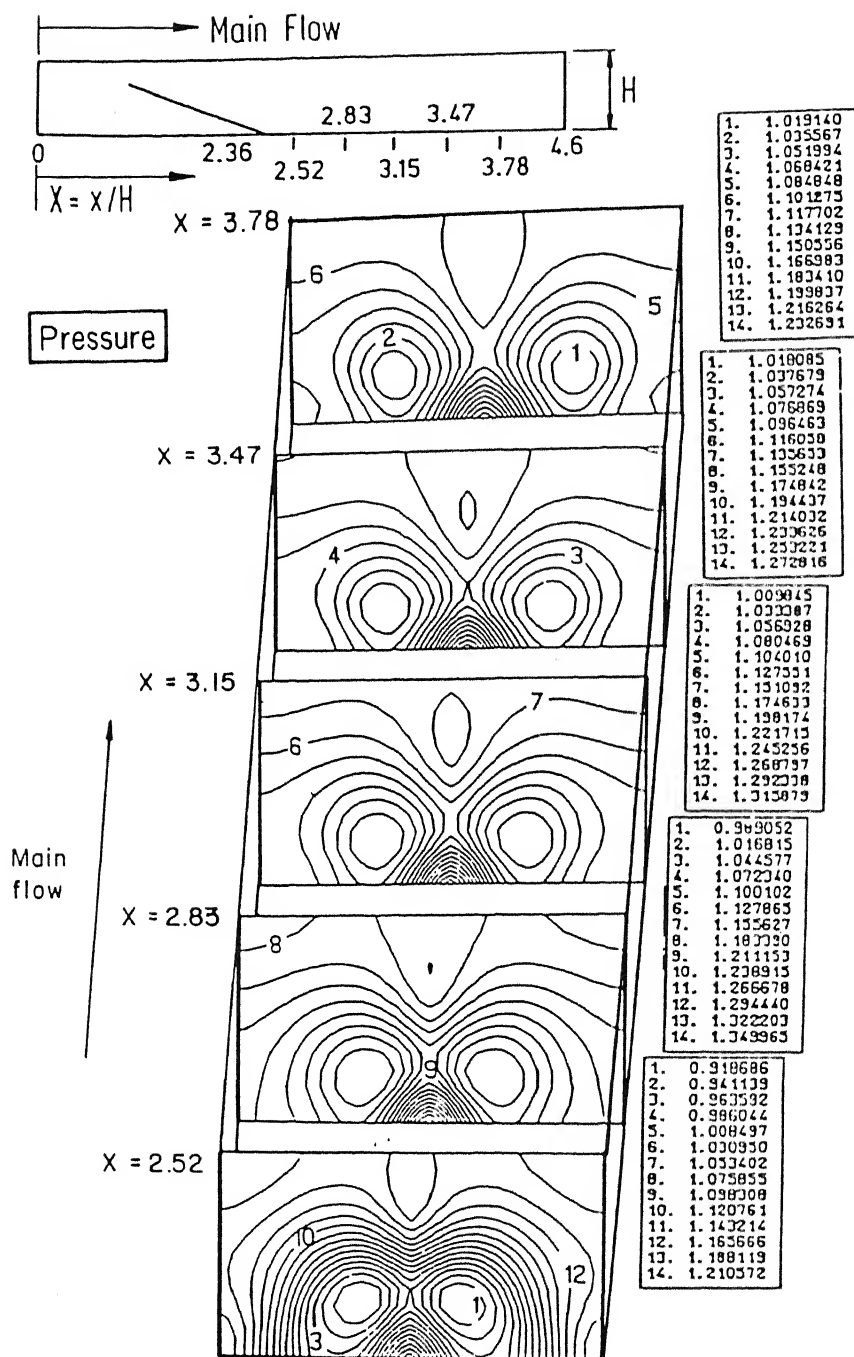


Figure 4.2: Static pressure distribution at different axial locations behind the delta wing

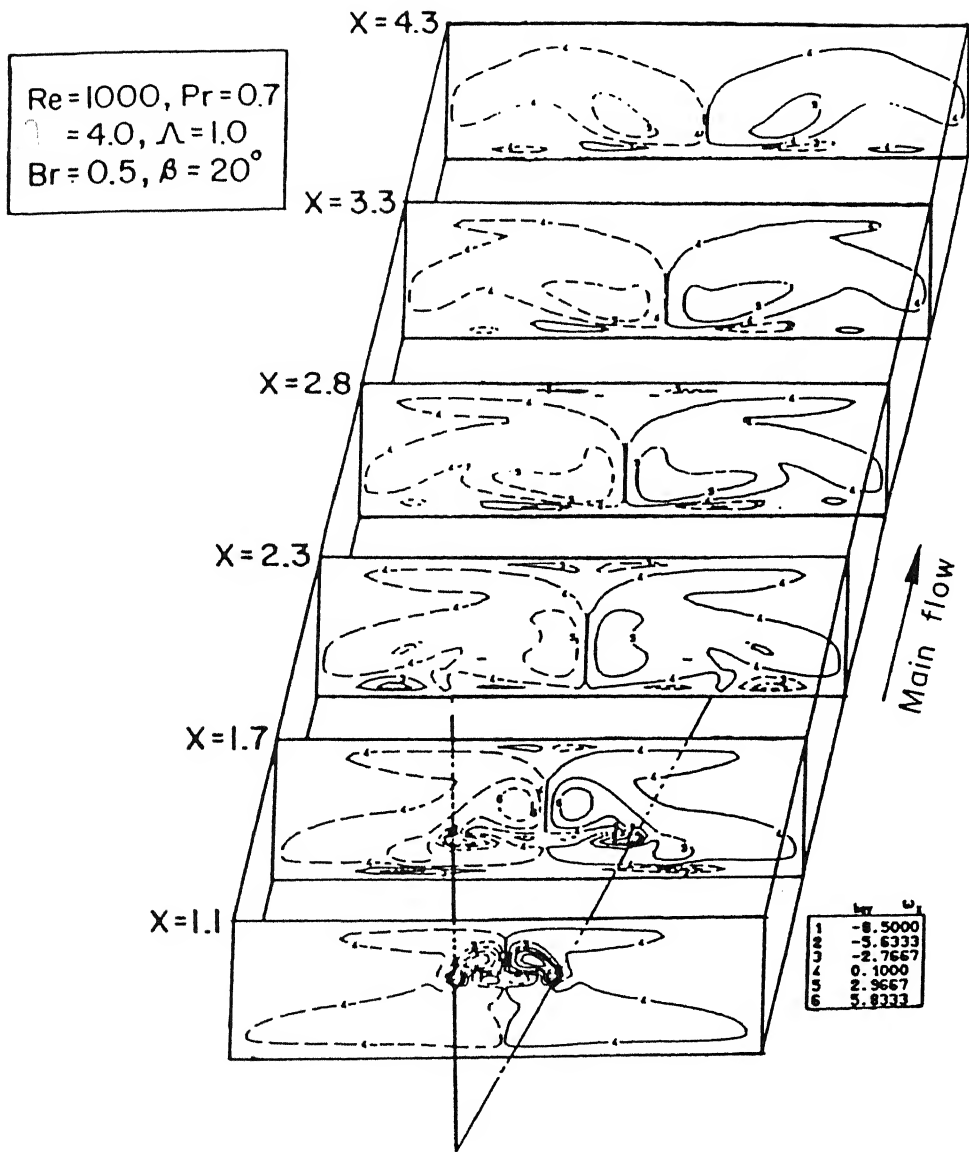


Figure 4.3: Contours of normalized streamwise vorticity at different cross-sections of the channel in presence of a delta wing

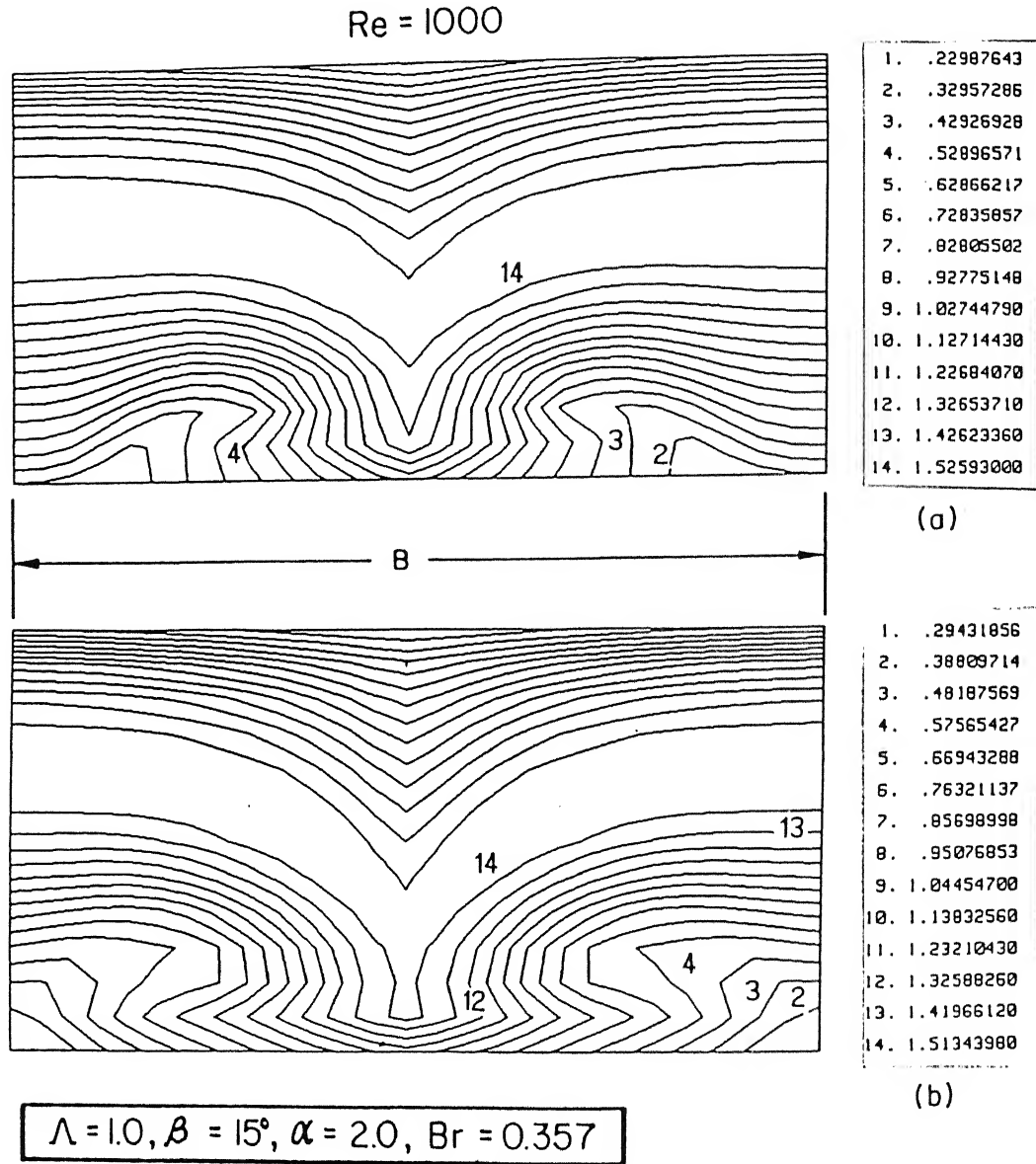


Figure 4.4: Isolines for axial velocity at two different cross-stream planes (a) 0.58 wing-chord downstream and (b) 1.74 wing-chord downstream of a delta wing

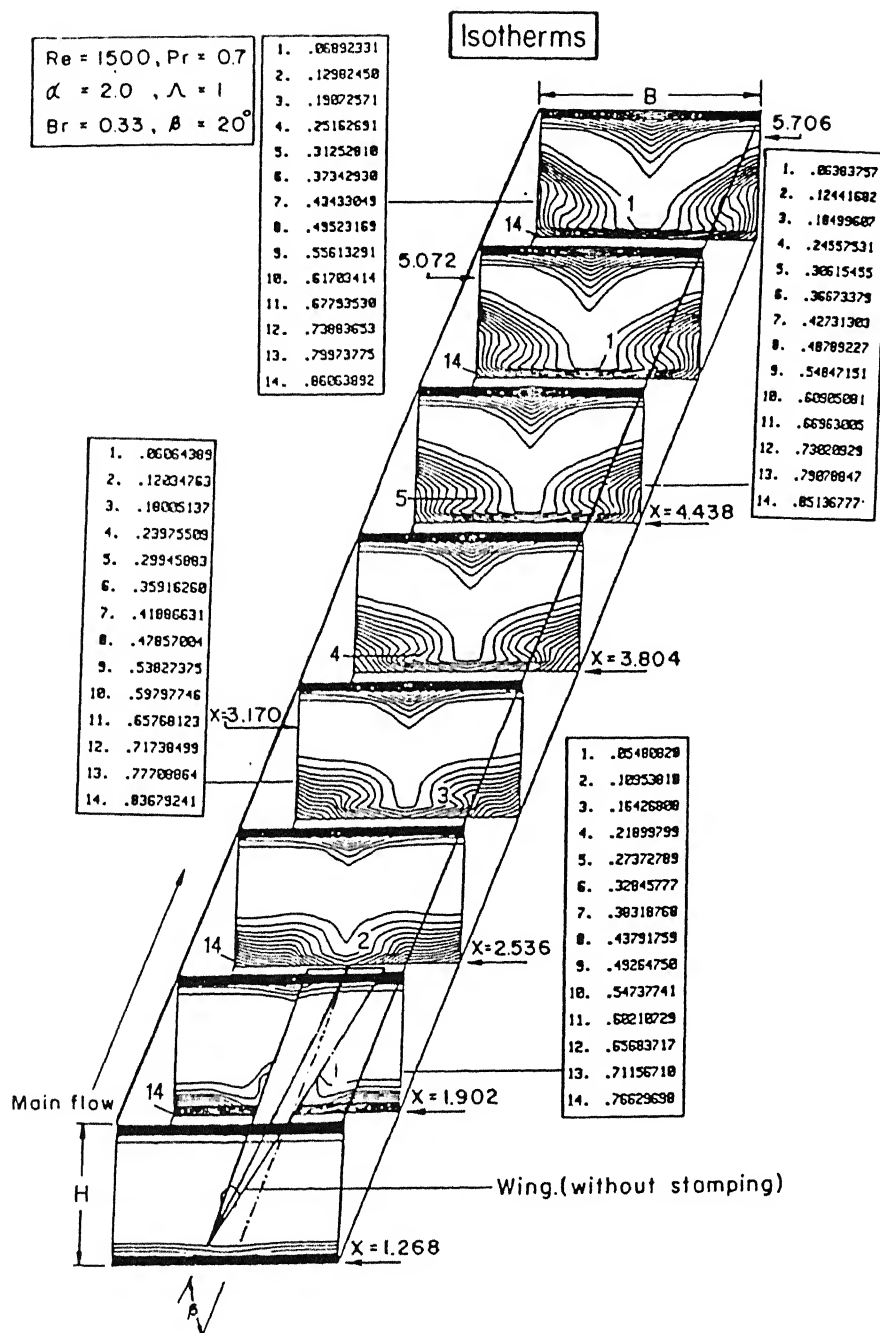


Figure 4.5: Isotherms at different cross-planes in the channel in presence of built-in delta wing

with higher strength which results in better heat transfer. At a nondimensional axial location of 4 from the inlet, for an angle of attack of 25° , we observe an enhancement of 37 percent in combined spanwise average Nusselt number over the case of channel without obstacle. Furthermore, at the same location, for $\beta=35$, an improvement of 8.87 percent in \overline{Nu}_{sa} is obtained over the case with $\beta = 25^\circ$.

In the above mentioned case, a fully developed velocity profile was considered at the inlet of the channel. For a developing flow, the effect of flow development in the channel and the effect of vortex generators on the flow field are superimposed in the downstream. In the earlier case, in order to distinguish the effect of vortex generators (to eliminate the effect of flow development), a fully developed velocity profile at the inlet was deployed. However, here we shall include the effect of developing flow and the influence of punched holes beneath the vortex generators on the heat transfer performance.

Figure 4.7 shows the comparison of cross-stream velocity vectors at different axial locations from the inlet of the channel for the cases without and with stamping on the solid walls. Due to the stamping on the walls, a velocity field normal to the vortex motion is induced in the downstream direction. This induced downward normal velocity field reduces the strength of the vortex flow and as compared with the case where there is no stamping, a decayed circulatory flow pattern is observed at the same axial location.

Figure 4.8 shows the heat transfer performance in a channel for a simultaneously developing flow (Kakac, Shah and Aung, 1987) in presence of a delta-wing. Figure 4.8 also compares the heat transfer on the channel walls for the with and without stamping cases. For the case of without stamping, in the region of the wing (from $X = 2.92$ to $X = 3.79$), the combined spanwise average Nusselt number rises to a high value of 10 and then takes a plunge. A small dead water zone exists in the immediate neighborhood behind the wing-wall junction which causes poor heat transfer at that location. However, in the downstream of the wing, heat transfer is increased remarkably as compared with the plane channel flow. As such, even for a very long channel ($X = 10.28$), the enhancement of the heat transfer at the exit of the channel is more than 46 percent. The enhancement is not so pronounced when the effect of a punched hole beneath the wing is taken into account. Due to the downward normal stream at the cross-planes (as shown in Fig.4.7), the strength of the longitudinal vortices is reduced to a great extent although a spiraling flow pattern still exists. The improvement in the heat transfer coefficient is relatively less than that of the case without any punched hole. However, at the exit of the channel, the improvement of heat transfer is about 29 percent as compared with the plane channel.

Figure 4.9 shows the lateral distribution of local heat transfer coefficients (local Nusselt numbers) at different axial locations behind the wing on the bottom plate of the channel. As one moves downstream, the peak of the local Nusselt number reduces and the lateral extent of the heat transfer enhancement widens slightly.

The effect of Reynolds number on combined spanwise average Nusselt number is clearly evident from Fig. 4.10. Higher Reynolds number signifies greater mass flow rate

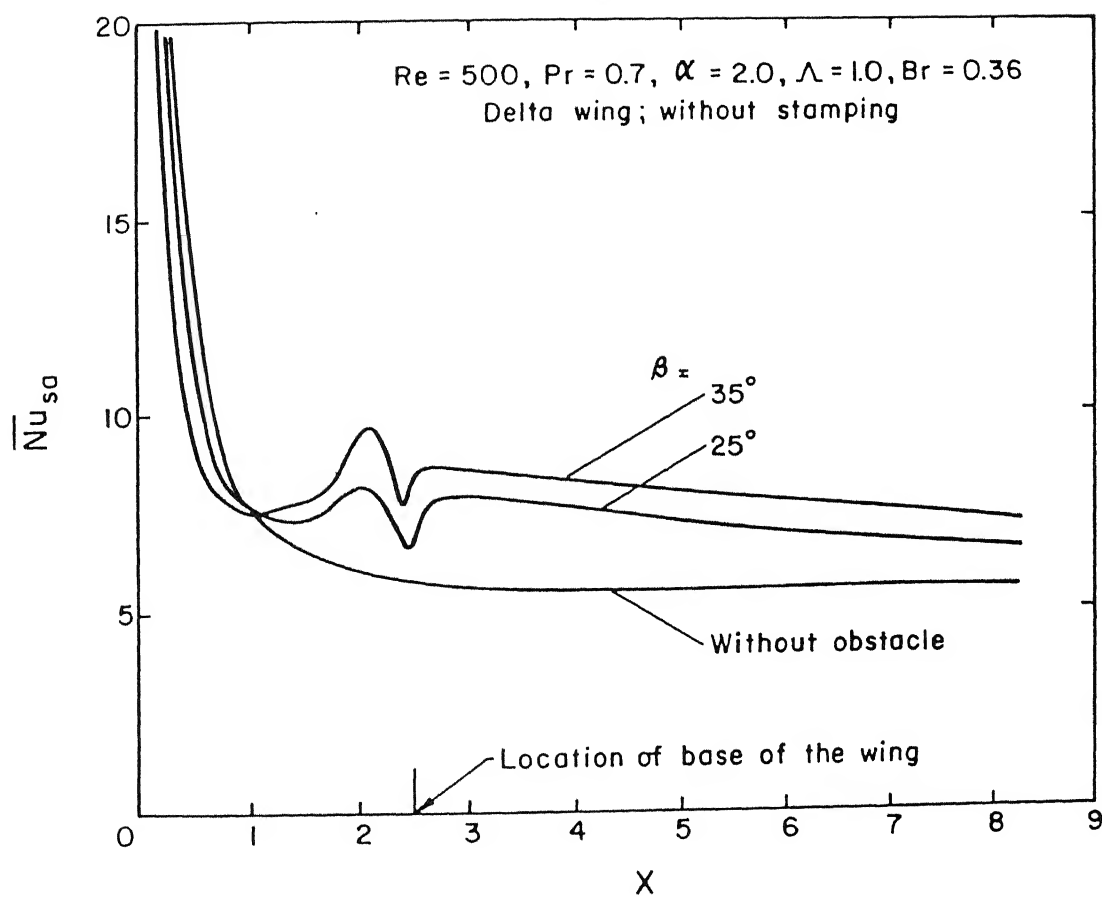


Figure 4.6: Effect of angle of attack of the delta wing on the distribution of combined spanwise-average-Nusselt-number in the channel

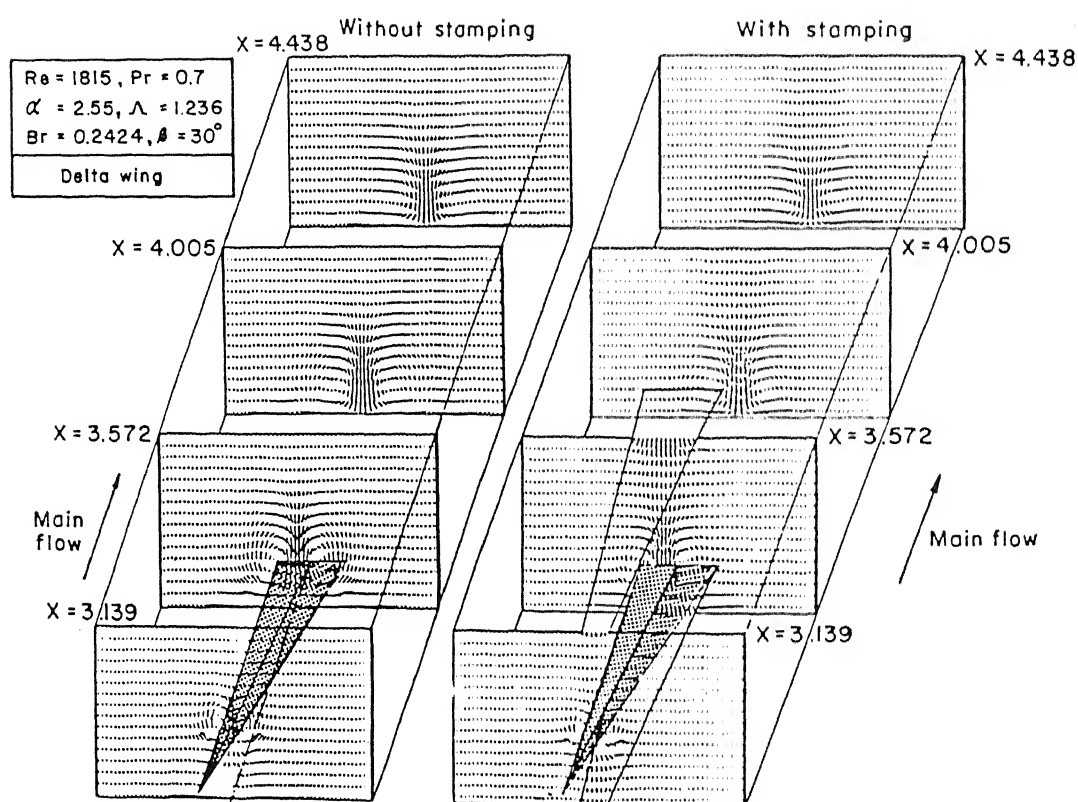


Figure 4.7: Effect of stamping on cross-stream velocity vectors at different axial locations in the channel with delta wing as the obstacle

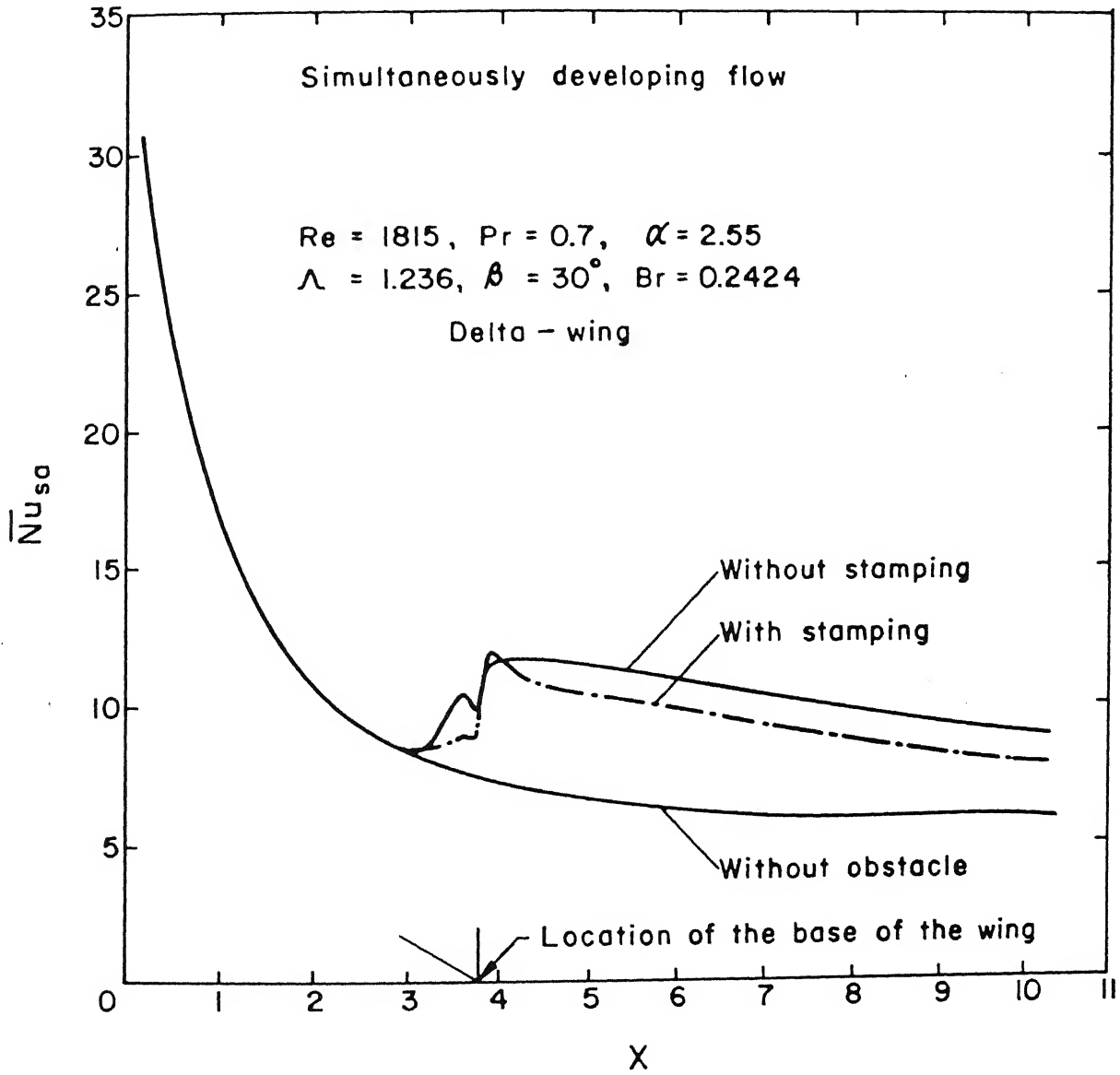


Figure 4.8: Effect of stamping on the distribution of combined spanwise average Nusselt number in the channel; simultaneously developing flow

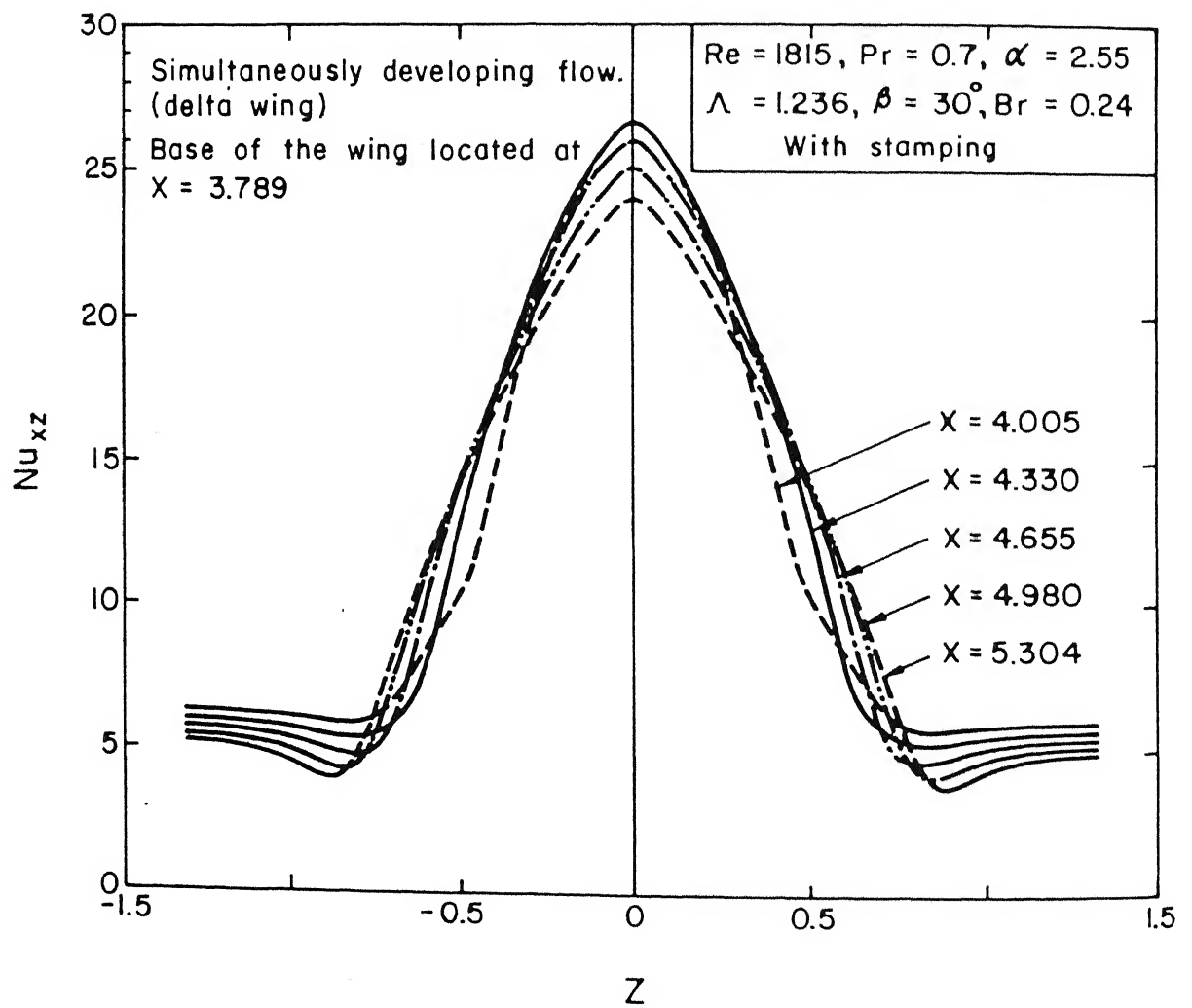


Figure 4.9: Lateral distribution of local Nusselt number at different axial locations in the channel

and consequently higher vortex strength is obtained ensuring better heat removal. At the exit of a moderately long channel ($X = 8.25$), \overline{Nu}_{sa} for $Re = 1000$ is 37 percent higher than that for $Re = 500$. However, at the same location, improvements of 69 and 96 percent over the case of $Re = 500$ are observed for the Reynolds numbers of 1500 and 2000 respectively. In each case, the Nusselt number distribution for plane channel flow has been shown by the dotted lines. In this study, the length of the channel is well below the thermal entry length. What we have illustrated here is the influence of Reynolds number on the enhancement of heat transfer in a thermally developing flow. It may be mentioned that the fully developed Nusselt number (in our case $Nu = hH/k$) for a channel flow with uniform wall temperature boundary condition is 3.77.

Augmentation of heat transfer is obtained at the price of increasing pressure drop. As we have mentioned earlier, the increase in pressure drop is relatively less when wing-type vortex generators are used for enhancing heat transfer coefficients. In order to show the aforesaid performance of wing-type vortex generators, the combined spanwise average friction coefficient has been defined as

$$\overline{C}_f = \frac{\mu[2 \int_0^{B/2} \left(\frac{\partial u}{\partial y}\right)_{y=0} dz + 2 \int_0^{B/2} \left(\frac{\partial u}{\partial y}\right)_{y=H} dz]}{\frac{\rho}{2} U_{av}^2 (2B)} \quad (4.2)$$

Figure 4.11 shows the effect of varying the vortex generator's angle of attack keeping the size constant. Increasing the angle of attack has the effect of increasing the vortex circulation which increases resistance and a higher value of combined spanwise average friction coefficient is obtained. We may mention here that our friction coefficient is not similar to Darcy's friction factor, rather, it is average Fanning's friction factor. However at the exit of the channel, $(\overline{C}_f \times Re)$ for $\beta = 25^\circ$ is 60 percent more than that for the plane channel and $(\overline{C}_f \times Re)$ for $\beta = 35^\circ$ is 12 percent more than that for $\beta = 25^\circ$. We have considered thermally developing and hydrodynamically developed flow herein. For the plane channel, $(\overline{C}_f \times Re)$ value remains unchanged (=12) throughout, which is the exact solution for plane Poiseuille flow. This observation is a check for computational accuracy as well.

Figure 4.12 shows the distribution of combined spanwise average friction coefficient $(\overline{C}_f \times Re)$ for three different cases. The plot clearly shows the effect of stamping on the distribution of the $(\overline{C}_f \times Re)$. Here we have considered a simultaneously developing flow. For a very long channel, at the exit ($X = 10.28$), the increase in $(\overline{C}_f \times Re)$ for the case with a built-in wing-type vortex generator (without stamping) over that for a plane channel is 64.71 percent, whereas this value of friction coefficient $(\overline{C}_f \times Re)$ is only 49.44 percent more than the plane channel value when the effect of the punched hole under the wing is taken into account. The reason for this reduction in friction coefficient is attributed to the spiraling flow with relatively less vortex strength. Strength of the vortical motion is reduced due to the interference with the downward normal stream created at the location of the punched hole which is also evident from Figure 4.7.

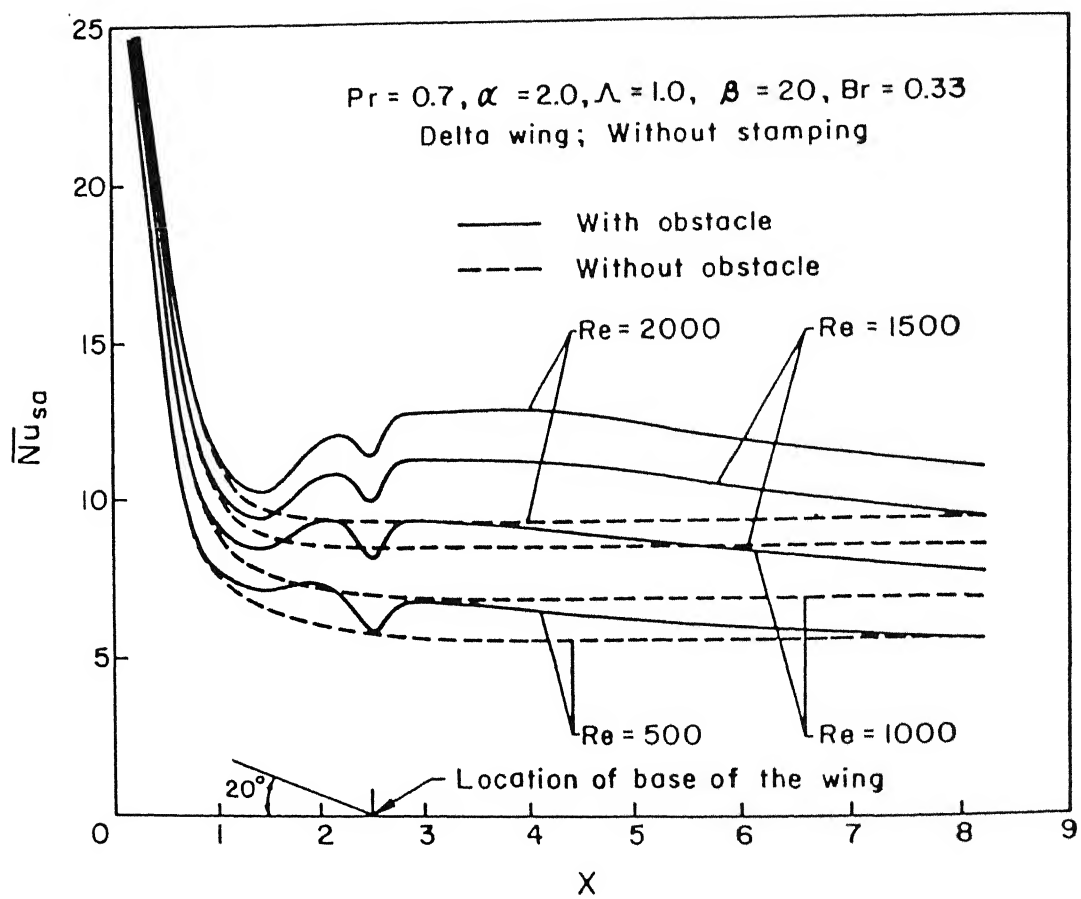


Figure 4.10: Effect of Reynolds number on the distribution of combined spanwise average Nusselt number in the channel with and without the delta wing

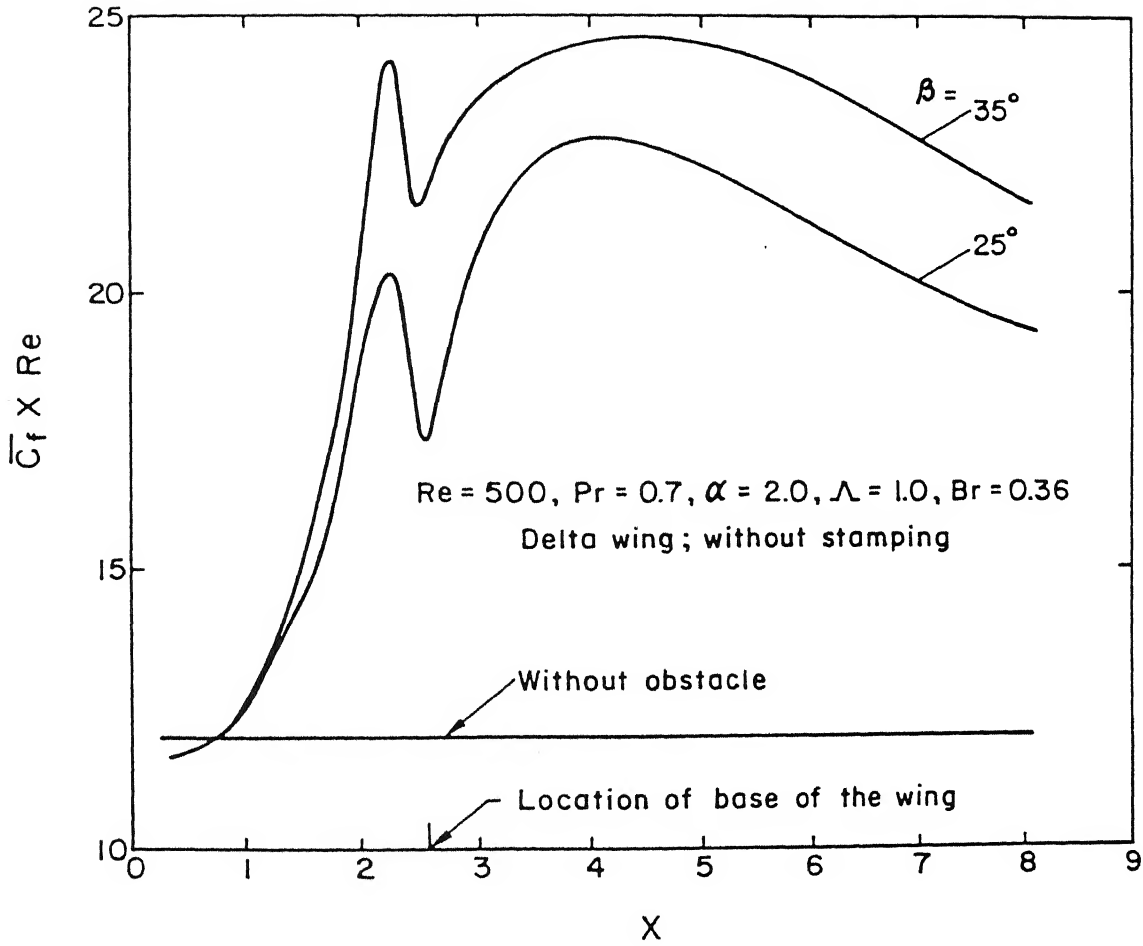


Figure 4.11: Effect of angle of attack of delta wing on the distribution of combined spanwise-average-friction-coefficient in the channel

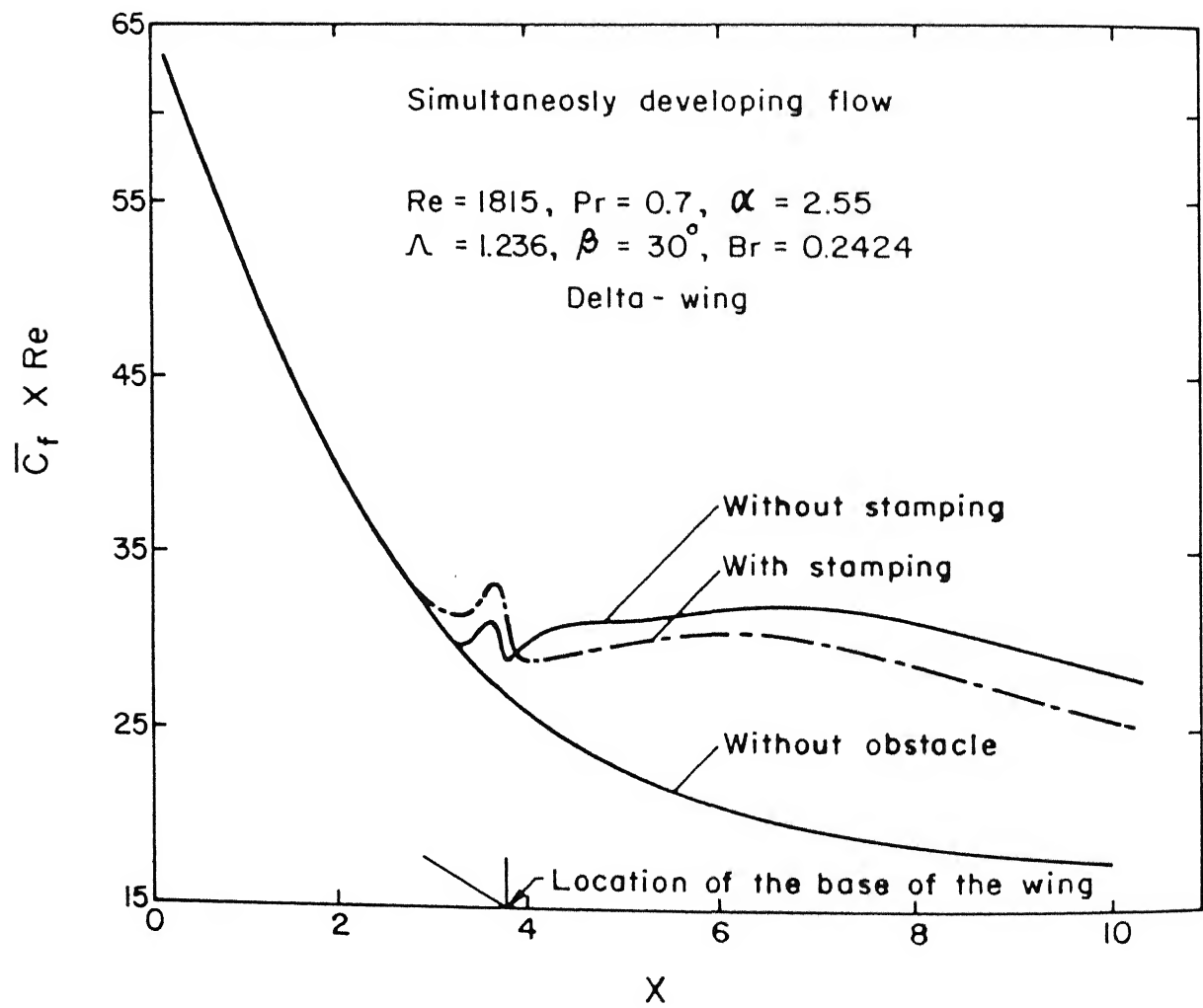


Figure 4.12: Effect of stamping on the distribution of combined spanwise average friction coefficient in the channel; simultaneously developing flow

Figure 4.13 shows the effect of Reynolds number on $(\bar{C}_f \times Re)$ while keeping the parameters related to channel and the vortex generator constant. At the exit of the channel ($X = 8.24$), $(\bar{C}_f \times Re)$ for $Re=1000$ is about 42 percent greater than that for $Re=500$. At the same location, $(\bar{C}_f \times Re)$ for $Re=1500$ and $Re=2000$ are about 76 percent and 101 percent greater than that for $Re=500$ respectively. A higher mass flow rate increases the strength of the vortices which eventually results in a higher drop in skin friction.

4.3 Performance of Delta Winglet-Pair Type Vortex Generators

As we have discussed earlier, the flow in a channel with an attached delta wing shows no trailing edge vortices. For the configuration of interest, the main difference between the wing and winglet is that the winglet has a free trailing edge whereas the wing has no trailing edge (wing span is attached to the plate).

Figure 4.14 shows cross-stream velocity vectors at various axial locations of the channel with a built-in winglet-pair. For the winglet-pair the vortices do not have to turn as abruptly near the trailing edge as they do for the wing. However, in order to have a lucid understanding of the structure secondary flow, various magnified scales for the average axial velocity have been used for different cross-stream planes.

Normalized streamwise vorticity contours for the above mentioned case have been shown in Fig. 4.15. The dotted lines indicate negative vorticity. Peak vorticity occurs in the vortex centers and near the symmetry sides (side walls) where the symmetry boundary conditions lead to rapid change in the direction of flow of the secondary vortices.

Figure 4.16 shows the isotherms at different cross-planes in a channel in presence of a delta winglet-pair. The vortex generators influence the temperature field strongly. The spreading of isotherms over a wider region of the cross-section implies that the bulk temperature is higher in the downstream from the trailing edges of the winglet-pair. The importance of the secondary flow and the higher heat transfer is evident from this picture.

Figure 4.17 shows the influence of angle of attack of the winglet-pair on combined spanwise average Nusselt number in the channel (equation 4.1). At a nondimensional distance of 4 from the inlet, for an angle of attack of 20° , we observe an enhancement of 30 percent in the combined spanwise average Nusselt number over the case of a plane channel. Now, at the same location, for an angle of attack of 26° , an improvement of about 6 percent in \overline{Nu}_{sa} over the case of the 20° angle of attack is obtained. However, at the same location, an improvement of 12 percent over the case of 20° angle of attack is discerned for $\beta = 32^\circ$. The winglets with higher angle of attack produce vortices with higher strength, which in turn results in improved heat transfer.

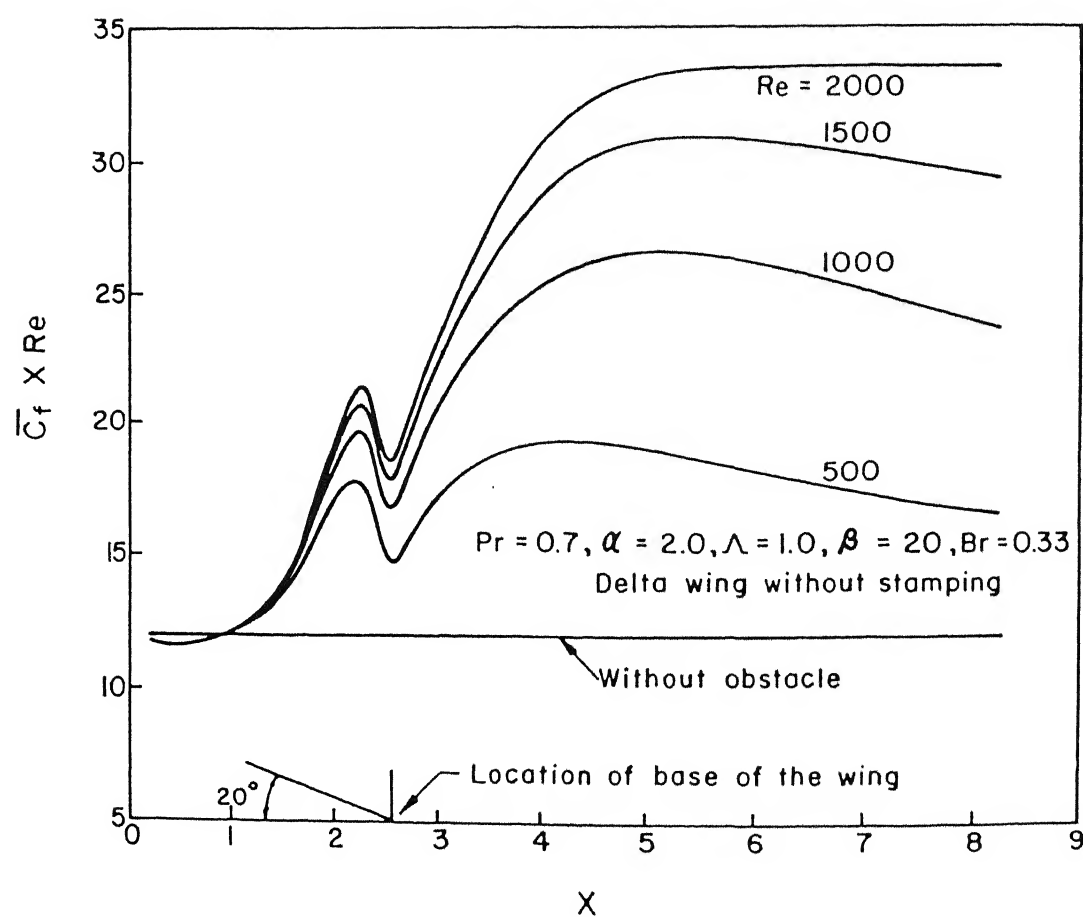


Figure 4.13: Effect of Reynolds number on the distribution of combined spanwise average friction coefficient in the channel with and without the delta wing

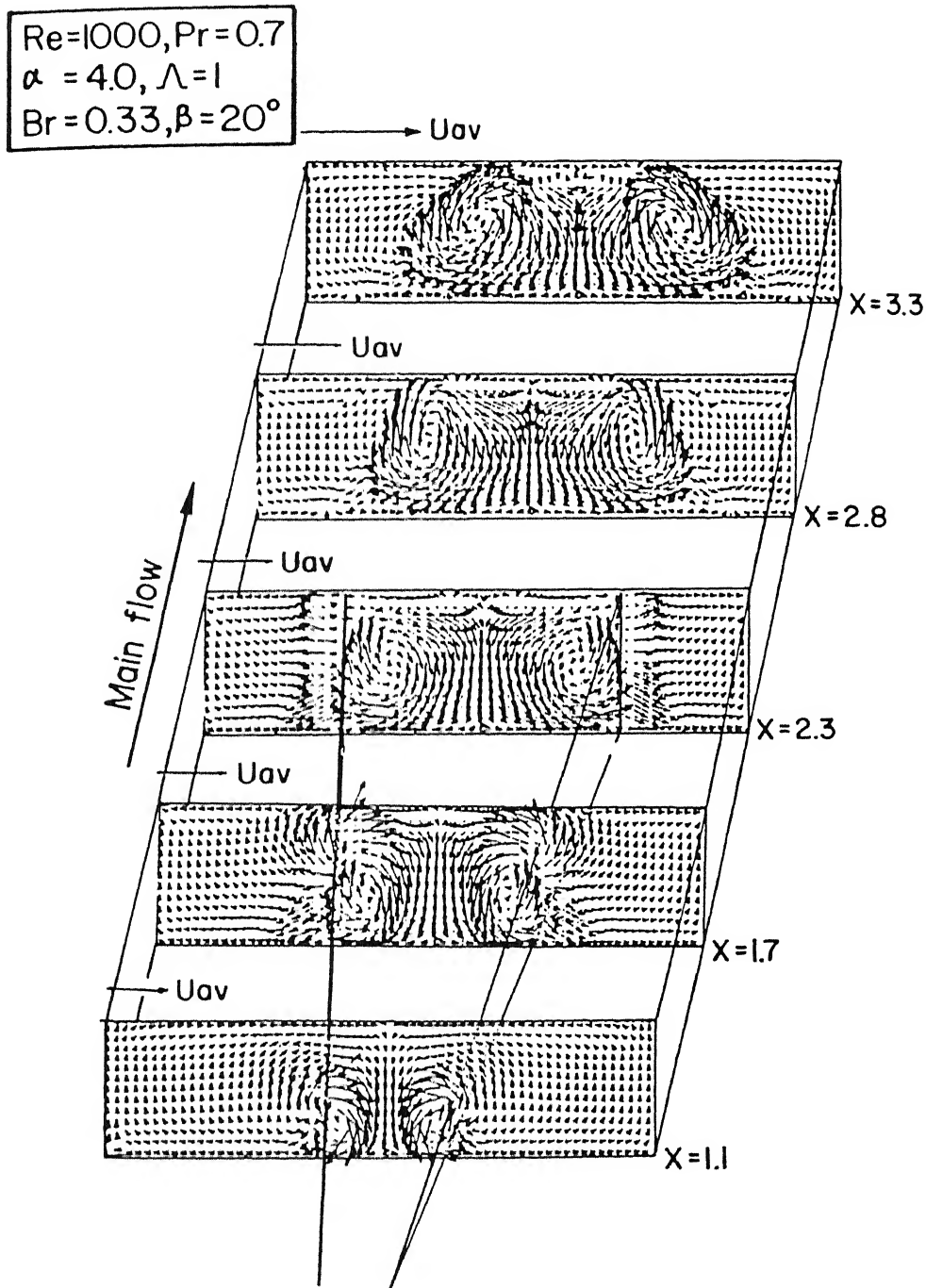


Figure 4.14: Cross-stream velocity vectors at different axial locations behind the winglet-pair in a channel

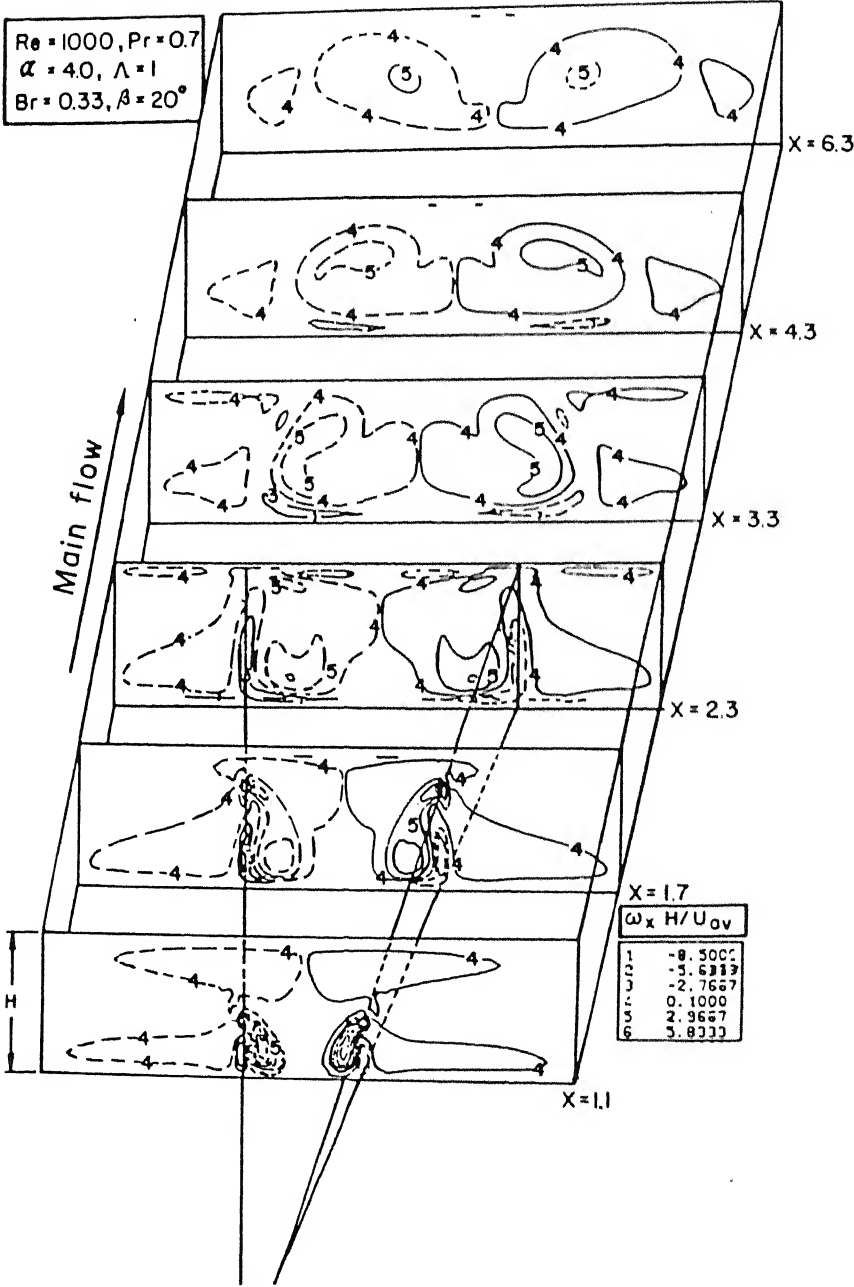


Figure 4.15: Contours of normalized streamwise vorticity at different cross-sections of the channel in presence of the winglet-pair

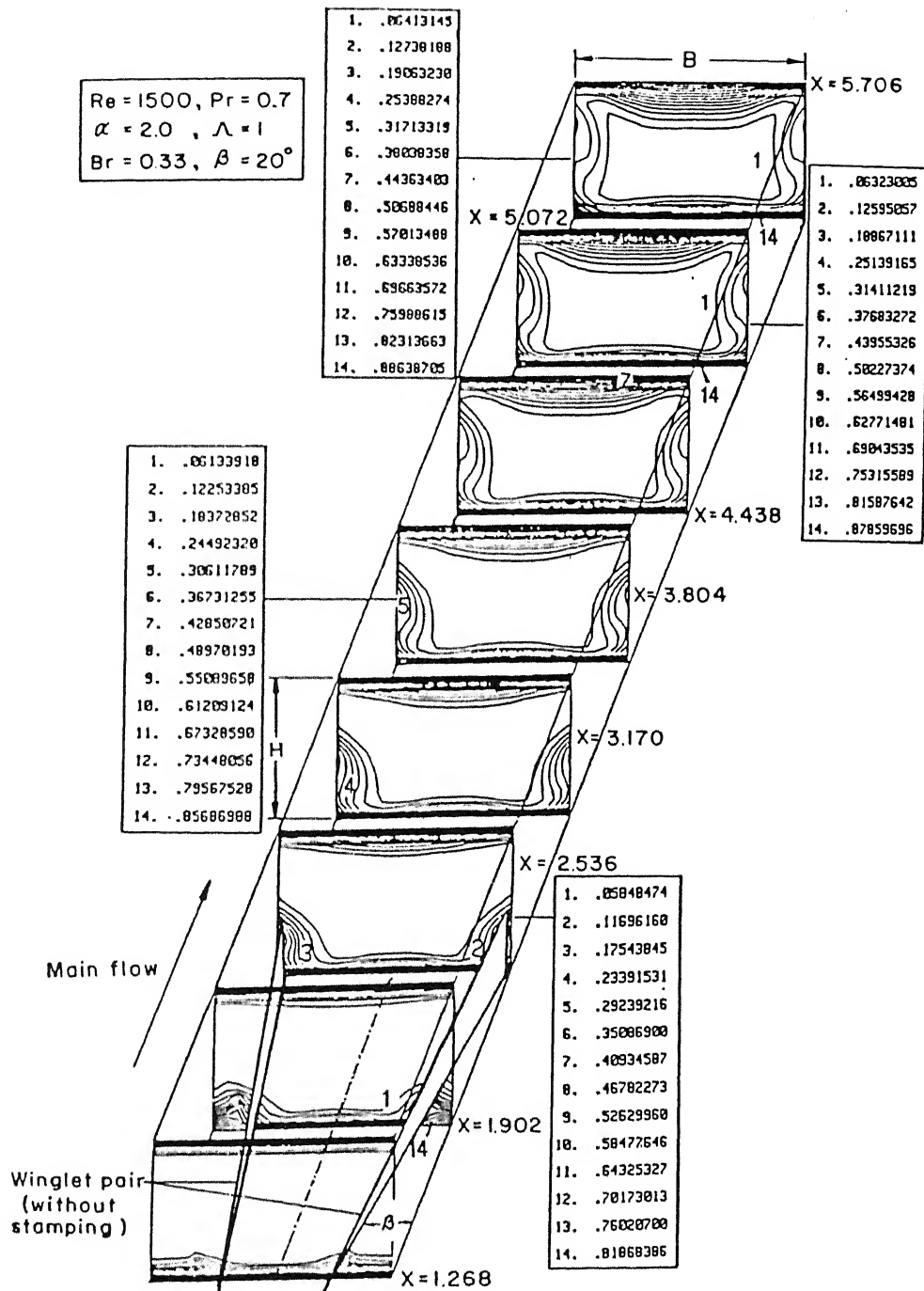


Figure 4.16: Isotherms at different cross-planes in a channel in presence of a built-in winglet-pair

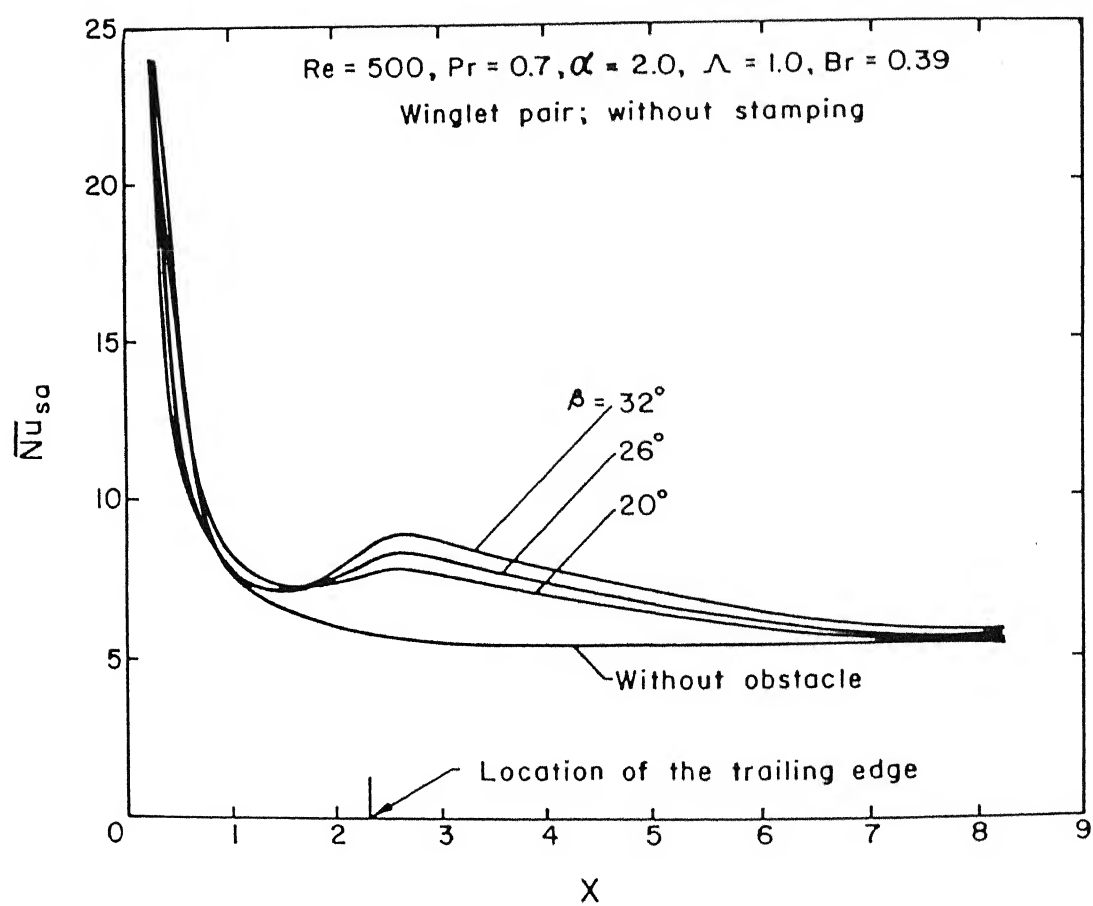


Figure 4.17: Effect of angle of attack of winglet-pair on the distribution of combined spanwise-average-Nusselt-number in the channel developed profile at the inlet

Figure 4.18 shows the effect of winglet-pair on distribution of \overline{Nu}_{sa} in a channel for various Reynolds numbers. Winglets with higher Reynolds number induce higher vortex strength and thereby higher heat transfer is brought about. For all the Reynolds numbers, the \overline{Nu}_{sa} distribution has been compared with the corresponding plane channel value. At a nondimensional distance of 2.5 from the inlet, for a Reynolds number of 2000, we observe an enhancement of 30 percent in the \overline{Nu}_{sa} over the corresponding value for a channel without any obstacle.

Figure 4.19 shows the effect of varying the angle of attack of the winglet on combined spanwise average skin friction coefficient ($\overline{C}_f \times Re$), given by equation 4.2, while keeping the size constant. Increasing the angle of attack has the effect of increasing vortex strength, which in turn increases resistance and consequently a higher value of combined spanwise average friction coefficient is obtained. At the exit of the channel, ($C_f \times Re$) for $\beta = 32^\circ$ is nearly 8 percent more than that for $\beta = 20^\circ$ and ($C_f \times Re$) for $\beta = 26^\circ$ is about 3 percent higher than that for $\beta = 20^\circ$.

Effect of Reynolds number on the distribution of ($\overline{C}_f \times Re$) for the built-in winglet-pair has been shown in Fig. 4.20. Increasing ($\overline{C}_f \times Re$) for higher Reynolds number is a consequence of increased vortex strength for higher flow velocities. For Reynolds number of 2000, the ($\overline{C}_f \times Re$) is 82 percent more than that of Reynolds number of 500 at the exit of the channel.

4.4 Comparison with Experiments

The model validation is performed through comparison with some published experimental results. Local Nusselt numbers along the centerline of the bottom plate with a delta-wing at an angle of attack of 20° were calculated. Reynolds and Prandtl numbers for this computation are 1815 and 0.7 respectively. Here local Nusselt number values are evaluated on the basis of entry temperature of the incoming stream as

$$Nu_{x_0} = \frac{-k[(\frac{\partial T}{\partial y})_{y=0, z=0}]_x (H/k)}{[T_{w1}(x) - T_\infty]_{y=0, z=0}} \quad (4.3)$$

Figure 4.21 shows that the computed values of local Nusselt numbers (with weighted average scheme) compare favorably with the experimental results of Fiebig *et al.* (1986). In the experiment (Fiebig *et al.*, 1986), the channel walls had punched holes on them and the experimental results are closer to the computed results for the case with stamping. The computational results due to QUICK discretization scheme (Leonard, 1979), have also agreed closely with the experiment with the exception near the exit of the channel. The local heat transfer coefficients were determined by unsteady liquid crystal thermography. Measurement error is indeed minimal in this process. The RSS uncertainty described by Moffat(1987) was below 4.3% for local heat transfer coefficients. However, the small discrepancy between the experimental and numerical results

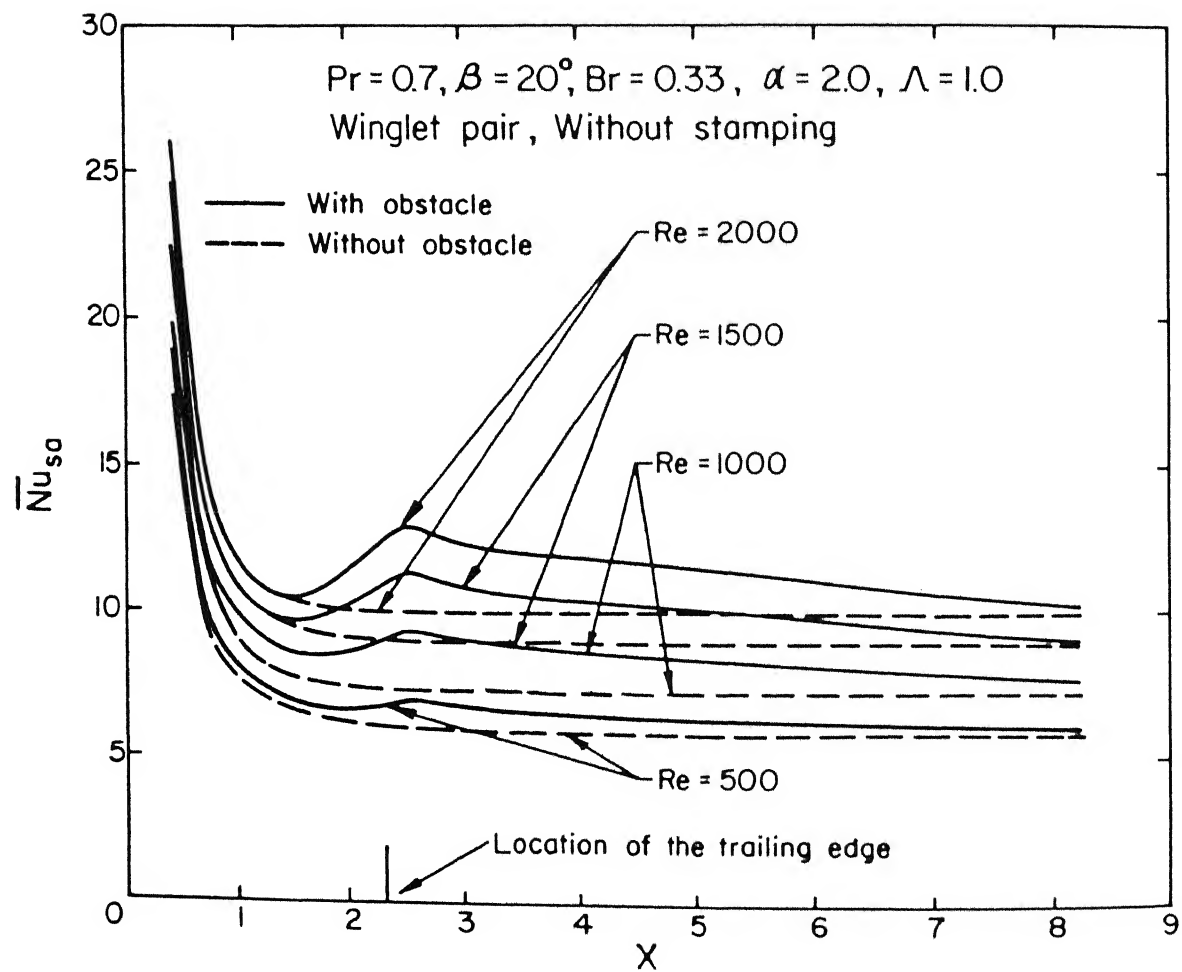


Figure 4.18: Effect of winglet-pair on combined spanwise average Nusselt number distribution of the channel for different Reynolds numbers

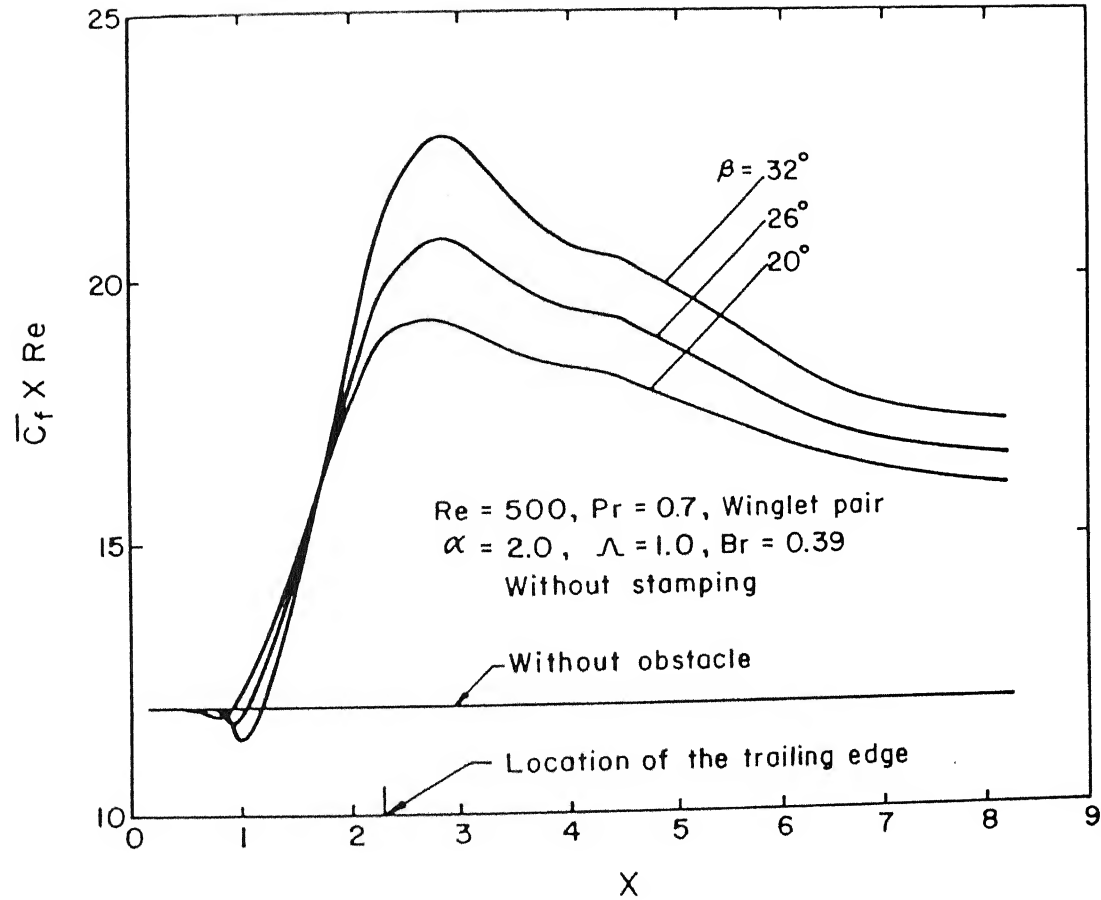


Figure 4.19: Effect of angle of attack of the winglet-pair on the distribution of combined spanwise average skin friction in the channel; developed profile at the inlet

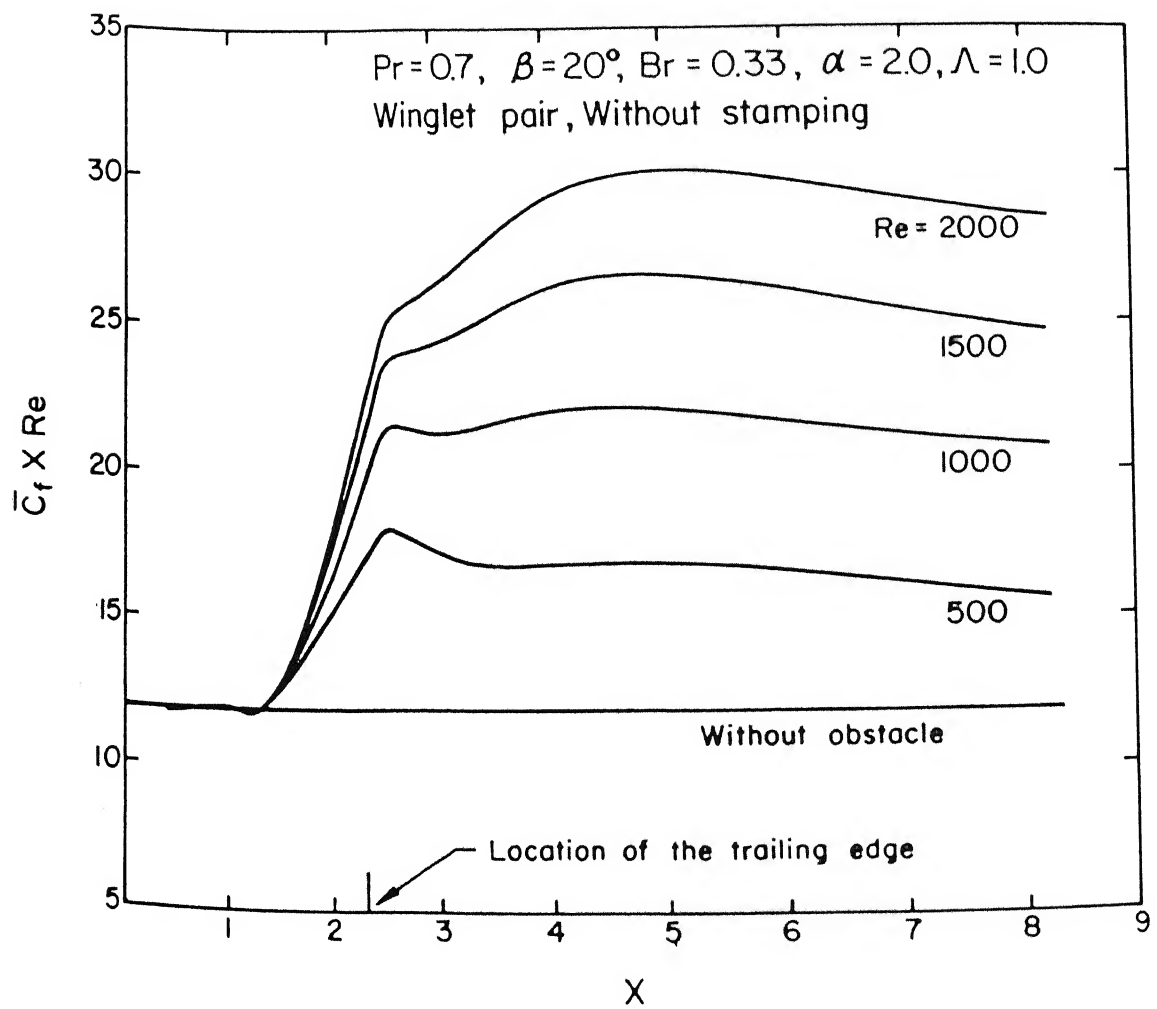


Figure 4.20: Effect of Reynolds number on the distribution of combined span-wise-average-skin-friction in the channel with built-in winglet-pair

could be attributed to physical boundary condition on the channel walls. Due to very small thickness (8.4×10^{-4} m) of the fin-plate (used in experiment), the axial heat conduction was not good and it was not possible to maintain perfect isothermal condition on the channel walls.

Overall heat transfer performance data is validated through comparison with respect to mean-Colburn-factor (j) using delta-wing for three different angles of attack. The experimental results were obtained from Fiebig *et al.* (1991). In the experiment, the reference plate-fin area started from the location of the base of the wing; its longitudinal extent was 7.5 wing chord lengths and its lateral extent was 4 times the wing span. Identifying this zone on the bottom plate as the reference area, experiments were conducted in a plane channel and in a channel with a built-in delta wing at different angles of attack. Figure 4.22 shows the mean-Colburn-factor(j) versus Reynolds number for a delta-wing of aspect ratio 1.25 at various angles of attack. The numerical model and the experiment corroborate with each other reasonably well. The curves can be represented by $j=C_n Re^n$, where n and C_n are constants.

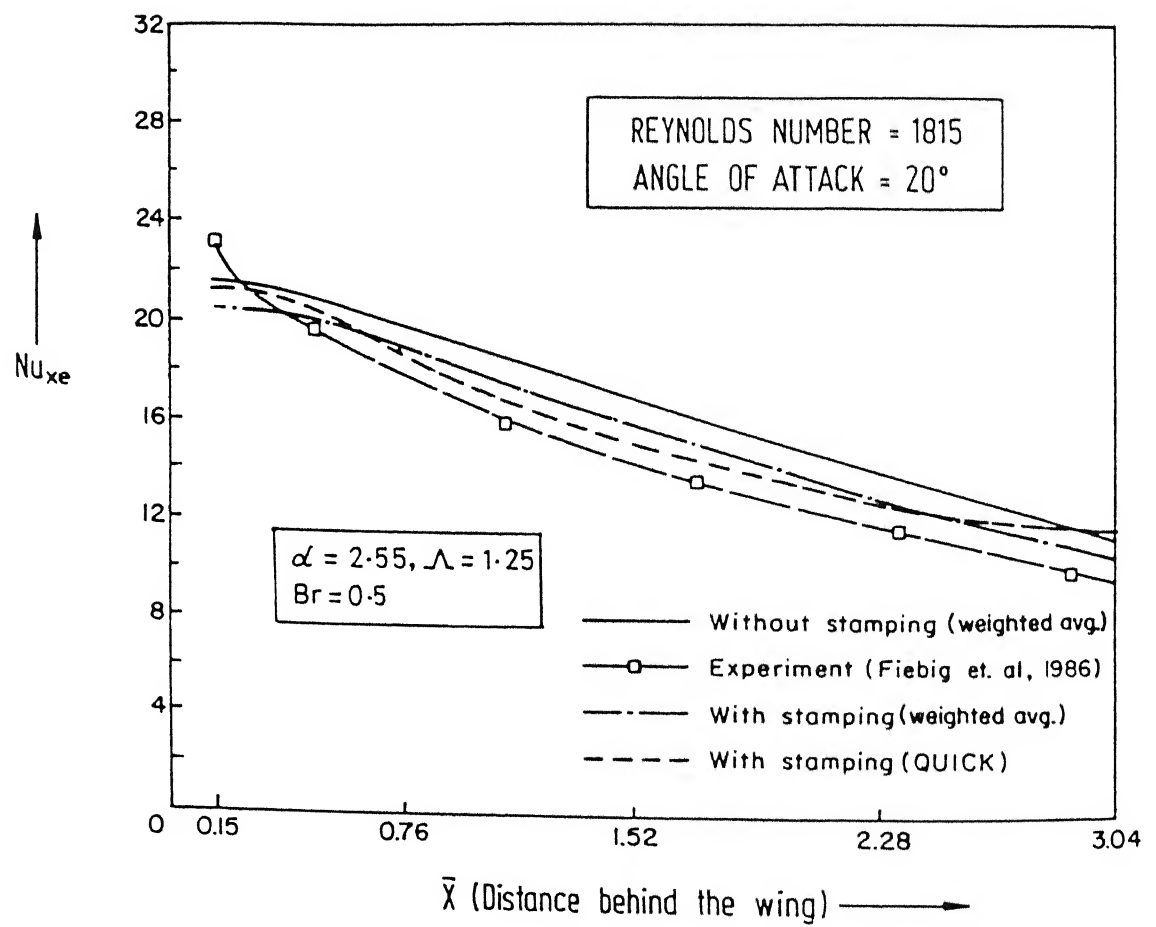


Figure 4.21: Comparison of computed results with experimental observation

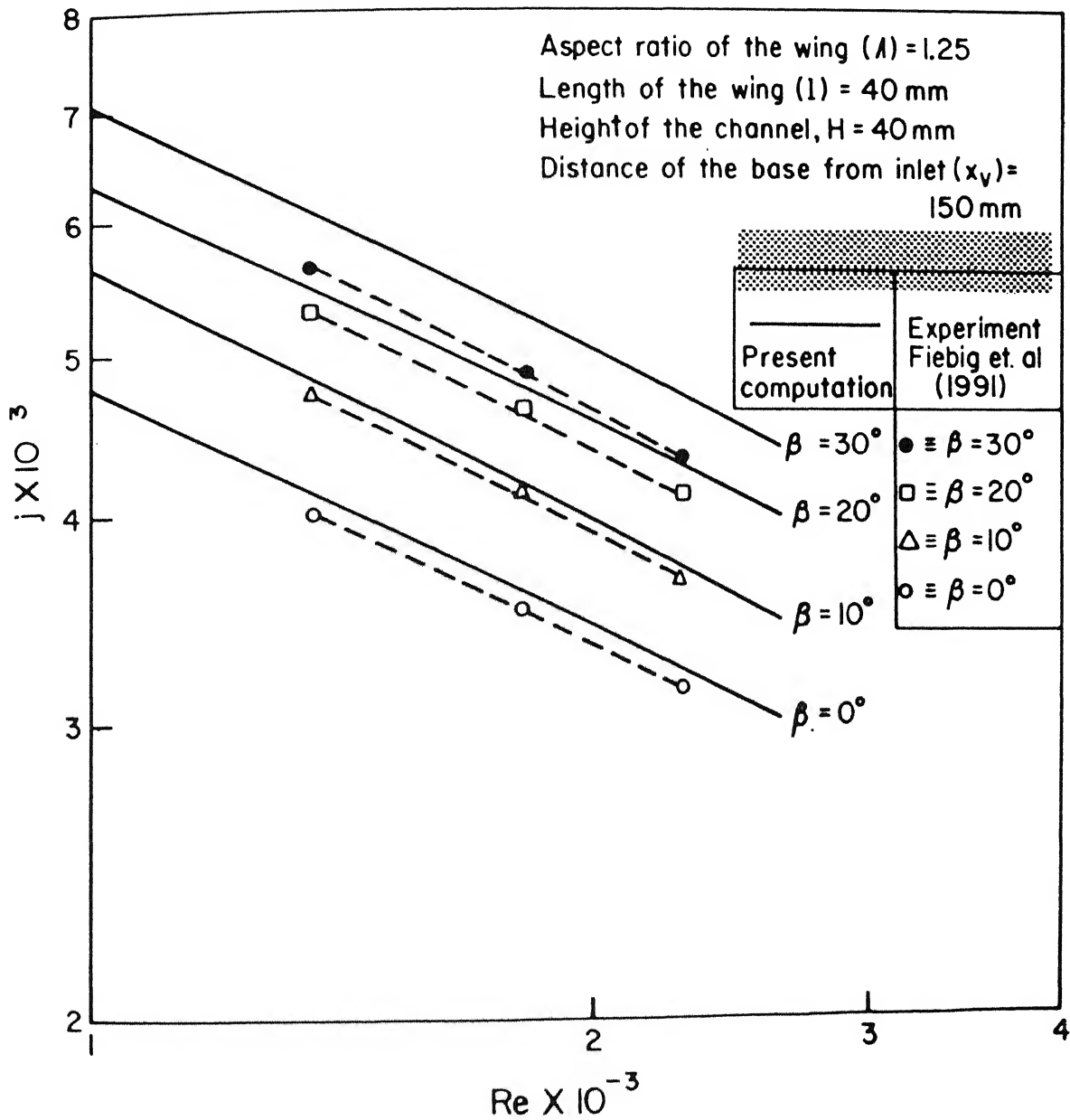


Figure 4.22: Comparison between computational and experimental results for Colburn factor as a function of Reynolds number at different angles of attack

Chapter 5

A Second Law Based Optimization for the Choice of Vortex Generators in the Laminar Flow Regime in the Laminar Flow Regime

"At first glance engineering thermodynamics may appear to be a dead discipline, but closer examination reveals a remarkably lively field of study. Its axioms have recently been reformulated in terms of heat transfer instead of mechanics. New graphic constructions are being used to summarize properties. And exergy analysis and refrigeration techniques are active pursuits for many engineers"

A. Bejan, Mechanical Engineering, p58, May 1988.

5.1 Introduction

Chapter-4 gives a quantitative performance data for a delta wing and winglet-pair in a channel with different angles of attack and a wide range of operating conditions. However, the performance of wings and winglets can be compared by taking into account two parameters: the augmentation of heat transfer and the associate flow losses. In the case of convective heat transfer two types of losses of useful work is encountered; one due to fluid friction and other due to heat transfer across finite temperature gradient. Both these phenomena are manifestations of irreversibility and therefore for a complete evaluation of heat transfer augmentation technique a detailed thermodynamic analysis is required. Thus, the present chapter incorporates an detailed analysis on the influence

of vortex generators (wings/winglets) on entropy generation and irreversibility. An evaluation of the exergy exchange process from the standpoint is called second law analysis (Bejan, 1977; Bejan, 1979). Based on an evaluation of irreversibility, this study is able to draw some conclusions about the efficient use of thermal energy.

5.2 Irreversibility Approach to Heat Transfer Process – A Brief Review

The concept of irreversibility can be employed as a general criterion for designing various thermal systems in order to minimize the wastage of usable energy (McClintock, 1951; Bejan, 1977; Bejan, 1979; Nag and Mukherjee, 1987). Irreversibility analysis through the use of Second Law of Thermodynamics considers the utilization of available energy (exergy) in contrast to the usual design procedure aimed at maximum transfer of heat in a heat exchange process.

McClintock (1951) is one of the pioneers who have used the Second Law of Thermodynamics in heat exchanger analysis. He has studied the production of irreversibility in a heat exchanger designed to exchange a specified amount of heat between the flow streams.

Irreversibility analyses by Bejan and Smith (1975) have successfully optimized the heat exchanger passage area along the flow path of helium vapor.

Bejan (1977) has introduced the concept of designing heat exchangers for fixed or for specified irreversibility in contrast with traditional design procedure based on specified amount of heat transferred. This approach is particularly useful in design of cryogenic systems where conservation of available refrigeration is of prime consideration.

Irreversibility analysis for fundamental convective heat transfer has been carried out by Bejan (1979a). Four fundamental flow configurations have been illustrated: forced convection in a round tube, flow over a flat plate, single cylinder in a crossflow and flow in the entrance region of a rectangular duct. The expressions obtained from this analysis serve as the basis of analyses for heat exchangers.

For insulation systems where the ratio of absolute temperatures across the insulation is high and where the conductance of the insulation is already reduced to the minimum acceptable economically, Bejan (1979b) has prescribed the temperature profile across the insulation that conserves the available refrigeration.

Sarangi and Chowdhury (1982) have analyzed counter flow heat exchangers to account for the entropy generated due to axial conduction and have derived an expression for optimum wall conductivity.

Nag and Mukherjee (1987) have shown that for a heat transfer process there exists an optimum ratio of heat transfer to pumping power. Simply maximizing this ratio is not often a good decision, since in that case the entropy generated may be far from the minimum possible and a large amount of the available energy may thus be irre-

The first term on the right-hand side of (5.2) may be written as :

$$-\frac{1}{T^2}(q \cdot \nabla T) = \frac{k}{T^2} \left[\left(\frac{\partial T}{\partial x} \right)^2 + \left(\frac{\partial T}{\partial y} \right)^2 + \left(\frac{\partial T}{\partial z} \right)^2 \right] \quad (5.3)$$

The second term on the right-hand side of equation (5.2) is expanded as

$$\begin{aligned} (\sigma : \nabla \bar{V}) &= (p + \frac{2}{3}\mu\Delta)\delta_{ij} \left(\frac{\partial u_i}{\partial x_j} \right) - \mu \left(\frac{\partial u_i}{\partial x_j} + \frac{\partial u_j}{\partial x_i} \right) \frac{\partial u_i}{\partial x_j} \\ \text{or, } (\sigma : \nabla \bar{V}) &= (p + \frac{2}{3}\mu\Delta)\Delta - \mu \left[2 \frac{\partial u}{\partial x} \frac{\partial u}{\partial x} + \left(\frac{\partial u}{\partial y} + \frac{\partial v}{\partial x} \right) \frac{\partial u}{\partial y} \right. \\ &\quad + \left(\frac{\partial u}{\partial z} + \frac{\partial w}{\partial x} \right) \frac{\partial u}{\partial z} + \left(\frac{\partial v}{\partial x} + \frac{\partial u}{\partial y} \right) \frac{\partial v}{\partial x} + 2 \frac{\partial v}{\partial y} \frac{\partial v}{\partial y} \\ &\quad + \left(\frac{\partial v}{\partial z} + \frac{\partial w}{\partial y} \right) \frac{\partial v}{\partial z} + \left(\frac{\partial w}{\partial x} + \frac{\partial u}{\partial z} \right) \frac{\partial w}{\partial x} \\ &\quad \left. + \left(\frac{\partial w}{\partial y} + \frac{\partial v}{\partial z} \right) \frac{\partial w}{\partial y} + 2 \frac{\partial w}{\partial z} \frac{\partial w}{\partial z} \right] \end{aligned} \quad (5.4)$$

After invoking the incompressibility condition, equation (5.4) can be written as :

$$\begin{aligned} -\frac{(\sigma : \nabla \bar{V})}{T} &= \frac{\mu}{T} \left[2 \left\{ \left(\frac{\partial u}{\partial x} \right)^2 + \left(\frac{\partial v}{\partial y} \right)^2 + \left(\frac{\partial w}{\partial z} \right)^2 \right\} \right. \\ &\quad \left. + \left(\frac{\partial u}{\partial y} + \frac{\partial v}{\partial x} \right)^2 + \left(\frac{\partial v}{\partial z} + \frac{\partial w}{\partial y} \right)^2 + \left(\frac{\partial u}{\partial z} + \frac{\partial w}{\partial x} \right)^2 \right] \end{aligned} \quad (5.5)$$

Use of equations (5.3) and (5.5) in equation (5.2) and nondimensionalization yields :

$$\begin{aligned} Ns_3 &= \frac{\dot{S}_3 H^2}{k} \\ &= \frac{(r-1)^2}{[\theta(r-1)+1]^2} \cdot \left[\left(\frac{\partial \theta}{\partial X} \right)^2 + \left(\frac{\partial \theta}{\partial Y} \right)^2 + \left(\frac{\partial \theta}{\partial Z} \right)^2 \right] \\ &\quad + \frac{Ec.Pr}{[\theta(r-1)+1]} \cdot \left[2 \left\{ \left(\frac{\partial U}{\partial X} \right)^2 + \left(\frac{\partial V}{\partial Y} \right)^2 + \left(\frac{\partial W}{\partial Z} \right)^2 \right\} \right. \\ &\quad \left. + \left(\frac{\partial U}{\partial Y} + \frac{\partial V}{\partial X} \right)^2 + \left(\frac{\partial V}{\partial Z} + \frac{\partial W}{\partial Y} \right)^2 + \left(\frac{\partial U}{\partial Z} + \frac{\partial W}{\partial X} \right)^2 \right] \end{aligned} \quad (5.6)$$

As expected, the irreversibility indicator Ns_3 contains two additive parts, one due to conduction in the presence of non-zero temperature gradient, and the other accounting

for viscous dissipation of mechanical power throughout the flow. However, if the velocity and temperature fields are completely known, we can find out the values of nondimensional entropy generation per unit volume (Ns_3) at each cell of the flow domain. After evaluating this quantity, we integrate Ns_3 over the entire volume to get nondimensional volumetric entropy generation in the channel as :

$$Ns = \iiint Ns_3 dXdYdZ \quad (5.7)$$

5.3.3 Merit Function

From this analysis, it is possible to evaluate the rate of energy transferred usefully as well as destruction of exergy due to irreversibilities.

If Q is the total rate of heat transfer, then $Q = \bar{h}_c(T_w - \bar{T}_b) 2BL$

$$\text{or, } Q = 2(B/H) \bar{Nu}_c kL (T_w - \bar{T}_b) \quad (5.8)$$

The equation (5.8) can be rearranged as :

$$Q = 2(B/H) kL \bar{Nu}_c T_w (1 - \frac{1}{r})(\theta_w - \bar{\theta}_b) \quad (5.9)$$

The rate of exergy transfer accompanying energy transfer at a rate of Q is given by Moran (1982) as

$$Q_a = Q \left[1 - \frac{T_a}{T_w} \right] = Q \left[1 - \frac{1}{r} \right] \quad (5.10)$$

where T_a , the exergy reference environment temperature has been considered as the ambient temperature T_∞ . The wall temperature T_w has been considered as a suitable temperature at the surface where heat transfer takes place. If \dot{S} is the total rate of entropy generation (dimensional), the destruction of exergy (Gouy-Stodola theorem) is

$$I = T_a \dot{S} = \frac{1}{r} T_w \dot{S} \quad (5.11)$$

As such, the total rate of entropy generation, \dot{S} , may be written as

$$\dot{S} = \frac{k}{H^2} \int \int \int Ns_3 d(HX) d(HY) d(HZ) \quad (5.12)$$

Invoking equation (5.7) in equation (5.12), we obtain

$$\dot{S} = HkNs \quad (5.13)$$

Finally, equation (5.11) and equation (5.13) will yield

$$I = \frac{1}{r} T_w H k Ns \quad (5.14)$$

A merit function is defined as the ratio of exergy transferred to the sum of exergy transferred and exergy destroyed

$$M = \frac{Q_a}{Q_a + I} \quad (5.15)$$

Substituting for Q_a from equations (5.9) and (5.10), and "I" from equation (5.14), we obtain,

$$M = \frac{2(B/H) (r-1)^2 \overline{Nu}_c (\theta_w - \bar{\theta}_b)}{2(B/H) (r-1)^2 \overline{Nu}_c (\theta_w - \bar{\theta}_b) + \frac{rH}{L} Ns} \quad (5.16)$$

This merit function is now evaluated for various flow parameters in a channel using delta wing or winglet-pairs as vortex generators. However, it might be observed that equation (5.16) is another form of second-law efficiency (Moran, 1982). The merit of the merit function lies in its simultaneous accountability of exergy transferred and its destruction caused by irreversibilities associated with exergy transport and momentum transport. Irreversibilities due to external interaction and internal dissipative effects are together taken care of by this parameter.

5.4 Results and Discussions

This chapter contributes a quantitative comparison between the performance of a delta wing and that of winglet-pair on enhancement of heat transfer. It will be of interest to accomplish the comparison by taking into account the irreversibilities associated with the heat transfer process.

Figure 5.1 illustrates the relative heat transfer performance of delta wing and winglet-pair configurations with other geometrical and flow parameters unchanged. The main difference between the wing and winglet is that the winglet has a free trailing edge, whereas the wing has no trailing edge (wing-span is attached to the plate). However, delta-wing produces streamwise vortices with higher strength, which brings about better improvement in heat transfer as compared with built-in winglet pair. In a moderately long channel ($X = 8.4$), the enhancement in combined spanwise Nusselt number for a built-in delta-wing ($\beta = 26^\circ$, $\Lambda=1$ and $Br=0.42$) at the exit of the channel, is more than 34 percent than that of a plane channel. This enhancement for the winglet-pair at the same location is about 14 percent. Therefore from heat transfer point of view, delta-wing is found to be more effective than the winglet-pair.

Figure 5.2 shows the distribution of combined spanwise average friction coefficient ($\overline{C}_f \times Re$) in the channel for the wing and winglet-pair and compares them with the distribution of ($\overline{C}_f \times Re$) in a plane channel. As mentioned earlier, delta-wing generates streamwise vortices with higher strengths. Increased frictional losses are due to steeper velocity gradients at the walls. These losses rise with vortex strength, and as a consequence, ($\overline{C}_f \times Re$) is higher for vortices with higher strength. At the channel exit

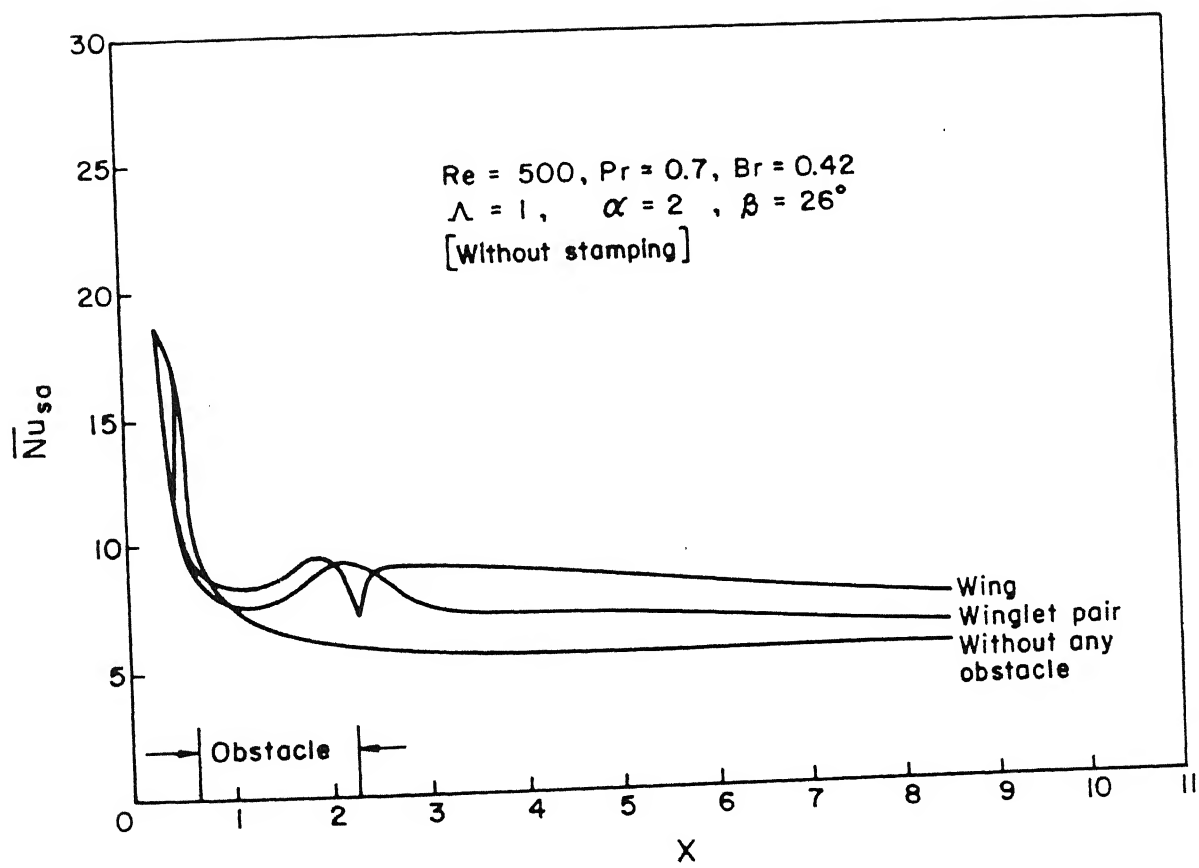


Figure 5.1: Effect of type of obstacle on the distribution of combined spanwise average Nusselt number in the channel; developed profile at the inlet

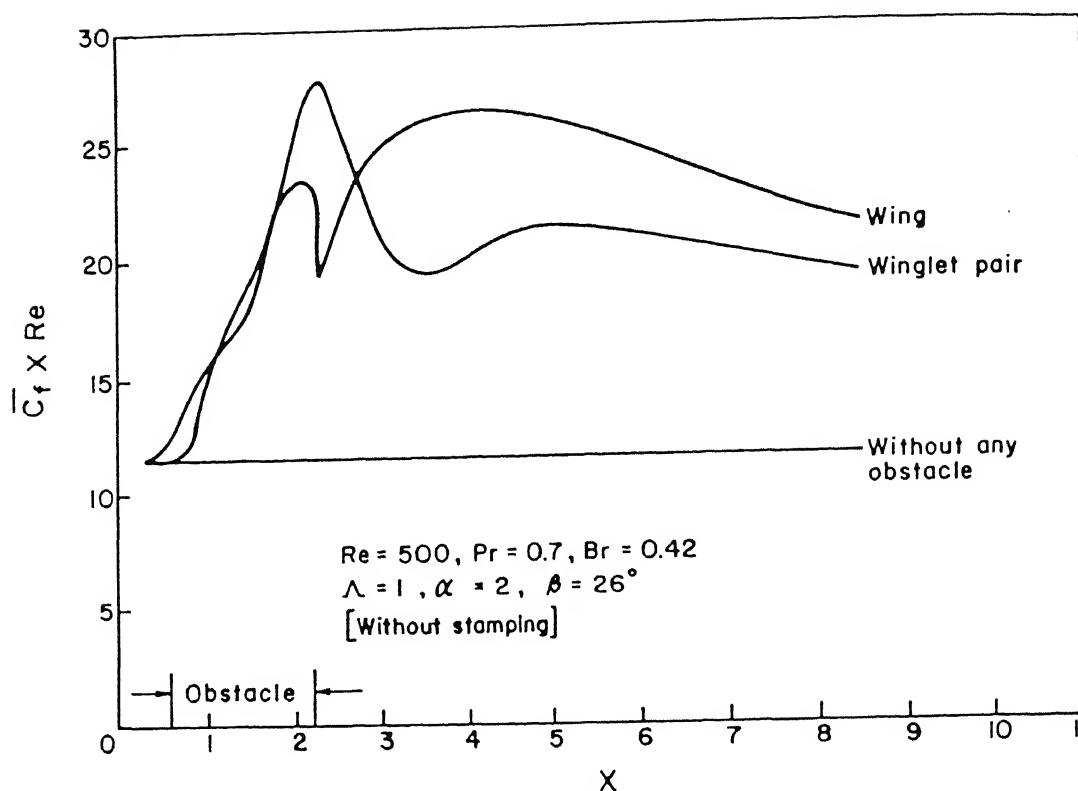


Figure 5.2: Effect of type of obstacle on the distribution of combined spanwise average friction coefficient in the channel; developed profile at the inlet

($X = 8.4$), $(\bar{C}_f \times Re)$ value for a delta-wing is about 79 percent more than for that of the plane channel flow. For winglet-pair, the increase in $(\bar{C}_f \times Re)$ value at the same location, over the case of a plane channel flow, is nearly 65 percent.

Figure 5.3 shows the total entropy generation in the channel at various Reynolds numbers (in the range of 500 – 3000) for two different cases, namely, with a built-in delta wing and winglet-pair. It is evident that for all the Reynolds numbers, the entropy generation in the case of a built-in delta wing is much more than that of a delta winglet-pair. With increasing Reynolds number, the delta-wing generates vortices of higher strengths. This culminates in steeper velocity gradients at the wall. As a result, frictional losses become high and consequently, the total generation of entropy becomes much more pronounced.

Figure 5.4 shows the variation of merit function, M with Reynolds number (in the range of 500 – 3000) for the built-in delta wing and winglet-pair. The delta winglet-pair shows better performance than delta wing with regard to merit function. For the case of heat transfer in a channel with a built-in winglet-pair, the increase in irreversibility associated with the increase in exergy transfer occurs at a relatively lower rate as com-

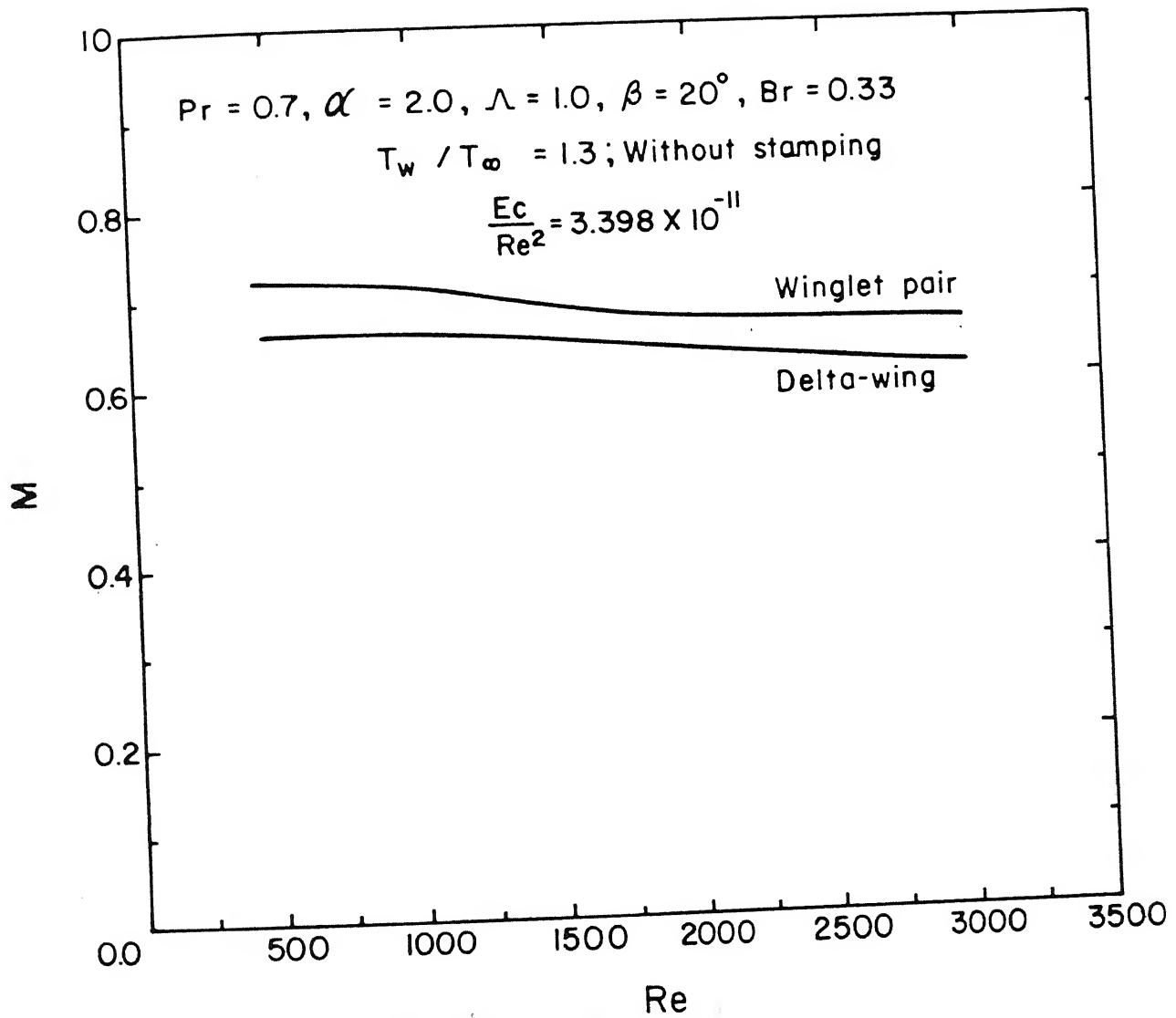


Figure 5.3: Effect of type of obstacle on the variation of volumetric entropy generation with Reynolds number

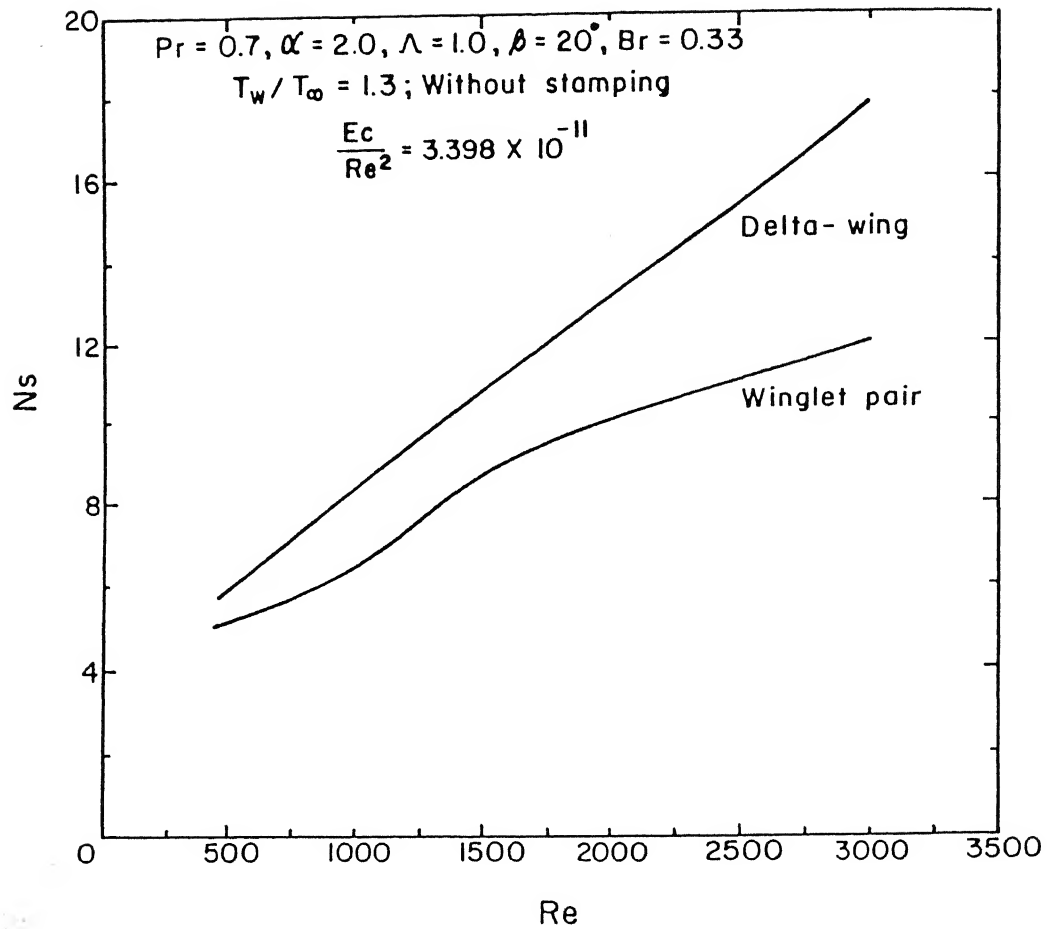


Figure 5.4: Effect of type of obstacle on the variation of merit function with Reynolds number

As compared to the case of a built-in delta wing. Although with regard to augmentation of heat transfer in the channel, the built-in delta wing shows better performance, it can be only argued that the built-in winglet-pair is more effective with respect to efficient use of energy.

Appraising Remarks

With above mentioned events in mind, we are now in a position to consider the practical application of this augmentation technique. The flow configuration resembles only a single element of a cascade in fin-tube or plate-fin crossflow heat exchangers or a row of vortex generators. In practice, for such an exchanger the channel may be allowed to be so long ($X \geq 8.0$), i.e., another row of vortex generators may

not be allowed to be so long ($X \geq 8.0$), i.e., another row of vortex generators may be punched out or mounted before this length is reached in the downstream direction. In that event, at about $X = 4$, (refer to Fig. 5.1), augmentation of heat transfer due to winglet-pair is also quite substantial. Moreover in the case of winglets, separation bubbles are not formed near the wing-plate junction. It has also been seen that the flow loss (corresponding to the combined spanwise average skin friction coefficient) due to the winglet-pair is less than that due to the wing. Besides, due to formation of trailing edge vortices for the free trailing edge of winglet, the small zone of poor heat transfer as it is observed with the wing can be avoided. Thus, based on this and a comparative study of second-law efficiency, the use of winglets appears to be a more attractive augmentation technique.

Chapter 6

Turbulent Flow and Heat Transfer

6.1 Introduction

It may be mentioned that the study of laminar flow in the present work is not for computational simplification. Usually, the fin spacing is so small and the mean velocity range is such that the flows are often laminar (Kakac *et al.*, 1981). However, for some special applications, the velocity becomes such that one may encounter turbulent flows in plate-fin type heat exchangers. Therefore, a detailed analysis of turbulent flow in an element of such heat exchangers is necessary. It may be mentioned that in plate-fin heat exchangers no holes should exist underneath the vortex generators in order to avoid mixing of the hot and cold streams. It is conjectured that in a laminar flow the coherent motions are dominant over the chaotic behavior of the flow. In the transitional flow chaotic and coherent behavior are equally dominant. When the chaotic behavior becomes dominant in relation to the coherent behavior, the flow is turbulent.

According to this statement the turbulent motion is chaotic and irregular. However, if it is entirely irregular or chaotic, turbulent motion will be inaccessible to any type of mathematical treatment. Instead, it can be assumed that the irregularity associated with turbulence is such that turbulent motion can be considered as an irregular condition of flow in which various quantities, *viz.*, velocity components and pressure show a random variation with time and space so that the statistical average of those quantities can be described.

The turbulent flow is dissipative in nature. Therefore if there is no external source of energy for the continuous generation of turbulence, the turbulent or irregular motion within a flow will decay. It is postulated that the fluctuations inherently come from disturbances and may either be viscosity damped or may grow by drawing energy from the free stream. At a Reynolds number less than critical, the kinetic energy of flow is not enough to sustain the random fluctuations in the face of viscous damping and in such cases laminar flow continues to exist. At somewhat higher Reynolds number than the critical Reynolds number, the kinetic energy of flow supports the growth of

fluctuations and transition to turbulence is induced.

However, the self-sustaining character of turbulence in a simple shear is that the turbulent velocity fluctuations in the direction of mean velocity gradient promote a growth in shear stress which in turn, serves to augment the intensity of streamwise fluctuations. Pressure interactions deflect some of this energy to fluctuations in the direction of the velocity gradient and thus the sequence repeats itself. Our aim is to mimic these processes in terms of time-mean properties. As such the most popular approach to resolve the issues of turbulent flow is to solve time-averaged (or Reynolds-averaged) equations and model the closure equations through some hypothesis. This approach has been widely used in engineering, but suffers from being problem dependent and non-universal. As we have seen, an extensive literature exists on the performance of the various turbulence models. The most popular turbulence model is the two-equation model. At the practical level, satisfactory results are obtained by making use of the two equation turbulence model due to Launder and Spalding (1974).

This chapter presents numerical simulation of flow and heat transfer in the configuration of interest (Fig. 3.1) for the turbulent regime. The governing equations and the boundary conditions have been discussed in section 3.2.3 and 3.2.4 respectively. Now we would like to highlight the basis of derivation of turbulent kinematic viscosity.

By analogy to molecular viscosity, we can write

$$\nu_t = v_s l_s \quad (6.1)$$

where, v_s is the turbulent velocity scale and l_s is the turbulent length scale.

On the other hand, k , the turbulent kinetic energy is given by

$$k = \frac{1}{2}(\overline{u'^2} + \overline{v'^2} + \overline{w'^2}) \quad (6.2)$$

Therefore a meaningful scale for velocity fluctuation is $k^{1/2}$. The length scale is related to the rate of dissipation of turbulent kinetic energy, ϵ , given by

$$l_s = \frac{k^{3/2}}{\epsilon} \quad (6.3)$$

Finally, the Prandtl-Kolmogorov relation is obtained from dimensional argument as

$$\nu_t = C_\mu k^2 / \epsilon \quad (6.4)$$

where C_μ is the constant of proportionality and is equal to 0.09. The nondimensional form of the equation (6.4) has been used as equation (3.13) in section 3.2.3.

6.2 Basis of the Wall-Function Treatment in Turbulence Modeling

The no-slip condition at a rigid boundary implicates that convective transport associated with the motion parallel to the solid wall vanishes there. Thus, very near

to the wall, the system of differential equations describing the mean and fluctuating fields become simply a function of normal coordinate, y . Therefore, with the requisite boundary conditions provided, the equations could be solved to obtain the distributions of the various dependent variables as a function of y and other relevant flow parameters. Any of the turbulence models discussed in the section 2.4.2 could serve a basis of generating such near wall solutions and the results obtained would be as accurate as a complete low-Reynolds-number near-wall treatment provided the neglect of streamwise variations is accomplished within the thin near-wall region ($Y^+ < 11.63$). This feature permits us to patch a three dimensional solution of the outer fully turbulent region to a one-dimensional near-wall solution in which all the near-wall influences are restored. The inner solution is conveniently expressed as a system of algebraic formulae, such as, equations (3.23) and (3.24) relating the dependent variables (U , W , k , ϵ etc.) in their dimensionless form to the independent variable y (also expressed dimensionlessly) and various parameters of flow. These formulae are commonly referred to as "Wall Functions".

The section 3.2.4 provides with the formulae used for two layer wall function (see Amano, 1984) treatment. It may be mentioned that in all the formulae, the friction velocity, u_τ is one of the most important characteristic quantity. However, in this section, the theoretical basis of expressing u_τ in terms of other quantities related to turbulent flows will be discussed.

The local equilibrium between the production and the dissipation rate of turbulent kinetic energy near the wall gives rise to

$$\overline{\rho u'v'} \frac{\partial \bar{u}}{\partial y} = \rho \epsilon \quad (6.5)$$

Just outside the viscous sublayer, the shear stress (still equal to τ_w) will be produced entirely by the turbulent eddies (Bradshaw, 1971) so that

$$\overline{\rho u'v'} = \tau_w \quad (6.6)$$

From equation (6.6) we can also write

$$\overline{u'v'} = \tau_w / \rho = \nu_t \frac{\partial \bar{u}}{\partial y} \quad (6.7)$$

Invoking $\nu_t = C_\mu k^2 / \epsilon$ in equation (6.7) we can write

$$\overline{u'v'} = \frac{C_\mu k^2}{\epsilon} \frac{\partial \bar{u}}{\partial y} \quad (6.8)$$

Substituting the value of $(\partial \bar{u} / \partial y)$ from equation (6.5) in the above equation, we get

$$-\overline{u'v'} = C_\mu k^2 \frac{1}{(-\overline{u'v'})}$$

or

$$(-\overline{u'v'})^2 = C_\mu k^2$$

or

$$\left(\frac{\tau_w}{\rho}\right)^2 = C_\mu k^2$$

Invoking $u_\tau = \sqrt{\tau_w/\rho}$, we get

$$u_\tau = C_\mu^{1/4} k^{1/2} \quad (6.9)$$

In nondimensional form, equation (6.9) may be written as

$$u_{\tau,n} = C_\mu^{1/4} k_n^{1/2} \quad (6.10)$$

The friction velocity is of paramount importance in deriving out the nondimensional form of the governing equations and the boundary conditions for turbulent flows.

6.3 Present Investigation

An effort has been made to investigate numerically the turbulent flows and associated temperature fields in channels with longitudinal vortex generators. The present investigation serves the following purposes:

- (a) validation of our model through comparison with the experiment results of Pauley and Eaton (1988 a,b) and Eaton (1993).
- (b) prediction of the heat transfer and flow losses in the configuration of interest. We envisage to predict the distribution of spanwise-average-Nusselt number and the distribution of spanwise-average-skin friction coefficient on the bottom plate of a channel with built-in vortex generators. It is implicit that the flow regime is turbulent.

6.4 Comparison of Numerical and Experimental Results

6.4.1 The Test Section and the Computational Domain

Experimental data for three-dimensional turbulent flows in a rectangular channel containing longitudinal vortex pairs have been presented in Pauley and Eaton (1988 a,b) and Eaton (1993). Figure 6.1 shows the schematic of the experimental facility. This facility has a 200 cm long test section with a 13 cm \times 61 cm cross-section and is operated at a normal free-stream velocity of $U_o = 16$ m/s. A pair of delta winglets is used as vortex generators and is located at 53 cm downstream from the inlet. The angles

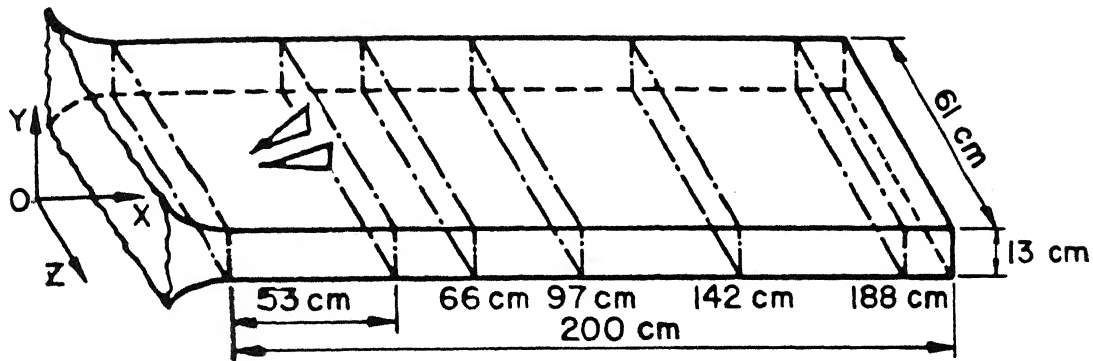


Figure 6.1: Schematic of the test section of Pauley and Eaton (1988 a,b)

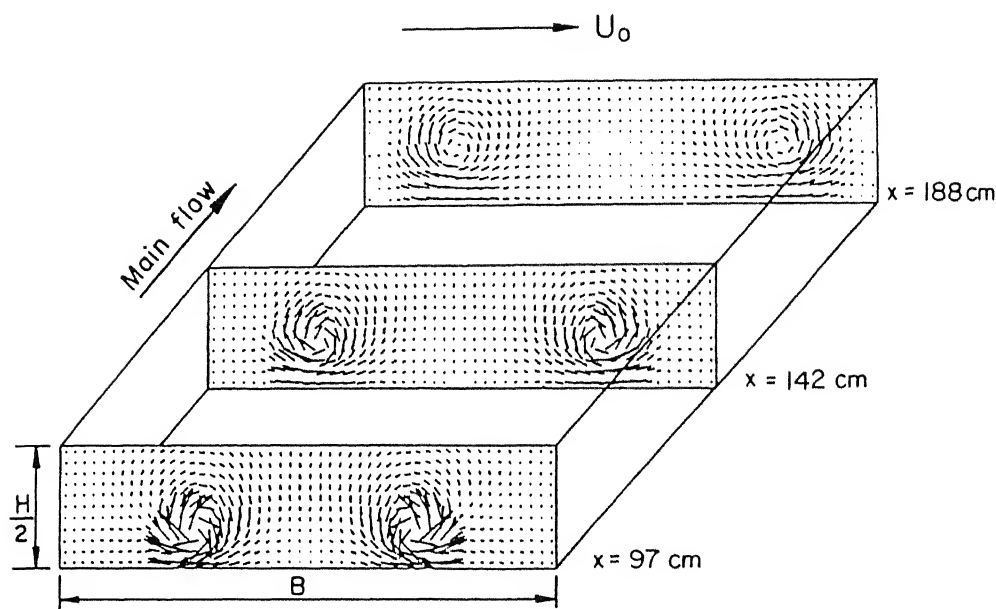
of attack of the vortex generators can be varied. The case with the winglet height of 2 cm and a length of 5 cm with 18° angle of attack, which has been referred to in Pauley and Eaton (1988 a,b) and Eaton (1993), is chosen for the present simulation. Pauley and Eaton (1988 a,b) and Eaton (1993) have conducted measurement at four cross-sections, namely, $x=66$, 97, 142 and 188 cm (see Fig. 6.1). The section $x=97$ cm is selected as inlet of the computational domain used for the comparison. No experimental data is available for the turbulent variables at the axial station of $x=66$ cm. The computational domain ends at the exit of the channel (i.e., at $x=200$ cm). The measured data of Pauley and Eaton (1988a) for u , v , w , k and ϵ at the cross-section $x=97$ cm are deployed as inlet profiles of these variables for the computational domain.

6.4.2 Comparison and Discussion

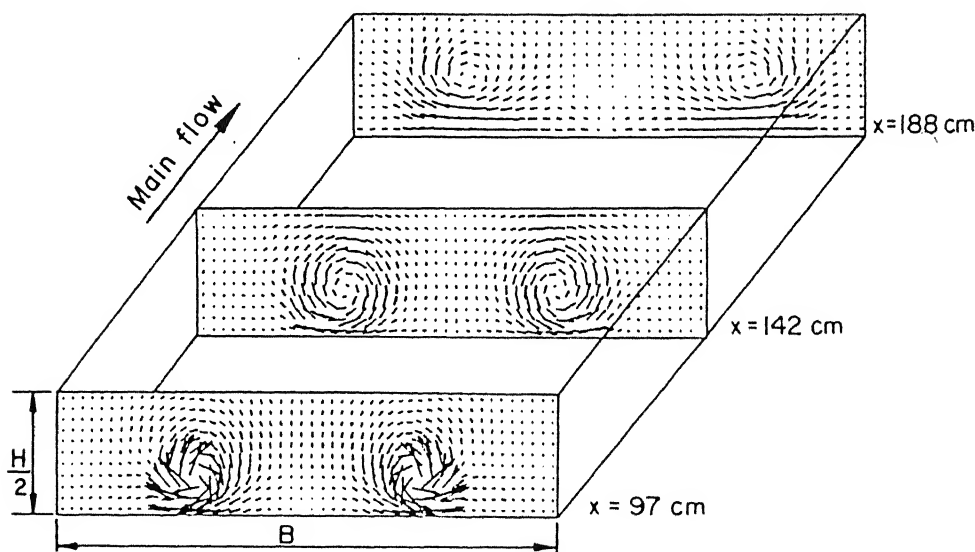
The flow is simulated for a Reynolds number of $Re_{H/2}=67000$, based on half height of the channel. Air has been used as a working fluid; hence Prandtl number of all computations is 0.7.

The comparison of secondary velocity vectors at three different planes in the channel can be observed through Fig. 6.2. A reasonably good agreement is confirmed between the experimental data and computed results. Both in the experiment and in the computation, the vortex transport and decay in the strength of secondary flow in various cross-sections are discerned.

Figure 6.3(a) shows isolines of the streamwise velocity at three different cross-stream planes of the channel. The boundary layer is thinned in the downwash region and seems remain unaffected in the upwash region. The vortices diverge as they move downstream. All such salient features are captured in computational results which are illustrated in Fig. 6.3(b).

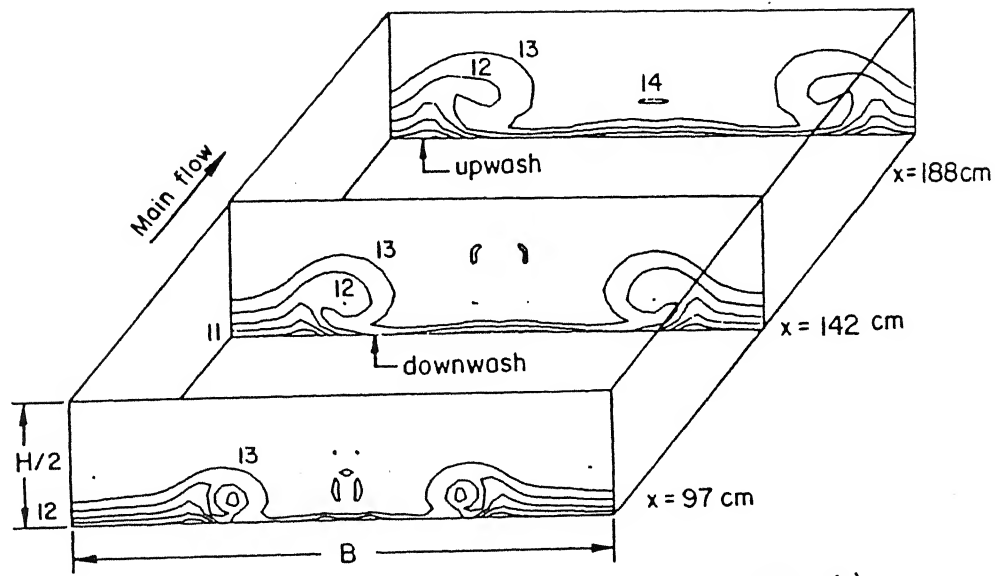


(a) Experiment due to Pauley and Eaton (1988 a, b)



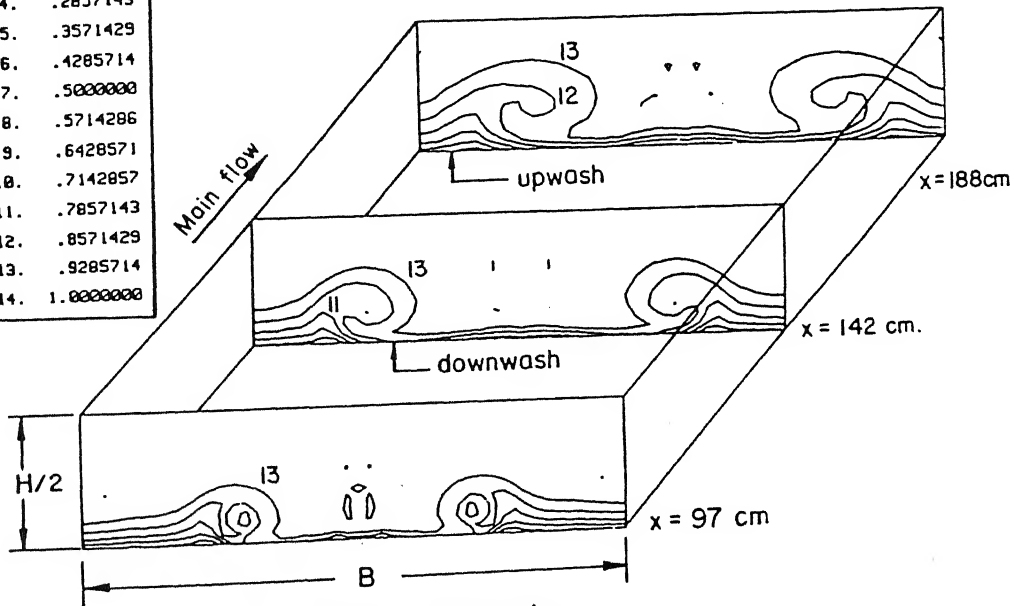
(b) Present computation

Figure 6.2: Vector Plots of secondary flow: $Re_{H/2}=67000$



(a) Experiment due to Pauley and Eaton(1988 a,b)

1.	.0714285
2.	.1428571
3.	.2142857
4.	.2857143
5.	.3571429
6.	.4285714
7.	.5000000
8.	.5714286
9.	.6428571
10.	.7142857
11.	.7857143
12.	.8571429
13.	.9285714
14.	1.0000000



(b) Present computation

Figure 6.3: Contours of streamwise velocity at different cross-sections for $Re_{H/2} = 67000$

Figure 6.4(a) shows the experimental values of isolines for the turbulent kinetic energy at two different cross-sections in the channel. In the downwash region, the boundary layer is thinned by the main vortex and the location for the peak value of turbulent kinetic energy comes closer to the wall. In the upwash region, the iso-kinetic energy lines are more uniformly placed. Although the $k-\epsilon$ model formally employs some restrictive assumptions, the results obtained from the present computation (Fig. 6.4(b)) seem to match surprisingly with the experiments.

An engineering computation of turbulent flow concerns determination of mean axial velocity profiles in a flow field and the effect of time-dependent fluctuations on them. Figures 6. 5 and 6.6 compare the experimental and computed axial velocity profiles (normalized) at different axial distances for five spanwise locations. In Fig. 6.5, the five spanwise locations at $z=2.4, 4.3, 6.2, 8.1$ and 10.0 cm represent the central core region (A), downwash region (B), region of vortex core (C), upwash region (D) and outer vortex region (E) of the cross-section at $x=142$ cm while in Fig. 6.6 the same spanwise locations stand for the similar five regions of the cross-section at $x=188$ cm. In the central region (A) of the cross-section at $x=142$ cm where the boundary layer is thinned significantly by the influence of strong downflow (refer to Fig. 6.2), the velocity profile shows a usual two dimensional distribution. However, in this region the agreement between the computational and experimental results is indeed good. In the upwash region (D) the streamwise velocity profile is not so correctly reproduced by the simulation. The departure of prediction from the experimental result goes up to 6 percent. In other regions of the cross-section at $x=142$ cm, a reasonably good agreement between the experimental results and the prediction is observed. Nearly similar trend of comparison between the experimental observations and the predictions is illustrated in the plots at $x=188$ cm.

Figure 6.7 compares the computed and measured values of turbulent kinetic energy distribution in the y -direction for different z locations at an axial station of $x=188$ cm. In some cases, (at $z=6.2$ cm), the computed results marginally overpredict the results of Eaton (1993). By and large, the comparison implicates acceptable agreement between the prediction and the computed results.

6.5 Prediction of Pertinent Performance Parameters

The predicted static pressure distribution at different axial locations in the channel for a Reynolds number of $Re = 5000$ is shown in Fig. 6.8. It is noteworthy that the longitudinal vortices persist in the downstream section influencing the entire velocity field. The basic free-vortex like structure is also observed in case of the turbulent flow. The location of the minimum pressure is at the vortex center. The minimum

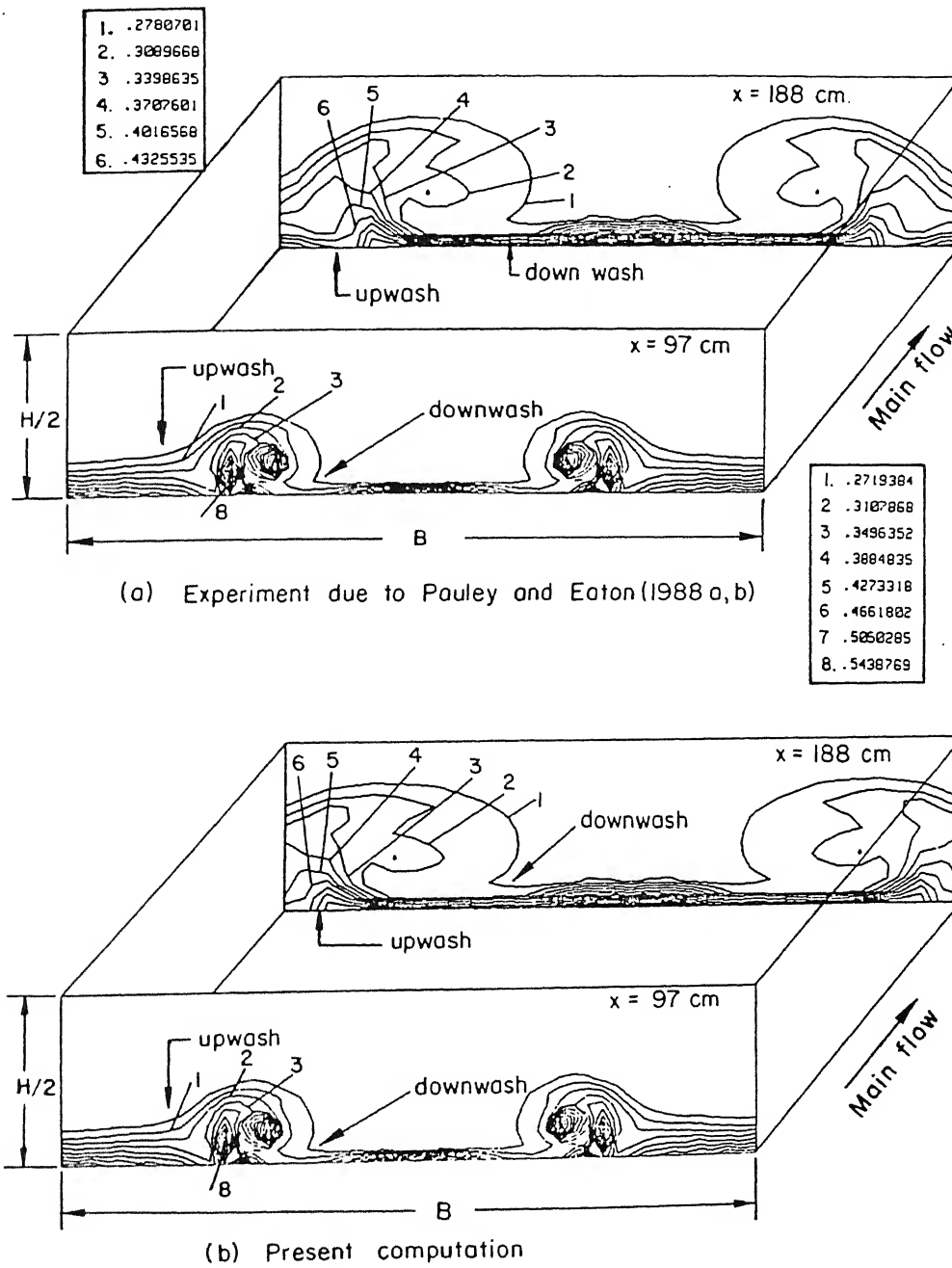


Figure 6.4: Isolines for turbulent kinetic energy at different cross-sections for $Re_{H/2} = 67000$

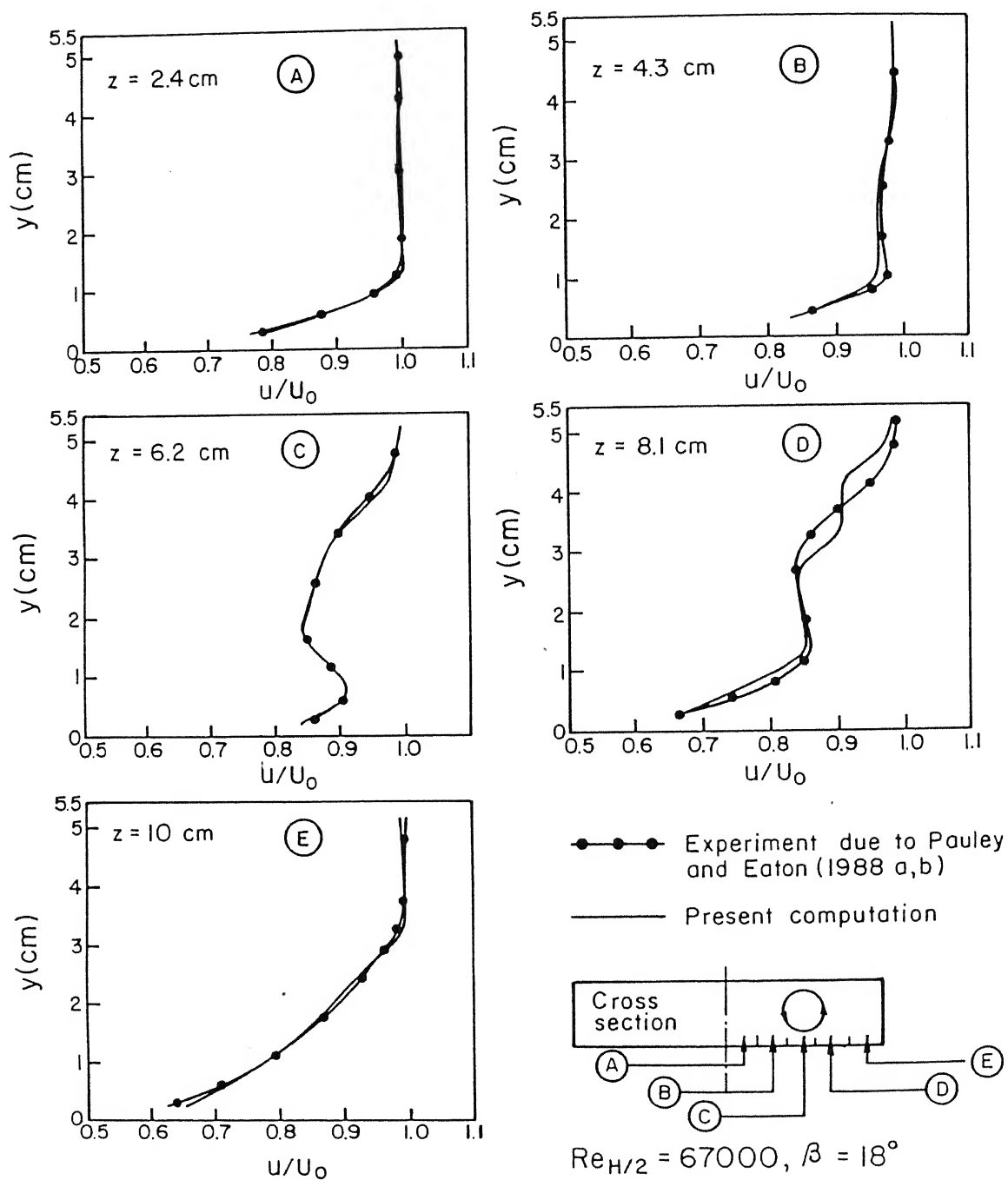
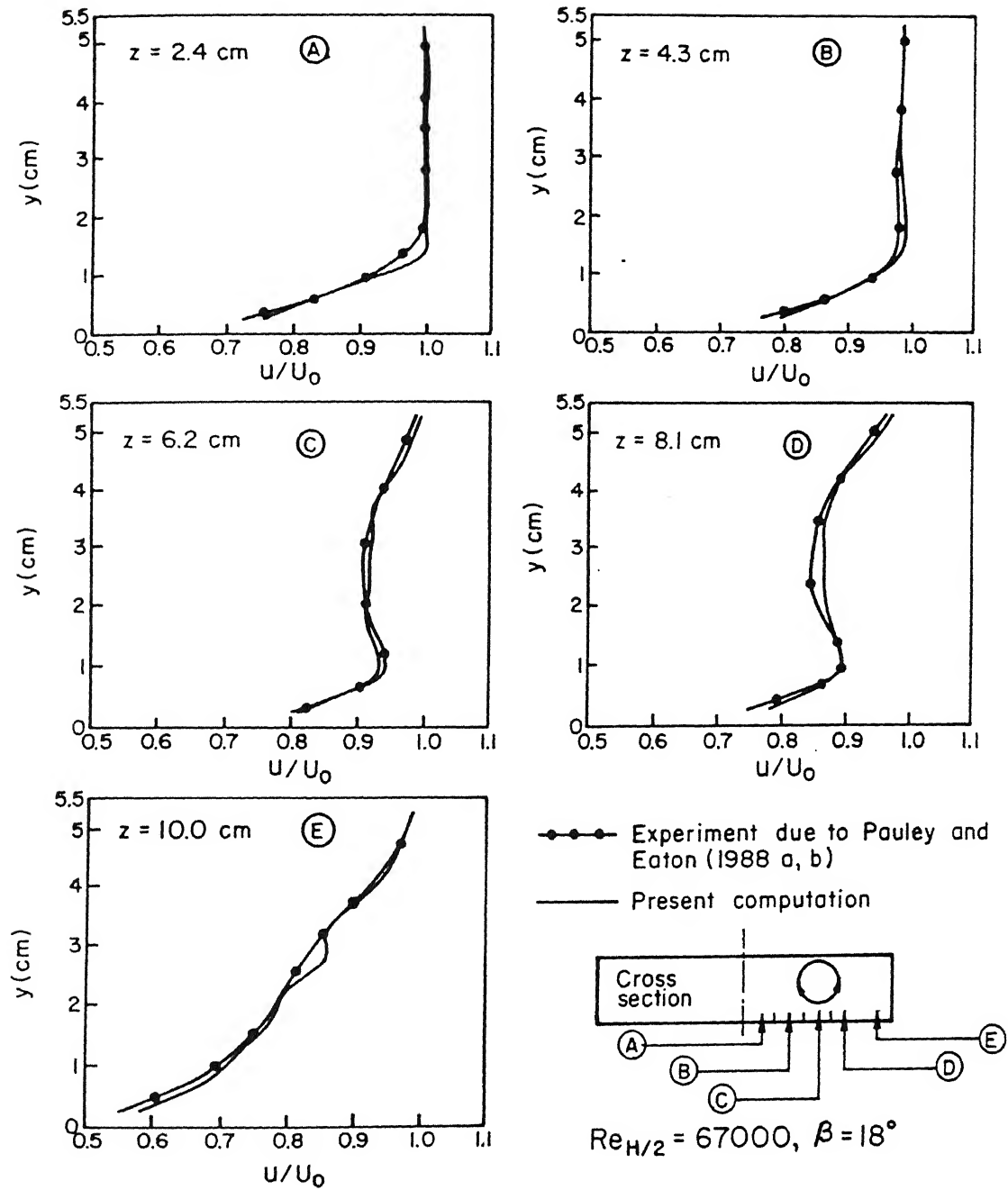


Figure 6.5: Streamwise velocity profiles at axial station $x=142$ cm for $Re_{H/2} = 67000$

Figure 6.6: Streamwise velocity profiles at axial station $x=188$ cm for $Re_{H/2} = 67000$

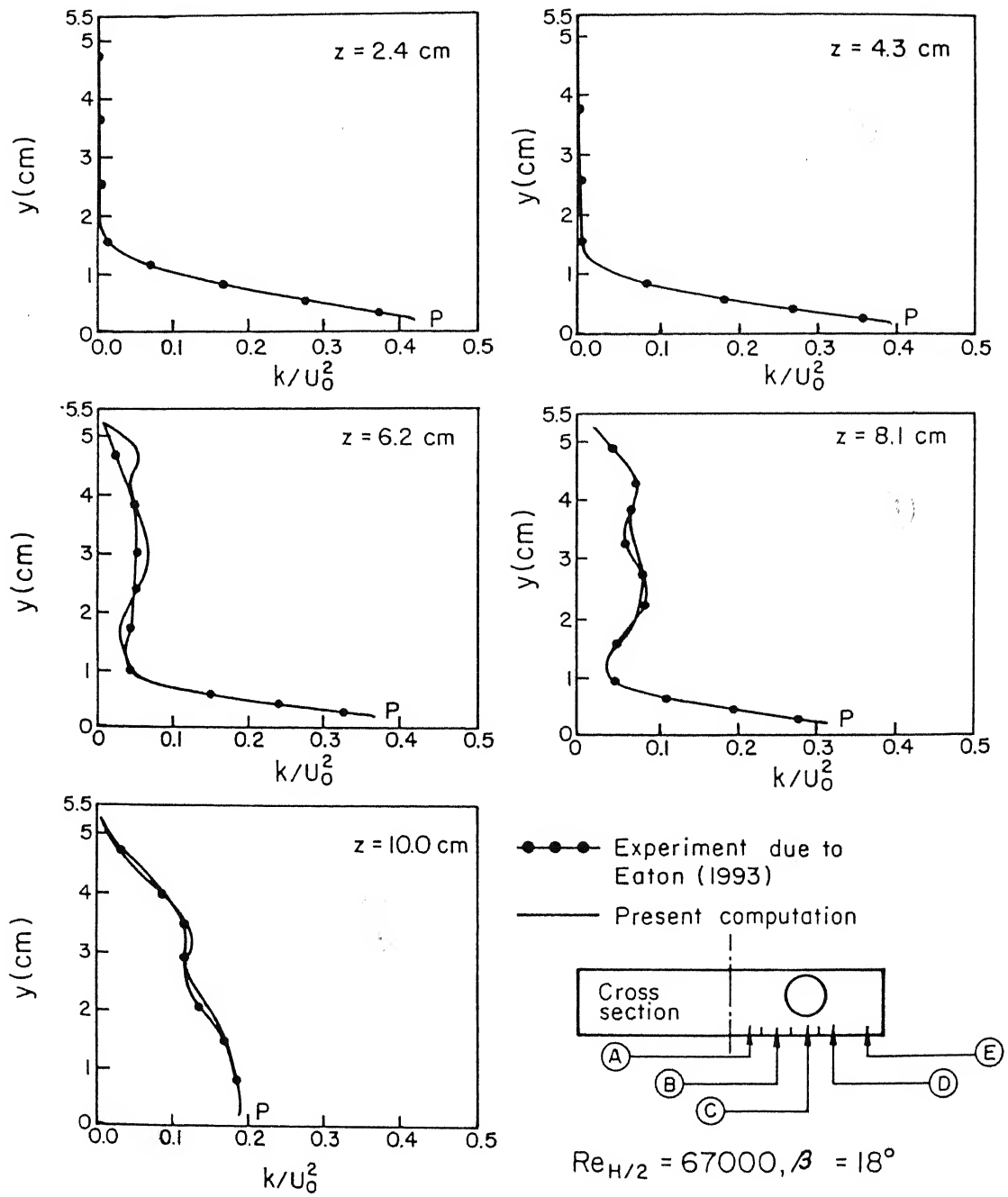


Figure 6.7: Turbulent kinetic energy profiles at axial station $x=188$ cm for $Re_{H/2} = 67000$

pressure zone moves downwards with increasing distance behind the trailing edge of the winglets. Figure 6.9 confirms a similar trend of static pressure for a Reynolds number of $Re = 15000$. Figure 6.10 shows the isolines for turbulent kinetic energy at two different axial locations in the channel for a Reynolds number of $Re = 5000$). The production of turbulent kinetic energy is maximum in the near-wall-region where the shear stress is also maximum. However, due to the influence of strong secondary flow another high kinetic energy zone is observed near the vortex center.

For the turbulent flows the transport rate for momentum is high and the vortex generators are rather small in size with a view not to enhance much of pressure penalty. Hence the height $(b/2)$ of the winglets for such computations are very small compared to the channel height $((b/2)/H=0.3)$.

The heat transfer and skin friction coefficients are the two most important performance parameters concerning any heat transfer process. In the following text, we shall discuss about these two parameters.

In order to predict the heat transfer performance at the wall, the local Nusselt number may be defined as

$$Nu_{(x,z)} = \frac{hH}{k}$$

or,

$$Nu(x, z) = h(T_w - T_b) \frac{\nu}{\alpha} \frac{1}{\rho c_p} \frac{1}{U_o(T_w - T_b)} \frac{U_o H}{\nu}$$

or,

$$Nu(x, z) = \frac{q_w Pr Re}{\rho c_p (T_w - T_b) U_o}$$

or,

$$Nu(x, z) = \frac{q_{w,n} Pr Re}{(\theta_w - \theta_b)} \quad (6.11)$$

where,

$$q_{w,n} = \frac{q_w}{\rho c_p (T_w - T_\infty) U_o}$$

Finally, the spanwise average Nusselt number on the bottom fin surface may be expressed as

$$\overline{Nu}_{s1} = \frac{2}{B} \int_0^{B/2} Nu(x, z) dz \quad (6.12)$$

Figure 6.11 shows the Nu_{s1} distribution on the bottom plate for the Reynolds number of 5000 and 15000. In both the cases, the turbulent intensity is 10 percent at the inlet of the channel. Significant enhancement is observed for the cases with built-in delta winglets over the corresponding cases without any obstacle. For example, in the case of Reynolds number of 5000, the enhancement is about 16 percent at the exit of the channel. It may be worthwhile to mention here that the size of the winglets used in

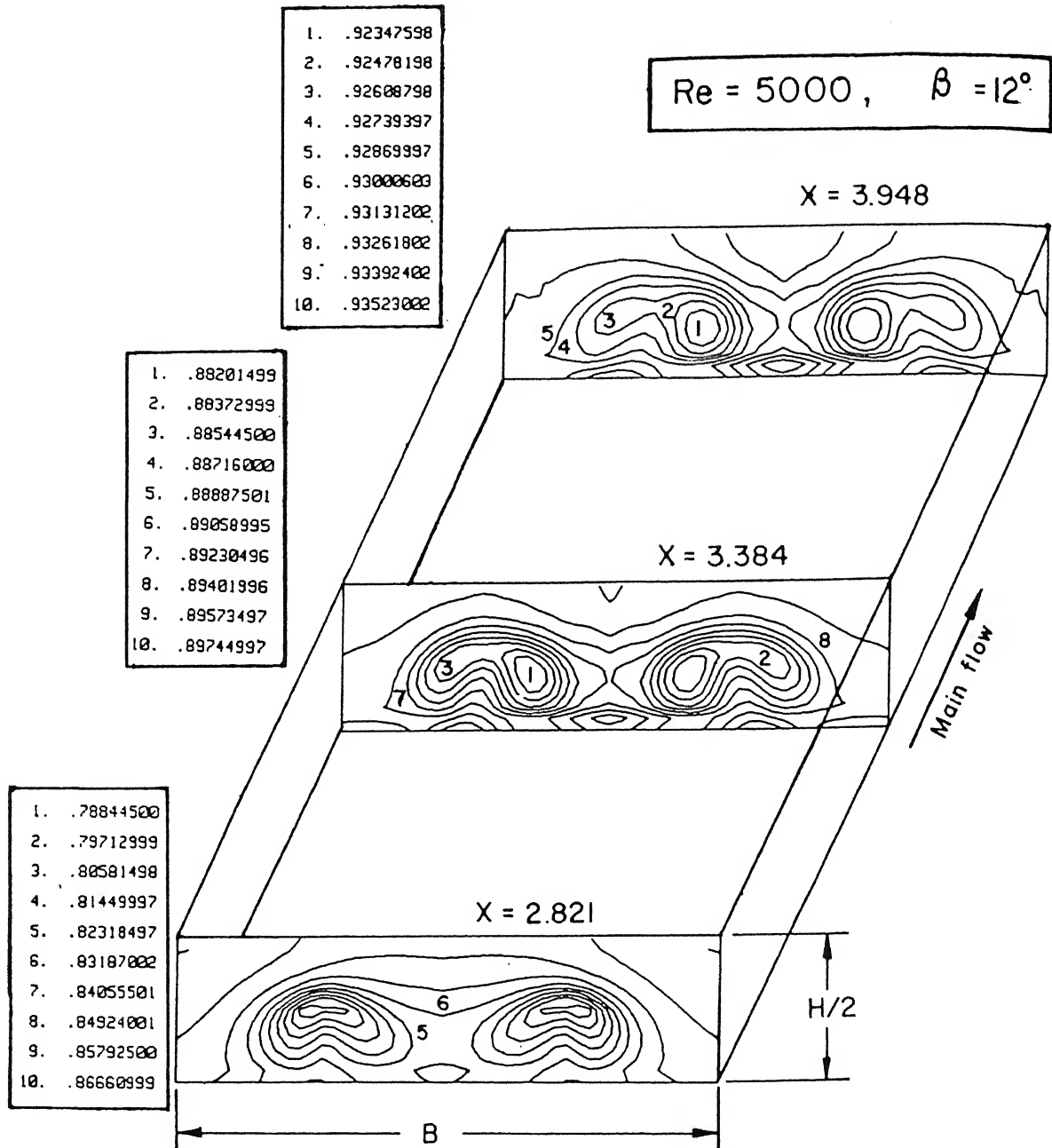


Figure 6.8: Isolines of static pressure at different cross-sections for $Re=5000$; trailing edge of the winglet is located at $X=2.5$ from the inlet

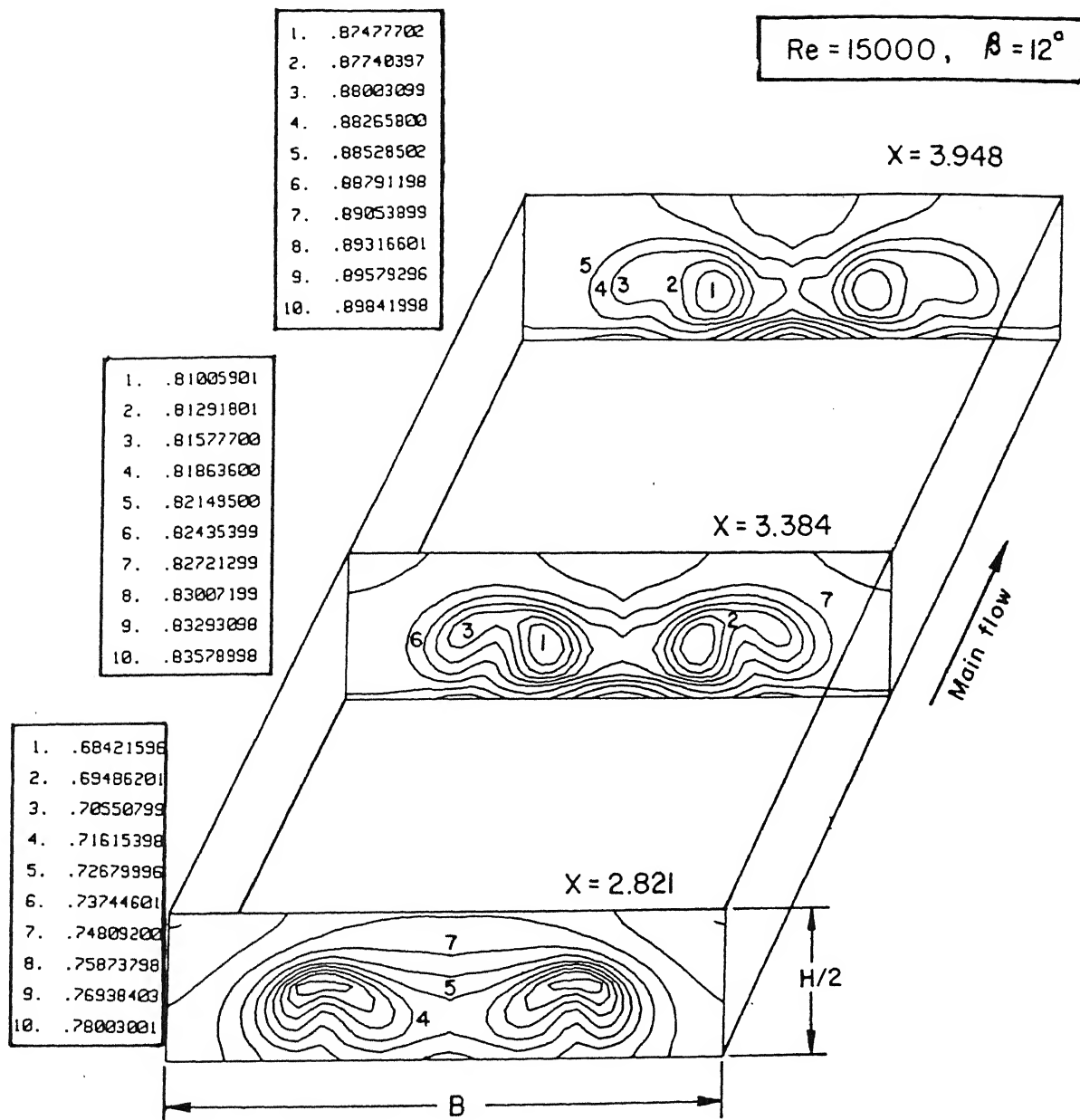


Figure 6.9: Isolines of static pressure at different cross-sections for $Re=15000$; trailing edge of the winglet is located at $X=2.5$ from the inlet

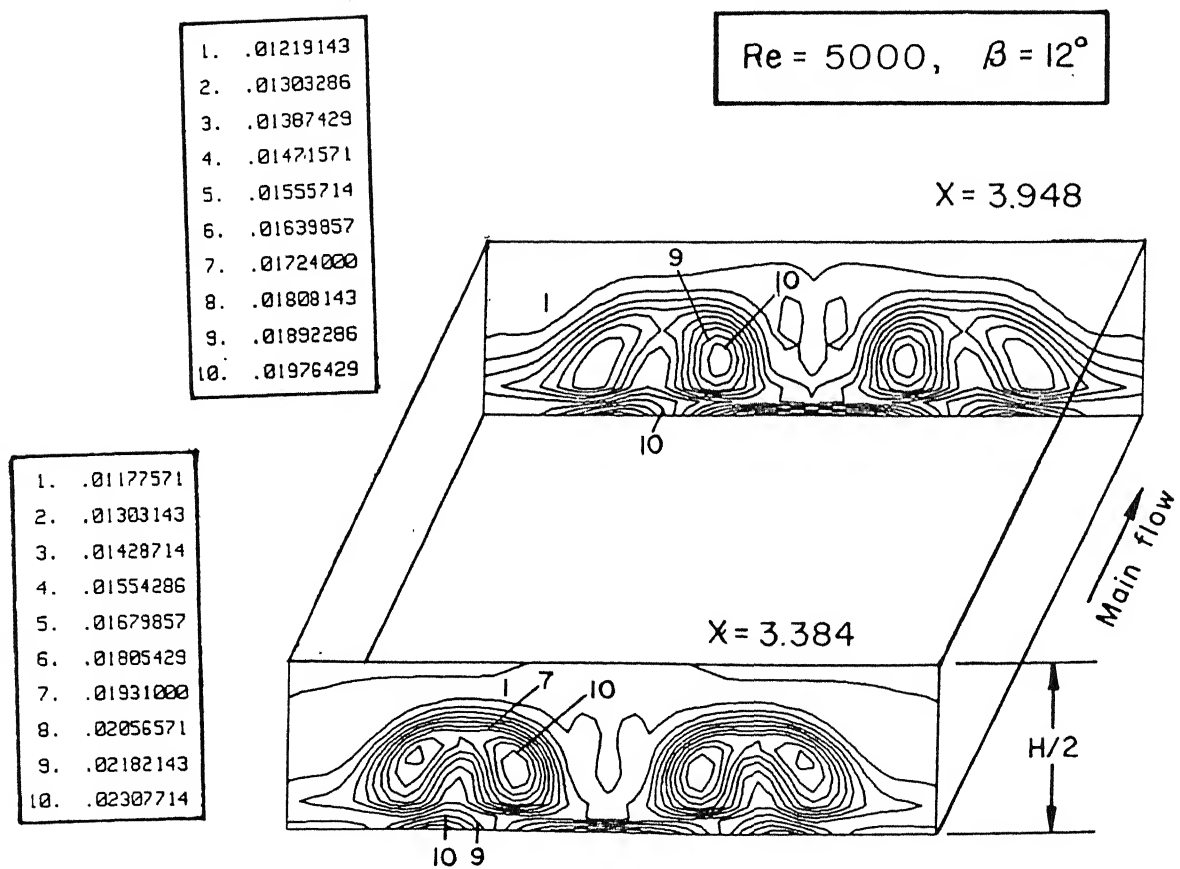


Figure 6.10: Isolines of turbulent kinetic energy at different cross-sections for $Re=5000$; trailing edge of the winglet is located at $X=2.416$ from the inlet

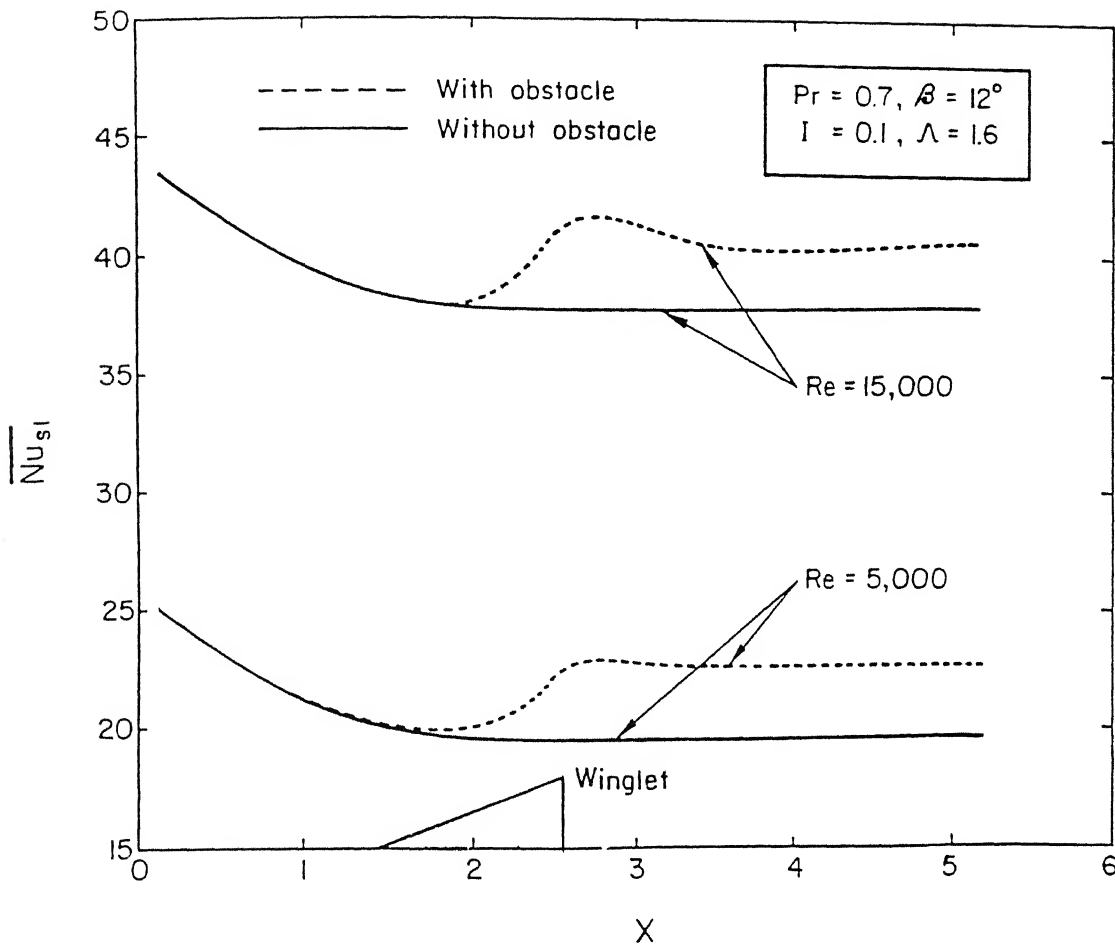


Figure 6.11: Distribution of spanwise average Nusselt number on the bottom plate for different Reynolds numbers

the study of turbulent flow is indeed smaller as compared to the size of the winglets used for the study in laminar flow. So, the enhancement in transport rate is not as high as laminar flows. The peak values are brought about just inboard of the vortex center where the lateral divergence is most pronounced (for both the cases, it is at $X=2.5$ from the inlet).

Figure 6.12 shows that at the location of the peak, the boundary layer is thinned by the strong downflow and lateral outflow of boundary layer fluid. In the downstream the secondary velocities decay and vortices spread apart causing a growth of the boundary layer. The spanwise distribution of local Nusselt number at $X=4.325$ on the bottom plate for two different Reynolds numbers are shown in Fig. 6.13. The level of heat transfer augmentation in the space between the vortices is high in both the cases.

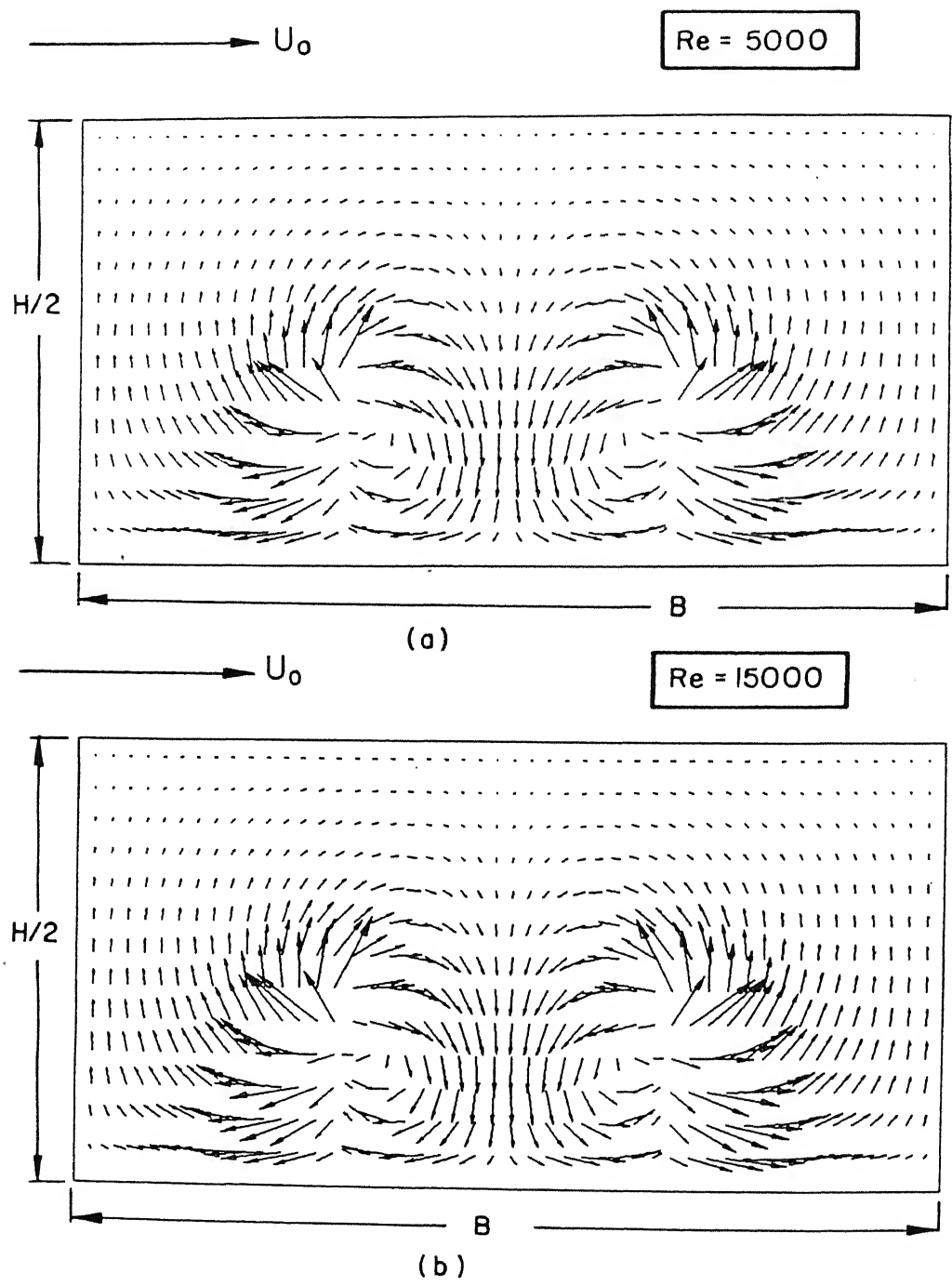


Figure 6.12: Cross-stream velocity vectors at $X=2.5$ from the inlet of the channel for two different Reynolds numbers

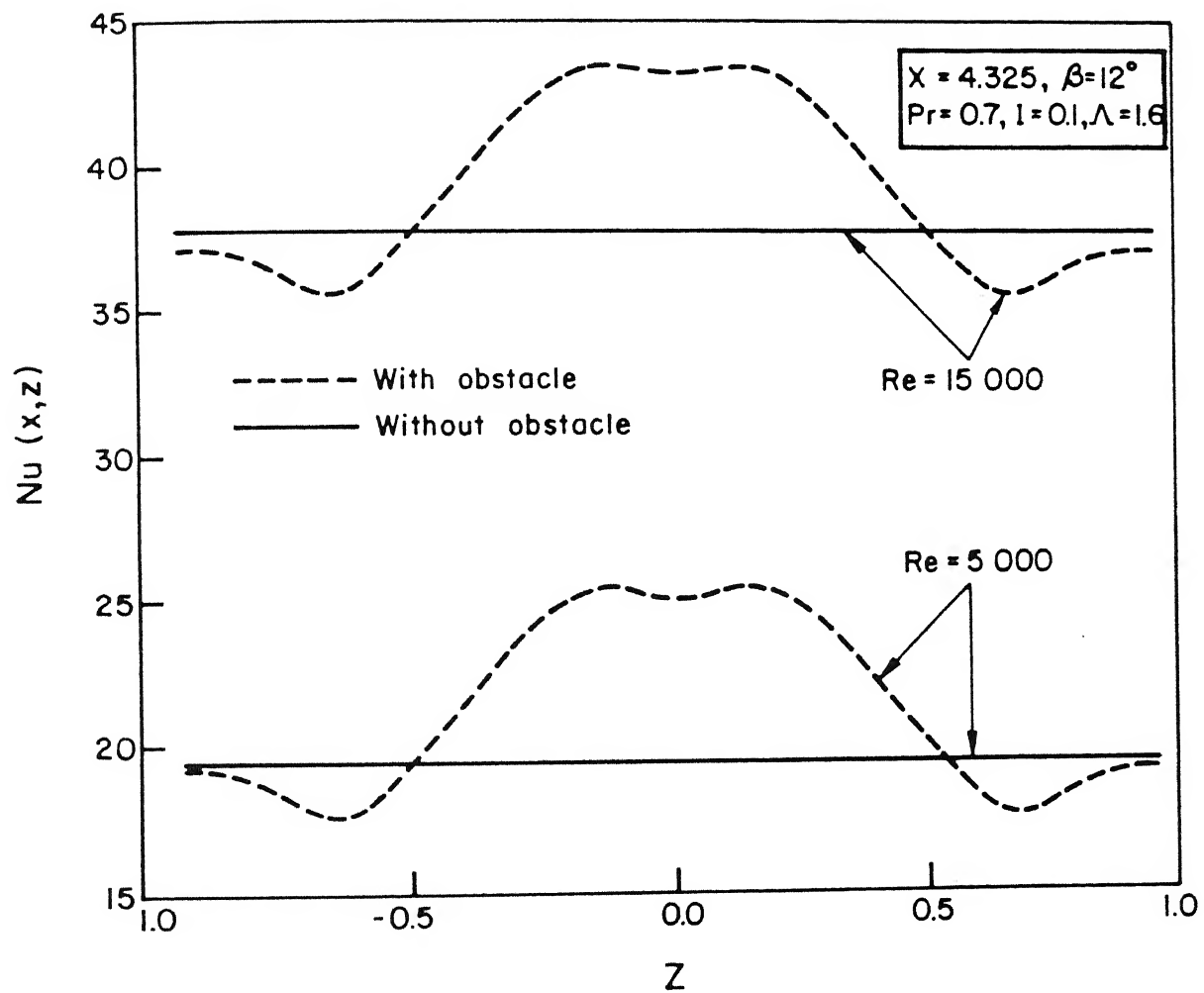


Figure 6.13: Spanwise variation of local Nusselt number for different Reynolds numbers at $X=4.325$

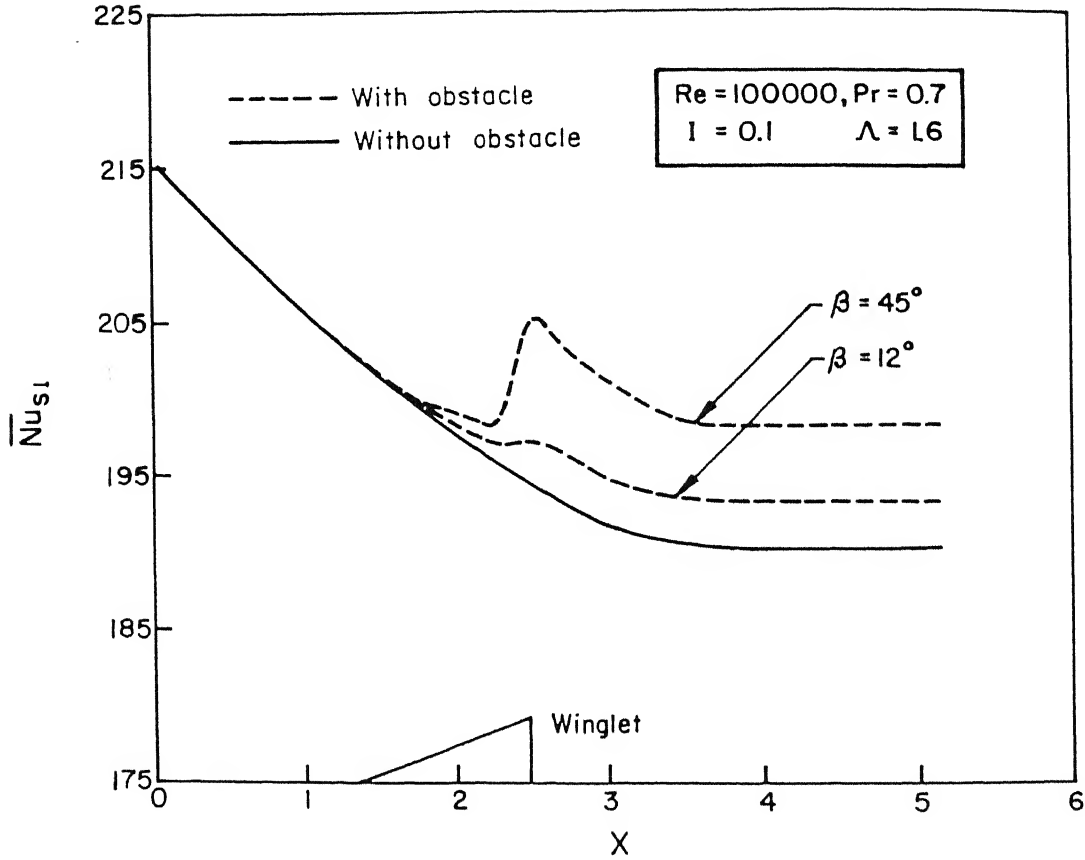


Figure 6.14: Distribution of spanwise average Nusselt number on the bottom plate for different angles of attack

Figure 6.14 shows the influence of angle of attack of the winglet-pair on the \overline{Nu}_{s1} over the bottom plate of the channel for a Reynolds number of 100000. Near the location of the trailing edge, for an angle of attack of 12° , we observe an enhanced \overline{Nu}_{s1} (absolute value of 4) over the case of a channel without any obstacle. The winglets with an angle of attack of 45° produce vortices with higher strength, which in turn result in further improvement of heat transfer. It may be mentioned that for the turbulent flow the transport rate is even otherwise high as compared to laminar flow. It is evident in Fig. 6.14 that even for a plane channel, the \overline{Nu}_{s1} value is reasonably high for the turbulent flow. Because of this reason, for the case of a built-in winglet-pair with an angle of attack of 45° , although the enhancement in \overline{Nu}_{s1} near the trailing edge is more than an absolute value of 12, in terms of percentage this value is not so high (6 percent).

The local skin friction coefficient at the bottom wall may be expressed as

$$C_f(x, z) = \frac{\tau_w}{\frac{1}{2}\rho U_o^2}$$

or,

$$C_f(x, z) = 2\tau_{w,n} \quad (6.13)$$

The spanwise average skin friction coefficient on the bottom wall is expressed as

$$C_{f,1} = \frac{2}{B} \int_0^{B/2} C_f(x, z) \, dz \quad (6.14)$$

The distribution of spanwise average skin friction coefficient ($\overline{C}_{f,1} \times Re$) for two different Reynolds numbers is shown in Fig. 6.15. The increase in peak values of the average skin friction coefficients are 33 and 27 percent for the Reynolds numbers of 5000 and 15000 respectively.

Effect of angle of attack on the distribution of spanwise average skin friction coefficient on the bottom plate of a channel for a Reynolds number of 100000 is shown in Fig. 6.16. At the location of the trailing edge, the vortex strength is boosted up by the trailing edge vortices. The near wake regions are highly distorted by the vortices but in the downstream, the vortices gradually lose their strength due to turbulent diffusion. However, for an angle of attack of 45° , at the location of the trailing edge, the increase in the spanwise average skin friction coefficient ($\overline{C}_{f,1} \times Re$) on the bottom wall is 8 percent more than that of the case of a plane channel. To summarize, it can be said the transport rate is usually very high for the turbulent channel flows even if there is no obstacle present in the channel. In presence of the vortex generators, the skin friction coefficient ($C_{f,1} \times Re$) increases by an absolute value of more than 19 but when this value is expressed in terms of percentage, the increase in flow loss appears to be somewhat less. It is also to be mentioned that the size of the vortex generators for turbulent flows is relatively small and the transport enhancement due to the vortex generators for turbulent flows is not as high as laminar flows.

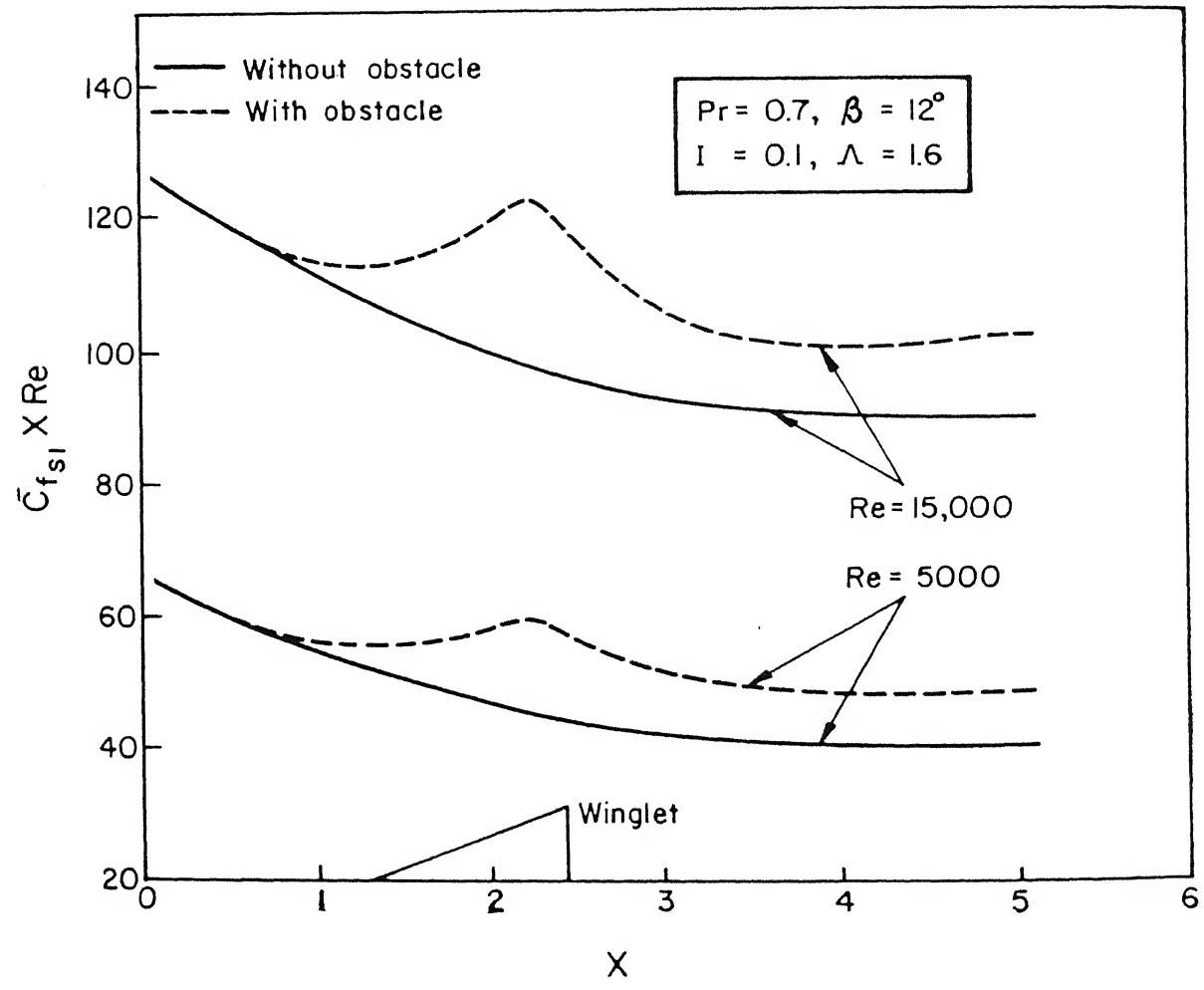


Figure 6.15: Distribution of spanwise average skin friction on the bottom plate for different Reynolds numbers

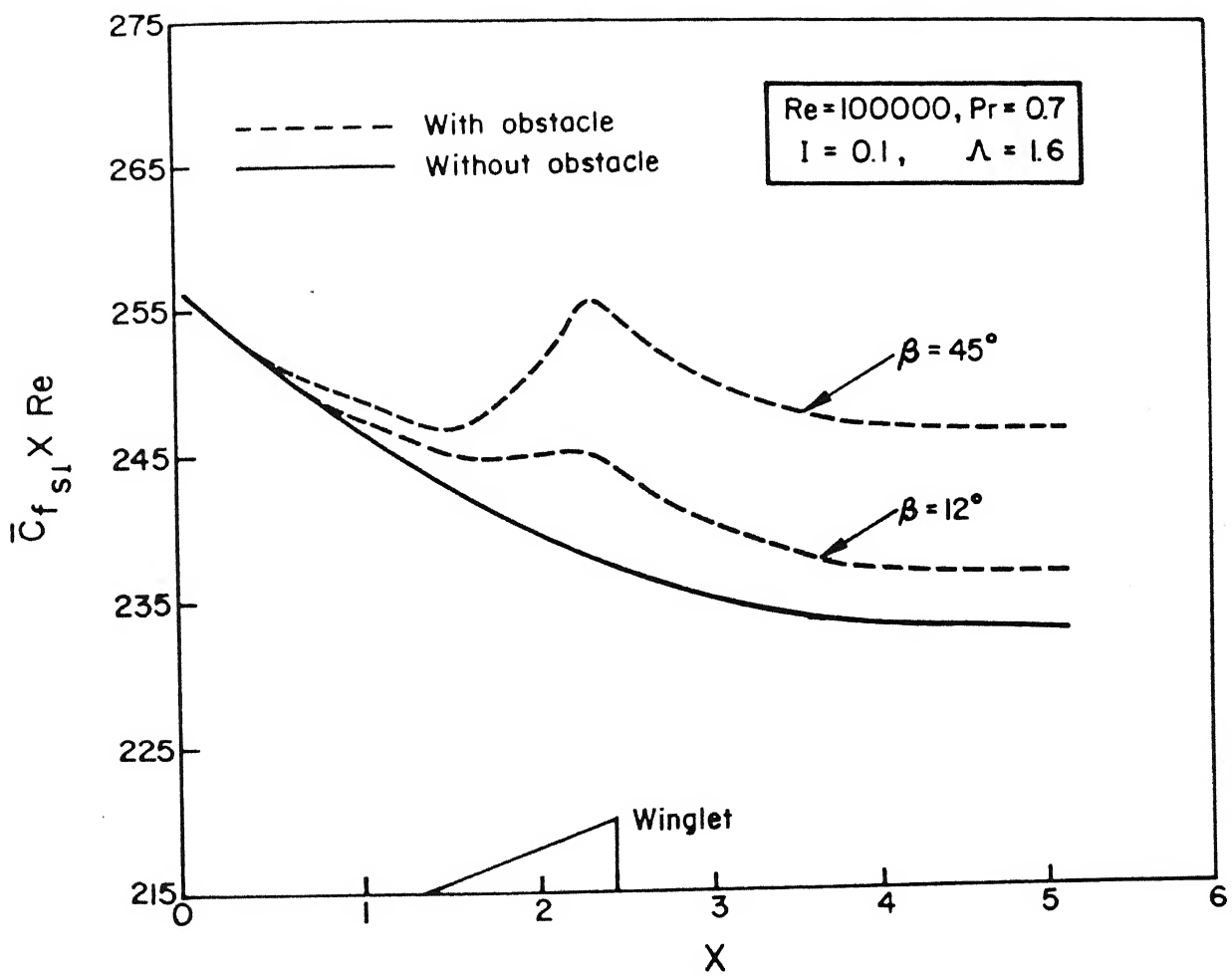


Figure 6.16: Distribution of spanwise average skin friction on the bottom plate for different angles of attack

Chapter 7

Concluding Remarks

The performance of heat exchanger surfaces can be significantly improved by mounting protrusions on the surfaces. Some typical examples of surface geometries which are popular in different industrial applications are wavy fins, offset strip fins, perforated fins and louvered fins. A somewhat different concept for the reduction of thermal resistance and consequent enhancement in heat transfer is to induce longitudinal vortices in the flow field. Longitudinal vortices generated by delta wings or winglets attached to the surface at an angle of attack persist over a long streamwise distance. The spiraling flow of these vortices serves to entrain fluid from their outside into their core. Thus, these vortices disrupt the growth of the boundary layer and serve ultimately to bring about enhancement of heat transfer between the fluid and its neighboring surfaces at the price of relatively less increase in pressure penalty.

The geometrical configuration considered in this thesis are representative of single elements of either a compact gas-liquid fin-tube crossflow heat exchanger or a plate-fin heat exchanger. A novel numerical model has been developed to study the suitability of the proposed modification on the surface-geometry of the above mentioned heat exchangers. The model involves computation of three dimensional Navier-Stokes and energy equations in a rectangular channel with a built-in wing or winglet-pair. A detailed evaluation of the performance parameters with regard to enhancement of heat transfer and associated flow losses using various wing-type vortex generators has been accomplished. Prediction of heat transfer in the laminar regime is validated through comparison with experiment results of a research group in the Ruhr University, Bochum of Germany. The numerical model and the experiment corroborate each other reasonably well.

From heat transfer point of view, delta wing is found to be more effective than winglet-pair. However, most convective heat transfer processes encounter two types of losses, *viz.*, losses due to fluid friction and those due to heat transfer across finite temperature gradient. Because these two phenomena are manifestations of irreversibility, an evaluation of the augmentation techniques is also made from a thermodynamic

viewpoint. Conclusions that are drawn thus identify winglet-pairs more efficient than the delta wings.

The model is also extended to compute turbulent flows. The flow is described by the unsteady Reynolds averaged Navier-Stokes equations and the k - ϵ model of turbulence. To mimic the transport processes near the wall, a two layer wall function treatment has been performed. The computed results are compared with the measurements of a research group in Stanford University of the USA. In general, the prediction is good although slight discrepancies are observed in the prediction of turbulent kinetic energy at places where the boundary layer is severely distorted by the vortices. Finally some important predictions are made with respect to enhancement of heat transfer for various Reynolds numbers in the turbulent regime.

It is understood that the wall function approach used in turbulent flow computations greatly reduces the storage and computational time as compared to those associated with the low Reynolds-number near-wall model of Jones and Launder (1973). However, it is also well-known that the wall-function approach is used on a rather simple intuition and it is not always consistent with complex physical picture near the wall. Instead of computing with the wall-function approach, two different but representative low-Reynolds number models designed for use with a standard k - ϵ two-equation turbulence model should be attempted. The models due to Lam and Bremhorst (1981) and Rodi and Mansour (1993) may be chosen for this purpose.

Bibliography

- Achaichia, A. and Cowell, T. W., 1988, Heat Transfer and Pressure Drop Characteristics of Flat Tube and Louvered Plate Fin Surfaces, *Experimental Thermal and Fluid Science*, vol. 1, pp 147-157.
- Acharya, S., and Patankar, S. V., 1985, Use of an Adaptive Grid Procedure for Parabolic Flow Problems, *Int. J. Heat Mass Transfer*, vol 28, pp 1057-1066.
- Acharya, S., Myrum, T. A., and Inamdar, S., 1991, Subharmonic Excitation of the Shear Layer Between Two Ribs: Vortex Interaction and Pressure Field, *AIAA J.*, vol. 29, pp. 1390-1399.
- Algifri, A. H., and Bharadwaj, R. K., 1985, Prediction of Heat transfer for Decaying Turbulent Swirl Flow in a Tube, *Int. J. Heat Mass Transfer*, vol. 28, pp 1637-1643.
- Amano, R. S., 1984, Development of a Turbulence Near-wall Model and its Application to Separated and Reattached Flows, *Numerical Heat Transfer*, vol. 7, pp 59-75.
- Amon, C. H., and Patera, A. T., 1989, Numerical Calculation of Stable Three-Dimensional Tertiary States in Grooved-Channel Flow, *The Phys. Fluids-A*, vol. 1, No. 12, pp. 2005-2009.
- Aung, W. and Goldstein, R. J., 1972, Heat Transfer in Turbulent Separated Flow Downstream of a Rearward Facing Step, *Israel J. Technol.*, vol. 10, no.1-2, pp. 35-41.
- Bakewell, H. P. Jr., and Lumley, J. L., 1967, Viscous Sublayer and Adjacent Wall Region in Turbulent Pipe Flow, *The Phys. Fluids*, vol. 10, No. 9, pp 1880-1889.
- Bejan, A., and Smith, J. L., Jr., 1975, Heat Exchangers for Vapour-Cooled Conducting Supports of Cryostats, *Advances in Cryogenic Engineering*, by K. D. Timmerhaus (Ed.), Plenum Press, vol. 21, pp. 247-256.
- Bejan, A., 1977, The Concept of Irreversibility in Heat Exchanger Design: Counterflow Heat Exchangers for Gas-to-Gas Applications, *Journal of Heat Transfer, ASME*, vol. 99, pp. 374-380.

- Bejan, A., 1978, General Criterion for Rating Heat Exchanger Performance, *Int. J. Heat Mass Transfer*, vol. 21, pp 655-658.
- Bejan., A., 1979a, A Study of Entropy Generation in Fundamental Convective Heat Transfer, *Journal of Heat Transfer*, vol. 101, pp 718-725.
- Bejan., A., 1979b, A General Variational Principle for Thermal Insulation System Design, *Int. J. Heat Mass Transfer*, vol. 22, pp 219-228.
- Bergles, A. E., 1978, Enhancement of Heat Transfer, *Heat Transfer 1978, Proceedings 6th International Heat Transfer Conference*, vol. 6, pp. 89-168.
- Bergles, A. E., Webb, R. L., Junkhan, G. H., and Jension, M. K., 1980, Bibliography on Augmentation of Convective Heat and Mass Transfer, *Heat Transfer Laboratory*, Department of Mechanical Engineering, Iowa State University, Ames, IA.
- Bergles, A. E., 1983, Augmentation of Heat Transfer, Heat Exchanger Design Handbook, Hemisphere Publishing Co., Washington DC, vol 2, pp 2.5.11-1-12
- Bergles, A. E., and Joshi, S. D., 1983, Augmentation Techniques for Low Reynolds Number In-Tube Flow, Low Reynolds Number Flow in Heat Exchangers, S. Kakac, Shah, R. K., and Bergles, A. E., 1981, Hemisphere, Washington, pp. 694-720.
- Bergles, A. E., 1985, Techniques to Augment Heat Transfer, Handbook of Heat Transfer Applications, McGraw-Hill, NewYork, pp. 3.1-80.
- Bernard, R. S., and Thompson, J. F., 1984, Mass Conservation on Regular Grids for Incompressible Flow, *AIAA-84-1669, 17th Fluid Dynamics, Plasma Dynamics and LASER Conference*.
- Bird, R. B., Stewart, W. E., and Lightfoot, E. N., 1960, Transport Phenomena, John Wiley & Sons, Inc., Singapore.
- Biswas, G., Mitra, N. K., and Fiebig, M., 1989, Computation of Laminar Mixed Convection Flow in a Channel with Wing type Built-inObstacles, *AIAA Journal of Thermophysics and Heat Transfer*, vol.3, pp 447-453.
- Biswas, G., Laschefski, H., Mitra, N. K., and Fiebig, M., 1990, Numerical Investigation of Mixed Convection Heat Transfer in a Horizontal Channel with a Built-In Square Cylinder, *Numerical Heat Transfer, Part - A*, vol. 18, pp. 173-188.

- Biswas, G. and Chattopadhyay, H., 1992, Heat Transfer in a Channel with Built-In Wing-Type Vortex Generators, *Int. J. of Heat and Mass Transfer*, vol 35, pp 803-814.
- Biswas, G., Mitra, N. K., and Fiebig, M., 1994, Heat Transfer Enhancement in Fin-Tube Heat Exchangers by Winglet-Type Vortex Generators, *Int. J. Heat Mass Transfer*, vol. 37, pp.283-291.
- Blum, H. A., and Oliver, L. R., 1966, Heat Transfer in Decaying Vortex System, *ASME Paper*, No. 66-WA/HT-62.
- Bozeman, J. D. and Dalton, C., 1973, Numerical Study of Viscous Flow in a Cavity, *J. Comp. Phys.*, vol. 12, pp 348-363.
- Bradshaw, P., 1971, An Introduction to Turbulence and its Measurement, Pergamen Press, Oxford.
- Brandt, A., Dendy, J. E., and Ruppel, H., 1980, The Multigrid Method for Semi-Implicit Hydrodynamics Codes, *J. Comp. Phys.*, vol. 34, pp. 348-370.
- Braza, M., Chassaing, P., and Ha-Minh, H., 1986, Numerical Study and Physical analysis of the Pressure and Velocity Fields in the Near Wake of a Circular Cylinder, *J. Fluid Mech.*, vol. 165, pp. 79-130.
- Brown, C. E., and Michael, W. H., 1954, Effect of Leading Edge Separation on the Lift of a Delta Wing, *J. Aero. Sci.*, vol. 21, pp. 690-694.
- Chorin, A. J., 1967, A Numerical Method for Solving Incompressible Viscous Flow Problems , *J. Comp. Phys.*, vol 2, pp 12-26.
- Christie, I. Griffiths, D. F., and Mitchell, A. R., 1976, Finite Element Methods for Second-Order Differential Equations with Significant First Derivatives, *Int. J. Numer. Methods Engg.*, vol. 10, pp. 1389-1396.
- Date, A. W., 1973, Flow in Tubes Containing Twisted Tapes, *Heating and Ventilating Eng.*, vol. 47, pp. 240-249.
- Date, A. W., 1974, Prediction of Fully-Developed Flow in a Tube Containing a Twisted Tape, *Int. J. Heat Mass Transfer*, vol. 17, pp. 845-859.
- Davis, R. W., and Moore, E. F., 1982, A Numerical Study of Vortex Shedding from

Rectangles, *J. Fluid Mech.*, vol. 116, pp. 475-506.

Dong, Y., 1989, Experimentelle Untersuchung der Wechselwirkung von Längswirbelzeugern und Kreiszylindern in Bezug auf Wärmeübergang und Strömungsverlust, Doctoral Thesis, Ruhr-Universität Bochum, Germany.

Dutta, S., and Acharya, S., 1993, Heat Transfer and Flow Past a Backstep with the Nonlinear $k-\epsilon$ Turbulence Model and the Modified $k-\epsilon$ Turbulence Model, *Numerical Heat Transfer*, Part A, vol. 23, pp 281-301.

Eaton, J. K., 1993, Personal Communications through a Data Tape of Experimental Results.

Edwards, F. J., and Alker, G. J. R., 1974, The Improvement of Forced Convection Surface Heat Transfer Using Surface Protrusions in the Form of (a) Cubes and (b) Vortex Generators, *Proceedings of the Fifth Int. Heat Transfer Conference*, Tokyo, vol. 2, pp. 2244-2248.

Eibeck, P. A. and Eaton, J. K., 1987, Heat Transfer Effects of a Longitudinal Vortex Embedded in a Turbulent Shear Flow, *Journal of Heat Transfer*, vol. 109 pp 16-24.

Faghri, M., Sparrow, E. M., and Prata, A. T., 1984, Finite Difference Solutions of Convection Diffusion Problems in Irregular Domains Using a Non-Orthogonal Coordinate Transformation, *Numerical Heat Transfer*, vol. 7, pp. 183-209.

Ferziger, J. H., 1987, Simulation of Incompressible Turbulent Flows, *J. Comp. Phys.*, vol. 69, pp 1-48.

Fiebig, M., Kallweit, P. and Mitra, N. K., 1986, Wing Type Vortex Generators For Heat Transfer Enhancement, *Proceedings of the Eighth Int. Heat Transfer Conference*, San Francisco, vol. 6, pp 2909-2913.

Fiebig, M., Brockmeier, U., Mitra, N. K. and Güntermann, T., 1989, Structure of Velocity and Temperature Fields in Laminar Channel Flows with Longitudinal Vortex Generators, *Numerical Heat Transfer - Part A*, vol.15, pp 281-302.

Fiebig, M., Kallweit, P., Mitra, N. K. and Tiggelbeck, S., 1991, Heat Transfer Enhancement and Drag by Longitudinal Vortex Generators in Channel Flow, *Experimental Thermal and Fluid Science*, vol. 4, pp 103 - 114.

- Fink, P. T., 1956, Wind-Tunnel Tests on a Slender Delta Wing at High Incidence, *Flugwiss*, vol. 4, pp. 247-249.
- Fletcher, C. A. J., 1988, Computational Techniques for Fluid Dynamics, vol. 1, (Fundamentals and General Techniques), Springer Verlag.
- Gal-Chen, T., and Somerville, R. C. J., 1975, Numerical Solution of the Navier Stokes Equations with Topography, *J. Comp. Phys.*, vol. 17, pp. 276-310.
- Galpin, P. F., and Raithby, G. D., 1986, Treatment of Nonlinearities in the Numerical Solution of the Incompressible Navier Stokes Equations, *Int. J. Numer. Methods Eng.*, vol 6, pp 409-426.
- Gambill, W. R., and Bundy, R. D., 1963, High Heat Flux Heat Transfer Characteristics of Pure Ethylene Glycol in Axial and Swirl Flow, *AIChE Journal*, vol. 9, pp 55-59.
- Garg, V. K., and Maji, P. K., 1987, Flow through a Converging-Diverging Tube with Constant Wall Enthalpy, *Numerical Heat Transfer*, vol 12, pp 285-305.
- Ghaddar, N. K., Korczak, K. Z., Mikic, B. B., and Patera, A. T., 1986a, Numerical Investigation of Incompressible Flow in Grooved Channels, Part 2- Stability and Self-Sustained Oscillations, *J. Fluid Mech.*, vol. 163, pp. 99-127.
- Ghaddar, N. K., Magen, M., Mikic, B. B., and Patera, A. T., 1986b, Numerical Investigation of Incompressible Flow in Grooved Channels, Part 1- Resonance and Oscillatory Heat-Transfer enhancement, *J. Fluid Mech.*, vol. 168, pp. 541-567.
- Ghia, U., Ghia, K. N., and Shin, C. T., 1982, High-Resolutions for Incompressible Flow Using the Navier-Stokes Equations and a Multigrid Method, *J. Comp. Phys.*, vol. 48, pp. 387-411.
- Gibson, M. M., and Launder, B. E., 1978, Ground Effects on the Pressure Fluctuations in the Atmospheric Boundary Layer, *J. Fluid Mech.*, vol. 86, pp 491-511.
- Gosman, A. D., and Rapley, C. W., 1980, Fully Developed Flow in Passages of Arbitrary Cross-section, Recent Advances in Numerical Methods in Fluids, C. Taylor and K. Morgan (Eds), Pineridge Press, Swansea.
- Harlow, F. H. and Welch, J. E., 1965, Numerical Calculation of Time-dependent Viscous Incompressible Flow of Fluid with Free Surface , *The Phys. Fluids* , vol 8, pp 2182-2188.

- Flow, F. H. and Amsden, A. A., 1970, The SMAC Method : A Numerical Technique for Calculating Incompressible Fluid Flows , Los Alamos Scientific Lab. Rept., LA 4370.
- Issan Y. A., Rice, J. G., and Kim, J. H., 1983, A Stable Mass Flow Weighted Two dimensional Skew Upwind Scheme, *Numerical Heat Transfer*, vol 6, pp 395-408.
- Patankar, J. O., 1987, Turbulence, McGraw-Hill Book Company.
- Patankar, C. W. and Cook, J. L., 1972, Calculating Three-Dimensional Flows around Structures and over Rough Terrain, *J. Comp. Phys.*, vol 10 , pp 324-340.
- Patankar, C. W., Nichols, B. D., and Romero, N. C., 1975, SOLA - A Numerical Solution Algorithm for Transient Fluid Flows, Los Alamos Scientific Laboratory Rept., LA-5652.
- Patankar, S. and Leschziner, M. A., 1989a, Computation of Highly Swirling Confined Flow with a Reynolds-Stress Turbulence Model, *AIAA J.*, vol. 27, pp 57-63.
- Patankar, S. and Leschziner, M. A., 1989b, Second-Moment-Closure Calculation of Strongly-wirling Confined Flow with Large Density Gradients, *Int. J. Heat and Fluid Flow*, vol. 10, pp 16-27.
- Patankar, S. W., and Bergles, A. E., 1976, Augmentation of Laminar Flow Heat Transfer by Means of Twisted Tape Inserts, *Journal of Heat Transfer*, vol. 98, pp. 252-256.
- Hummel, D., and Srinivasan, P. S., 1967, Vortex Breakdown Effects on the Low-Speed Aerodynamic Characteristics of Delta Wings in Symmetrical Flow, *J. Roy. Aero. Soc.*, vol. 71, pp. 319-322.
- Hummel, D., 1973, Study of the Flow Around Sharp-Edges Slender Delta Wings with Large Angles of Attack, NASA TTF -15, vol. 107.
- Hummel, D., 1978, On the Vortex Formation over a Slender Wing at Large Angles of Incidence, *Fluid Dynamics Panel Symposium*, Sandefjord, Norway, AGARD-CP-247, pp 15.1-15.17.
- Incropera, F. P., and Schutt, J. A., 1985, Numerical Simulation of Laminar Mixed Convection in the Entrance Region of Horizontal Rectangular Ducts, *Numerical Heat Transfer*, vol. 8, pp. 707-729.
- Incropera, F. P., Knox, A. L., Maughan, J. R., 1987, Mixed-Convection Flow and

Heat Transfer in the Entry Region of a Horizontal Rectangular Duct, *Journal of Heat Transfer*, vol. 109, pp. 434-439.

Issa, R. I., Gosman, A. D. and Watkins A. P., 1986, The Computation of Compressible and Incompressible Recirculating Flows by a Non-iterative Implicit Scheme, *J. Comp. Phys.*, vol. 62, pp 66-82.

Jang, D. S., Jetli, R. and Acharya, S., 1986, Comparison of PISO, SIMPLER and SIMPLEC Algorithms for the Treatment of the Pressure Velocity Coupling in Steady Flow Problems, *Numerical Heat Transfer*, vol. 10, pp 209-228.

Johnson, F. T., Lu, P., Brune, G., W., Webber, J. A., and Rubbert, P. E., 1976, An Improved Method for Prediction of Complete Three-Dimensional Aerodynamic Load Distribution on Configurations with Leading-Edge Separation, *AIAA J.*, AIAA Paper no. 76-147.

Jones, W. P. and Launder, B. E., 1972, The Prediction of Laminarization with a Two-Equation Model of Turbulence, *Int. J. Heat Mass Transfer*, vol.15, pp 301-314.

Jones, W. P. and Launder, B. E., 1973, The Calculation Of Low-Reynolds-Number Phenomena with a Two-Equation Model of Turbulence, *Int. J. Heat Mass Transfer*, vol.16, pp 1119-1130.

Junkhan, G. H., Bergles, A. D., Nirmalan, V., and Ravigururajan, T., 1985, Investigation of Turbulators for Five Tube Boilers, *Journal of Heat Transfer*, vol. 107, pp. 354-360.

Kakac, S., Shah, R. K., Bergles, A. E., 1981, Low Reynolds Number Flow Heat Exchangers, Hemisphere Publishing Corp, Washington.

Kakac, S., Shah, R. K., and Aung, W., 1987, Handbook of Single Phase Convective Heat Transfer, John Wiley & Sons, pp 4.55.

Kandil, O. A., Mook, D. T. and Nayfeh, A. H., 1976, Nonlinear Prediction of Aerodynamic Loads on the Lifting Surfaces, *J. Aircraft*, vol. 13, pp. 22-28.

Kawamura, T., Kuwahara, K., and Takami, H., 1986, Computation of High Reynolds Number Flow Around a Circular Cylinder with Surface Roughness, *Fluid Dynamics Research*, vol. 1, pp. 145-162.

Kim, S. W., and Benson, T. J., 1992, Comparison of SMAC, PISO and Iterative Time-Advancing Schemes for Unsteady Flows, *Computers & Fluids*, vol. 21, pp. 435-454.

Kreith, F., and Margolis, D., 1959, Heat Transfer and Friction Factor in Turbulent Vortex Flow, *Applied Scientific Research*, vol. 8, pp 457-473.

Kirkwood, J. G., and Crawford, B. L. Jr., 1952, The Macroscopic Equations of Transport, *J. Phys. Chem.*, vol. 56, pp. 1048-1051.

Lam, C. K. G., and Bremhorst, K., 1981, A Modified Form of the $k-\epsilon$ Model for Predicting Wall Turbulence, *J. Fluids Engg. (ASME)*, vol.103, pp 456-460.

Launder, B. E., Reace, G. J., and Rodi, W., 1975, Progress in the Development of a Reynolds-Stress Closure, *J. Fluid Mech.*, vol. 68, pp 537-566.

Launder, B. E., and Spalding, D. B., 1972, Mathematical Models of Turbulence, Academic Press, London.

Launder, B. E., and Spalding, D. B., 1974, The Numerical Computation of Turbulence Flows, *Comp. Methods in App. Mech. and Engg.*, vol.3, pp 269-289.

Lawal, A., and Mujumdar, A. S., 1985, Laminar Flow and Heat Transfer in Power Law Fluids Flowing in Arbitrary Cross-sectional Ducts, *Numerical Heat Transfer*, vol. 8, pp 217-244.

Lawford, J. A., 1964, Low Speed Wind Tunnel Experiments on Series of Sharp-Edged Delta Wings, Part 2, RAE, Rep. Aero. 2954.

Leonard, B. P., 1979, A Stable and Accurate Convective Modelling Procedure Based on Quadratic Upstream Interpolation, *Comput. Methods Appl. Mech. Eng.*, vol 19, pp 59-98.

Leonard, B. P., 1984, Third-Order Upwinding as a Rational Basis for Computational Fluid Dynamics, *Computational Techniques & Applications*, CTAC-83, edited by J. Noye and CAJ Fletcher, pp 106-120.

Leschziner, M. A., and Rodi, W., 1981, Calculation of Annular and Twin Parallel Jets

- Using Various Discretization Schemes and Turbulence-Model Variations, *J. of Fluids Engg. (ASME)*, vol.103, pp 352-360.
- Ligrani, P. M., Subramanian, C. S., Craig, D. W., Kaisuwan, P., 1991, Effects of Vortices With Different Circulations on Heat Transfer and Injectant Downstream of a Row of Film-cooling Holes in a Turbulent Boundary Layer, *Journal of Heat Transfer*, vol. 113, pp 79-90.
- Majumdar, D., and Amon, C. H., 1992, Heat and Momentum Transport in Self-Sustained Oscillatory Viscous Flows, *Journal of Heat Transfer*, vol. 114, pp. 866-873.
- Majumdar, S., Rodi, W., and Zhu, J., 1992, Three-Dimensional Finite-Volume Method for Incompressible Flows with Complex Boundaries, *J. of Fluids Engg. (ASME)*, vol. 114, pp. 496-503.
- Maliska, C. R., and Raithby, G. D., 1984, A Method for Computing Three-Dimensional Flows Using Non-Orthogonal Boundary Fitted Coordinates, *Int. J. Numer. Methods Fluids*, vol. 4, pp. 519-537.
- Mangler, K. W., and Smith, J. H. B., 1959, A Theory of Flow Past a Slender Delta Wing with Leading Edge Separation, *Proc. Roy. Soc. Lond*, vol. A251, pp. 200-217.
- McClintock, F., A., 1951, The Design of Heat Exchangers for Minimum Irreversibility, ASME Paper No. 51-A-108, Presented at the 1951 Annual Meeting of the ASME (1951).
- Marsden, D. J., Simpson, R. W., and Rainbird, W. J., 1958, The Flow Over Delta Wing at Low Speeds with Leading Edge Separation, *College of Aeronautics, Cranfield*, Rep. 114.
- Migay, V. K., and Golubev, L. K., 1970, Friction and Heat Transfer in Turbulent Swirl Flow with a Variable Swirl Generator in a Pipe, *Heat Transfer - Soviet Research*, vol. 2, pp. 68-73.
- Moffat, R. J., 1987, Describing the Uncertainties in Experimental Results, *Experimental Thermal and Fluid Science*, vol.1, pp 3-17.
- Moran, M. J., 1982, Availability Analysis :A Guide to Efficient Energy Use, Prentice Hall, Englewood Cliffs, NJ, pp 58-85.
- Mukherjee, P., Biswas, G., and Nag, P. K., 1987, Second Law Analysis of Heat Transfer

BIBLIOGRAPHY

- g Flow Through a Cylindrical Duct, *Journal of Heat Transfer*, vol. 109, pp
- adhyay, A., Sundararajan, T., and Biswas, G., 1993, An Explicit Transient m for Predicting Incompressible Viscous Flows in Arbitrary Geometry, *Int. J. Methods Fluids*, vol. 17, pp. 975-993.
- T. A., Acharya, S., Inamdar, S., and Mehrotra, A., 1992, Vortex Generator Heat Transfer Augmentation Past a Rib in a Heated Duct Air Flow, *Journal Transfer*, vol. 114, pp. 280-284.
- K., and Mukherjee, P., 1987, Thermodynamic Optimization of Convective Heat r Through a Duct with Constant Wall Temperature, *Int. J. Heat Mass Trans-* . 30, pp. 401-405.
- my, M., 1987, Turbulence Models and their Applications to the Prediction of l Flows: A Review, *Computers & Fluids*, vol.15, pp 151-194.
- kumar, K., Masliyah, J. H., and Law, H. S., 1985, Bifurcation in Steady Lami- xed Convection Flow in Horizontal Ducts, *J. Fluid Mech.*, vol. 152, pp. 145-161.
- s, B. D., and Hirt, C. W., 1971, Improved Free Surface Boundary Conditions merical Incompressible-Flow Calculations, *J. Comp. Phys.*, vol. 8, pp. 434-448.
- kar, S. V., Ramadhyani, S., and Sparrow, E. M., 1978, Effect of Circumferen- Nonuniform Heating on Laminar Combined Convection in a Horizontal Tube, *al of Heat Transfer*, vol. 100, pp. 63-70.
- kar, S. V. and Spalding, D. B., 1972, A Calculation Procedure for Heat Mass Momentum Transfer in Three-dimensional Parabolic Flows , *Int. J. Heat Mass sfer*, vol 15, pp 1787-1806.
- kar, S. V., 1980, Numerical Heat Transfer and Fluid Flow, Hemisphere , Wash- n D.C.
- nk, S. V., 1981, A Calculation Procedure for Two-Dimensional Elliptic Situa- , *Numerical Heat Transfer* , vol 4, pp 409-425.
- ey, W. R., and Eaton, J. K., 1988a, The Fluid Dynamics and Heat Transfer Ef- of Streamwise Vortices Embedded in a Turbulent Boundarylayer, *Rept. MD-51, rmosciences Division*, Department of Mechanical Engineering, Stanford Univer-

sity, USA.

Pauley, W. R., and Eaton, J. K., 1988b, Experimental Study of the Development of Longitudinal Vortex Pairs Embedded in a Turbulent Boundary Layer, *AIAA J.*, vol. 26, No.7, pp.816-823.

Pearcy, H. H., 1961, Shock-Induced Separation in Boundary Layers, in Boundary Layers and Flow Control, vol. 2, Pergamon Press, New York.

Peric, M., 1985, A Finite Volume Method for the Prediction of Three-Dimensional Fluid Flow in Complex Ducts, Ph.D. Thesis, University of London.

Peric, M., Kessler, R., and Scheuerer, 1988, Comparison of Finite-Volume Numerical Methods with Staggered and Collocated Grids, *Computers & Fluids*, vol. 16, pp. 389-403.

Peyret, R., and Taylor, T. D., 1983, Computational Methods for Fluids Flow, Springer-Verlag, New York.

Pollard, A. and Siu, L. W. A., 1982, The Calculation of Some Laminar Flows Using Various Discretization Schemes, *Comput. Methods Appl. Mech. Eng.*, vol 35, pp 293-313.

Pope, S. B., 1978, The Calculation of Turbulent Recirculating Flows in General Orthogonal Coordinates, *J. Comp. Phys.*, vol. 26, pp. 197-217.

Rai, M. M., and Moin, P., 1991, Direct Simulations of Turbulent Flow Using Finite-Difference Schemes, *J. Comp. Phys.*, vol.96, pp 15-53.

Raithby, G. D., 1976, Skew Upstream Differencing Schemes for Problems Involving Fluid Flow, *Comput. Methods Appl. Mech. Eng.*, vol 9, pp 153-164.

Rehbach, C., 1976, Numerical Investigations of Leading-Edge Vortex for Low Aspect-Ratio Thin Wings, *AIAA J.*, vol. 14, pp. 253-255.

Rhie, C. M., and Chow, W. L., 1983, Numerical Study of the Turbulent Flow Past an Airfoil with Trailing Edge Separation, *AIAA J.*, vol. 21, pp. 1525-1532.

Roache, P. J., 1972, Computational Fluid Dynamics, Hermosa Publ., Albuquerque, New Mexico.

Roberts, K. V. and Weiss, N. O., 1966, Convective Difference Schemes, *Math. Comp.*, vol. 20, pp 272-299.

Robichaux, J., Tafti, D. K., and Vanka, S. P., 1992, Large-Eddy Simulations of Turbulence on the CM-2, *Numerical Heat Transfer*, Part-B, vol. 21, pp 367-388.

Rodi, W., 1976, A New Algebraic Relation for Calculating the Reynolds-Stresses, *ZAMM*, vol. 56, pp 219-221.

Rodi, W., and Mansour, N. N., 1993, Low Reynolds Number $k-\epsilon$ Modelling with the Aid of Direct Simulation Data, *J. Fluid Mech.*, vol.250, pp 509-529.

Rodi, W., and Spalding, D. B., 1970, A Two-Parameter Model of Turbulence, and its Application to Free Jets, *Wärme und Stoffübertragung*, vol.3, pp 85-95.

Rodi, W., 1984, Turbulence Models and their Application in Hydraulics, IAHR, Delft, The Netherlands.

Runchal, A. K., 1987, CONDIF : A Modified Central Difference Scheme for Convective Flows, *Int. J. Numer. Methods Eng.*, vol 24, pp 1593-1608.

Runchal, A. K., and Wolfstein, M., 1969, Numerical Integration Procedure for the Steady State Navier-Stokes Equations, *J. Mech. Engg. Sci.*, vol. 11, pp. 445-452.

Russels, C. M. B., Jones, T. V., and Lee, G. H., 1982, Heat Transfer Enhancement Using Vortex Generators, *Proceedings of the Seventh Int. Heat Transfer Conference*, Munich, vol. 3, pp. 283-288.

Sanchez, M., Mitra, N. K., Fiebig, M., 1989, Numerical Investigation of Three-Dimensional Laminar Flows in a channel with Built-in Circular Cylinder Wing-Type Vortex Generators, *Proc. Eighth GAMM-Conference on Numerical Methods in Fluid Mechanics (Vieweg)*, pp. 484-492.

Sarangı, S., and Chowdhury, K., 1982, On the Generation of Entropy in Counter Flow Heat Exchangers, *Cryogenics*, vol. 22, pp 63-65.

Schlichting, H., 1987, Boundary Layer Theory, McGraw Hill Book Company, New York.

Schmidt, H., and Schumann, U., 1989, Coherent Structure of the Convective Boundary Layer Derived from Large-Eddy simulations, *J. Fluid Mech.*, vol.200, pp 511-562.

- Schumann, U., 1975, Subgrid Scale Model for Finite-Difference Simulations of Turbulent Flows in Plane Channels and Annuli, *J. Comp. Phys.*, vol. 18, pp 376-404.
- Shah, R. K., and London, A. L., 1978, Laminar Flow Forced Convection in Ducts, *Advances in Heat Transfer*, Suppl. 1, Academic Press, New York, pp 169 -176.
- Shirayama, S., 1992, Construction of Modified Third-Order Upwind Schemes for Stretched Meshes, *AIAA J.*, vol 30, pp 1237-1242.
- Shyy W., 1985, A Study of Finite Difference Approximations to Steady State, Convection Dominated Flow Problems, *J. Comp. Phys*, vol 57, pp 415-438.
- Smith, J. H. B., 1968, Improved Calculations of Leading Edge Separation from Slender Delta Wings, *Proc. Roy. Soc. Lond*, vol. A306, pp. 67-90.
- Smithberg, E., and Landis, F., 1964, Friction and Forced Convection Heat Transfer Characteristics in Tube with Twisted Tape Swirl Generator, *Journal of Heat Transfer*, vol. 86, pp. 39-49.
- Som, S. K., Mitra, A. K., and Sengupta, S. P., 1990, Second Law Analysis of Spray Evaporation, *Journal of Energy Resources Technology*, (ASME), vol. 112, pp 130-135.
- Spalding, D. B., 1972, A Novel Finite Difference Formulation for Differential Expressions Involving Both first and Second Derivatives, *Int. J. Numer. Methods Eng.*, vol 4, pp 551-559.
- Sparrow, E. M., and Chaboki, A., 1984, Swirl Affected Turbulent Fluid Flow and Heat Transfer in a Circular Tube, *Journal of Heat Transfer*, vol. 106, pp. 766-773.
- Speziale, C. G., 1987, On Nonlinear $k-l$ and $k-\epsilon$ Models of Turbulence, *J. Fluid Mech.*, vol.178, pp. 459-475.
- Tamamidis, P., and Assanis, D. N., 1993, Three-Dimensional Incompressible Flow Calculations with Alternative Discretization Schemes, *Numerical Heat Transfer*, Part - B, vol. 24, pp 57-76.
- Thakur, S., and Shyy, W., 1993, Some Implementational Issues of Convection Schemes for Finite-Volume Formulations, *Numerical Heat Transfer*, Part - B, vol 24, pp 31-55.
- Thomas, J. L., Krist, S. T., and Anderson, W. K., 1990, Navier Stokes Computa-

tions of Vortical Flows over Low-Aspect-Ratio Wings, *AIAA J.*, vol. 28, pp. 205-212.

Thompson, J. F., Warsi, Z. U. A., and Mastin, C. W., 1982, Boundary Fitted Coordinate System for Numerical Solution of Partial Differential Equations - A Review, *J. Comp. Phys.*, vol. 47, pp. 1-108.

Tiggelbeck, S., Mitra, N. K., and Fiebig, M., 1992, Flow Structure and Heat Transfer in a Channel with Multiple Longitudinal Vortex-Generators, *Experimental Thermal and Fluid Science*, vol.5, pp 425-436.

Timin, T, and Esmail, M. N., 1983, A Comparative Study of Central and Upwind Difference Schemes Using the Primitive Variables, *Int. J. Numer. Methods Fluids*, vol. 3, pp. 295-305.

Valencia, A., 1992, Wärmeübergang und Druckverlust in Lamellen-Rohr-Wärmeübertragern mit Langswirbelerzeugern, Doctoral Thesis, Ruhr-Universität Bochum, Germany.

Van Doormaal, J. P. and Raithby G. D., 1984, Enhancements of the SIMPLE Method for Predicting Incompressible Fluid Flows, *Numerical Heat Transfer*, vol 7, pp 147-163.

van Dyke, M., 1982, An album of fluid motion, Dept. of Mechanical Engineering, Stanford University and Parabolic Press, USA.

Vanka, S. P., Chen, B. C. J. and Sha W. T., 1980, A Semi - Implicit calculation Procedure for Flows Described in Boundary Fitted Coordinate Systems, *Numerical Heat Transfer*, Part - B, vol 3, pp 1-19.

Vanka, S. P., 1987, Second-Order Upwind Differencing in a Recirculating Flow, *AIAA J.*, vol. 25, pp. 1435-1441.

Velusamy, K., and Garg, V. K., 1993, Entrance Flow in Elliptical Ducts, *Int. J. Numer. Methods Fluids*, vol. 17, pp. 1079-1096.

Viecelli, A. J., 1971, A Computing Method for Incompressible Flows bounded by Moving Walls, *J. Comp. Phys.*, vol 8, pp 119-143.

Webb, B. W., and Ramadhyani, S., 1985, Conjugate Heat Transfer in a Channel with Staggered ribs, *Int. J. Heat Mass Transfer*, vol. 28, pp. 1679-1687.

Webb, R. L., 1987, Enhancement of Single-Phase Convective Heat Transfer, Handbook of Single Phase Convective Heat Transfer, John Wiley & Sons, New York.

Weber, J. A., Brune, G. W., Johnson, F. T., Lu, P., and Rubbert, P. E., 1976, Three-Dimensional Solution of Flow over Wings with Leading Edge Vortex Separation, *AIAA J.*, vol. 14, pp. 519-525.

Winter, H., 1956, Strömungsvorgänge on Plattern and Profilerten Körpern bei Kleinen Spannweiten, *Forsch. Ing. Wes.*, vol. 6, pp. 247-249.

Westphal, R. V., and Mehta, R. D., 1987, Interaction of an Oscillating Vortex with a Turbulent Boundary Layer, *AIAA 19th Fluid Dynamics and Laser Conference*, Hawaii, AIAA Paper no. 87 - 1246.

Zhu, J. X., Fiebig, M., and Mitra, N. K., 1993, Comparison of Numerical and Experimental Results for a Turbulent Flow Field with a Longitudinal Vortex Pair, *J. Fluids Engg. (ASME)*, vol.115 , pp 270-274.

Appendix A

The Program Substructure

In order to solve the full Navier-Stokes and energy equations for both laminar and turbulent flows, a computer code has been developed based on the numerical methods described in Chapter-3. The code has been written in FORTRAN-77 language. The code consists of several subroutines each of which has a set of specific tasks to carry out. The main program (DELTAM) and the subroutines are written in the form of modules. A flow chart is provided in Fig. A-1 showing the operational sequence of the various subroutines with their major communication links with the main program. A short description of different indices and the main functions of different subroutines are given below:

INIT	This is a subroutine which initializes the entire calculations for a set of input variables such as Reynolds number, Prandtl number, grid sizes etc.
IREST	This is an index which denotes whether a restart from a set of existing field variables are desired (=1) or the computation should start from the beginning (=0)
START	This subroutine creates the guessed field for the dependent variables and initiates computation
RESTAR	This is a subroutine where the field variables are equated to a data field which was existing beforehand

CONTI	This is a subroutine which controls the pressure-velocity iteration loop
JSTAM	This is a parameter which denotes whether there is a stamping on the walls (=1) or not (=0) in the computation for laminar flows
BCC	This subroutine deals with the boundary conditions for continuity equation
BCCST	This subroutine deals with the boundary conditions for continuity equation in the presence of stampings on the walls
BCO	In this subroutine some of the geometrical parameters for the obstacle are defined
CEQCP	This is a subroutine where divergence of velocity vector (D) is evaluated and the pressure correction is done
EPSI	A small value prescribed as the upper-bound for the velocity divergence in each cell
BCNS	This subroutine deals with the boundary conditions for Navier-Stokes equations
BCNSST	This subroutine deals with the boundary conditions for Navier-Stokes equations in the presence of stampings on the walls
VELALT	This is a subroutine which stores the current solution (velocity) for time level (n) in order to start a new time cycle of (n+1) level
ITUR	This is an index which denotes whether a laminar flow(=0) or a turbulent flow (=1) is being computed

TURBU	This subroutine controls the subroutines for computation of turbulent viscosity with the help of k and ϵ equations
BCKD	This subroutine deals with the boundary conditions for k and ϵ
KDALT	This subroutine stores the current variables of k and ϵ in order to start next iteration
KDEQCP	This is a subroutine where the k and ϵ for the next iteration are explicitly evaluated
TURVIS	This is a subroutine where the turbulent kinematic viscosity for each cell is calculated
DIVKD	This parameter denotes maximum discrepancy of k and ϵ between two iterative steps
EPKD	A small value that determines the convergence for the calculation of the equations for k and ϵ
TICORR	In this subroutine where the value of the time increment (Δt) and the donor cell coefficient (α_p) are calculated
DIVMAX	This is a parameter which denotes the maximum time increment of field variables
STAT	A small value which determines the conditions for steady solution
ITA	Number of iterations in the time (one way) coordinate or number of time steps
ITAMAX	Maximum number of allowable iterations in the time direction

NSEQCP	This is a subroutine where the velocities for the next time step are explicitly evaluated from the discretized Navier-Stokes equations
BCOV	In this subroutine the velocity boundary conditions for the obstacle are specified. This is used in conjunction with BCO
TIGRAD	This is a subroutine where the time-gradients of the velocity components are calculated
ENERGY	This is a subroutine which controls the solution of energy equation by a SOR or equivalent technique
BCT	This subroutine deals with the temperature boundary conditions for the confining surfaces of the channel
BCTST	This subroutine deals with the temperature boundary conditions for the confining surfaces in the presence of stampings on the walls
BCOT	This subroutine deals with temperature boundary conditions for the obstacle
TEQCP	This is a subroutine where the temperature field is calculated
DIVT	This parameter denotes maximum discrepancy of the temperature between two iterative steps
TSTAT	A small value that determines the convergence for steady solution of the energy equation
OUTPUT	This is a subroutine which prints the output in the assigned output files

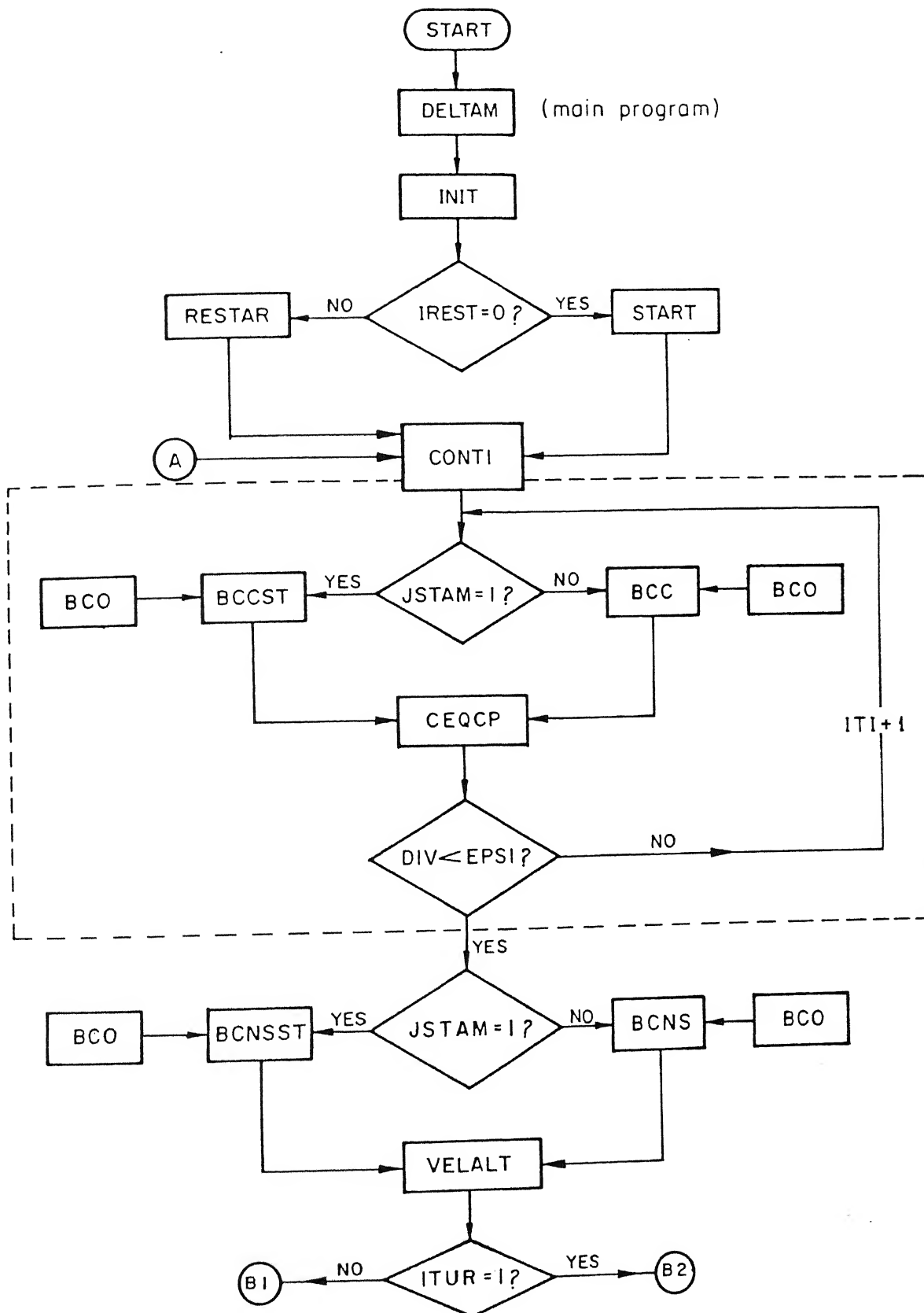


Fig. A-1

Contd.....

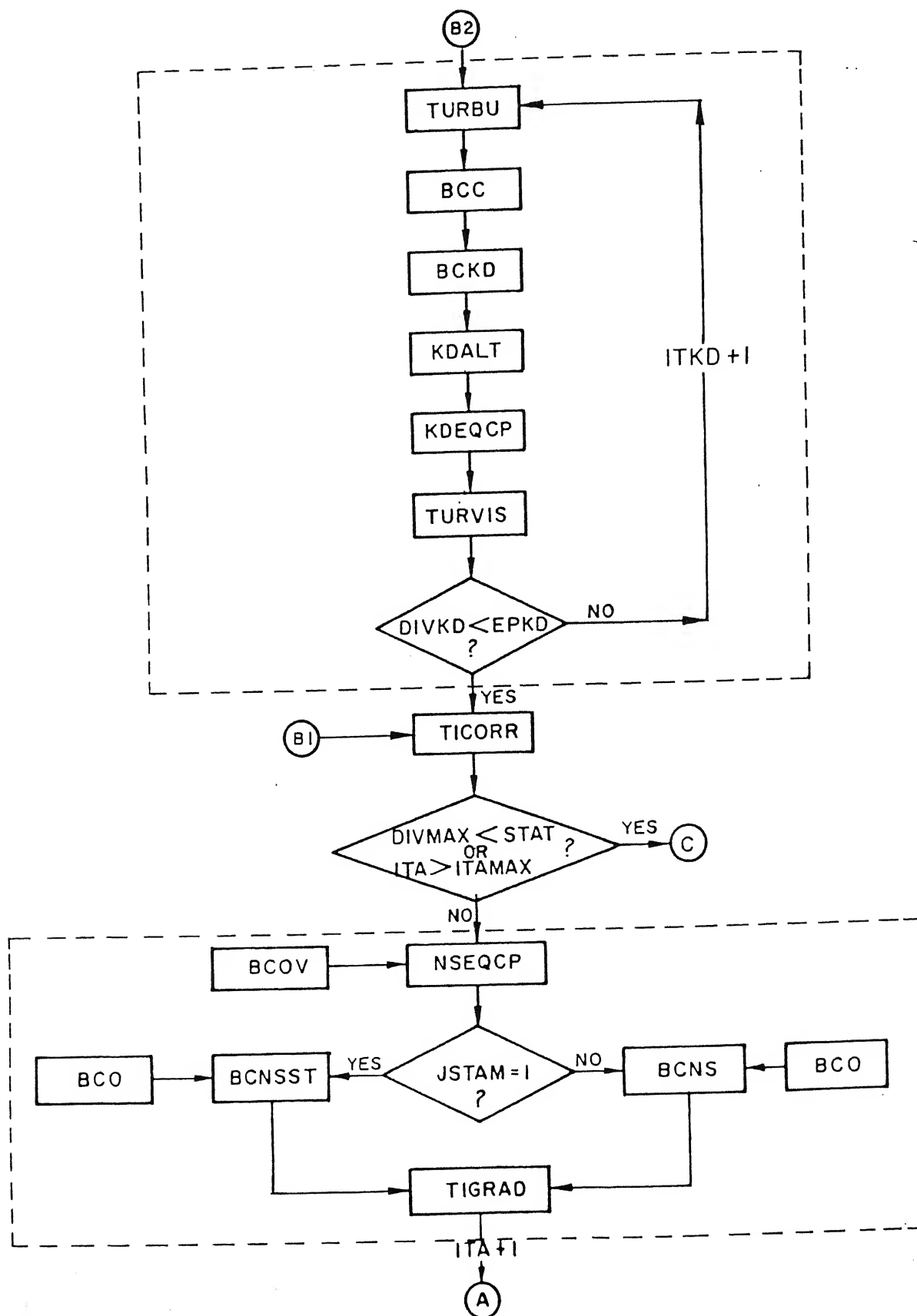


Fig. I - A

Contd

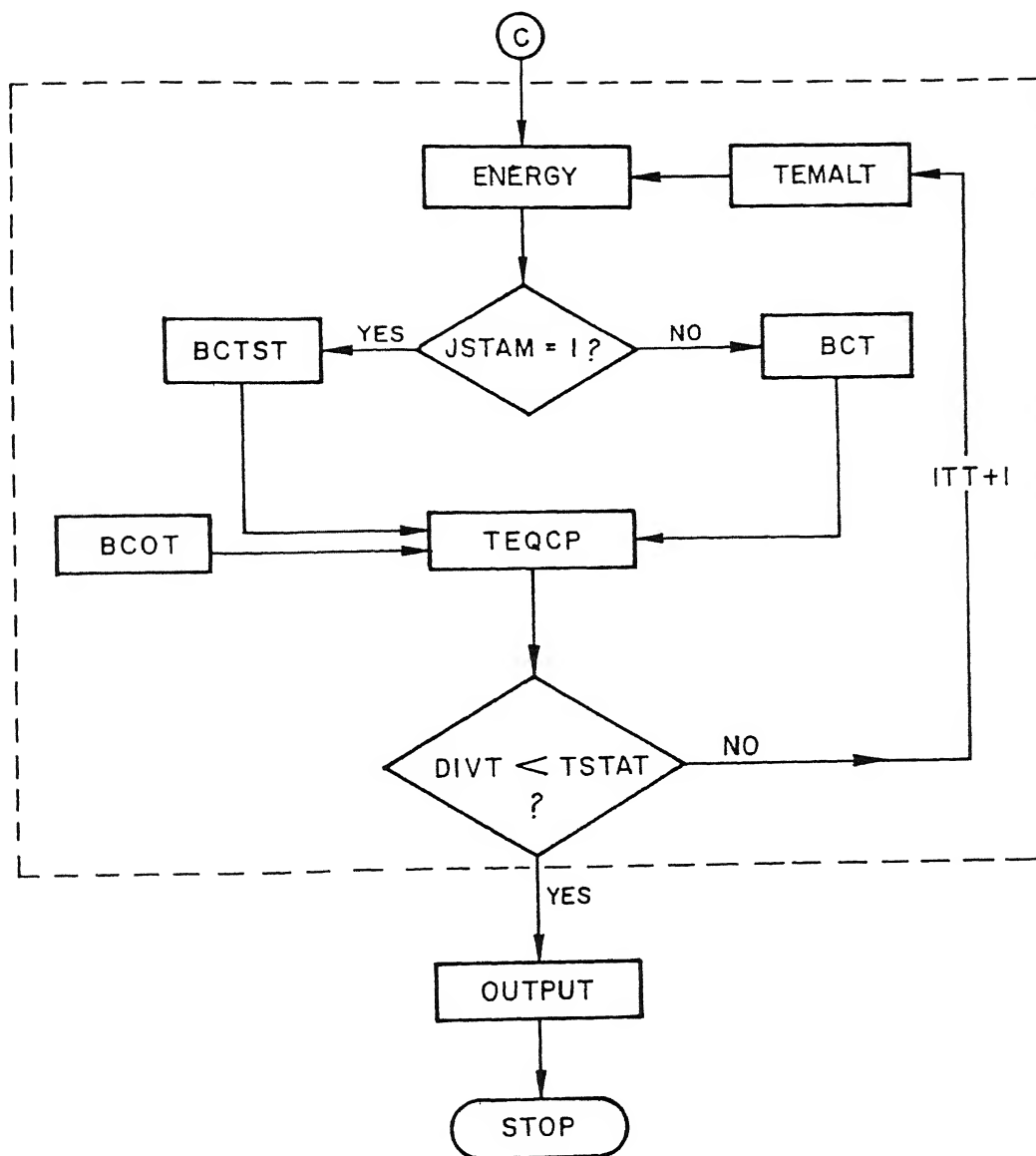


Fig. A-1